

From the field of Medical Biochemistry and Molecular Biology

Theoretical Medicine and Biosciences

Of the Faculty of Medicine

Of the Saarland University, Homburg/Saar

## **AXER in Focus: Molecular Interplay and Structural Aspects in Cellular Models**

Dissertation for obtaining the Degree of Doctor of Natural Sciences

of the Faculty of Medicine

SAARLAND UNIVERSITY

2024

Submitted by: Dražena Hadžibeganović

Born on: 14.04.1979 in Tuzla (B&H)

Day of oral examination: March 20, 2025

Dean of the Faculty: Univ.-Prof. Dr. med. dent. Matthias Hannig

Examinants: Prof. Dr. Martin Jung

Prof. Dr. Barbara Anne Niemeyer-Hoth

Prof. Dr. Magali Madry

*Dedicated to my daughter*



## Table of Contents

Table of Contents .....	1
Table of Figures .....	4
Table of Tables.....	6
Abbreviations.....	7
Abstract .....	11
Zusammenfassung.....	12
<b>I. INTRODUCTION</b> .....	<b>14</b>
I.1. Cell energy metabolism.....	14
I.1.1. ATP-producing pathways.....	14
I.1.2. Metabolic alterations.....	15
I.1.3. AMPK - the intracellular energy sensor .....	16
I.2. Endoplasmic reticulum - great organelle, great duties, great energy demand .....	18
I.3. Molecular mechanism of the ATP <sub>ER</sub> import .....	21
I.3.1. AXER-mediated ATP <sub>ER</sub> import.....	22
I.3.1.1. Putative regulatory mechanisms of the ER energy homeostasis .....	24
I.4. BiP – the master ATP <sub>ER</sub> -consumer.....	26
I.4.1. BiP regulation of Sec61-channel .....	27
I.4.2. BiP regulation of UPR signaling.....	29
I.5. Objectives.....	32
<b>II. MATERIAL AND METHODES</b> .....	<b>34</b>
II.1. Materials.....	34
II.1.1. Devices and software .....	34
II.1.2. Chemicals, enzymes, and kits .....	35
II.1.3. Antibodies .....	37
II.1.3.1. Primary antibodies .....	37
II.1.3.2. Secondary antibodies.....	38
II.1.4. Peptide.....	38
II.1.5. Oligonucleotides .....	38
II.1.5.1. RNA oligonucleotides (siRNA) .....	38
II.1.5.2. DNA oligonucleotides (Primers).....	39
II.1.6. Plasmids .....	40
II.1.7. Rough microsomes.....	42
II.1.8. Bacterial cells.....	42
II.1.9. Cell line .....	43
II.1.9.1. HeLa cells .....	43

II.1.9.1.1. HeLa- $\mu$ s cells .....	43
II.2. Cell culture and cell manipulation.....	43
II.2.1. Cell cultivation and cell counting.....	43
II.2.2. siRNA-based cell manipulation .....	43
II.2.3. Plasmid-based cell manipulation .....	44
II.2.4. Preparation of whole-cell lysate.....	45
II.2.5. Preparation of semi-permeabilized cell.....	45
II.2.6. Sample preparation for mass spectrometry .....	47
II.3. Molecular biology and nucleic acid manipulation .....	47
II.3.1. Total RNA isolation .....	47
II.3.1.1. Quantity and purity of nucleic acids .....	47
II.3.1.2. RNA integrity .....	48
II.3.1.3. Real-time quantitative polymerase chain reaction .....	48
II.3.1.4. RNA sequencing .....	49
II.3.2. Strategies for cloning.....	50
II.3.2.1. Designing primers .....	51
II.3.2.2. Polymerase chain reaction.....	52
II.3.2.3. Agarose gel electrophoresis.....	53
II.3.2.4. Restriction digestion.....	54
II.3.2.5. Ligation of restricted DNA .....	54
II.3.2.6. Bacterial transformation with plasmid vector.....	55
II.3.2.7. Cultivation of transformed bacterial cells .....	55
II.3.2.8. Plasmid DNA extraction .....	56
II.3.2.9. Sequencing of plasmid DNA .....	56
II.4. Biochemical analysis .....	57
II.4.1. SDS-polyacrylamide gel electrophoresis .....	57
II.4.2. Western blot analysis.....	58
II.4.3. NanoBIT system – detection of protein-protein interaction .....	60
II.4.4. Live-cells metabolic analysis .....	62
II.4.4.1. Measuring mitochondrial respiration .....	66
II.4.4.2. Measuring glycolytic activity.....	66
II.5. Statistical analysis .....	66
II.6. Additional experiments .....	67
II.6.1. Spot peptide array analysis .....	67
<b>III. RESULTS.....</b>	<b>68</b>
III.1. Evaluation of optimal time interval for AXER siRNA-mediated silencing .....	68

III.2. RNA sequencing analysis after AXER depletion .....	70
III.2.1. GO enrichment analysis .....	73
III.2.2. KEGG pathway analysis .....	76
III.3. Quantitative proteomic analysis after AXER silencing .....	79
III.4. RT-qPCR and Western blot analysis used to verify the “-omic” results .....	81
III.5. Changes in cell metabolism due to AXER depletion .....	85
III.6. Detection of dynamic protein-protein interactions in living cells using the NanoBiT system .....	87
III.6.1. The interactions of the Sec61-complex subunits $\beta$ and $\gamma$ .....	88
III.6.2. How ER stress affects the Sec61-complex interaction with BiP .....	90
III.6.2.1. Effect of chemically caused ER stress .....	91
III.6.2.1.1. Is NanoBiT luciferase $\text{Ca}^{2+}$ -dependent? .....	95
III.6.2.1.2. ER stress affects the additional luminal protein-protein interaction .....	97
III.6.2.2. Effect of physiological ER stress .....	98
III.6.3. Identification of AXER playmates in intact cells .....	102
III.6.3.1. Is AXER capable of homo-oligomerization? .....	105
III.7. Additional results .....	107
III.7.1. Spot peptide array data .....	107
<b>IV. DISCUSSION</b> .....	109
IV.1. “-Omic” analysis revealed the molecular changes occurring after AXER knockdown ..	109
IV.2. Cellular energy-producing activities affected by loss of AXER .....	113
IV.3. Valuable insights into protein-protein interactions of the ER residents .....	114
IV.3.1. Interactions of the ER protein translocase demonstrated in living cells .....	114
IV.3.1.1. BiP-Sec61 interaction disrupted by ER stress .....	115
IV.3.2. AXER interaction partners identified in intact cells .....	117
IV.3.3. Putative AXER homo-oligomer .....	119
IV.4 Conclusion and further directions .....	121
Appendix .....	123
References .....	125
Publications .....	141
Acknowledgements .....	142
Curriculum Vitae .....	143

## Table of Figures

Figure 1. Structure and activation of AMPK .....	17
Figure 2. Organization of the Sec61, TRAP and ribosome-translocon complex .....	20
Figure 3. Hypothetical model of hSLC35B1 (AXER) .....	23
Figure 4. Two regulatory mechanisms of the ER energy homeostasis .....	25
Figure 5. BiP ATPase cycle.....	27
Figure 6. Organization of the Sec61 $\alpha$ , BiP and its co-chaperon Sec63 .....	28
Figure 7. Three UPR signaling branches triggered by BiP releasing .....	30
Figure 8. Graphical summary of the objectives .....	33
Figure 9. Total RNA quality analysis using the Agilent Bioanalyzer system .....	48
Figure 10. The workflow - from RNA sample preparation to RNA-seq analysis.....	50
Figure 11. Graphic of molecular cloning.....	51
Figure 12. Principle of the NanoBiT system .....	60
Figure 13. Microplate setup for measuring mitochondrial respiration and glycolytic activity ..	63
Figure 14. The signal profile of MitoXpress Xtra and pH-Xtra .....	65
Figure 15. AXER gene silencing affected cell viability and proliferation depending on different silencing duration and type of targeting siRNA .....	68
Figure 16. AXER depletion efficiency validated by RT-qPCR .....	69
Figure 17. Comparison of differentially expressed genes (DEGs) upon AXER depletion .....	71
Figure 18. Comparison of differentially expressed genes (DEGs) upon AXER depletion illustrated by volcano plots .....	72
Figure 19. Gene Ontology (GO) enrichment analysis of differentially expressed genes (DEGs) from the AXER siRNA #1 treatment .....	74
Figure 20. Gene Ontology (GO) enrichment analysis of differentially expressed genes (DEGs) from the AXER siRNA #4 treatment .....	75
Figure 21. KEGG enrichment analysis of differentially expressed genes from the AXER siRNA #1 treatment .....	77
Figure 22. KEGG enrichment analysis of differentially expressed genes from the AXER siRNA #4 treatment .....	78
Figure 23. mRNA expression levels after AXER silencing validated by RT-qPCR .....	82
Figure 24. Different protein abundance in response to AXER silencing, determined by Western blot analysis.....	83
Figure 25. Statistical analysis of Western blot results upon AXER depletion.....	84
Figure 26. Extracellular acidification upon AXER depletion .....	85
Figure 27. Mitochondrial respiration upon AXER depletion.....	86
Figure 28. ER-luminal protein-protein interactions of Sec61-complex .....	89
Figure 29. Cartoon view of disrupted PPIs between Sec61 subunits ( $\beta$ and $\gamma$ ) and BiP, caused by Tg/Tun treatment .....	91
Figure 30. Effect of chemically caused ER stress on Sec61-complex interaction with BiP in HeLa cells.....	92
Figure 31. Effect of chemically caused ER stress on Sec61-complex interaction with BiP in HeLa- $\mu_s$ cells .....	94
Figure 32. cAMP-dependent protein kinase A (PKA) construct pair served as control for luciferase calcium dependency .....	96
Figure 33. Effect of chemically caused ER stress on BiP interaction with Sec63. ....	97
Figure 34. Effect of physiological ER stress on Sec61-complex interaction with BiP .....	99
Figure 35. Effect of physiological ER stress on PKA positive control pair.....	101
Figure 36. AXER interaction with Sec61-complex.....	102

Figure 37. AXER interaction with TRAP-complex .....	104
Figure 38. AXER putative homo-oligomerization .....	106
Figure 39. Possible interaction sites of AXER-Sec61 and AXER-TRAP .....	108
Figure 40. Possible interaction sites of AXER-AXER.....	108
Figure 41. Putative AXER dimer .....	120
Figure 42. Graphical summary of the main findings of the study .....	122
Figure 43. Heatmap summarizing the tested PPIs of AXER.....	124

## Table of Tables

Table 1. Devices and software .....	34
Table 2. Chemicals, enzymes, and kits.....	35
Table 3. Primary antibodies used in this work.....	37
Table 4. Secondary antibodies used in this work.....	38
Table 5. Peptide used in this work .....	38
Table 6. RNA oligonucleotides used in this work .....	38
Table 7. Primers used for RT-qPCR experiments.....	39
Table 8. Primers used for mutagenesis and sequencing .....	39
Table 9. Plasmids used for cell culture transfection .....	40
Table 10. Pipetting protocol for the preparation of SDS-polyacrylamide gel.....	58
Table 11. Instrumental setup for M200 Tecan Infinite microplate reader .....	63
Table 12. Quantity and quality of RNA samples prepared for RNA sequencing.....	70
Table 13. Changes in protein level after AXER depletion. ....	80
Table 14. Differently expressed genes (DEGs) upon AXER depletion .....	123
Table 15. Genes/proteins with similar trends of regulation/expression upon AXER depletion. .....	124

## Abbreviations

%	percent
°C	degree Celsius
μ	micro
~	approximately
α	alpha (subunit)
β	beta (subunit)
γ	gamma (subunit)
δ	delta (subunit)
aa	amino acids
ADP	adenosine diphosphate
AMP	adenosine monophosphate
Amp	ampicillin
AMPK	AMP-activated protein kinase
ANT	adenine nucleotide translocator
ATF4	activating transcription factor 4
ATF6	activating transcription factor 6
ATF6-N	cleaved activating transcription factor 6 with N-terminus
ATP	adenosine triphosphate
ATP <sub>ER</sub>	adenosine triphosphate in the ER
ATP2A	ATPase sarcoplasmic/endoplasmic reticulum calcium transporting protein
AXER	ATP/ADP exchanger in the ER
BiP	binding immunoglobulin protein (also known as Hsp70, GRP78)
bp	base pair
BP	biological process
BSA	bovine serum albumin
C-	carboxy terminus
Ca <sup>2+</sup>	calcium ions
Ca <sup>2+</sup> -CaM	calcium (2+)-calmodulin
CaATiER	Ca <sup>2+</sup> -antagonized transport into the ER
CaM	calmodulin
CaMKK2	calcium/calmodulin dependent kinase kinase 2
CC	cellular components
cDNA	complementary DNA
CHO	Chinese hamster ovary (cells)
CHOP	C/EBP homologous protein
cm	centimeter
Co-IP	co-immunoprecipitation
Cryo-EM	cryo-electron microscopy
Ctrl	control
DMEM	Dulbecco's Modified Eagle Medium
DMSO	dimethyl sulfoxide
dNTP	deoxyribonucleotide triphosphate
ds	double-stranded
<i>E.coli</i>	<i>Escherichia coli</i>
e.g.	for example
EGTA	ethylene glycol-bis(aminoethylether)-N,N,N',N'-tetraacetic acid
eIF2	eukaryotic translation initiation factor 2
EMC	ER membrane complex
ER	endoplasmic reticulum
ERAD	ER-associated degradation
ERj	ER-resident J-domain-containing protein
et al.	et alia / and others
ETC	electron transport chain
FADH <sub>2</sub>	flavin adenine dinucleotide

f.c.	final concentration
FPKM	Fragments Per Kilobase per Million mapped fragments
Fwd	forward
g	gram
GFP	green fluorescent protein
GO	gene ontology
GOI	gene of interest
GTP	guanosine triphosphate
h	hours
HaBiT	High affinity NanoBiT peptide
HeLa	"Henrietta Lacks" cervical cancer cells
HEPES	4-(2-Hydroxyethyl)piperazine-1-ethane-sulfonic acid
Hsp	heat shock protein
HSPA5	heat shock protein family A member 5 gene (encodes BiP)
HSV-TK	herpes simplex virus-1 thymidine kinase
i.e.	that is (in other words)
Ig	immunoglobulin
IMM	inner mitochondrial membrane
INS-1	(rat) insulin secreting beta cell
lowER	ER low energy response
IP <sub>3</sub> Rs	inositol 1,4,5-trisphosphate receptors
IRE1	inositol-requiring enzyme 1
Kan	kanamycin
KCl	potassium chloride
K <sub>D</sub>	dissociation constant
KD	kinase domain
kDa	kilo Dalton
KEGG	Kyoto Encyclopedia of Genes and Genomes
l	liter
LB	lysogeny broth
LgBiT	Large BiT -tag of NanoBiT systems
LKB1	liver kinase B1 (also known as STK11)
LU	luminescence units
M	molar concentration
mA	milliampere
MAM	mitochondria-associated ER membrane (also known as MERC)
MCS	membrane contact site
MERC	mitochondria-endoplasmic reticulum contact
MF	molecular function
mg	milligram
MgCl <sub>2</sub>	magnesium chloride
Mif	mifepristone
min	minutes
ml	milliliter
mM	millimolar concentration
mRNA	messenger ribonucleic acid
mTOR	mammalian target of rapamycin
N-	amino terminus
NaCl	sodium chloride
NADH	nicotinamide adenine dinucleotide
NanoBiT	nanoluciferase binary technology
NBD	nucleotide binding domain
NEF	nucleotide exchange factor
Ng	nanogram
nM	nanomolar concentration
OST	oligosaccharyltransferase complex

OXPHOS	oxidative phosphorylation
P <sub>i</sub>	inorganic phosphate
pAMPK	phosphorylated AMP-activated protein kinase
PCR	polymerase chain reaction
PERK	protein kinase RNA-like endoplasmic reticulum kinase
<i>Pfu</i>	<i>Pyrococcus furiosus</i>
PKA	protein kinase A
PLAC	Pepstain A, Leupetin, Antipain, Chymostatin
PMSF	phenylmethylsulfonyl fluoride
PPI	protein-protein interaction
PVDF	polyvinylidene difluoride
rER	rough endoplasmic reticulum
Rev	reverse
RFU	relative fluorescence units
RIN	RNA integrity number
RLU	relative luminescence units
RM	rough microsome
RNA	ribonucleic acid
RNAse	ribonuclease
rpm	rotation per minute
RT	room temperature
RT-qPCR	real-time quantitative PCR
RyR	ryanodine receptor
s	seconds
SBD	substrate binding domain
scr	scrambled
SDS-PAGE	sodium dodecyl sulfate-polyacrylamide gel electrophoresis
sER	smooth endoplasmic reticulum
SERCA	sarco/endoplasmic reticulum calcium ATPase
siRNA	small interfering RNA
SLCs	solute carriers
SLC35B1	solute carrier family 35 member B1
SmBiT	Small BiT -tag of NanoBiT systems
SP	signal peptide
SPCs	semi-permeabilized cells
SPR	signal recognition particle
SQSTM1	sequestosome1
SR	signal recognition particle receptor
SRP	signal recognition particle
SRPRA	SRP receptor subunit alpha gene (encodes SR $\alpha$ )
SRPRB	SRP receptor subunit beta gene (encodes SR $\beta$ )
STK11	serine/threonine kinase 11
TB	terrific broth
TCA	tricarboxylic acid
Tg	thapsigargin
T <sub>m</sub>	melting temperature
TMH	transmembrane helix
TMD	transmembrane domain
Tun	tunicamycin
TRAM	translocon-associated membrane protein
TRAP	translocon-associated protein complex
Tris	tris(hydroxymethyl)aminomethane
U	Unit
UdS	“Universität des Saarlandes” (Saarland University)
UPR	unfolded protein response
UTR	untranslated region

UV	ultraviolet
V	Volt
v/v	volume per volume
w/v	weight per volume
WG	working group
Xbp1	X-box binding protein 1

Single and three-letter codes for amino acid

A (Ala) Alanine	C (Cys) Cysteine	D (Asp) Aspartic acid
E (Glu) Glutamic acid	F (Phe) Phenylalanine	G (Gly) Glycine
H (His) Histidine	I (Ile) Isoleucine	K (Lys) Lysine
L (Leu) Leucine	M (Met) Methionine	N (Asn) Asparagine
P (Pro) Proline	Q (Gln) Glutamine	R (Arg) Arginine
S (Ser) Serine	T (Thr) Threonine	V (Val) Valine
W (Trp) Tryptophan	Y (Tyr) Tyrosine	

Nucleotide

A	Adenine	C	Cytosine
T	Thymine	G	Guanine
U	Uracil		

## Abstract

Unlike other cellular compartments, such as the cytosol (enabling glycolysis) or mitochondria (enabling oxidative phosphorylation), the endoplasmic reticulum (ER) operates without an autonomous metabolic pathway for the regeneration or de novo synthesis of adenosine triphosphate (ATP). Instead, the ER heavily relies on the regulated import of ATP. Recently, SLC35B1 was characterized as the ATP/ADP exchanger of the mammalian ER membrane and termed AXER. It was found that AXER is integrated into a broader signaling cascade, which includes calcium ( $\text{Ca}^{2+}$ ) as a potent second messenger. However, ongoing debates persist regarding (i) the precise role of  $\text{Ca}^{2+}$  as a regulator of AXER activity and (ii) the sources of ATP for the ER import. Also, unresolved inquiries revolve around AXER's interaction partners, earlier investigated *in vitro* by co-immunoprecipitation (co-IP) studies.

To expand upon previous research, this work aimed to verify and extend interaction partners of AXER in living cells, preferably using the biomolecular luminescence complementation (BiLC). In conjunction with various experimental methodologies, including RNA sequencing (RNA-seq) and proteomic analysis, the BiLC approach successfully identified key players involved in the ER protein import and/or the ER  $\text{Ca}^{2+}$  homeostasis as components of the AXER interactome. Furthermore, it was observed that AXER potentially functions as a dimer or higher order oligomer. To better understand the metabolic integration of this functionally unique ER protein, the live monitoring of cellular energetic processes (glycolysis and oxidative phosphorylation) was performed after AXER depletion, revealing a decline in the overall ATP-production in cells. These findings not only bolster the earlier discoveries, but also indicate AXER's involvement in total cellular energy flow and its connection to the complex  $\text{Ca}^{2+}$  signaling. Clearly, both findings warrant further examination.

The BiLC approach was also instrumental in demonstrating for the first time the interaction between the ER protein translocase and the luminal chaperone BiP in living, intact cells. To further investigate the dynamics of the detected protein-protein interactions (PPIs) cells were confronted with a short-term chemically induced ER stress as well as a prolonged stress condition. These studies elegantly underline the dynamic and transient nature of BiP's interaction with the Sec61-complex, and its co-chaperone Sec63. In sum, the data offer valuable insights into the changes occurring in response to ER stress in living cells and support the idea of a regulatory function triggered by BiP binding and dissociating from partner proteins.

## Zusammenfassung

### AXER im Fokus: Molekulares Zusammenspiel und strukturelle Aspekte in Zellmodellen

Im Gegensatz zu anderen zellulären Kompartimenten, wie dem Zytosol (Ort der zellulären Glykolyse) oder den Mitochondrien (Ort der oxidativen Phosphorylierung) arbeitet das endoplasmatische Retikulum (ER) ohne einen autonomen Stoffwechselweg für die Regeneration oder de-novo-Synthese von Adenosintriphosphat (ATP). Stattdessen ist das ER auf den regulierten Import von ATP angewiesen. Vor kurzem wurde SLC35B1 als der ATP/ADP-Austauscher der ER-Membran von Säugetieren identifiziert. Dieses Membranprotein wurde entsprechend seiner Funktion als AXER bezeichnet. Es wurde weiterhin festgestellt, dass AXER in eine Signalkaskade eingebunden ist, die auch Kalzium ( $\text{Ca}^{2+}$ ) als potenten Botenstoff miteinschließt. Allerdings wird weiterhin ausgiebig über (i) die genaue Rolle von  $\text{Ca}^{2+}$  als regulatorischer Faktor zur Beeinflussung der Aktivität von AXER und (ii) die Quellen des ATP für dessen ER Import diskutiert. Offene Fragestellungen drehen sich auch um die Interaktionspartner von AXER, die zuvor *in vitro* durch Co-Immunopräzipitationsstudien (Co-IP) identifiziert wurden.

Um in dieser Arbeit bisherige Forschungsergebnisse zu verifizieren und erweitern, sollten putative AXER-Interaktionspartner direkt in lebenden Zellen mit Hilfe eines biomolekularen Lumineszenz-Komplementations-Assays (BiLC) untersucht werden. In Verbindung mit verschiedenen experimentellen Methoden, einschließlich RNA-Sequenzierung (RNA-seq) und Proteomanalysen, identifizierte der BiLC-Ansatz erfolgreich wichtige Akteure des AXER-Interaktoms. Gefundene Interaktionspartner von AXER agieren als Schlüsselkomponenten beim ER-Proteinimport und/oder der ER- $\text{Ca}^{2+}$ -Homöostase. Darüber hinaus wurde festgestellt, dass AXER möglicherweise als Homo-Oligomer mit zwei oder mehr Kopien funktioniert. Zum besseren Verständnis der metabolischen Integration dieses funktionell einzigartigen ER-Proteins wurden die energetischen Prozesse Glykolyse und oxidative Phosphorylierung nach AXER-Deletion in lebenden Zellen untersucht. Es zeigte sich ein Rückgang der gesamten ATP-Produktion in den Zellen. Die Ergebnisse bestätigten nicht nur die früheren Entdeckungen, sondern deuten auch auf AXERs Beteiligung am gesamten zellulären Energiefluss und seine Verbindung zur komplexen  $\text{Ca}^{2+}$ -Signalisierung hin. Beide Erkenntnisse erfordern eindeutig weiterführende Untersuchungen.

Der BiLC-Ansatz war auch entscheidend, um erstmals die Interaktion zwischen der ER-Proteintranslokase und dem ER-luminalen Chaperon BiP in lebenden, intakten Zellen zu demonstrieren. Zur Untersuchung der Dynamik der nachgewiesenen Protein-Protein-Interaktionen (PPIs) wurden die Zellen mit einem kurzzeitigen chemisch induzierten ER-Stress

sowie mit lang-anhaltenden Stressbedingungen ausgesetzt. Diese Studien verdeutlichen die dynamische und vorübergehende Natur von BiPs Interaktion mit dem Sec61-Komplex und seinem Co-Chaperon Sec63. Insgesamt bieten die Daten wertvolle Einblicke in die Veränderungen, die als Reaktion auf ER-Stress in lebenden Zellen auftreten und unterstützen die Idee einer regulatorischen Funktion, die durch die Bindung und Dissoziation von BiP mit Partnerproteinen ausgelöst wird.

## I. INTRODUCTION

### I.1. Cell energy metabolism

Energy is essential for proper functionality of all living organisms. The set of biochemical processes by which cells gain, transform, and use energy is called cell energy metabolism. For storage and use at the cellular level, energy is mainly provided by the hydrolysis of adenosine triphosphate (ATP) to adenosine diphosphate (ADP) and free inorganic phosphate ( $P_i$ ). Although other nucleotides (e.g., guanosine triphosphate, GTP) and phosphate metabolites (e.g., phosphoenolpyruvate) have a role in the overall energetic contribution, ATP is the principal fuel for most of the energy consuming processes. A great repertoire of cellular processes revolves around the production and consumption of ATP, from cellular signaling to post-translational modifications of proteins and nucleic acids synthesis (Kamerlin et al., 2013; Rajendran et al., 2016). In human adult, each ATP molecule is recycled 1000-1500 times to meet daily ATP requirements, that corresponds to approximately 65 kg ATP recycled (Zimmerman et al., 2011).

The current metabolic conditions within the cell dictate the type and rate of ATP production, that can occur in a presence of oxygen as well as in an anaerobic environment. Intracellular glucose, serving as a primary energy source, is catabolized in three consecutive pathways to yield ATP: glycolysis, tricarboxylic acid (TCA) cycle, and oxidative phosphorylation (OXPHOS).

#### I.1.1. ATP-producing pathways

Glycolysis is the first ATP-producing process, when one molecule of glucose is converted into two pyruvate molecules in cell cytosol. Due to initial energy investment, glycolysis ends with quite low energy production, generating two ATPs per molecule of glucose only (plus two reduced nicotinamide adenine dinucleotide (NADH) electron-carrier molecules; Chandel, 2021). From this stage, depending on cellular conditions, the pyruvate molecule has two possible fates: to be reduced to lactate (I.1.2), or to be oxidized to acetyl coenzyme A (acetyl-CoA) and  $CO_2$ . Under aerobic conditions, acetyl-CoA enters the second metabolic pathway called TCA cycle (Krebs cycle or the citric acid cycle; Kennedy and Lehninger, 1949). Pyruvate oxidation and the TCA cycle, both occur within mitochondria producing a single molecule of ATP (or GTP). Additionally, four reduced NADH and one reduced flavin adenine dinucleotide ( $FADH_2$ ) are generated in the process. Subsequently, these coenzymes donate electrons to the electron transport chain (ETC) and drive OXPHOS - the third energy-producing process that yields a generous amount of ATP (Bonora et al., 2012). Four redox enzyme complexes (Complex I, II, III, and IV), studded along the inner mitochondrial membrane (IMM), are involved in electron transport chain. Electrons are shuttled from one protein complex to the next, and lastly to molecular oxygen, that is reduced to  $H_2O$ . In response to electron transfer,

hydrogen ions ( $H^+$ , protons) are moved from the mitochondrial matrix to the intermembrane space, producing the “proton motive” force. Re-entry of hydrogen ions into the mitochondrial matrix through the Complex V (ATP synthase) is accompanied by the phosphorylation of ADP (oxidative phosphorylation), yielding on average 34 ATP molecules from two molecules of pyruvate. Thus, catabolism of a single glucose molecule ends on average with synthesis of 38 ATPs (Lodish et al., 2016; Nolfi-Donagan et al., 2020).

Catabolic processes of amino acids (oxidative deamination and transamination) and fatty acids (beta-oxidation) are additional reactions that can generate acetyl-CoA and eventually satisfy the cell energy-demands all depending on factors including the current cellular environment as well as cell type (Stryer, 1995).

### **I.1.2. Metabolic alterations**

In the oxygen-rich state, the majority of cells use OXPHOS as the ruling pathway for ATP generation. If oxygen is not available, pyruvate cannot be efficiently oxidized to acetyl-CoA, and cells primarily rely on glycolysis. Under these conditions, glucose conversion into pyruvate is followed by lactate generation, and consumption of two newly produced NADH molecules to restore the NAD tank. The process is catalysed by lactate dehydrogenase and ends with total energetic contribution of two ATP molecules (Bonora et al., 2012.; Lee, 2021). Due to slower oxygen supply from the blood, lactate is generated in muscles during dynamic exercise (Gladden, 2004). However, the production and increased concentration of lactate are not strictly associated to the oxygen deficiency. The lack of mitochondria makes erythrocytes incompetent to yield ATP via oxidative phosphorylation, and consequently dependent on the glycolytic pathway (Van Wijk and Van Solinge, 2005). The main characteristic of cancer cells is energy generation in an  $O_2$ -independent way, preferentially relying on glycolysis. Even though there is a huge mathematical disparity in ATP production by glycolysis (2 ATPs) compared to oxidative phosphorylation (total 38 ATPs), cancer cells overcome this energy imbalance rising the glucose intake and generating lactate (Ganapathy-Kanniappan and Geschwind, 2013). This tumor metabolic alteration was first noticed in 1920s by Otto Warburg, the German scientist who proposed the phenomenon of aerobic glycolysis, later known as the “Warburg effect”. Based on Warburg’s hypothesis, mitochondrial dysfunctionality causes the aerobic glycolysis that is the mayor reason for cancer development as well as cancer universal metabolic modification (Warburg et al., 1927; Warburg, 1956a; Warburg, 1956b; Liberti and Locasale, 2016). Over the past decades, innovative experimental approaches, and new insights into genetically administered cell transformations improve the understandings on biological significance of cancer-associated glycolysis. Contrary to what Warburg hypothesized, the upregulation of glycolysis is not generally related to dysfunctional mitochondria (Vaupel and Multhoff, 2021). Metabolic alterations support cell survival,

progressive growth, and rapid proliferation, creating the specific tumor hallmarks (Vander Heiden et al., 2009; Pavlova and Thomson, 2016; Pascale et al., 2020; X. Li et al., 2022; Pavlova et al., 2022). The chemoresistance, promoted by higher glycolytic rate, is one of the examples of undisturbed growth of cancer cells (Ganapathy-Kanniappan and Geschwind, 2013).

### **I.1.3. AMPK - the intracellular energy sensor**

The AMP-activated protein kinase (AMPK) complex is a central player of a very sophisticated signaling pathway, and highly conserved through evolution of eukaryotic cells. This advanced system serves as an adaptor of cellular metabolism, responding to energy changes and nutrients availability. When the cellular AMP:ATP or ADP:ATP ratio rises, an allosteric mechanism stimulates the activity of the AMPK, which then regulates energy homeostasis supporting catabolic and preventing anabolic processes (Herzig and Shaw, 2018). Three subunits constitute the AMPK complex,  $\alpha$  (catalytic subunit),  $\beta$  and  $\gamma$  (regulatory subunits) (Figure 1). The human AMPK subunits exhibit several isoforms, each encoded by a distinct gene. This includes two isoforms of  $\alpha$  and  $\beta$  subunits ( $\alpha 1$ ,  $\alpha 2$ ;  $\beta 1$ ,  $\beta 2$ ) and three isoforms of the  $\gamma$  subunit ( $\gamma 1$ ,  $\gamma 2$  and  $\gamma 3$ ). Diverse  $\alpha\beta\gamma$ -isoform combinations create 12 possible AMPK complexes. The compositions may have different subcellular locations as well as different functions, and different regulation by adenine nucleotides (the latter refers to  $\gamma$  subunit isoforms; Ross et al., 2016). The complex is activated by phosphorylation of threonine residue (Thr172), located on the amino (N)-terminal kinase domain (KD) of the  $\alpha$  subunit, that is directly followed by an autoinhibitory domain (AID). The two main activating kinases are tumour suppressor liver kinase B1 (LKB1; also known as serine/threonine kinase 11, STK11), and calcium (2+)/calmodulin-dependent protein kinase kinase  $\beta$  (CaMKK $\beta$ ; CaMKK2) (Stein et al., 2000; Yan et al., 2018). The association of the AMPK with glycogen is facilitated by the carbohydrate binding module (CBM) on the  $\beta$  subunit. The C-terminus of  $\gamma$  subunit contains four tandem repeats, noted as cystathionine- $\beta$ -synthase (CBS) domains. The CBS1, CBS3 and CBS4 are functional AMP/ADP/ATP binding sites that enable AMPK to respond to energy changes in the cell (Herzig and Shaw, 2018; Yan et al., 2018; Trefts and Shaw, 2021). Based on the Kyoto Encyclopedia of Gene and Genomes (KEGG) database, some of the AMPK-related processes are: glycolysis and gluconeogenesis; fatty acid biosynthesis; mTOR signaling pathway; PI3K-Akt signaling pathway; cell cycle and autophagy ([KEGG PATHWAY: AMPK signaling pathway - Reference pathway \(genome.jp\)](#), last checked at 14/06/24). The activated AMPK complex regulates downstream pathways by phosphorylation of target-components. The AMP binding to the  $\gamma$  subunit initiates the AMPK activation, causing conformational changes that enable Thr172-phosphorylation on the catalytic  $\alpha$  subunit (Figure 1; Kim et al., 2016). Additionally, the AMP-binding serves as a protection against

dephosphorylation of active, phosphorylated complex by protein phosphatases (Davies et al., 1995). Intricate AMPK-activation mechanism also involves two upstream kinases, LKB1 and CaMKK $\beta$ , as mentioned earlier (Figure 1). When cellular energy is distressed, the main part of AMPK activation is induced by LKB1 (Shackelford and Shaw, 2009). On the other hand, AMPK activation by CaMKK $\beta$  occurs regardless of AMP/ADP/ATP levels. The CaMKK $\beta$ -mediated phosphorylation of the Thr172 residue is associated with the fluctuations of intracellular calcium (2+), suggesting the connection between energy metabolism and calcium signaling (Woods et al., 2005; Marcelo et al., 2016).

Across the cellular compartments, diverse stimuli actuate the LKB1 and CaMKK $\beta$ , which then activate the AMPK complex. In this manner, regulating and connecting the sectional energy homeostasis, the AMPK becomes the major regulator of total energy homeostasis in eucaryotic cells (Trefts and Shaw, 2021). In addition to its well-known connection with mitochondria (Herzig and Shaw, 2018), the AMPK interacts with endoplasmic reticulum (ER) through calcium signaling and lipid homeostasis (Trefts and Shaw, 2021).

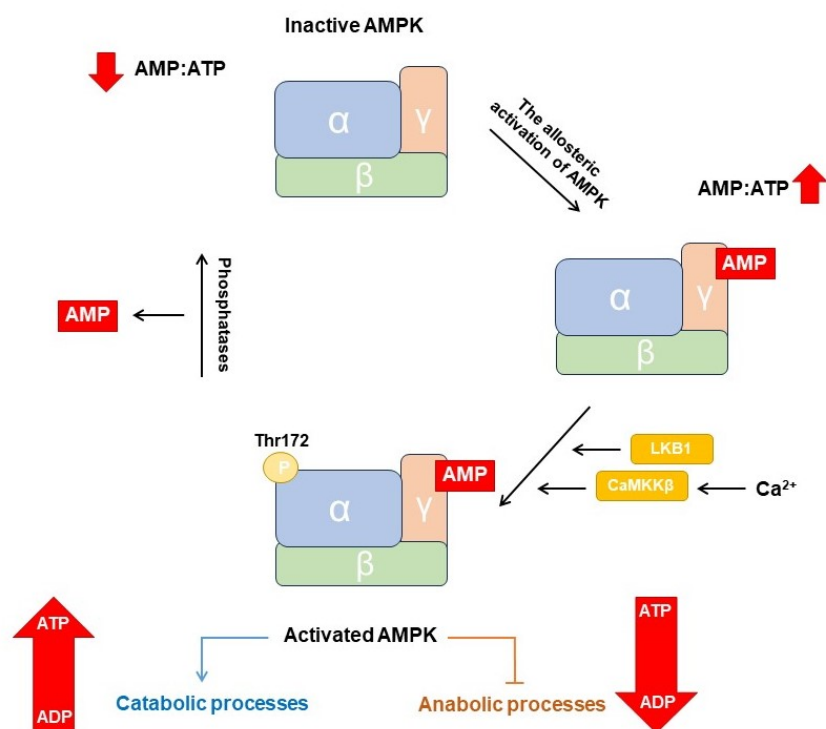


**Figure 1. Structure and activation of AMPK.** Schematic representation of three AMPK subunits:  $\alpha$  (blue),  $\beta$  (green) and  $\gamma$  (orange). The intracellular AMP:ATP ratio raises under metabolic stress. Consequently, AMP binds to the  $\gamma$  subunit leading to allosteric activation of AMPK. That allows upstream kinases (LKB1 or CaMKK $\beta$ ) to mediate phosphorylation of the Thr172 residue on the catalytic  $\alpha$  subunit. Once activated, AMPK regulates its downstream signal pathways, inhibiting anabolic processes to prevent ATP consumption, and stimulating catabolic processes to increase ATP production. AMPK, AMP-activated protein kinase; ATP, adenosine triphosphate; ADP, adenosine diphosphate; LKB1, liver kinase B1; CaMKK $\beta$ , calcium (2+)/calmodulin-dependent protein kinase kinase  $\beta$ ; P, phosphorylation.

## **I.2. Endoplasmic reticulum - great organelle, great duties, great energy demand**

The endoplasmic reticulum is a dynamic, single-copy organelle in eukaryotic cells. In 1945, it was visualized by electron microscopy and described like a “delicate lace-work extending throughout the cytoplasm” (Porter et al. 1945). Almost a decade after, the current name *endoplasmic reticulum* was coined based on its morphology and intracellular location (Palade and Porter, 1954). The ER is composed of two distinct morphological domains: interconnected tubules and flat cisternae (sheets), which are continuous with the nuclear envelope and extend across the cytoplasm reaching (close to) the plasma membrane (Porter and Palade, 1957; Voeltz et al., 2002; Schwarz and Blower, 2016). This unique form makes it aside from the cell nucleus the largest cellular organelle, occupying approximately 9 times the mitochondrial volume and 37 times the Golgi volume (Valm et al., 2017). The tubular structure of the ER is known as smooth endoplasmic reticulum (sER), while sheets-like structure is called rough endoplasmic reticulum (rER). The cytosolic surface of the rER is studded with ribosomes (polysomes), that gives it a “rough” appearance. It is involved in biogenesis of secretory and membrane proteins, including their translocation, folding, glycosylation, and secretion. It also plays a decisive role in protein quality control, ensuring that terminally misfolded proteins are recognized and targeted for degradation. Due to the lack of ribosomes, the sER is considered “smooth”. It is the site of various metabolic reactions, such as phospholipid, fatty acid, and steroid synthesis as well as detoxification (Ellgaard and Helenius, 2003; Shibata et al., 2006; Puhka et al., 2007; Hebert and Molinari, 2007; Shibata et al., 2010; Zimmermann et al., 2011; Cherepanova et al., 2016; Almanza et al., 2019).

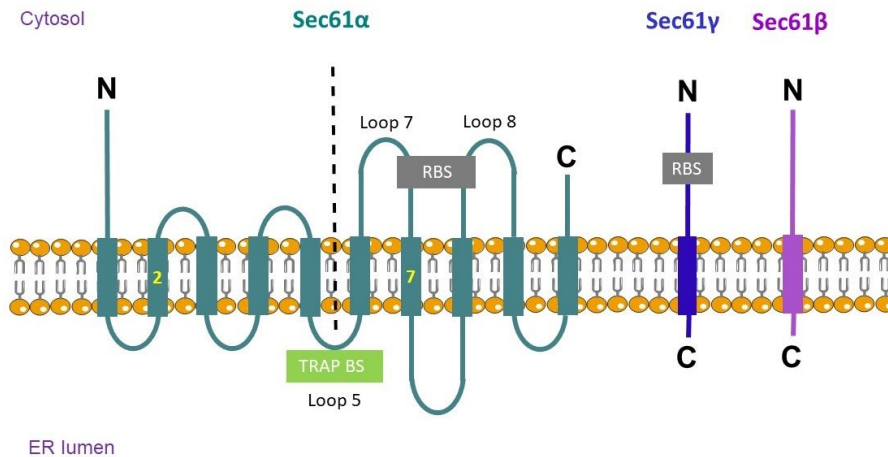
The expansive network of the ER enables quick and effective intra- and intercellular signaling by forming membrane interactions with other organelles as well as with the plasma membrane. Areas where organelle membranes come into proximity and align, without fusing, are known as membrane contact sites (MCSs). Discovered in the early 1950s, one of the well-studied MCSs are mitochondria-endoplasmic reticulum contacts (MERCs), also known as mitochondria-associated ER membranes (MAMs). MAMs are enriched with proteins and operate in many processes, such as  $\text{Ca}^{2+}$  homeostasis, lipid metabolism, mitochondrial biogenesis, UPR and inflammatory responses (Giacomello and Pellegrini, 2016; Gomez-Suaga et al., 2017; Simmen and Herrera-Cruz, 2018; Panda et al., 2021). The ER also interacts with Golgi apparatus, endosomes, peroxisomes, and lipid droplets (Malmersjö and Mayer, 2013; Phillips and Voeltz, 2016). These extensive ER contacts with multiple intracellular compartments significantly contributes to the overall cellular organisation and function and underline the significance of the ER as important organelle.

The ER is involved in the transport of one-third of all proteins in eucaryotic cells. The newly synthesized polypeptide chains, recognized by hydrophobic N-terminal signal peptides (SP) or N-terminal transmembrane helices (TMH), are transported across or into the ER membrane

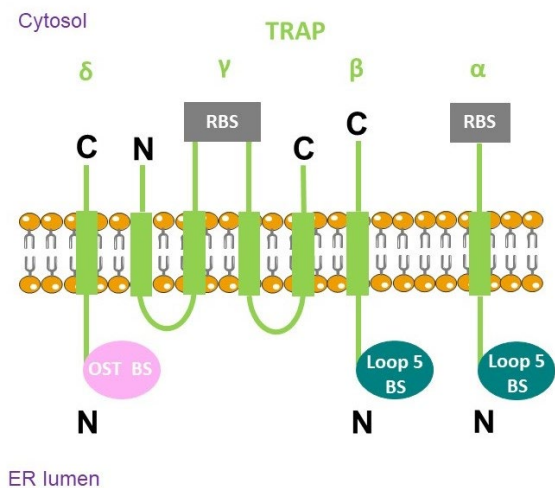
via the Sec61-channel (Figure 2: A, C; Zimmermann et al., 2011; Dudek et al., 2015; Pfeffer et al., 2016). There are mainly two mechanisms of protein targeting and transport: a co-translational mechanism, that occurs during protein synthesis at the ribosome, and involves signal recognition particle (SRP) and its receptor (Walter et al., 1981; Rapoport et al., 1996; Matlack et al., 1998); or a post-translational mechanism, that occurs after a protein is fully synthesized (Schlenstedt and Zimmermann, 1987; Kutay et al., 1995). The Sec61-channel is formed by three subunits:  $\alpha$ ,  $\beta$  and  $\gamma$ . The Sec61 $\alpha$  is the central channel-forming subunit, accompanied by a single  $\beta$  and  $\gamma$  subunits (Figure 2: A; Lang et al., 2017). Synchronized activity of the Sec61-complex and further accessory proteins helps the translocation and modification of nascent polypeptide chains. The post-translational mechanism of protein transport via the Sec61-channel is supported by the two membrane proteins Sec62 and Sec63 (ER-resident J-domain-containing protein 2, ERj2). The luminal J-domain of Sec63 allows protein-interaction and cooperation with the ER chaperone BiP (Lakkaraju et al., 2012; Lang et al., 2012; Linxweiler et al., 2017; Jung and Kim, 2021). BiP activity is promoted by other co-chaperons (ERjs) and the nucleotide-exchange factors (NEFs; I.4). Additionally, protein folding in the ER involves the chaperones calnexin and calreticulin (Danilczyk et al., 2000), and folding catalysts protein such as disulfide isomerases (PDIs) and peptidylprolyl-cis/trans-isomerases (PPIases; Schönbrunner and Schmid, 1992). Another component often accompanying the Sec61-complex is the translocon-associated protein complex (TRAP). It is heterotetrameric membrane complex assembled by the proteins TRAP $\alpha$ , TRAP $\beta$ , TRAP $\gamma$  and TRAP $\delta$  (Figure 2: B). The complex supports translocation of proteins with specific SPs, assists membrane protein topogenesis, and has a role in N-glycosylation (Sommer et al., 2013; Losfeld et al., 2014; Pfeffer et al., 2017; Nguyen et al., 2018). Furthermore, the oligosaccharyl-transferase complex (OST; Figure 2: C) is an integral membrane protein complex which catalyses the N-linked protein glycosylation of newly synthesized proteins. There are two paralogous forms of the catalytic OST subunit, STT3A and STT3B, each coupled with at least six accessory subunits (Mohorko et al., 2011; Pfeffer et al., 2014; Braunger et al., 2018). In addition, the translocating chain-associating membrane protein (TRAM) has a supportive role in protein transport in the ER, modulating the phospholipid bilayer (Klein et al., 2020).

Misfolded polypeptides are subjected to the ER-associated protein degradation (ERAD; Christianson and Carvalho, 2022), while prolonged protein misfolding in the ER lumen triggers the unfolded protein response (UPR; I.4.2; Read and Schröder, 2021).

A



B



C

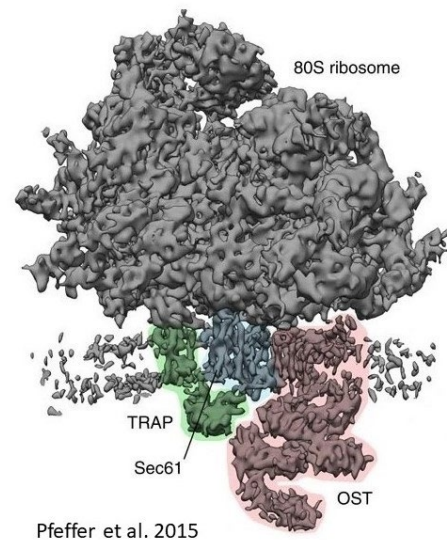


**Figure 2. Organization of the Sec61, TRAP and ribosome-translocon complex.** (A) Topology of the Sec61 $\alpha$  subunit (ten TMDs) and two associated tail-anchored subunits,  $\beta$  and  $\gamma$ . Regions that interact with the ribosome and the TRAP-complex are indicated for  $\alpha$  and  $\gamma$  subunits. Yellow marked TMD2 and TMD7 of the Sec61 $\alpha$  represent lateral gate forming helices. The vertical dashed line defines two pseudo-symmetrical halves. (B) Topology of the TRAP-complex. Regions that interact with the Sec61 $\alpha$  loop 5, OST and ribosome are indicated for each TRAP subunit ( $\alpha$ ,  $\beta$ ,  $\gamma$  and  $\delta$ ). (C) Cryo-electron microscopy (cryo-EM) map depicting native ribosome-translocon complex: Sec61 (blue), TRAP (green), OST (light pink), and the ribosome (grey) (Pfeffer et al., 2015). ER, endoplasmic reticulum; RBS, ribosome-binding site; BS, binding site; OST, oligosaccharyl-transferase; N, amino-terminus; C, carboxy-terminus.

Besides its role in protein synthesis, the ER is an integral part of well-coordinated processes that meet the cellular calcium ( $Ca^{2+}$ ) homeostasis. It serves as the largest  $Ca^{2+}$  reservoir with an estimated luminal concentration of 100-800  $\mu M$ , whereas the  $Ca^{2+}$  concentration in the cytosol

is around 100 nM under resting conditions (Clapham, 2007; Lemmer et al., 2021). The active release of  $\text{Ca}^{2+}$  ions from the ER (and sarcoplasmic reticulum) is mainly achieved by the inositol 1,4,5-trisphosphate receptors ( $\text{IP}_3\text{Rs}$ ) and ryanodine receptors (RyRs; Amador et al., 2013; Seo et al., 2015). Conversely,  $\text{Ca}^{2+}$  ions are continuously imported into the ER via the sarcoplasmic/endoplasmic reticulum ATPase (SERCA) that maintains the  $\text{Ca}^{2+}$  gradient between the ER lumen and cytosol (Wuytack et al., 2002). Also, SERCA faces the challenge of passive  $\text{Ca}^{2+}$  leakage that is mostly mediated by the Sec61-channel (Schäuble et al., 2012). In addition, there is the ER-to-mitochondria  $\text{Ca}^{2+}$  flux via MAMs that is related to the mitochondrial ATP production and cell survival (Marchi et al., 2013).

A recent review (Depaoli et al., 2019) provides details about ER related energy-consuming processes, mostly occurring on the cytosolic side of the ER membrane (e.g., ATP-dependent SERCA activity). The luminal ATP is primarily required for the chaperone-mediated processes (Adams et al., 2021).

Considering the large volume of the ER, its structural complexity, variety of its duties and high-energy requirements, it might be surprising that such a remarkable organelle is unable to generate ATP by itself. Then, how is ATP imported into the ER? The answer came recently, when Klein et al. (2018) showed that human SLC35B1 protein in the ER membrane is responsible for the  $\text{ATP}_{\text{ER}}$  import.

### **1.3. Molecular mechanism of the $\text{ATP}_{\text{ER}}$ import**

Quite a number of energy-requiring processes are associated with the ER, including protein folding, unfolded protein response (UPR) and ER-associated protein degradation (ERAD; Depaoli et al., 2019). Since the ER is not able to generate ATP by itself, ATP import from the cytosol is a prerequisite for the energy-requiring processes within the ER lumen, mainly chaperone-mediated protein folding (Clairmont et al., 1992; Hirschberg et al., 1998; Csala et al., 2007; Balchin et al., 2020). The key player in protein folding and dominant ATP-consumer in the ER lumen is the Hsp70-type molecular chaperone BiP (1.4).

Regarding mammalian cells, the molecular mechanism for importing ATP into the ER was a puzzle. Over the years, different experimental approaches were used for analysis of the ER membrane proteins from algae, plants, yeast, and mammals, in effort to determine the ATP carrier or ATP/ADP exchanger. (Mayinger and Meyer, 1993; Guillén and Hirschberg, 1995; Kim et al., 1996; Kochendörfer et al., 1999; Shin et al., 2000; Leroch et al., 2008; Chu et al., 2017). Still, it remained unknown, with exception of the carriers ER-ANT1 (plant *Arabidopsis thaliana*) and PtNTT5 (alga *Phaeodactylum tricornutum*), both with the no yeast and mammalian orthologs (Leroch et al., 2008; Hoffmann et al., 2013; Chu et al., 2017). Recently, the focus was directed towards the human ER membrane protein SLC35B1 (solute carrier family 35 member B1) as potential ATP carrier. The protein caught the eye based on screening

databases of the solute carriers (SLCs) that display two specific characteristics: location in the ER membrane and a similar expression pattern as BiP (Hediger et al., 2013; Schlessinger et al., 2013; Klein et al., 2018).

### **I.3.1. AXER-mediated ATP<sub>ER</sub> import**

As a member of the nucleotide-sugar transporter family, SLC35B1 was denoted as UDP-galactose transporter-related protein 1 (UGTrel1; Hadley et al., 2019). Its orthologs can be found across a wide range of eukaryotic organisms. In *Saccharomyces cerevisiae*, *Schizosaccharomyces pombe* and *Caenorhabditis elegans*, depletion of the Hut1 ortholog induced protein folding disruption, chronic stress, and larval growth defect and lethality (Nakanishi et al., 2001; Dejima et al., 2009).

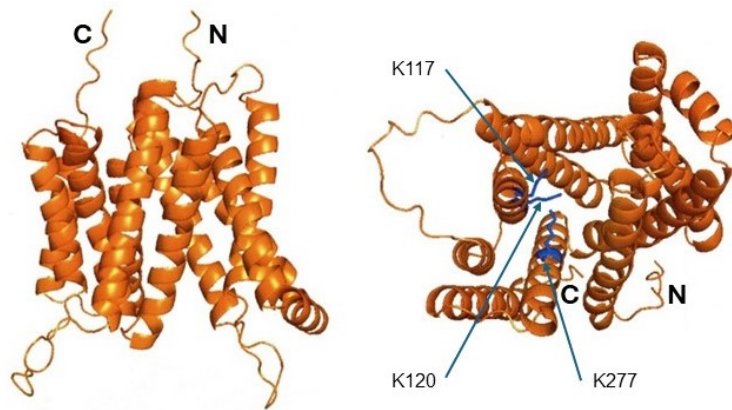
Human SLC35B1 (hSLC35B1) exhibits several splice variants, giving rise to at least three known isoforms (Klein et al., 2018). The predicted protein structure has ten transmembrane domains (TMDs) with the amino and carboxy terminus being placed on the cytosolic side of the ER membrane (UniProtKB/Swiss-Prot: P78383). In the cytosolic loop between TMD2 and TMD3, mammalian SLC35B1 comprises a putative IQ motif, indicating that the protein may associate or being regulated by calcium (2<sup>+</sup>)-calmodulin (Ca<sup>2+</sup>-CaM; Figure 3: B; Klein et al., 2018).

A recent report provided some answers about molecular mechanism of the mammalian ATP<sub>ER</sub>-import. Namely, Klein et al. (2018; team from our lab) showed that the human SLC35B1 exchanges ATP<sub>in</sub> and ADP<sub>out</sub> across the ER membrane, and as such, the protein was termed AXER (ATP/ADP exchanger in the ER membrane). The authors heterologously expressed hSLC35B1 in *Escherichia coli* to investigate its potential role as an ATP/ADP transporter. Indeed, the assay demonstrated that hSLS35B1 is a transporter with a high specificity for ATP and ADP. Also, the energy status in the ER was measured upon hSLC35B1 knockdown demonstrating a reduced level of the luminal ATP, and consequently reduced BiP activity. After the chemically induced Ca<sup>2+</sup> release from the ER (using thapsigargin; Christensen et al., 2021), the measured ATP<sub>ER</sub> level was elevated, as it was suggested earlier by Vishnu et al. (2014). All together, the current results indicate that SLC35B1 operates as an ATP/ADP exchanger in the mammalian ER membrane (Klein et al., 2018). In addition to HeLa cells, these findings were confirmed for CHO and INS-1 cell lines (Yong et al., 2019).

Newly, the assay which included the expression of hSLC35B in yeast, purification, and subsequent reconstitutions in liposomes loaded with ADP, showed the import [ $\alpha^{32}\text{P}$ ]-ATP (Schwarzbaum et al., 2022). These results confirmed the study from Klein et al. (2018), showing that SLC35B1 acts as an ATP/ADP exchanger. Further experiments revealed that hSLC35B1 expresses asymmetrical affinities for ATP transport. Lower affinity was detected on the cytosolic side of the ER membrane, while the luminal side displayed higher affinity

(Schwarzbaum et al., 2022). Based on these findings, the authors speculate that hSLC35B1 transporter “may promote ER uptake of ATP at submaximal speeds and may change ATP transport rates according to the effective ATP concentration at the ER surface”. Plus, combining bioinformatics and mutational analysis, it was detected that positively charged lysine residues K117 and K120 (TMD4) and K277 (TMD9) of SLC35B1 perform the key roles during transport process (Figure 3: A). These lysines represent evolutionary conserved residues (Schwarzbaum et al., 2022).

**A**



**B**

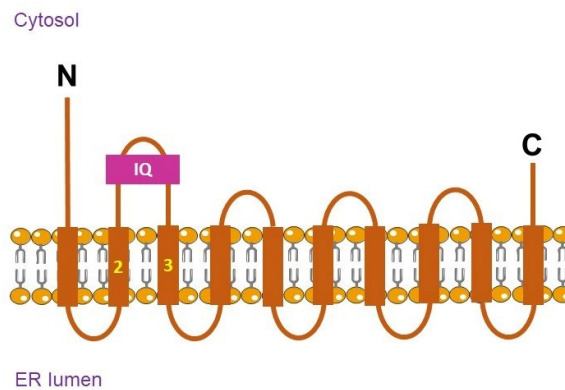


**Figure 3. Hypothetical model of hSLC35B1 (AXER).** (A) Ribbon representation of hSLC35B1 structure created by PyMOL Molecular Graphic System (version 1.1); view from the plane of the ER membrane (left); view from the ER lumen (right). The key residues for transport process: K117 and K120 residues of TMD4, and K277 residue of TMD9 (Schwarzbaum et al., 2022) are indicated (blue). (B) Topology of hSLC35B1 with ten transmembrane domains, and both N- and C- terminus on the cytosolic side of the ER membrane. Putative IQ motif on the connecting loop of TMD2 and TMD3 (yellow marked; Klein et al., 2018). ER, endoplasmic reticulum; TMD, transmembrane domain; IQ, IQ motif; N, amino-terminus; C, carboxy-terminus.

### I.3.1.1. Putative regulatory mechanisms of the ER energy homeostasis

To date, two regulatory mechanisms of the ER energy homeostasis are suggested, and both models present AXER as the crucial mediator of the ATP import and ADP export in mammalian cells. In the first proposed model AXER is a part of  $\text{Ca}^{2+}$ -dependent regulatory circuit (Klein et al., 2018). This regulatory mechanism, named lowER, also involves the ER luminal chaperone BiP and Sec61-complex at the ER membrane (Figure 4: A). When ATP:ADP ratio is high, BiP binds to the Sec61-channel, limiting  $\text{Ca}^{2+}$  leakage from the ER to the cytosol (Schäuble et al., 2012). Due to increased protein import or folding/misfolding, the advanced BiP's engagement triggers a lowering of the ATP:ADP ratio. This condition leads to chaperon's dissociation from the Sec61-channel inducing  $\text{Ca}^{2+}$  leakage from the ER (Schäuble et al., 2012). On the cytosolic side of the ER,  $\text{Ca}^{2+}$  binds to calmodulin (CaM; I.4.1; Erdmann et al., 2011) presumably initiating CaMKK $\beta$ -mediated phosphorylation and activation of AMPK, the master energy sensor in the cell. Phosphorylated AMPK (pAMPK) then activates 6-phospho-fructo-2-kinase (PFK2) which triggers glycolytic ATP production. Afterwards,  $\text{ATP}_{\text{ER}}$  import is mediated by AXER. Directly or indirectly, calcium ( $2+$ ) efflux from the ER could also activate AXER via putative IQ motif (Vishnu et al., 2014; Klein et al., 2018). Subsequently, ATP:ADP ratio is normalized, BiP limits  $\text{Ca}^{2+}$  leakage binding to the Sec61-channel and the lowER is inactivated. ER calcium ( $2+$ ) levels are balanced by SERCA. Since the lowER was proposed based on the experiments in HeLa cells, the authors pointed out that MAMs and OXPHOS are expected to be involved in the lowER in non-cancer cells.

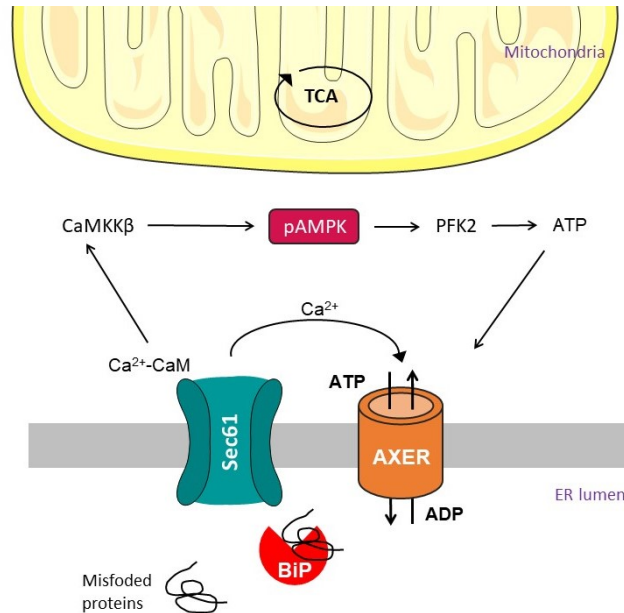
Another proposed regulatory mechanism is named CaATiER (short for  $\text{Ca}^{2+}$ -antagonized transport into the ER; Figure 4: B; Yong et al., 2019). Based on experiments in three cell lines (HeLa, INS-1, and CHO), the authors came to conclusion that mitochondrial OXPHOS is the main source of  $\text{ATP}_{\text{ER}}$  in response to ER protein misfolding. Released from the ER lumen,  $\text{Ca}^{2+}$  ions are transferred into mitochondria to boost TCA cycle. On the other hand,  $\text{ATP}_{\text{ER}}$  import, mediated by AXER, is limited by extended  $\text{Ca}^{2+}$  release. Interestingly, SERCA-inhibition induced the short-term elevation of the  $\text{ATP}_{\text{ER}}$  levels, which was neglected due to following long-term reduction (over the next ten minutes).

Thus, the lowER ( $\text{Ca}^{2+}$  dependent) and CaATiER ( $\text{Ca}^{2+}$  inhibited) models of AXER-mediated  $\text{ATP}_{\text{ER}}$  import seem like certain opponents.

Attempting to clarify enigmatic regulation of the ER energy homeostasis, Zimmermann and Lang (2020) nicely tied these two regulatory mechanisms, involving MAMs, and proposed a model termed ER holo-Care (homeostasis, lowER, CaATiER, recovery). The authors suggested that the lowER and CaATiER constitute a unified regulatory mechanism of the ER energy homeostasis that is selectively activated (in phases) in response to specific cell conditions. In the case of increasing protein folding (or minor misfolding) in the ER lumen, BiP's ATP consumption is boosted resulting with a low ATP:ADP ratio. The lowER is activated as an

immediate response, serving for a prompt energy recovery and protein misfolding prevention. If it fails, increasing protein misfolding and consequently high ATP demand in the ER lumen trigger the CaATiER.

**A**



**B**

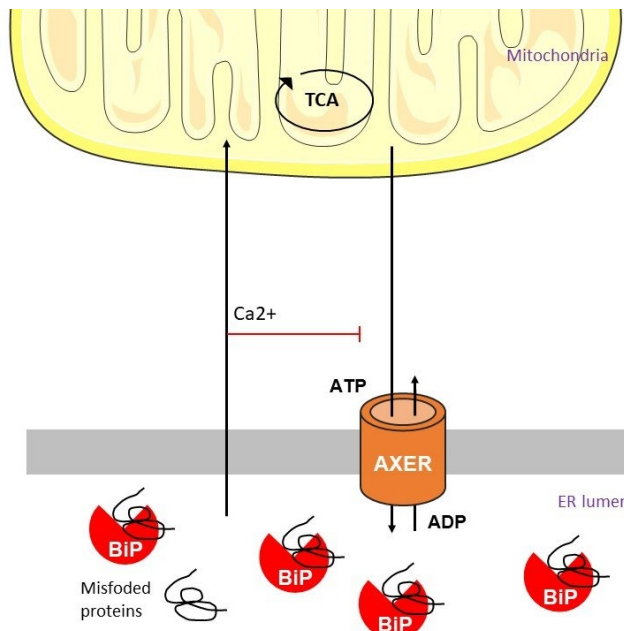


**Figure 4. Two regulatory mechanisms of the ER energy homeostasis. (A)** The lowER model (ER low energy response): Increased protein import/folding/misfolding in the ER lumen activates the signaling cascade. Luminal chaperon BiP dissociates from the Sec61-channel allowing Ca<sup>2+</sup> leakage from the ER. Calcium (2+) ions, on the cytosolic side of the ER membrane, provoke a downstream signaling process that include AMPK activation

(phosphorylated AMPK, pAMPK) and subsequent glycolytic ATP production.  $\text{Ca}^{2+}$  ions also directly activate AXER for the  $\text{ATP}_{\text{ER}}$  import. **(B)** The CaATiER model ( $\text{Ca}^{2+}$ -antagonized transport into the ER): ER luminal ATP demand is increased due to the occurrence of misfolded proteins. Predominantly,  $\text{ATP}_{\text{ER}}$  supply is generated by mitochondrial OXPHOS. Extended  $\text{Ca}^{2+}$  release from the ER causes inhibition of AXER-mediated  $\text{ATP}_{\text{ER}}$  import. (Text contains more details about these regulatory mechanisms; 1.3.1.1). ER, endoplasmic reticulum; ATP, adenosine triphosphate; ADP, adenosine diphosphate; TCA, tricarboxylic acid cycle;  $\text{Ca}^{2+}$ -CaM, calcium (2+)-calmodulin; CaMKK $\beta$ , calcium (2+)/calmodulin-dependent protein kinase kinase  $\beta$ ; PFK2, 6-phospho-fructo-2-kinase.

#### **I.4. BiP – the master $\text{ATP}_{\text{ER}}$ -consumer**

Housed in the ER lumen, binding immunoglobulin-heavy chain protein (BiP) is an indispensable molecular chaperone involved in protein translocation, unfolded protein response (UPR), ER-associated protein degradation (ERAD) and calcium signaling. Since glucose starvation triggers its synthesis, BiP is called glucose-regulated protein 78 (Grp78), but also HSPA5 (Haas and Wabl, 1983; Hendershot et al., 1988; Wang et al., 2017). The concentration of BiP reaches the millimolar range (Lang et al., 2017) and aligns with the ER burden, such as in the case of the accumulation/aggregation of misfolded proteins when the chaperone level is rapidly increased (Gülow et al., 2002). The cell lines, tissue type and species play a significant role in the fluctuations of BiP's half-life, which varies from relatively short-lived BiP of a few hours, to the long-lived BiP of a several days. The diverse half-life range of BiP can be ascribed to variations in genetic background, as well as differences in epigenetic, transcriptional, and translational regulation (Wang et al., 2017).

The BiP chaperon structure is typical for the members of Hsp70 family, enabling it to participate in protein folding process. It contains two functional domains: nucleotide binding domain (NBD; N-terminal) that binds and hydrolyzes ATP, and substrate binding domain (SBD; C-terminal) that binds a protein substrate (Figure 5). While the  $\text{Mg}^{2+}$ -binding site of NBD stimulates ATPase activity, the  $\text{Ca}^{2+}$ -binding site has an inhibitory effect. The functional domains, NBD and SBD are bonded with a flexible linker region (Sriram et al., 1997; Smock et al., 2010; Kumar et al., 2011; Genest et al., 2019). Two SBD subdomains serve as a substrate-binding pocket (SBD $\beta$ ) and a pocket lid (SBD $\alpha$ ) (Figure 5; Wang et al., 2017). The BiP ATP-bound form is characterized by the SBD open conformation with a low substrate affinity. ATPase activity is stimulated by the interaction between BiP and one of the Hsp40 co-chaperones with J-domain (ERjs), ending with the hydrolysis of ATP and conversion into the BiP ADP-bound form that shows a high substrate affinity (Figure 5). Nucleotide exchange factor (NEF) mediates substrate release, that is accompanied by the ADP-to-ATP exchange and BiP re-conversion into the form with a low substrate affinity (Figure 5). BiP is ready for the next ATPase cycle (Dudek et al., 2009; Otero et al., 2010; Pobre et al., 2019; Melnyk et al., 2022). Since each reversible BiP-with-substrate interaction requires the expense of one ATP molecule (ATP

hydrolysis to ADP plus one inorganic phosphate), and considering the BiP' s millimolar concentration, this process in the ER lumen is energetically quite expensive.

In addition to its role in protein folding, BiP takes part in the regulation of the ER  $\text{Ca}^{2+}$  homeostasis. It acts as an  $\text{Ca}^{2+}$ -binding protein able to store 25% of the ER  $\text{Ca}^{2+}$  (Lièvremonet et al., 1997), helps assemble  $\text{IP}_3\text{R1}$  into tetramers (Kiviluoto et al., 2013), and participates in the closing of Sec61-complex preventing passive  $\text{Ca}^{2+}$  leakage from the ER to the cytosol (Schäuble et al., 2012). Dissociating from the Sec61-complex,  $\text{IP}_3\text{R}$ , and three UPR activator proteins (PERK, IRE1, and ATF6; I.4.2) during ER stress, BiP causes  $\text{Ca}^{2+}$  release from the ER that potentially triggers apoptotic event (Parys and Van Coppenolle, 2022).

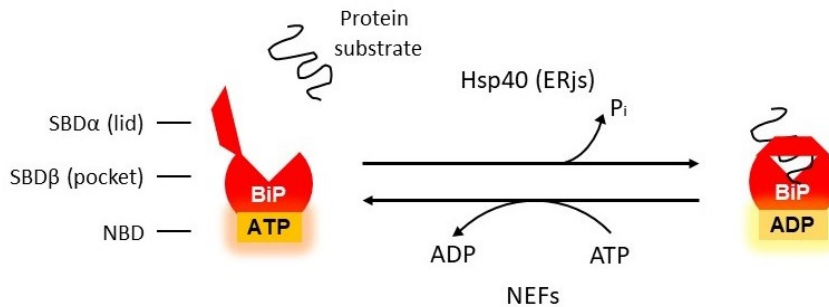


**Figure 5. BiP ATPase cycle.** Two functional domains of BiP: the nucleotide binding domain (NBD) and the substrate binding domain (SBD). The NBD binds ATP, converting BiP into the ATP-bound form with a low affinity for substrate. The SBD subdomains act as a pocket (SBD $\beta$ ) and lid (SBD $\alpha$ ) for substrate binding and dissociation. ATPase activity hydrolysis ATP to ADP and converts BiP into the ADP-bound form with a high affinity for substrate. The process is assisted by one of the Hsp40 co-chaperones (ERjs). Polypeptide release is mediated by a nucleotide exchange factor (NEF) that turns BiP back into the form with a low affinity for substrate, and the new ATPase cycle starts. In human cells, a substrate specificity is mediated by the set of eight currently known ERjs (ERj1-ERj8) and two NEFs (Grp170 and Sil1) (Behnke et al., 2015; Melnyk et al., 2022). ATP, adenosine triphosphate; ADP, adenosine diphosphate.

#### I.4.1. BiP regulation of Sec61-channel

Ribosome-free (closed) state of the mammalian Sec61-channel has a pore diameter of 9-15 Å. On the other hand, the pore diameter in ribosome-bound (opened) state is 40-60 Å, and as such can allow  $\text{Ca}^{2+}$  flux disturbing the  $\text{Ca}^{2+}$  gradient across the ER membrane (Hamman et al., 1997; Wirth et al., 2003; Van Coppenolle et al., 2004; Lang et al., 2011). Therefore, controlled Sec61-channel gating is imperative.

ER chaperon BiP has a significant role in the regulation of the Sec61-channel gating (Zimmermann, 2016). Together with Sec63 (ERj2; Figure 6), BiP serves as an allosteric modulator of the Sec61-complex, supporting channel opening in a substrate-specific manner (Nguyen et al., 1991; Lyman and Schekman, 1995; Lang et al., 2012; Lang et al., 2017). Binding to the polypeptide in transit through the open Sec61-channel, BiP serves as a

molecular ratchet ensuring the unidirectional transport, and mediates completion of translocation (Nicchitta and Blobel, 1993; Tyedmers et al., 2003; Alder et al., 2005; Dudek et al., 2009). The Sec61 $\alpha$  minihelix within luminal loop 7 was determined as a BiP-binding site (Figure 6). Both the SubAB-mediated BiP depletion (subtilase cytotoxin, inactivates BiP; Paton et al., 2006) and SEC61A1 Y344H mutant expression (unable to bind BiP; Figure 6) in HeLa cells showed the overlapping effect on protein transport of BiP-dependent precursor polypeptides, confirming the Sec61 $\alpha$  loop 7 as BiP-binding site (Schäuble et al., 2012).

Also, BiP binding to the Sec61 $\alpha$  induces channel closing limiting passive Ca<sup>2+</sup> leakage from the ER to the cytosol. Limited concentration of BiP in HeLa cells verified its role in closing the Sec61-channel. Induction of protein misfolding by short-term chemical treatment or BiP gene knockdown, coupled with live cell Ca<sup>2+</sup> imaging, revealed an increased Ca<sup>2+</sup> leakage from the ER (Schäuble et al., 2012). The same effect was observed upon depletion of luminal Hsp40 co-chaperones ERj3 and ERj6, specifically assisting BiP in Sec61-channel closing (Schorr et al., 2015). Additionally, increased Ca<sup>2+</sup> leakage was detected in SEC61A1 Y344H mutant HeLa cells (Schäuble et al., 2012). Thus, BiP binding to luminal Sec61 $\alpha$  loop 7 is involved in channel closing, equally to BiP-mediated channel opening.

Furthermore, calmodulin (CaM) operates with BiP in channel closing and limiting Ca<sup>2+</sup> leakage. In the cytosol, Ca<sup>2+</sup> ions bind CaM, and then Ca<sup>2+</sup>-CaM bind to the N-terminal IQ motif of the Sec61 $\alpha$  (Figure 6) minimizing further Ca<sup>2+</sup> leakage from the ER (Erdmann et al., 2011). Here, as in the case of BiP-to-Sec61 $\alpha$  loop 7 interaction, the binding energy may induce channel closure (Lang et al., 2017). Using the CaM antagonists, Ca<sup>2+</sup> leakage was increased (Erdmann et al., 2011). In addition, an EF-hand in the cytosolic C-terminus of Sec62 can bind Ca<sup>2+</sup> and support binding of Ca<sup>2+</sup>-CaM (Linxweiler et al., 2013).

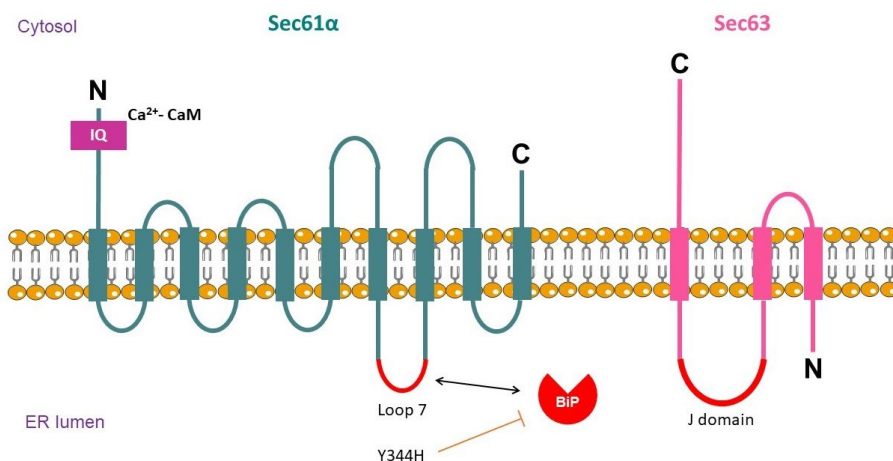


**Figure 6. Organization of the Sec61 $\alpha$ , BiP and its co-chaperon Sec63.** Sec61 $\alpha$  subunit with elements related to its function as Ca<sup>2+</sup>-leak channel. The cytosolic N-terminus calcium (2+)-calmodulin (Ca<sup>2+</sup>-CaM) binding site (IQ; purple) and the luminal BiP-binding loop 7 (red) are indicated, including the Y344H-mutation which disrupts the Sec61 $\alpha$ -BiP interaction.

Additionally, J domain (red) of the Sec63 (ERj2) is shown. IQ, IQ motif; N, amino-terminus; C, carboxy-terminus.

#### **I.4.2. BiP regulation of UPR signaling**

The cellular state caused by perturbation of the ER homeostasis is defined as ER stress. Confronted with ER stress, mammalian cells activate an intricate stress-resistance mechanism tailored towards the perturbing agent as well as the stress intensity and duration. Unmanageable and excessive stress triggers the mechanisms that promote cell death, usually in the form of apoptosis (Walter and Ron, 2011; Sano and Reed, 2013; Smith and Wilkinson, 2017; Andhavarapu et al., 2019).

Hsp70-type chaperone BiP is essential for effective protein folding in the ER. Binding to exposed hydrophobic regions of the polypeptide chains, BiP inhibits their aggregation and promotes polypeptides folding and achieving their native conformation. It aids maintain stability of the client proteins and facilitates their trafficking through the ER. Considering this activity of BiP as folding catalyst it is not surprising that BiP is ideally suited and works as direct ER stress sensor. When the ER-influx of nascent polypeptides exceeds the capacity of the folding machinery, the unfolded/misfolded proteins accumulate. In such cases, BiP initiates the unfolded protein response (UPR) with the intention to (i) reduce the influx of nascent polypeptides, (ii) increase the capacity of the folding machinery, (iii) fold or eliminate aberrantly folded proteins, and (iv) re-establish normal ER function (Gülow et al., 2002; Xu et al., 2005; Adams et al., 2019; Chipurupalli et al., 2021). The major signaling branches of the UPR in mammalian cells are regulated by ER-transmembrane proteins: inositol requiring enzyme 1 (IRE1), protein kinase RNA-like endoplasmic reticulum kinase (PERK) and activating transcription factor 6 (ATF6). Those activator proteins consist of three domains: a cytosolic domain (IRE1 and PERK C-terminus; ATF6 N-terminus), a single membrane-spanning domain, and an ER luminal domain (IRE1 and PERK N-terminus; ATF6 C-terminus). The luminal domains are thought to bind BiP that prevents their activation during normal physiological conditions (i.e., no ER stress; Almanza et al., 2019; Chipurupalli et al., 2021). Accumulation of misfolded proteins recruit BiP that at a certain threshold releases the three UPR activator-proteins (Figure 7). Thus, besides its crucial role in protein folding, BiP operates as a negative regulator of the UPR under normal physiological conditions, and as direct ER stress sensor when the ER homeostasis is disturbed.

When BiP dissociates from the luminal domains of IRE1 and PERK, it triggers their homo-oligomerization and trans-autophosphorylation (Cui et al., 2011; Ferri et al., 2020). Afterwards, an unconventional splicing of the X-box binding protein 1 (Xbp1) mRNA is mediated by IRE1. The corresponding protein, spliced XBP1 (XBP1s) is functionally active transcriptional factor that regulates expression of specific genes including chaperones, folding enzymes, and

components of the ERAD (Figure 7; Yoshida et al., 2001; Lee et al., 2002; Park et al., 2021). Next, PERK phosphorylates the  $\alpha$  subunit of eukaryotic translation initiation factor 2 (eIF2 $\alpha$ ), restricting translation and preventing further folding failure until protein homeostasis is restored. Interestingly, the restriction of ribosomal protein synthesis mediated by PERK is not a global shutdown. Instead, the selective translation of specific mRNAs is still possible. For example, one selectively synthesized protein is ATF4, the transcription factor of stress-responsive genes including DDIT3 (CHOP) (Figure 7; Harding et al., 2000; Vattem and Wek, 2004; Nishitoh, 2012). Released from BiP, ATF6's luminal Golgi-localisation sequences are exposed, leading to protein translocation to the Golgi. There, ATF6 is cleaved, and its cytosolic fragment (ATF6-N) is further translocated to the nucleus where it regulates expression of the UPR genes including Xbp1 and HSPA5 (BiP) (Figure 7; Shen et al., 2002; Hillary and FitzGerald, 2018).

Altogether, the UPR reduces the ER-influx of the nascent polypeptides on different biological levels and timely scales. These include gene expression, mRNA translation and stability, protein synthesis and their post-translational fate as well as structural re-organisation of the ER organelle.

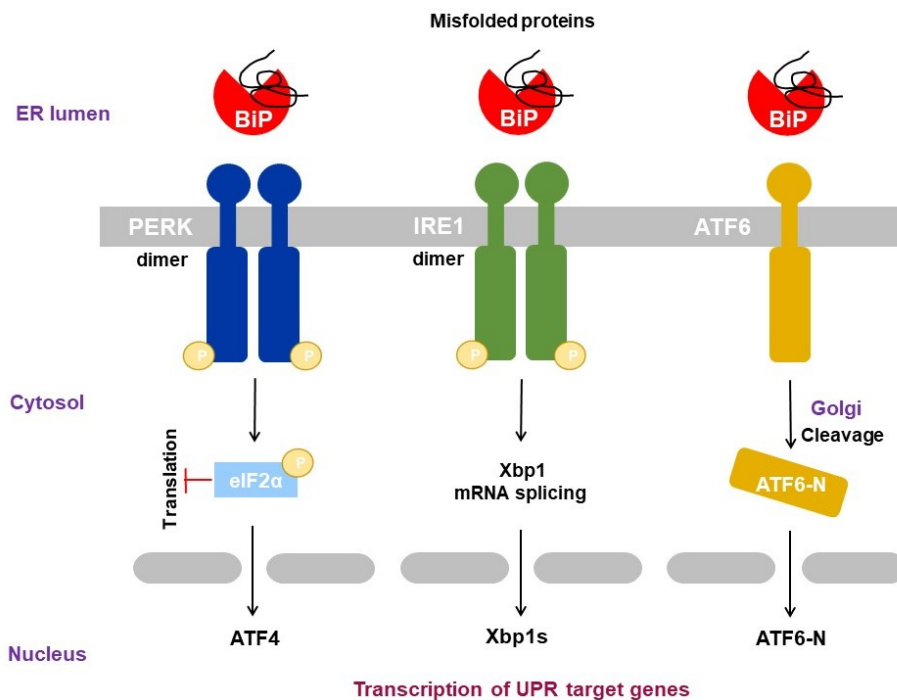


**Figure 7. Three UPR signaling branches triggered by BiP releasing.** Due to elevated level of misfolded proteins in the ER, BiP (red) releases the luminal tails of three UPR activator proteins: PERK (blue), IRE1 (green) and ATF6 (yellow). Releasing triggers homo-dimerization and phosphorylation of PERK and IRE1. PERK phosphorylates the translation initiation factor 2 (eIF2 $\alpha$ ; light purple) which restricts translation and activates ATF4 for transcription of stress-responsive genes. Unconventional splicing of Xbp1 mRNA is mediated by IRE1, and transcriptional factor XBP1s regulates gene expression. ATF6 is translocated to the Golgi, cleaved (ATF6-N) and then moved to the nucleus to induce transcription. Overall, activated

UPR proteins restrict translation to prevent aggregation of unfolded proteins in the ER, trigger selective transcription that include molecular chaperones, and resolve the over-accumulation of misfolded proteins. For a more detailed description of the UPR activation, see text. ER, endoplasmic reticulum; PERK, protein kinase RNA-like endoplasmic reticulum kinase; IRE1 inositol requiring enzyme 1; ATF6 and ATF4, activating transcription factor 6 and 4; Xbp1, X-box binding protein 1; XBP1s, spliced XBP1; P, phosphorylation.

## **I.5. Objectives**

The ATP transporter of the mammalian ER membrane has been a long-standing question, until the recent identification of AXER as the ER ATP/ADP exchanger. Furthermore, a set of its potential interaction partners has been unveiled, including key participants in the ER protein import and ER calcium homeostasis. Despite this, AXER's interactome has remained ill-defined, motivating the primary objective of this work. In tandem with diverse experimental methods, the biomolecular luminescence complementation (BiLC) approach was employed to investigate the interactome in living cells, providing insights into the AXER's structure and spatial relationship with neighboring residents of the ER membrane.

In addition to its crucial role in providing ATP for the ER, preliminary evidence suggested that AXER is integrated into a broader signaling cascade that encompasses calcium ( $Ca^{2+}$ ) as a powerful second messenger. However, discussions regarding the source of ATP and the role of  $Ca^{2+}$  have yielded conflicting perspectives. Therefore, this work also intended to enhance our understanding of AXER's metabolic integration and regulatory circuit by tracking the changes in cellular bioenergetics following AXER knockdown.

The secondary objective involved the identification of interactions between the ER protein translocon and the luminal chaperone BiP in intact cells. By subjecting cells to stress conditions, the dynamics in the detected protein-protein interactions (PPIs) were monitored in real time.

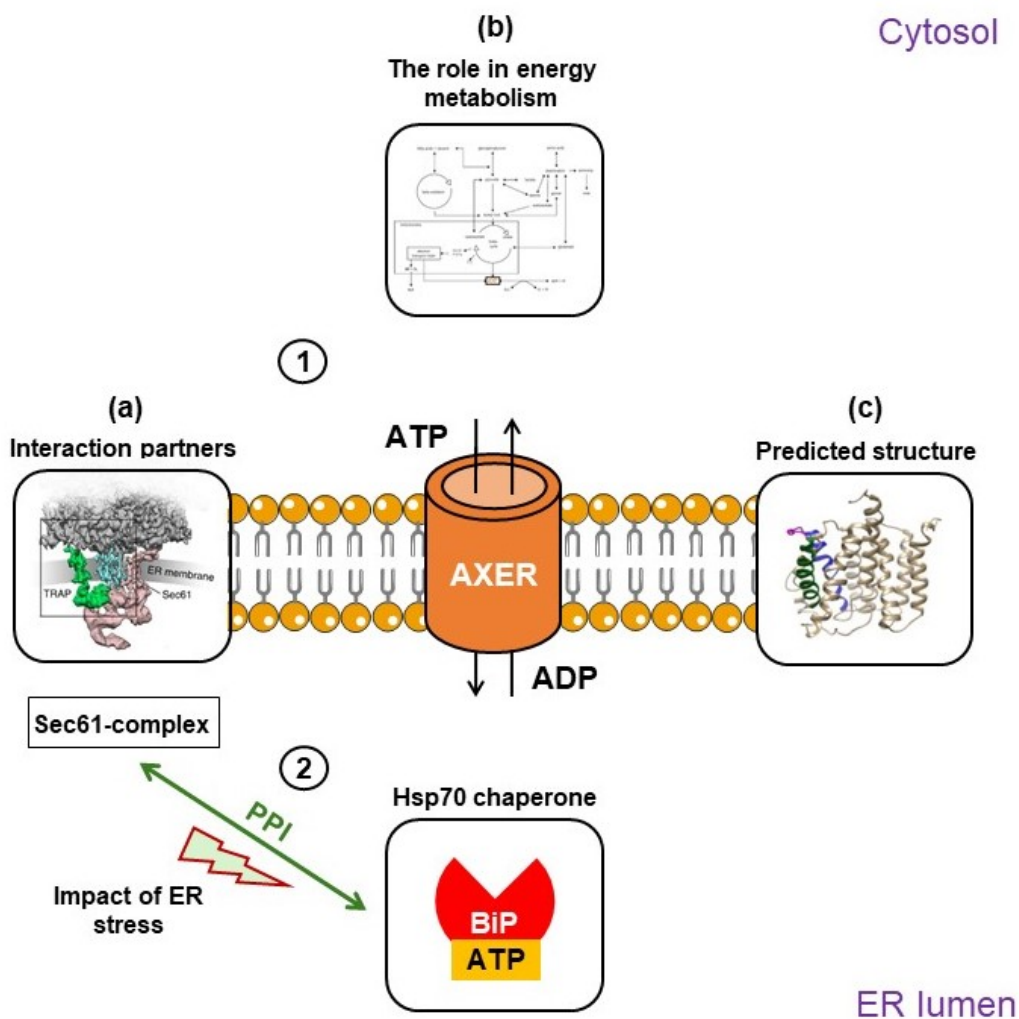


**Figure 8. Graphical summary of the objectives.** (1) This work centered around the ER membrane protein AXER, recognized as the ATP/ADP exchanger. The primary objective was to (a) examine AXER's interaction partners; (b) investigate its role in the cellular energy metabolism; and (c) verify AXER's interactome in living cells and determine its structure and position in the native membrane environment. (2) The secondary objective was to demonstrate protein-protein interactions (PPIs) of the ER protein translocase and the luminal Hsp70 chaperon BiP in living cells. Further, inspect the dynamics of the identified PPIs during ER stress.

[(a) Native ribosome-translocon complex, Pfeffer et al., 2015; (c) Hypothetical structural model of AXER, Klein et al., 2018]

## II. MATERIAL AND METHODES

### II.1. Materials

#### II.1.1. Devices and software

Table 1 shows the list of devices and software that were used in this work, excluding refrigerators and freezers used daily.

**Table 1. Devices and software.**

Manufacturer	Consumables / device / software
Abena, Eberdingen	Gloves
Abimed, Düsseldorf	Gilson Pipette (2; 20; 200; 1000 and 5000 µl)
Agilent Technologies, USA	Bioanalyzer: 2100 instrument, RNA Nano LabChip; chip priming station, syringe, chip vortex and software
Applied Biosystems-Thermo Fisher Scientific, Waltham, MA, USA	qPCR-Cycler StepOnePlus, StepOnePlus software, v2.3, Optical 96-well reaction plate
Beckmann, München	GS-6KR centrifuge, J2 MC centrifuge, JA-20 rotor, polypropylene centrifuge tubes
Biomolecular Structures Group, Glaxo Wellcome Research & Development Stevenage, Hertfordshire, UK	RASWin v2.6, program for molecular graphic visualisation, based on RasMol v2.6 by Roger Sayle
Braun, Melsungen	Syringes, cannulas
Carl Roth, Karlsruhe	Parafilm (H66.1); cell scraper (245 mm, 20 mm); pH indicator paper ROTILABO Eco pH 5.5-9.0
DNASTAR Inc, WI, USA	Lasergen Softwares (SeqMan, SeqBuilder)
Duran, Wertheim	Laboratory glassware
Eppendorf, Hamburg	Reaction tube (1.5 ml), refrigerated centrifuge 5402, centrifuge 5430, FA45-30-11 rotor, thermostat 5320, benchtop centrifuge 5415R
Fröbel Labortechnik, Wasserburg	Rocking shaker; clean bench
GE Healthcare, Uppsala, SWE	Electrophoresis Power Supply EPS 601, Typhoon Trio (9410), Typhoon Scanner Control v5.0 Software, ImageQuant TL 7.0 software, ImageQuant 5.1 Software, Image Scanner 3, Labscan software
Gelaire Flow Laboratories, Meckenheim	Clean bench 82126
Gilson, Middelton, WI, USA	Multipipette (5-100 µl)
Greiner Bio-One-GmbH, Frickenhausen	Cell culture flasks (25 cm <sup>2</sup> and 75 cm <sup>2</sup> ), cell culture plates Ø 6 cm; 96-well microplatte black/clear and white
Greiner Labortechnik, Frickenhausen	Rotating shaker
Heraeus, Hanau	Cell culture incubator Hera Cell 150; bactifuge
Hirschmann Laborgeräte, Eberstadt	Pipetus-Akku
Infors, Bottmingen, CH	Incubator AJ112/6
Insightful Science LLC, CA, USA	SnapGene Viewer
Intavis, Tübingen	ResPep SL automated peptide synthesizer
Invitrogen, Darmstadt	Countess Automated Cell Counter, Countess Cell counting chamber slides
Isotherm KGW, Karlsruhe	Liquid nitrogen dewar

Janke & Kunkel KG, Staufen i. Breisgau	Magnetic stirrer IKA-COMBIMAG RCO
Julabo, Seelbach	Water bath VC 5
Marienfeld, Lauda-Königshofen	Tumble roller mixer
Memmert und Co KG, Schwabach	Incubator warming cabinet BE500
Microsoft, WA, USA	Office 365 application
Millipore Co, MA, USA	Immobilon-P transfer membrane (0.45 µm pore size), Milli-Q Integral water purification system
Neolab, Heidelberg	Ice bath 1-6031; Magnetic stir bars; tumble roller mixer
Panasonic, Hamburg	Microwave
Peqlab, Erlangen	Nanodrop ND-1000 UV/Vis, PCR-Cycler Primus 96, UV-Table ECX-20.L, Fusion SL luminescence imaging system and software
Pharmacia Biotech AB, Freiburg	Power supply EPS 500/400, EPS 600, EPS 601, EPS 3500, Image Master Gel Documentation System, MultiTemp II
Sarstedt, Nürnberg	Pipette tips (0.1-5000 µl); reaction tubes (1.5; 15 and 50 ml); transfer pipettes
Sartorius, Göttingen	Micro scales BP61, BP4100, LA420, ED5201
Schleicher & Schuell, Dassel	Filter papers
Schrödinger, NY, USA	PyMOL Molecular Graphic System v1.1
Schütt, Göttingen	Autoclave; Typ Bioklav
Scientific Industries, NY, USA	Vortex-Mixer (Genie 2)
Serva GmbH, Dassel	Whatman FP30/0.2 (0.2 µm)
Systec GmbH, Wetzlar	Autoclave DX-65
Tecan, Männedorf, CH	Plate Reader Infinite M200
Th. Geyer GmbH & CO. KG, Renningen	Pasteur pipettes glass 150 mm
Thermo Fisher Scientific, Dreieich	Sterilbank MSC Advantage, Nalgene Bottle-Top Filter units (150 ml); HERAccl 150i CO2 incubator
Waters-Millipore, Milford USA	Millipore water system Milli-Q
Wenzel Glaserei, München	Glass plates
Workshop Medical Biochemistry, Homburg	Electrophoresis chambers; plexiglass tubes
WTW, Weilheim	pH-meter pH537
Zeiss, Jena	Binoculars microscope Axiolab (brightfield)
Ziegler, Isernhagen	Ice maker

### II.1.2. Chemicals, enzymes, and kits

Chemicals, enzymes, and kits used in this work are shown in Table 2. The components of specific buffers or solutions are given in the section of the respective experiment.

**Table 2. Chemicals, enzymes, and kits.**

Manufacturer	Chemicals / enzymes / kits
Agilent Technologies, USA	Bioanalyzer kit; MitoXpress assay kit; pH-Xtra assay kit
Applied Biosystems, Darmstadt	TaqMan Gene Expression master mix
Biochrom AG, Berlin	Foetal Calf Serum (FCS)

Biofrox, Einhausen	BSA blocking solution
Biotium, Fermont, Can	GelRed nucleic acid stain
Biospec Products, Bartlesville, OK, USA	Glas beads 0.5 mm
Calbiochem, Merck, Darmstadt	Digitonin
Carl Roth, Karlsruhe	LB-agar, LB medium, TB-medium, milk powder, Agar-Agar, agarose, sodium hydroxide, HEPES, glucose, EGTA, Albumin Fraktin V (BSA)
Eurofines MWG, Ebersberg	DAN-oligonucleotides
Invitrogen, Darmstadt	Trypan Blue stain (0.4%), thapsigargin, SuperScript VILO cDNA synthesis kit
Merck, Darmstadt	DMSO, EDTA, glycerol, glycine, potassium chlorid, magnesium acetat, magnesium chloride, magnesium sulfate, sodium chloride, sodium dihydrogen phosphate, tris, tunicamycin
MP Biomedicals, Illkirch, FRA	Trypsin-inhibitor (Soybean)
New England Biolabs GmbH, Frankfurt a.M.	Alkaline phosphatase
Promega Biotec, WI, USA	FuGENE HD, DNA purification kit, NanoBiT PPI MCS Starter System, PureYield Plasmid Miniprep System
Qiagen, Hilden	HiPerFect transfection reagent, siRNA oligonukleotide, QIAquick PCR Purification Kit, Plasmid Midi Kit, QIAquick Gel Extraction Kit, RNeasy Mini Kit
Riedel de Haën, Hannover	Potassium acetat, 2-propanol
Roche, Mannheim	Trypsin, DNase I, Nonidet P 40, phosphoenolpyruvate
Serva, Heidelberg	40% acrylamid, 2-acrylamido-2-methylpropane sulfonic acid (AMPS), bromphenolblau, calcium chloride, TritonX-100, potassium hydrogen phosphate, magnesium chloride, N, N, N, N'-tetramethylethylenediamine (TEMED), N, N'-methylene bisacrylamide 2x, SDS
Sigma-Aldrich, Steinheim	Ampicillin, $\beta$ -mercaptoethanol, PMSF, glucose, DMSO, kanamycin, Fetal Bovine Serum (FBS), pyruvate kinase/lactic dehydrogenase, Tween 20
Thermo Fisher Scientific, Dreieich	0.05% Trypsin-EDTA (1x), Gibco DMEM + GlutaMAX <sup>TM</sup> -I, 1x PBS, Opti-MEM, Opti-MEM without phenol red, penicillin/ streptomycin, 50 bp/ 1 kb DNA ladder, Pfu-Polymerase, Page Ruler Prestained Protein Ladder, SuperSignal West Pico PLUS, T4 DNA ligase, T4 DNA ligase buffer 10x, Tango buffer 10x, restriction enzymes (Nhe I, Xho I)
VWR International, Belgien	Calciumchloride
Uni SB ZCHL (Central warehouse for chemicals, Saarbrücken)	Ethanol, methanol, acetone

### II.1.3. Antibodies

#### II.1.3.1. Primary antibodies

All primary antibodies used in this work are listed in Table 3. The custom-made antibodies were obtained from blood-immunized rabbits. All necessary steps, starting with peptide synthesis or polypeptide purification, immunization, blood sampling, and final serum collection, were carried out by Professor Dr. Martin Jung and his working group (Medical Biochemistry and Molecular Biology, Saarland University). The article number is indicated if the antibody was commercially purchased.

**Table 3. Primary antibodies used in this work.**

UdS = Saarland University; UGOE = University of Göttingen.

Antibody	Internal identifier	Characteristic	Origin/Source	Dilution
β-Actin	/	Monoclonal	Mouse/ Sigma (A5441)	1:10000
AMPKα1 and AMPKα2	AMPK	Monoclonal	Rabbit/ abcam (ab207442)	1:1000
AMPKα1 (phospho T183) and AMPKα2 (phospho T172)	pAMPK	Monoclonal	Rabbit/ abcam (ab133448)	1:1000
BiP	950	Polyclonal	Rabbit/ UdS	1:500
CAMKK2	CAMKK2	Polyclonal	Rabbit/ Proteintech (11549-1-AP)	1:500
Sec61α1	α-Sec61α1	Polyclonal	Rabbit/ UGOE	1:2500
SQSTM1	SQSTM1	Monoclonal	Mouse/ abcam (ab56416)	1:2000
SRα	178a	Polyclonal	Rabbit/ UdS	1:500
SRβ	510	Polyclonal	Rabbit/ UdS	1:500
SSR3	TRAPγ	Polyclonal	Rabbit/ Sigma	1:500
TRAPα	1342	Polyclonal	Rabbit/ UdS	1:300
TRAPβ	302	Polyclonal	Rabbit/ UdS	1:300

### II.1.3.2. Secondary antibodies

For immunological detection, ECL Plex secondary antibodies were used (Table 4). The horseradish peroxidase-based version was used in cases of less efficient antibodies or low protein levels.

**Table 4. Secondary antibodies used in this work.**

Antibody	Label	Origin/Source	Article Nr.	Dilution
$\alpha$ -Mouse-IgG	ECL Plex Cy3	Goat/Sigma	C2181	1:2500
$\alpha$ -Rabbit-IgG	ECL Plex Cy5	Goat/GE Healthcare	PA45011	1:1000
$\alpha$ -Rabbit-IgG	horseradish peroxidase	Goat/Sigma	A8275	1:1000

### II.1.4. Peptide

The HaBiT peptide, used for the NanoBiT experiments (II.4.3), was designed by Professor Dr. Martin Jung and his working group (Medical Biochemistry and Molecular Biology, Saarland University). The sequence, length, and molecular weight are shown in Table 5. The peptide (20 mM stock concentration) was dissolved in DMSO prior to use.

**Table 5. Peptide used in this work.**

No.	Name	Sequence	Length	MW [g/mol]
1788	High affinity NanoBiT (HaBiT) peptide	VSGWRLFKKIS	11	1321

### II.1.5. Oligonucleotides

#### II.1.5.1. RNA oligonucleotides (siRNA)

The RNA oligonucleotides used for siRNA-mediated gene silencing are listed in Table 6. The siRNAs, supplied lyophilized by the manufacturer, were dissolved in RNase-free water to a concentration of 20  $\mu$ M and stored at -20°C for long-term use.

**Table 6. RNA oligonucleotides used in this work.**

UTR = untranslated region.

Internal identifier	Gene (organism)	Sequence (sense strand)	Concentration
Ctrl	/	Sequence unknown (AllStars negative control, Quiagen)	20nM
SLC35B1 #1 -UTR	SLC35B1 (Homo sapiens)	GAGACUACCUCCACAUCAAtt	20nM

SLC35B1 #4	SLC35B1 (Homo sapiens)	GGUACCCUGCCAUCAUCUAtt	20nM
------------	---------------------------	-----------------------	------

### II.1.5.2. DNA oligonucleotides (Primers)

The sequences created from a few nucleotides were used for the effective identification or manipulation of specific nucleic acid targets.

ThermoFisher Scientific primers (Table 7) were used in the real-time quantitative polymerase chain reaction (RT-qPCR) to detect a target mRNA (cDNA) after siRNA-mediated gene silencing.

**Table 7. Primers used for RT-qPCR experiments.**

Gene	Number	Description
ACTB	Hs00357333_g1	$\beta$ -Actin primer for RT-qPCR (control)
ATP2A2	Hs00544877_m1	SERCA2 primer for RT-qPCR
HSPA5	Hs99999174_m1	BiP primer for RT-qPCR
Sec61A1	Hs00273698_m1	Sec61 $\alpha$ primer for RT-qPCR
Sec61B	Hs00606455_m1	Sec61 $\beta$ primer for RT-qPCR
SLC35B1	Hs00195184_m1	AXER primer for RT-qPCR
SQSTM1	Hs01061917_g1	SQSTM1 primer for RT-qPCR
SRPRA	Hs01112418_g1	SR $\alpha$ primer for RT-qPCR
SRPRB	Hs00253639_m1	SR $\beta$ primer for RT-qPCR
SSR1	Hs00162340_m1	TRAP $\alpha$ primer for RT-qPCR
SSR2	Hs00162346_m1	TRAP $\beta$ primer for RT-qPCR

The custom-designed oligonucleotides (Table 8) were purchased from Eurofins Genomics Company. The oligonucleotides were used for the amplification of the target gene with specific sites applied to generate the NanoBiT plasmids (II.3.2) or for target sequencing (II.3.2.9).

**Table 8. Primers used for mutagenesis and sequencing.**

The column "Primer" indicates direction of binding primer, where forward primer (5'→3') is marked as "+", and reverse primer (3'→5') as "-".

Primer ID	Target/ Gene	Primer	Sequence (5'→3')	Used for
RZ758	/	+	GCATATTAAGGTGACGCGTG	NanoBiT plasmid sequencing

RZ759	/	-	CCTCCCCCTGAACCTGAAAC	NanoBiT plasmid sequencing
RZ844	SLC35B1	+	CAGATCTGCTAGCGAATGGCCTCTAG CAGCTC	Nhe1 insertion; C-terminus
RZ845	SLC35B1	-	ACCACCGCTCGAGCCGTGGGATGTC TTCTTAG	Xho1 insertion; C-terminus
RZ846	SLC35B1	+	GTGGAGGCTCGAGCATGGCCTCTAG CA GCTC	Xho1 insertion; N-terminus
RZ847	SLC35B1	-	AAGATCTGCTAGCTTCTAGTGGGATG TCTTCTTAG	Nhe1 insertion; N-terminus

### II.1.6. Plasmids

Table 9 shows the list of plasmids used in cell culture for the expression of target proteins in different types of experiments (II.3.2; II.4.3).

**Table 9. Plasmids used for cell culture transfection.**

Amp = ampicillin; Kan = kanamycin; UdS = Saarland University.

Plasmid ID	Target protein	Resistance	Source	Description
N196	/	Amp	Promega	LgBiT C-terminal vector pBiT1.1-C[TK/LgBiT]
N197	/	Amp	Promega	SmBiT C-terminal vector pBiT2.1-C[TK/SmBiT]
N198	/	Amp	Promega	LgBiT N-terminal vector pBiT1.1-N[TK/LgBiT]
N199	/	Amp	Promega	SmBiT N-terminal vector pBiT2.1-N[TK/SmBiT]
N202	Halo C SmBiT	Kan	Promega	Halo-tag (negative control SmBiT)
N203	rPKA C LgBiT	Kan	Promega	Regulatory subunit of protein kinase A, (positive control LgBiT)
N204	cPKA C SmBiT	Kan	Promega	Catalytic subunit of protein kinase A, (positive control SmBiT)
N211	TRAP $\alpha$ C LgBiT	Amp	UdS, Dr. M. Sicking	TRAP $\alpha$ protein with the LgBiT at the C-terminus
N212	TRAP $\alpha$ C SmBiT	Amp	UdS, Dr. M. Sicking	TRAP $\alpha$ protein with the SmBiT at the C- terminus
N213	TRAP $\beta$ C LgBiT	Amp	UdS, Dr. M. Sicking	TRAP $\beta$ protein with the LgBiT at the C-terminus
N214	TRAP $\beta$ C SmBiT	Amp	UdS, Dr. M. Sicking	TRAP $\beta$ protein with the SmBiT at the C- terminus

N215	Sec61 $\alpha$ C LgBiT	Amp	UdS, Dr. M. Sicking	Sec61 $\alpha$ protein with the LgBiT at the C-terminus
N216	Sec61 $\alpha$ C SmBiT	Amp	UdS, Dr. M. Sicking	Sec61 $\alpha$ protein with the SmBiT at the C- terminus
N217	Sec61 $\alpha$ N LgBiT	Amp	UdS, Dr. M. Sicking	Sec61 $\alpha$ protein with the LgBiT at the N-terminus
N226	Sec63 N SmBiT	Amp	UdS, Dr. M. Sicking	Sec63 protein with the SmBiT at the N- terminus
N227	Sec61 $\beta$ C LgBiT	Amp	UdS, Dr. M. Sicking	Sec61 $\beta$ protein with the LgBiT at the C-terminus
N228	Sec61 $\beta$ C SmBiT	Amp	UdS, Dr. M. Sicking	Sec61 $\beta$ protein with the SmBiT at the C- terminus
N229	Sec61 $\beta$ N LgBiT	Amp	UdS, Dr. M. Sicking	Sec61 $\beta$ protein with the LgBiT at the N-terminus
N230	Sec61 $\beta$ N SmBiT	Amp	UdS, Dr. M. Sicking	Sec61 $\beta$ protein with the SmBiT at the N- terminus
N239	BiP SmBiT	Amp	UdS, Dr. M. Sicking	BiP protein with the SmBiT inserted upstream of the KDEL- coding sequence at the C-terminus
N243	Sec61 $\gamma$ C SmBiT	Amp	UdS, M. Lerner	Sec61 $\gamma$ protein with the SmBiT at the C- terminus
N244	Sec61 $\gamma$ C LgBiT	Amp	UdS, M. Lerner	Sec61 $\gamma$ protein with the LgBiT at the C-terminus
N245	Sec61 $\gamma$ N SmBiT	Amp	UdS, M. Lerner	Sec61 $\gamma$ protein with the SmBiT at the N- terminus
N246	Sec61 $\gamma$ N LgBiT	Amp	UdS, M. Lerner	Sec61 $\gamma$ protein with the LgBiT at the N-terminus
N263	TRAP $\gamma$ C LgBiT	Amp	UdS, M. Lerner	TRAP $\gamma$ protein with the LgBiT at the C-terminus
N264	TRAP $\gamma$ C SmBiT	Amp	UdS, M. Lerner	TRAP $\gamma$ protein with the SmBiT at the C- terminus
N265	TRAP $\gamma$ N LgBiT	Amp	UdS, M. Lerner	TRAP $\gamma$ protein with the LgBiT at the N-terminus
N266	TRAP $\gamma$ N SmBiT	Amp	UdS, M. Lerner	TRAP $\gamma$ protein with the SmBiT at the N- terminus
N267	AXER C SmBiT	Amp	UdS, this work	AXER (SLC35B1) protein with the SmBiT at the C-terminus
N268	AXER N LgBiT	Amp	UdS, this work	AXER (SLC35B1) protein with the LgBiT at the N-terminus
N269	AXER N SmBiT	Amp	UdS, this work	AXER (SLC35B1) protein with the SmBiT at the N-terminus

N274	AXER C LgBiT	Amp	UdS, this work	AXER (SLC35B1) protein with the LgBiT at the C-terminus
N275	AXER-loop3 SmBiT	Amp	UdS, this work	AXER (SLC35B1) protein with the SmBiT inserted in the ER-luminal loop3; N197 vector backbone
N279	BiP LgBiT	Amp	UdS, this work	BiP protein with the LgBiT inserted upstream of the KDEL-coding sequence at the C-terminus; N197 vector backbone
BiP_LgBiT_KDEL-Ct	BiP LgBiT	Amp	UdS, this work; created and ordered from ThermoFisher GeneArt Instant Designer	BiP protein with the LgBiT inserted upstream of the KDEL-coding sequence at the C-terminus; pMA-RQ vector backbone
SLC35B1 Iso1 "lang"	SLC35B1	Amp	OriGene	SLC35B1 (AXER) Isoform 1 with GFP-Tag at the C-terminus; pCMV6 vector backbone

### II.1.7. Rough microsomes

Rough microsomes (RMs) are small vesicles of the endoplasmic reticulum (ER) and attached ribosomes, isolated together when eukaryotic cells are homogenized and centrifuged. They are suitable for studying protein in a cell-free system. The RMs used in this work were isolated by Professor Dr. Martin Jung (Medical Biochemistry and Molecular Biology, Saarland University) from canine pancreas according to the established method (Walter and Blobel, 1983). Containing proteins at a significantly high concentration, RMs served as positive control for Western blot assays (II.4.2) and spot peptide array analyses (II.6.1).

### II.1.8. Bacterial cells

Plasmids amplification was performed using *Escherichia coli* (*E. coli*) bacterial cells with the following genotypes:

1. *E. coli* DH5 $\alpha$  (protein-coding plasmids used for cell culture transfection; II.3.2.6):  
F<sup>-</sup>,  $\phi$ 80dlacZ $\Delta$ M15,  $\Delta$ (lacZYA-argF) U169, deoR, recA1, endA1, hsdR17(rk<sup>-</sup>, mk<sup>+</sup>), phoA, supE44,  $\lambda$ <sup>-</sup>, thi-1, gyrA96, relA1;
2. *E. coli* JM101 (newly generated plasmids after mutagenesis; II.3.2.6):  
supE thi-1  $\Delta$ (lac-proAB) [F' traD36 proAB lacIqZ $\Delta$ M15].

## **II.1.9. Cell line**

### **II.1.9.1. HeLa cells**

The experiments and datasets are based on the established human cell line HeLa (ATCC, No. CCL-2). Since 1951, when they were isolated from a cervical carcinoma of a 31-year-old patient Henrietta Lacks, HeLa cells grow and multiply perpetually in a laboratory. Labeled as “immortal”, these cells are used as a model of human biology and have contributed to many significant scientific discoveries. However, the HeLa genome revealed the aneuploidy, chromosomal rearrangements, as well as fragments/sequences of the Human Papilloma Virus 18 (HPV-18) genome, which should be taken into account during experimental design and analysis (Lucey et al., 2009; Landry et al., 2013; Lin et al., 2019).

#### **II.1.9.1.1. HeLa- $\mu_s$ cells**

HeLa- $\mu_s$  cells (clone 3.7; Bakunts et al., 2017) are a generation of the HeLa cell line that inducibly expresses transgenes. Provoked by the synthetic steroid mifepristone (Mif), HeLa- $\mu_s$  cells persistently express the secretory heavy chain ( $\mu_s$ ) of immunoglobulin M (IgM). The cells were kindly provided by WG Cavalié (Saarland University) and used in this work for protein-protein interaction (PPI) studies (II.4.3).

## **II.2. Cell culture and cell manipulation**

### **II.2.1. Cell cultivation and cell counting**

HeLa cells were cultivated in standard culture medium (Gibco DMEM + GlutaMAX-I) supplemented with 10% fetal bovine serum (FBS) and 1% penicillin-streptomycin (P/S). The same medium was used for HeLa- $\mu_s$  cells, supplemented with 5% FBS and 1% P/S. Cells were cultured in 14 ml of medium in a 75 cm<sup>2</sup> flask and kept in a humidified incubator with 5% CO<sub>2</sub> at 37°C. After reaching ~80% confluency (48-72 hours), the medium was removed, and cells were washed with 1x PBS. Trypsin was added (2 ml), and cells were incubated for 5 min at 37°C. By adding the culture medium, trypsin was inactivated. Cell number was determined by cell counter (Table 1), using trypan blue staining mixed with the cell suspension (1:1 ratio). Subsequently, cells were seeded at the desired density. The culture medium and trypsin were kept in a refrigerator and heated to 37°C in a water bath prior to use.

### **II.2.2. siRNA-based cell manipulation**

RNA interference (RNAi) is a regulatory mechanism of gene suppression, known for over two decades (Fire et al., 1998). This sequence-specific process occurs naturally through the

production of pre-microRNA (pre-miRNA) that migrates into the cytoplasm and become mature microRNA (miRNA) by DICER enzyme. The process can also be induced experimentally by small interfering RNA (siRNA), formed from synthetic double-stranded RNA (dsRNA). The miRNA or siRNA then creates the miRNA-RISC or siRNA-RISC complex, binding to the RNA-induced silencing complex (RISC), that further binds to complementary sequence of messenger RNA (mRNA). It enzymatically cleaves target sites forming a non-functional mRNA and inhibiting translation into protein (Shukla et al., 2011; Lam et al., 2015).

Since siRNA may induce an off-target gene silencing (Birmingham et al., 2006; Ui-Tei et al., 2008), two AXER-silencing siRNAs (Table 6) were used in this work, together with the control siRNA that has no sequence homology with any human mRNA.

HeLa cells were cultivated and harvested as described in II.2.1. The cell number was adjusted to  $1.55 \times 10^5$  cells per ml by adding fresh medium. For gene silencing,  $6 \times 10^5$  cells (3.9 ml of cell mixture) were seeded in a 6 cm dish and transfected with the targeting siRNA or control, using the lipid-based transfection reagent (HiPerFect). The siRNA transfection mix was prepared separately in a 1.5 ml reaction tube following the pipetting scheme (below), and added into a properly labeled culture dish, after being incubated for 10 min at room temperature (RT). The final concentration of all siRNAs was 20 nM (Table 6).

siRNA transfection mix:

OptiMEM	76 $\mu$ l
HiPerFect	20 $\mu$ l
<u>siRNA (20 nM)</u>	<u>4 <math>\mu</math>l</u>
Total volume	100 $\mu$ l

The next day, cells were refreshed by changing the medium (4 ml), and the new transfection mixture was added dropwise. After a certain time interval (24 or 48 hours), cells were harvested and treated according to requirements of the following experiment. Silencing efficiency was evaluated using RT-qPCR (II.3.1.3).

### **II.2.3. Plasmid-based cell manipulation**

Cellular transfection was a part of the NanoBiT experiment (II.4.3), used for protein-protein interaction (PPI) detection in living cells. During this process, an exogenous DNA (plasmid) was delivered into the cells by a transfection reagent. For this purpose, the non-liposomal reagent FuGENE HD was used. The foreign DNA was transported to the nucleus and transcribed into mRNA, which was then translated into the protein of interest. The cell preparation and transfection procedures are described in II.4.3. The plasmid constructs are listed in Table 9.

## II.2.4. Preparation of whole-cell lysate

The preparation of whole-cell lysate includes protein extraction and solubilization from the cellular matrix. After gene silencing, HeLa cells were washed two times with PBS (4 ml) and incubated with trypsin (200  $\mu$ l) for 5 min. Cells were harvested, counted, and pelleted by centrifugation for 5 min at 2500 rpm. Based on the total cell count of each condition, the total lysis volume was calculated. Adjusting cell density is crucial for equal sample loading (II.4.1) and subsequent protein intensity quantification. Freshly prepared 1x cell lysis buffer (80% of the total lysis volume) was added to the reaction tube with the cell pellet. Samples were incubated for 30 minutes at 37°C at 700 rpm. Detergents in the buffer disrupted the cells and released proteins. Cellular enzyme activity, which occurs immediately after cell lyses, was minimized by protease and phosphatase inhibitors. To achieve a final concentration of  $1 \times 10^4$  cells/ $\mu$ l, samples were diluted in 5x Laemmli sample buffer (20% of the total lysis volume; Laemmli, 1970) with the addition of glass beads. The buffer, containing glycerol, allows samples to sink easily into gel pockets. Bromophenol blue (tracking dye) indicates the progress of protein separation by migrating through the gel first. The sample buffer also contains sodium dodecyl sulfate (SDS) and  $\beta$ -mercaptoethanol (reducing agent) for protein denaturation. Samples were heated for 10 min at 56°C. Afterwards, samples were stored at -20°C for later analysis (if not used immediately; II.4.1).

### 1x Cell-lysis buffer:

Tris/HCl, pH 8	10 mM
NaCl	10 mM
MgCl <sub>2</sub>	3 mM
NP40	0.5% (v/v)
PMSF	0.1 mM
PLAC	0.1% (v/v)
DNase	0.1 mg/ml
in H <sub>2</sub> O distilled	

### PMSF:

PMSF	1 M
dissolved in acetone	
diluted in EtOH (f.c. 0.1 M)	

### 5x Laemmli buffer:

Tris/HCl, pH 6.8	300 mM
Glycerol	50% (v/v)
SDS	10% (w/v)
$\beta$ -mercaptoethanol	25% (v/v)
Bromophenol blue	0.01% (w/v)
in H <sub>2</sub> O distilled	

### PLAC solution:

Pepstatin A	3 mg/ml
Leupeptin	3 mg/ml
Antipain	3 mg/ml
Chymostatin	3 mg/ml
in DMSO	

## II.2.5. Preparation of semi-permeabilized cell

Samples of semi-permeabilized cells (SPCs) were used to determine the abundance of target proteins by Western blot analysis (II.4.2), minimizing background signal. For this purpose, the preparation of SPCs was carried out based on a “quick” version of a previously established

protocol (Lang et al., 2012). Knock-down of the target gene was performed as previously described (II.2.2). After removing the medium from 6 cm cell culture dishes, HeLa cells were washed two times with PBS (4 ml) and incubated with trypsin (250  $\mu$ l) for 5 min. Trypsinization was inactivated by adding 2 ml of KTI solution (1 ml of KHM buffer containing 2.5  $\mu$ l of trypsin inhibitor; f.c. 125  $\mu$ g/ml) per dish. Cells were harvested, counted, and instantly pelleted by centrifugation for 3 min at 1800 rpm at 4°C. Based on the total cell count of each condition, the amount of digitonin was calculated (1  $\mu$ l of digitonin per  $1 \times 10^6$  cells). The cell pellet was resuspended in 1 ml of cold KHM buffer, transferred into a 1.5 ml reaction tube, and treated with digitonin. Incubation was carried out for 5 minutes on ice. Digitonin is a mild non-ionic detergent that permeabilizes the plasma membrane by binding to cholesterol-rich membranes (Frenkel et al. 2014; Fan and Heerklotz, 2017). After centrifugation for 3 min at 1200 rpm, the supernatant was removed, and the pellet was resuspended in 150  $\mu$ l of cold KHM buffer. Nucleic acids were digested by adding nuclease (1  $\mu$ l) and  $\text{CaCl}_2$  (0.5  $\mu$ l). After 12 min of incubation at RT, EGTA solution (2  $\mu$ l) was added to inactivate the nuclease. Then, cold KHM buffer (1.5 ml) was added to the reaction tube, and cells were centrifugated for 3 min at 2000 rpm. The pellet was resuspended in 1-1.5 ml of cold KHM buffer, adjusted according to the assessed cell number (approximately  $1 \times 10^6$  cells/ml). Subsequent cell counting was essential for to adjust equal cell concentration per condition. Cells were centrifuged for 2 min at 3000 rpm. Finally, the cell pellet was resuspended in KHM buffer to achieve a final concentration of 40 000 cells per 1  $\mu$ l. Samples were diluted in 2x Laemmli sample buffer (f.c. 20 000 cells/ $\mu$ l) with the addition of glass beads and heated at 56°C for 10 min before use. If not used immediately, samples were stored at -20°C (II.4.1).

KHM-buffer:

$\text{CH}_3\text{CO}_2\text{K}$                     110 mM  
 $\text{Mg}(\text{CH}_3\text{COO})_2$                 2 mM  
 HEPES/KOH; pH 7.2    20 mM  
 in  $\text{H}_2\text{O}$  distilled

KTI- buffer:

Trypsin inhibitor                125  $\mu$ g/ml  
 in KHM-buffer

Digitonin:

Digitonin                        40 mg/ml  
 in  $\text{H}_2\text{O}$  distilled

Nuclease:

Nuclease                        4000 U/ml  
 in  $\text{H}_2\text{O}$  distilled

$\text{CaCl}_2$ :

$\text{CaCl}_2$                             200 mM  
 in  $\text{H}_2\text{O}$  distilled

EGTA:

EGTA                             200 mM  
 in  $\text{H}_2\text{O}$  distilled

## **II.2.6. Sample preparation for mass spectrometry**

After 72 h of siRNA-mediated AXER silencing (II.2.2), the medium in each dish was aspirated, and cells were washed two times with PBS (4 ml). Washing PBS was removed and, instead of trypsin, fresh PBS (2 ml) and a cell scraper were used to carefully dislodge cells from the dish bottom. The cells were then gently mixed by pipetting, transferred into 1.5 ml reaction tubes, counted, and instantly pelleted using centrifugation at 1800 rpm for 3 min. The minimum required cell number was  $1 \times 10^6$  cells per ml, determined using an automated cell counter. After centrifugation, the supernatant was discarded, and samples were stored at  $-80^{\circ}\text{C}$  before further processing (mass spectrometry).

## **II.3. Molecular biology and nucleic acid manipulation**

### **II.3.1. Total RNA isolation**

As a pre-step, siRNA-mediated AXER silencing was performed (II.2.2). After 72 hours, the culture medium was removed from each dish, cells were washed two times with PBS (4 ml) and incubated with trypsin (200  $\mu\text{l}$ ) for 5 min. Trypsin was inactivated by adding 1 ml of culture medium, and then the cell suspension was transferred into a 1.5 ml reaction tube. Cells were counted and pelleted by centrifugation for 3 min at 3000 rpm. After aspirating the supernatant, 1 ml of PBS was added, and the centrifugation and aspiration steps were repeated. Total RNA was isolated using the RNeasy Mini Kit (Qiagen), following the manufacturer's recommended procedure. Prior to downstream experiments, the quantity and purity of extracted RNA were evaluated using an UV-Vis spectrophotometer (II.3.1.1). RNA integrity was assessed using a Bioanalyzer (II.3.1.2). Since RNA is less stable than DNA, samples were stored at  $-80^{\circ}\text{C}$  to ensure integrity and prevent RNA degradation.

#### **II.3.1.1. Quantity and purity of nucleic acids**

The UV-Vis spectrophotometer NanoDrop ND-1000 (Peqlab) was used to determine the concentration and purity of nucleic acids (DNA or RNA) in the samples. It provides direct measurement of purity ratios:  $A_{260}/A_{280}$  ( $\sim 1.8$  for pure DNA;  $\sim 2.0$  for pure RNA) and  $A_{260}/A_{230}$  (ideal is 1.8-2.2). A considerably lower  $A_{260}/A_{280}$  or  $A_{260}/A_{230}$  ratio indicates the sample contamination. The advantage of this UV-Vis measurement is that it requires only a small sample volume to determine nucleic acid concentration with high accuracy, and there are no specific requirements for sample preparation or dyes. Volume of 1.1  $\mu\text{l}$  of DNA or RNA sample was used, added by inverse pipetting to prevent the introduction of air bubbles and measurement errors.

### II.3.1.2. RNA integrity

Total RNA was isolated from HeLa cells after siRNA-mediated AXER silencing. Samples were prepared for RNA sequencing (NovoGene company, UK), and performing sample quality control was essential. RNA integrity was evaluated using the Agilent Bioanalyzer (Model 2100; Agilent Technologies). It is an automated electrophoresis system that provides a reliable RNA integrity number (RIN) ranging from 1 to 10. RIN 1 indicates strongly degraded RNA, while RIN 10 indicates the highest possible RNA quality. Samples were analyzed with the Agilent RNA 6000 Nano kit following the manufacturer's instructions. After the run, an electropherogram and a gel-like (digital gel) image were obtained from the Agilent Bioanalyzer (Figure 9).

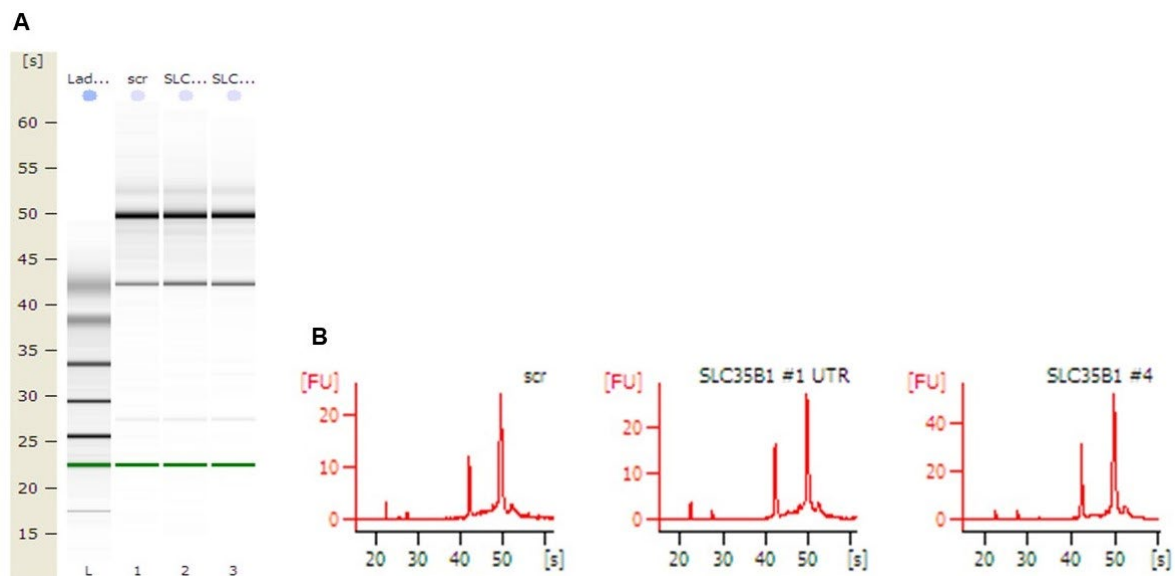


**Figure 9. Total RNA quality analysis using the Agilent Bioanalyzer system.** Total RNA was isolated from HeLa cells after AXER-gene silencing. The Agilent RNA 6000 Nano kit was used for the analysis, and images were gained from the Agilent Bioanalyzer after the run. **(A)** Digital gel image shows 18S and 28S rRNA bands ratio for each condition. RNA ladder is shown in the lane marked with “L”; lane 1 shows sample treated with scr siRNA; SLC35B1 (AXER) depleted samples are shown in the lanes 2 (#1 UTR) and 3 (#4). **(B)** Electropherograms demonstrate the 18S and 28S ribosomal RNA peaks ratio indicating the intact RNA levels for each condition.

### II.3.1.3. Real-time quantitative polymerase chain reaction

For measuring mRNA levels, real-time quantitative polymerase chain reaction (RT-qPCR) was performed using the StepOnePlus Real-Time PCR System (Applied Biosystem) with StepOnePlus Software v2.3 (Applied Biosystems). The extracted RNA (II.3.1) was reverse transcribed into complementary DNA (cDNA) using the Superscript Vilo cDNA synthesis kit. The product was purified (QIAquick PCR purification Kit, Qiagen), and a UV-Vis spectrophotometer (II.3.1.1) was used to determine the concentration of nucleic acid. For the

RT-qPCR analysis, 10  $\mu$ l of reaction mix (below) was pipetted into a 96-well reaction plate. As a negative control, 4.5  $\mu$ l of nuclease-free water was added instead of cDNA. The reaction plate was centrifuged at 1000 rpm for 1 min (Eppendorf centrifuge 5430, FA45-30-11 rotor) before the run.  $\Delta$ Ct values were calculated using  $\beta$ -actin as a standard. Values were normalized based on the control sample. The primers used in this work are listed in Table 7.

Reaction mix (per well):

TaqMan gene expression Master Mix	5.0 $\mu$ l
Expression Assay Primer and Probe	0.5 $\mu$ l
<u>cDNA (25 ng cDNA + H<sub>2</sub>O)</u>	<u>4.5 <math>\mu</math>l</u>
Total volume	10.0 $\mu$ l

Thermal cycle conditions:

50°C	02:00 min	
95°C	10:00 min	
95°C	00:15 min	} 40 cycles
60°C	01:00 min	

#### II.3.1.4. RNA sequencing

RNA sequencing (RNA-seq) is a powerful tool for investigating the transcriptome (the total content of RNAs in a cell.) Transcriptome analysis reveals the connection between genome information and functional protein expression.

In this work, RNA-seq analysis was performed to investigate potential transcriptional changes induced by AXER-gene silencing. HeLa cells were transfected, harvested, and total RNA was isolated, as described previously (II.2.2; II.3.1). Before sending the samples to NovoGene company for RNA sequencing, RNA quality control of RNAs was carried out using a UV-Vis spectrophotometer (II.3.1.1) and Bioanalyzer (II.3.1.2). The low quality and purity of RNA could lead to poor results or library preparation failure. Therefore, additional quality control was performed by the company upon samples arrival.

The RNA-seq protocol begins with reverse transcription of RNA into complementary DNA (cDNA). Following processes of fragmentation, adapters ligation, and amplification, the cDNA library is sequenced into a computer-readable format. Raw read data is then aligned to a reference genome, generating a raw counts table (Kukurba and Montgomery, 2015). The next phase involves RNA-seq data processing. Numerous tools are available that can help to quantify transcriptional levels and analyze RNA-seq data (Corchete et al., 2020). To determine differentially expressed genes (DEGs), two approaches are typically used: (1) intergroup comparison, which assesses difference between experimental conditions and control; and (2) intragroup comparison, which assesses variability within experimental conditions (Koch et al., 2018). DEGs can be illustrated in various forms, such as heatmap, volcano plot and Venn

diagram. In this work, comparisons were made between AXER-depleted samples (treated with different AXER siRNAs; AXER #1 and AXER #4) and control (Ctrl), as well as between AXER #1 and AXER #4. Correlations between conditions were generated using normalized FPKM (Fragments Per Kilobase per Million mapped fragments; [How to choose Normalization methods \(TPM/RPKM/FPKM\) for mRNA expression - Novogene](#)) counts. There is also an enrichment analysis where biological relevance is assigned to a set of genes. It provides useful information regarding differentially affected gene ontology (GO) terms (biological processes (BP), molecular functions (MF), and cellular components (CC); Koch et al., 2018) and cellular pathways (KEGG pathway database). The entire workflow, from RNA sample preparation to RNA-seq analysis, is illustrated in Figure 10. Key genes identified through RNA-seq data were subsequently validated using RT-qPCR (II.3.1.3).

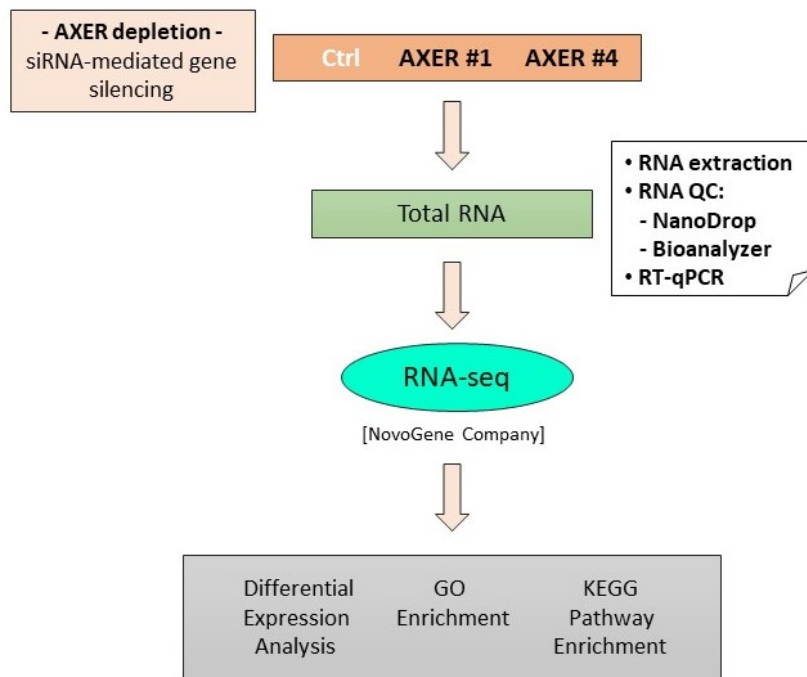


**Figure 10. The workflow - from RNA sample preparation to RNA-seq analysis.** The figure demonstrates all steps, from the AXER-gene silencing, RNA isolation and quality control (QC), to the RNA-seq analysis provided by NovoGene company. RNA-seq analysis includes the differentially expressed genes (DEGs), GO (gene ontology) enrichment and KEGG (Kyoto Encyclopedia of Genes and Genome) pathway enrichment.

### II.3.2. Strategies for cloning

Molecular cloning is a multistep process that begins with the amplification of a DNA fragment (gene of interest) using the polymerase chain reaction (PCR), incorporating restriction sites at its ends. In the ligation step, the DNA insert is joined to the plasmid of interest before cell

transformation. The process is illustrated in Figure 11, and details are described in the subsequent sections.

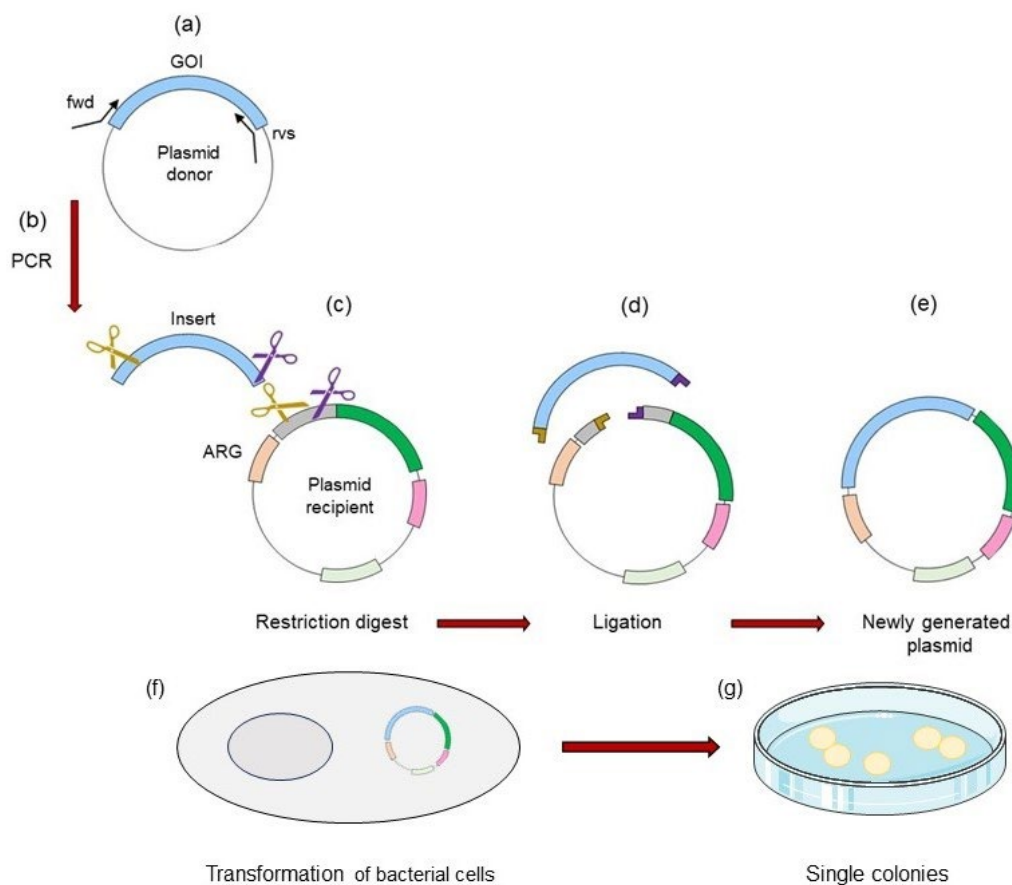


**Figure 11. Graphic of molecular cloning.** Cartoon shows the main steps of cloning process. **(a)** Designe of forward (fwd) and reverse (rvs) primers that anneal to the 5'- and 3'- end of the gene of interest (GOI); **(b)** Amplification of the GOI by the polimerasa chain reaction (PCR); **(c)** Restriction digestion of the PCR product (insert) and plasmid recipient with the antibiotic resistance gene (ARG); **(d)** Ligation of the insert and plasmid, fusion via “sticky ends“; **(e)** Newly generated plasmid; **(f)** Transformation of bacterial cells with the newly generated plasmid; **(g)** Single colonies on LB-agar antibiotic plate (only cells that contain the plasmid are able to grow on a plate due to antibiotic resistance); The further steps, including plasmid DNA purification, sequencing, amplification and final purification, are not shown.

The AXER-plasmid constructs were generated for use in the NanoBiT experiment (II.4.3). The DNA sequence of the AXER gene was inserted into four different backbone plasmids (C LgBiT; C SmBiT; N LgBiT; N SmBiT; Table 9). Additionally, the AXER loop3 SmBiT construct and the BiP construct with LgBiT-tag incorporated into the gene sequence were generated (Table 9).

### II.3.2.1. Designing primers

Primers were designed to add restriction enzyme sites at the ends of the target gene sequence (gene of interest, GOI). The purpose was to incorporate the DNA insert into a plasmid of

interest (plasmid recipient), and eventually label the protein with one of the BiT-tags on the N- or C-terminus (Table 9). Commercially available plasmids from Promega were used, containing the Large BiT (LgBiT) or Small BiT (SmBiT) sequence (II.4.3), positioned either 5' or 3' to a multiple cloning site. To achieve C-terminally labeled protein, the terminal stop sequence of the GOI was removed so the tag could also be translated. The basic primer for cloning consists of (a) a hybridization sequence, a region that binds to the GOI sequence; (b) the chosen restriction site, and (c) a "tail" sequence, the primer 5' extra base pares that assist with the restriction enzyme. The GOI was isolated from the rest of the DNA (plasmid donor) and multiple copies were generated using the polymerase chain reaction (PCR).

### II.3.2.2. Polymerase chain reaction

The GOI was amplified by polymerase chain reaction (PCR) using designed primes with appropriate restriction enzyme sites (Table 8). To minimize the risk of mutations, a high-fidelity polymerase should be used in this step. The pipetting scheme and thermal cycle conditions (below) were used to generate the AXER insert with a C-tag (966 bp), shown here as an example. The selection of the annealing temperature was based on the melting temperature (T<sub>m</sub>) of the primers, predicted using the ThermoFisher homepage:

<https://www.thermofisher.com/de/de/home/brands/thermo-scientific/molecular-biology/molecular-biology-learning-center/molecular-biology-resource-library/spotlight-articles/optimizing-tm-and-annealing.html>.

#### Pipetting scheme for PCR:

10x PCR-buffer with MgSO <sub>4</sub>	10.0 µl	
dNTP	2.0 µl	(f.c. 0.2 mM)
Fwd Primer (RZ 844)	2.0 µl	(f.c. 0.1 µM)
Rvs Primer (RZ 845)	2.0 µl	(f.c. 0.1 µM)
DNA (Plasmid)	2.0 µl	(f.c. 2.0 ng/µl)
<i>Pfu</i> -Polymerase (2 min/kb)	1.0 µl	(f.c. 0.025 U/µl)
<u>H<sub>2</sub>O distilled</u>	<u>81.0 µl</u>	
Total volume	100.0 µl	

#### Thermal cycle conditions:

110°C	L heat	
95°C	120 sec	
95°C	30 sec	} 35 cycles
65°C	30 sec	
72°C	120 sec	
72°C	120 sec	
8°C	∞	

The correct size of the PCR product was verified using agarose gel electrophoresis (II.3.2.3). After isolating it from the reaction mix using the PCR Purification Kit (Qiagen), the pure PCR product was prepared for restriction digestion (II.3.2.4). If not used immediately, the product was stored in a refrigerator at 4°C.

### II.3.2.3. Agarose gel electrophoresis

Gel electrophoresis is a commonly used method for DNA separation, based on the size (length in base pairs). Negatively charged DNA migrates in response to the electric field through an agarose gel matrix towards the anode (Lee et al. 2012). Since shorter DNA fragment travels faster through the gel than longer ones, approximate fragment size can be determined by using appropriate DNA ladder. Low-percentage gels (0.5% w/v agarose) were used to separate longer fragments (> 5 kb), while high-percentage gels (1-2% w/v agarose) were used for shorter fragments.

Gel electrophoresis was performed to separate and identify PCR products (II.3.2.2) or DNA fragments after restriction digestion (II.3.2.4). An agarose gel was prepared by dissolving the appropriate amount of agarose in 100 ml 1x TAE-buffer, heating it in a microwave until completely dissolved. The hot liquid agarose was poured into a gel tray containing a plastic comb to crate gel pockets. A solidified gel (after 15 min at 4°C) was placed in a horizontal electrophoresis chamber, with the pockets oriented towards the cathode, and completely immersed in 1x TAE-buffer. The DNA ladder (4 µl; 1 kb) was loaded into the first well (pocket) of the gel. Each DNA sample was mixed with 6x DNA-sample-buffer (loading day), in a 1:6 ratio, and loaded into following pocket. The buffer increases sample density, allowing it to sink easily into the gel pockets and indicates the progress of fragment migration. The gel run at 200 V for 1 hour. Afterwards, the gel was immersed in 1xTAE-buffer containing GelRed solution (nucleic acid dye) and left overnight. DNA bands were visualized using the Image Master VDS.

#### 1x TAE- buffer:

Tris-acetate, pH 8     40 mM  
EDTA                     1 mM  
in H<sub>2</sub>O distilled

#### GelRed solution:

GelRed (10000x)     7 µl  
in 100 ml 1x TAE-buffer

#### 6x DNA-sample-buffer:

(3000 bp)  
Xylene cyanol         0.25%  
Sucrose                 40%  
in H<sub>2</sub>O distilled

### II.3.2.4. Restriction digestion

Restriction enzymes were used to cleave both the DNA insert and the plasmid recipient at specific sequences, generating compatible ends that could be ligated together. The selection of restriction enzymes was initially performed during primer design (Table 8), using the sequence analysis program SeqBuilder (DNASTAR).

Properties of the restriction enzymes were checked on the ThermoFisher homepage:

<https://www.thermofisher.com/de/de/home/brands/thermo-scientific/molecular-biology/thermo-scientific-restriction-modifying-enzymes/restriction-enzymes-thermo-scientific/double-digest-calculator-thermo-scientific.html>.

The appropriate buffers, enzymes, reaction temperatures, and durations were suggested. The pipetting scheme (below) is related to the insert described in II.3.2.2 and the recipient vector N196 (plasmid; Table 9). Samples were incubated in two steps at 37°C for one hour. To prevent re-circularization, the linearized vector was treated with phosphatase (2 µl; calf intestine phosphatase, CIP), and additionally incubated for one hour at 37°C. Afterwards, gel electrophoresis was performed (II.3.2.3) to identify the DNA fragment and corresponding vector. The DNAs were cut out and isolated from the gel matrix using the QIAquick Gel Extraction Kit (Qiagen).

<u>Insert:</u>		<u>Plasmid:</u>	
PCR product	20.0 µl	Plasmid	2.0 µl
10x Tango buffer	4.0 µl	10x Tango buffer	4.0 µl (f.c. 1x Tango)
Nhe I	0.2 µl	Nhe I	0.2 µl
<u>H<sub>2</sub>O</u>	<u>15.8 µl</u>	<u>H<sub>2</sub>O</u>	<u>33.8 µl</u>
Total volume	40.0 µl	Total volume	40.0 µl

Incubation

10x Tango buffer	5.0 µl	10x Tango buffer	5.0 µl (f.c. 2x Tango)
Xho I	0.2 µl	Xho I	0.2 µl

Incubation

### II.3.2.5. Ligation of restricted DNA

To insert the DNA fragment into the vector (plasmid of interest), both generated by restriction digestion (II.3.2.4), ligation was performed using the T4 DNA ligase enzyme. During this process, the compatible overhangs (“sticky ends“) annealed to one another forming a complete, circular plasmid. The DNA ligase covalently linked the fragments together. The ratio between the entry vector (plasmid) and the inset was 1:3. Ligation was carried out for 1 hour at RT. Afterwards, the ligation product was used for the transformation of *Escherichia coli* cells

(II.3.2.6). The success of ligation and transformation was assessed by culturing the transformed cells on appropriate LB-agar plate (II.3.2.7).

Ligation:

Insert	3.0 µl
Plasmid	1.0 µl
10x Ligation-buffer	1.0 µl
T4-Ligase	0.4 µl
H <sub>2</sub> O	4.6 µl
Total	10.0 µl

**II.3.2.6. Bacterial transformation with plasmid vector**

For plasmid amplification, *Escherichia coli* (*E. coli*) cells were used (II.1.8): JM101 cells, when the newly generated plasmids were transformed into bacterial cells for the first time; and DH5α cells for the amplification of protein-coding plasmids used for the cell culture transfection. After bacterial cells (100 µl) were thawed on ice, 3 µl of ligation product (II.3.2.5) or 1 µl of plasmid DNA (1 µg/µl conc.) was added, gently mixed by flicking the bottom of reaction tube, and then incubated on ice for 30 min. The transformation (plasmid DNA ingestion) was promoted by the heat shock at 42°C (JM101, 90 sec; DH5α, 60 sec) in water bath, followed by 1 min cooling on ice. After adding 500 µl of LB-medium, *E. coli* cells were incubated at 37°C for 1 h on a rotary shaker.

LB-medium:

LB-medium (*lysogeny broth*) 2.5%  
in H<sub>2</sub>O distilled

**II.3.2.7. Cultivation of transformed bacterial cells**

Using the incubator with a horizontal shaker, the transformed DH5α cells (II.3.2.6) were cultivated in a 1000 ml flask containing 100 ml of LB-medium at 37°C, overnight. According to plasmid resistance (Table 9), the appropriate antibiotic (ampicillin or kanamycin) was added in the LB-medium (1:1000 ratio). The amplified plasmid DNA was extracted from bacteria as described in the following section.

For newly generated plasmid, the transformed JM101 cells (II.3.2.6) were centrifuged for 1 min at 5000 rpm, and 500 µl of the supernatant was discarded. The remaining 100 µl of transformed bacteria was resuspended, transferred onto an LB-agar plate containing the appropriate antibiotic, and spread evenly using a sterile tool. The plates were then placed in an incubator at 37°C, overnight. The next day, single colonies were gently picked with a sterile wooden stick and placed into a glass tube with 2 ml of TB-medium (50.8 g of *terrific broth* per 1 l H<sub>2</sub>O distilled)

containing the appropriate antibiotic (1:1000 ratio). The colonies were incubated at 37°C for at least 12 hours on a rotary shaker.

LB-agar plate:

LB-medium 2.5%  
LB Agar 1.5%  
Antibiotic 1:1000  
in H<sub>2</sub>O distilled

Antibiotic:

Ampicillin 100 mg/ml  
Kanamycin 25 mg/ml  
each in H<sub>2</sub>O distilled

### II.3.2.8. Plasmid DNA extraction

Plasmid DNA was extracted from the transformed *E. coli* cells (II.3.2.7) using two different kits and following manufacturer's instructions: PureYield Plasmid Miniprep System (Promega) or PlasmidMidi Kit (Qiagen). The kit was chosen based on the volume of bacterial culture obtained during the transformation experiment: the Mini kit for 2 ml, and the Midi kit for 100 ml. The principle is identical for both kits. The bacterial culture was centrifuged, the supernatant was discarded, and the cell lysis was carried out by adding a lysis buffer. Afterwards, a neutralization solution was added, and the samples were centrifuged. The supernatant was transferred to a column which binds DNA, and the washing step was repeated several times. According to the Midiprep protocol, the plasmid DNA was eluted from the column matrix and precipitated by adding isopropanol. After centrifugation, the pellet was washed with ethanol. Subsequently, the plasmid DNA was resuspended in TE-buffer or H<sub>2</sub>O distilled. The plasmid DNA extracted using the Miniprep protocol was eluted with nuclease-free water directly from the column matrix. Quantification of the DNA was performed using the NanoDrop UV/Vis spectrophotometer (II.3.1.1). The concentration was adjusted to 1 µg/µl, and the plasmid DNA was stored at -20°C for follow-up experiments.

TE-buffer:

Tris/HCl, pH 8 10 mM  
EDTA 1 mM  
in H<sub>2</sub>O distilled

### II.3.2.9. Sequencing of plasmid DNA

The generated plasmids (II.3.2.8) were sent for sequencing to LGC Genomics company in Berlin. The samples were prepared according to the company's requirements: a total volume of 14 µl per reaction tube, containing the plasmid and the primer (5 µM; forward RZ758, or reverse RZ759; Table 8) in distilled water. The sequence and quality of the results were available on the company's online portal. Using the SeqMan software (DNASTAR), the

sequence was aligned to the predicted sequence created *in silico* (SeqBuilder, DNASTAR), and the generated inserts were identified.

Samples for sequencing:

Primer	4 $\mu$ l (f.c. 1.4 $\mu$ M)
DNA	X $\mu$ l (f.c. 100 ng/ $\mu$ l)
<u>in H<sub>2</sub>O distilled</u>	
Total volume	14 $\mu$ l

## II.4. Biochemical analysis

### II.4.1. SDS-polyacrylamide gel electrophoresis

Sodium dodecyl sulfate-polyacrylamide gel electrophoresis (SDS-PAGE) is a commonly used method for separating protein mixtures based on protein molecular weight. Since a low molecular weight allows a faster migration, gels with a higher acrylamide concentration are used for proteins with a lower molecular weight. Proteins migrate in response to the electric field through the gel that acts as a sieving matrix. Natively folded proteins have a net charge that can be negative or positive, depending on the balance of negative and positive amino acids. Moving in an electrical field, proteins of the same molecular weight may travel at different speed. Therefore, to separate proteins based on their molecular weight only, it is essential to reduce the proteins to linear molecules and coat them with the uniform (negative) charge. During sample preparation, Laemmli buffer (below) was added, containing  $\beta$ -mercaptoethanol and SDS for protein denaturation (II.4.2). Also, SDS masks proteins with a negative charge (Weber and Osborn, 1969). Approximately 1.4 g of SDS reacts with 1 g of protein, meaning that SDS binds to proteins quite uniformly (Smith, 1984). To maintain this state during the run, SDS is also present in a gel.

The pipetting scheme for preparing the polyacrylamide gel (Table 10) is designed for self-made gel chambers with dimensions of 14 cm (width) x 11 cm (height) x 0.1 cm (depth). After sealing the bottom of the gel chamber with 2% agarose gel, a mixture of running gel was added. It was covered with isopropanol to maintain gel moisture during polymerization. Approximately 2 h later, the isopropanol was removed, and a mixture of stacking gel was added. A plastic comb was placed at the top to create gel pockets. After 30 min, the finished polyacrylamide gel was transferred to a vertical electrophoresis chamber filled with electrophoresis buffer. Samples, either 30  $\mu$ l of whole-cell lysate (II.2.4) or 20  $\mu$ l of semi-permeabilized cells (II.2.5), were loaded into the gel pockets. Two additional pockets were used: one for 10  $\mu$ l of RM (II.1.7) to determine the position of target proteins, and another for 4  $\mu$ l of marker (Page Ruler Prestained Protein Ladder) for protein size identification. The loaded gels were run for 3h at 45 mA or overnight at 5 mA. Afterwards, the gels were subjected to Western blot analysis (II.4.2).

**Table 10. Pipetting protocol for the preparation of SDS-polyacrylamide gel.** Depending on the size of proteins of interest, SDS-PAGE gels contain different concentration of acrylamide (%).

Solution \ Percentage	Separating gel				Stacking gel
	10	12.5	15	17.5	5
40% (w/v) acrylamide (ml)	3.8	4.7	5.6	6.6	0.9
2% (w/v) bisacrylamide (ml)	1	1.3	1.5	1.8	0.2
H <sub>2</sub> O distilled (ml)	4	2.9	1.7	0.4	5
1.875 M Tris/HCl, pH 8.8 (ml)	6				-
1 M Tris/HCl, pH 6.8 (ml)	-				0.9
10% (w/v) SDS (μl)	150				72
20% (w/v) AMPS (μl)	45				67.5
TEMED (μl)	5				10.5
Total volume (ml)	15				7.2

1x Laemmli buffer:

Tris/HCl, pH 6.8	60 mM
Glycerol	10% (v/v)
SDS	2% (w/v)
β-mercaptoethanol	5% (v/v)
Bromophenol blue	0.01% (w/v)

1x Electrophoresis buffer:

Glycine	384 mM
Tris	50 mM
SDS	0.1% (w/v)
in H <sub>2</sub> O bi-distilled	

#### II.4.2. Western blot analysis

Since its introduction by Towbin et al. in 1979, Western blot has become extensively used technique for protein analysis. It involves three main steps: 1) protein separation based on molecular weight, 2) transfer to a membrane as a solid support, and 3) detection of target proteins marked with appropriate primary and secondary antibodies.

After separation, a protein mixture was transferred from the SDS gel (II.4.1) to a polyvinylidene difluoride (PVDF) membrane using the Wet/Tank Blotting system (Trans-Blo Cell, Bio-Rad). PVDF membranes are mechanically and chemically stable (Gültekin and Heermann, 1988), allowing blots to be re-probed and stored. Before transfer, the membrane was activated in methanol for one minute. Afterwards, both the SDS gel and the blotting membrane were equilibrated in a transfer buffer (below). The transfer sandwich was assembled as follows: sponge (fiber pad), filter paper (Whatman paper), gel, PVDF membrane, filter paper, sponge. The filter paper and sponge were also soaked in transfer buffer. The gel and membrane were in a close contact without any air bubbles. Migration of the negatively charged proteins in the gel-to-membrane direction was achieved by placing the membrane between the gel and positive electrode. The assembled sandwich was enclosed in a cassette and placed in a blot chamber filled with transfer buffer. Blotting was performed at 400 mA for 3 h. A constant water

flow was cooling the system down to keep the temperature at 14°C and prevent protein degradation.

Transfer buffer:

Glycine                    96 mM  
Tris                        12.4 mM  
in H<sub>2</sub>O distilled

The next step was blocking, which prevents a non-specific binding to the membrane. Blocking was done with non-fat dried milk at RT for 1 h, gently rocking. In the case of an anti-phosphoprotein antibody, a 5% (w/v) BSA blocking solutions was used, since milk contains the phosphoprotein casein, which interferes with assay results. Blocking was followed by five-minute washing steps, alternating TBS-buffer, TBS-T and TBS again. The membrane was placed in a rolling-box and incubated with appropriate dilutions of the primary antibody for 90 min at RT or overnight at 4°C. The secondary antibody was fluorophore-coupled, and incubation was carried out for 90 min at RT in the absence of light. After incubation, the washing steps were performed (30 s TBS, 2x5 min TBS-T, 5 min TBS). The thoroughly dried membrane was scanned using the Typhoon Trio imaging system in combination with the ImageQuant TL image analysis software 7.0 (GE Healthcare).

In the case of a small amount of protein or weak antibody, a POD-coupled secondary antibody was used (Table 4). The procedure and dilution remained unchanged, but the blot was not dried before detection. Instead, it was covered with the Luminol/Enhancer and Stable/Peroxide (1:1 ratio; SuperSignal West Pico PLUS kit, Thermo Scientific). Afterwards, the membrane was placed between two transparent plastic sheets free of air bubbles to improve the distribution of the chemiluminescent mixture. Detection and analysis were performed using the Fusion SL chemiluminescence imager (Peqlab) and Fusion software.

TBS-buffer:

NaCl                        150 mM  
Tris/HCl, pH 7.4        10 mM  
in H<sub>2</sub>O distilled

TBS-T buffer:

Triton X-100 0.05% (v/v)  
in TBS-buffer

Blocking solution:

non-fat dry milk        2% (w/v)  
in TBS-buffer

Antibody solution:

Blocking solution  
with antibody (II.1.3)

### II.4.3. NanoBiT system – detection of protein-protein interaction

Modifying the luciferase from a deep-sea shrimp (*Oplophorus gracilirostris*), the company Promega developed the NanoLuc Binary Technology (NanoBiT) system. It is based on a complementation assay first mentioned in literature in 2016 (Dixon et al., 2016; Oh-Hashi et al., 2016). The ATP-independent luciferase is divided into two complementary subunits: the large subunit (LgBiT; 18 kDa) and the small subunit (SmBiT; 11 amino acids), which are fused to proteins of interest. In the case of protein-protein interaction (PPI), the two subunits reconstitute a functional enzyme. By adding the substrate furimazine, the reunited luciferase provides a light signal that can be measured (Figure 12). This is known as NanoLuc luciferase (England et al., 2016). The subunits do not form a functional enzyme spontaneously, due to their low affinity for each other (the intrinsic affinity of the two subunits has a  $K_D$  of 190  $\mu\text{M}$ ; Dixon et al., 2016). In most cases, one of the BiT subunits is tagged at the N- or C- terminus of the protein of interest with a linker sequence of 13-15 amino acids. Overexpression of reporter proteins in cells, and consequent measurement of a false positive signal, is prevented by the weak HSV-TK promoter upstream of the respective gene sequences (Ali et al., 2018). The advantage of this measurement is a possibility to track the changes in a protein-protein interaction, in real time.

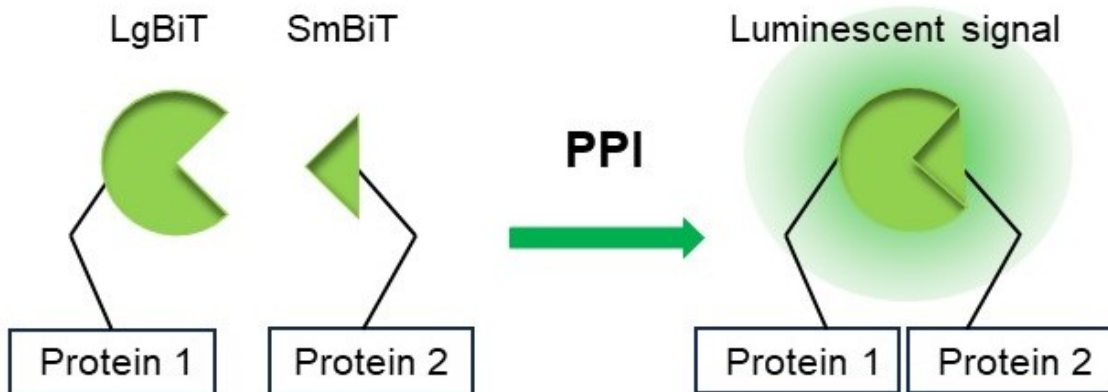


**Figure 12. Principle of the NanoBiT system.** Two complementary luciferase subunits, the Large subunit (LgBiT) and Small subunit (SmBiT), are fused to proteins of interest. Protein-protein interaction (PPI) reunites a functional enzyme providing a bright luminescent signal (green orb) upon addition of the cell-permeable substrate (furimazine; not shown).

On day one, cells were harvested, counted, and the cell number was adjusted to  $2 \times 10^5$  cell/ml. Afterwards, cells were seeded in a white 96-well plate with a flat bottom, adding 100  $\mu\text{l}$  of cell suspension per well ( $2 \times 10^4$  cell/100 $\mu\text{l}$ ), and incubated at 37°C and 5%  $\text{CO}_2$ . The next day (after 20-24 hours), cells were transfected with a plasmid transfection mix (containing a reporter pair) that was prepared separately for each well:

Transfection mix (two plasmids):

OptiMEM without phenol red	16.71 $\mu$ l
Plasmid 1 (0.1 $\mu$ g/ $\mu$ l)	1.27 $\mu$ l
Plasmid 2 (0.1 $\mu$ g/ $\mu$ l)	1.27 $\mu$ l
<u>FuGENE HD</u>	<u>0.75 <math>\mu</math>l</u>
Total volume	20.00 $\mu$ l

Each plasmid construct was pre-diluted in OptiMEM (without phenol red) to achieve a concentration of 0.1  $\mu$ g/ $\mu$ l. The FuGeneHD transfection reagent was added last. After a 10-min incubation at RT, 8  $\mu$ l of the transfection mix was added to the appropriate well, resulting in a final concentration of 50 ng/well for each plasmid (LgBiT-tagged and SmBiT-tagged). The medium in the wells was not exchanged before transfection. The plate content was gently mixed by circular hand movements.

After 24 hours, the culture medium was aspirated from each well and replaced with 100  $\mu$ l of pre-warmed (37°C) OptiMEM without phenol red. The furimazine substrate, consisting of the Nano-Glow Live Cell reagent and Nano-Glow Live Cell Substrate Dilution Buffer (1:20 ratio), was freshly prepared for each experiment. The microplate reader (M200 Tecan Infinite, Tecan iControl software) was pre-warmed to 37°C for 20 min before measurement. The measurement settings were as follows:

Instrument set up:

Duration: 9 min

Measuring interval: 1 min

Shake before each measurement: 2 s; 2 mm orbit

Integration time: 1000 ms

Settle time: 50 ms

After a baseline measurement (9 min), the substrate (20  $\mu$ l) was added to each well, and the measurement was started again (9 min). To verify the expression of the LgBiT-tagged fusion construct, two additional measurements were performed. By adding digitonin (5  $\mu$ l; diluted in OptiMEM without phenol red), the cells were semi-permeabilized, and eventually, the synthetic HaBiT peptide (10  $\mu$ l; Table 5) was added. Due to its high affinity for LgBiT ( $K_D$  700 pM; Sicking et al., 2021), HaBiT served as a control for sufficient expression of the LgBiT-tagged construct. Each transfection with the reporter pair (LgBiT- and SmBiT- tagged fusion proteins) was followed by a non-interacting pair of the LgBiT-tagged fusion protein plus Halo-SmBiT. Provided by the manufacturer, Halo-SmBiT served as a negative control, replacing the SmBiT fusion protein. According to the manufacturer, a detected protein-protein interaction (PPI) is considered specific if its luminescent signal is at least 10-fold higher compared to the luminescent signal of the appropriate negative control.

Certain protein-protein interactions were challenged with physiological or chemically induced ER stress. To provoke ER stress and measure a possible change of the luminescent signal, the chemical stressors thapsigargin and tunicamycin were used, individually or mixed. DMSO served as the control. Stressors were added to the corresponding wells right before a baseline measurement. Physiological ER stress was triggered by the synthetic steroid mifepristone (Mif). Treatment was performed before or during cellular transfection at different time points (4; 7; 17; 30 and 48 hours before measurement). As a control, ethanol (EtOH) was added to the corresponding wells. Mifepristone (10 mM) was diluted in cell medium (DMEM) to a concentration of 50 nM (f.c. 0.5 nM per well).

Chemicals - final concentration per well:

Digitonin (5.5%)	0.002%
HaBiT peptide (20 mM)	100 nM
Thapsigargin (1 mM)	1 $\mu$ M
Tunicamycin (10 mg/ml)	10 $\mu$ g/ml

The HaBiT peptide was weighed and dissolved in DMSO, and then diluted in OptiMEM without phenol red. Thapsigargin and tunicamycin were diluted in DMSO.

#### **II.4.4. Live-cells metabolic analysis**

Two main metabolic processes, glycolysis and mitochondrial respiration, were measured in living cells using kits from Agilent (pH-Xtra and MitoXpress Xtra assay kits). Although the experiments were performed following the basic manufacturer's instructions, two adapted protocols were established (II.4.4.1; II.4.4.2) to measure the changes in metabolic activity upon AXER depletion. Both assays were carried out using fluorescence plate reader, providing a functional kinetic measurement of metabolic activity in real time.

The Extracellular Acidification Rate (ECAR) and Oxygen Consumption Rate (OCR) were measured using the pH-Xtra and MitoXpress Xtra assay, respectively. The main contributor to extracellular acidification is lactate production, thus the ECAR measurement indicates cellular glycolytic activity. On the other hand, the MitoXpress Xtra reagent is quenched by O<sub>2</sub>, and the reduction of extracellular oxygen levels leads to an increase in the fluorescent signal, indicating cellular respiration. The pH-Xtra reagent is an H<sup>+</sup>-sensing fluorophore, while the MitoXpress Xtra reagent is an oxygen-sensing fluorophore. Both reagents are cell-impermeable, chemically stable, and water-soluble.

To determine the optimal number of HeLa cells per well, a cell seeding density experiment was performed. Cells were seeded at densities of 4x10<sup>4</sup>, 5x10<sup>4</sup>, 8x10<sup>4</sup>, 1x10<sup>5</sup> and 1.5x10<sup>5</sup> cells/well.

Based on the setup and experimental conditions, the highest tested cell density was considered optimal.

Prior to use, the medium and solutions were warmed at 37°C, and a 96-well plate (black well/clear bottom) was placed on a plate-block heater during preparation. The microplate reader (M200 Tecan Infinite, Tecan iControl software) was pre-warmed at 37°C, 20 min before the measurement starts. The instrumental setup is shown in Table 11, and the microplate setup is presented in Figure 13.

**Table 11. Instrumental setup for M200 Tecan Infinite microplate reader.** Measurement settings for the pH-Xtra Glycolysis Assay and the MitoXpress Xtra Oxygen Consumption Assay (Agilent).

	pH-Xtra assay	MitoXpress Xtra assay
Method	Time-resolved fluorescence	Time-resolved fluorescence
No. of lables	One	One
Kinetic duration	Two hours	Two hours
Interval time	Minimal	Minimal
Kinetic measurement	Well-wise	Well-wise
Measurement mode	TRF intensity, top read	TRF intensity, bottom
Emission	380 (9) nm	380 (9) nm
Emission	615 (20) nm	650 (20) nm
Settle time	0 ms	0 ms
No. of flashes	25	25
Gain	180	180
Lag time	100 µs	30 µs
Integration time	100 µs	100 µs

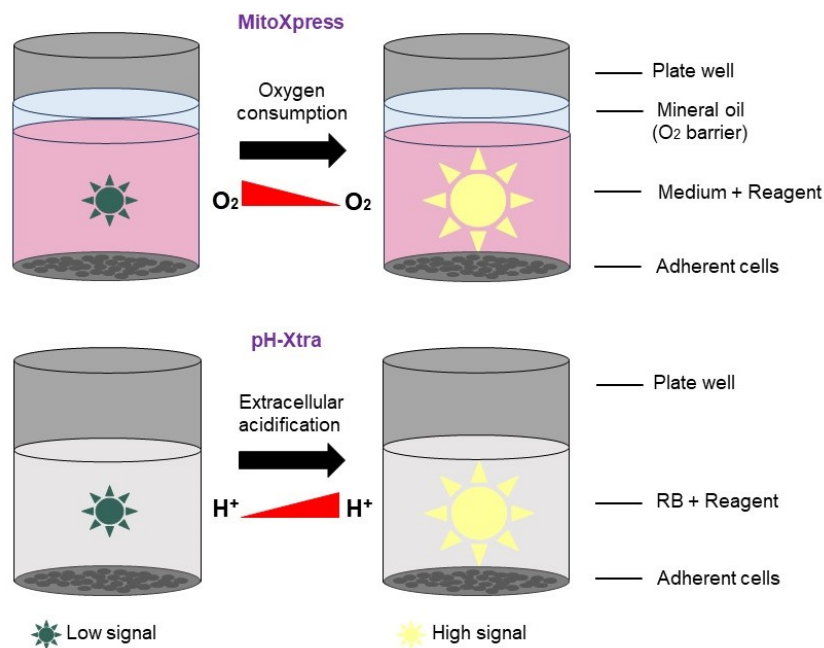


**Figure 13. Microplate setup for measuring mitochondrial respiration and glycolytic activity.** The mitochondrial respiration and glycolytic activity were measured in HeLa cells (adherent cells) using the commercially available kits from Agilent. Cells were harvested,

counted, seeded in a 96-well plate (black well/clear bottom; 100 µl/well) and incubated at 37°C and 5% CO<sub>2</sub>, overnight. To remove CO<sub>2</sub>, the plates prepared for pH-Xtra assay were placed in a CO<sub>2</sub>-free incubator for 2 h before measurement. Afterwards, the medium was replaced with respiration buffer (90 µl), prepared according to the manufacturer's instructions. In the MitoXpress Xtra assay plates, the medium was replaced with 90 µl of fresh medium. Corresponding reagent (MitoXpress or pH-Xtra; 10 µl) was added in the plate wells, and the measurement was started. In addition, the wells with MitoXpress reagent were covered with one drop of mineral oil that served as an O<sub>2</sub>-barrier. The change in signal was measured kinetically using a fluorescence plate reader. (**Upper panel**) Mitochondrial respiration decreases the oxygen concentration, causing a higher fluorescent signal. (**Lower panel**) Due to extracellular acidification, the pH of assay buffer is reduced, leading to an increased fluorescent signal. Text contains more details about both assays (II.4.4.1, II.4.4.2). Medium, cell medium (DMEM); RB, respiration buffer (pH 7.4).

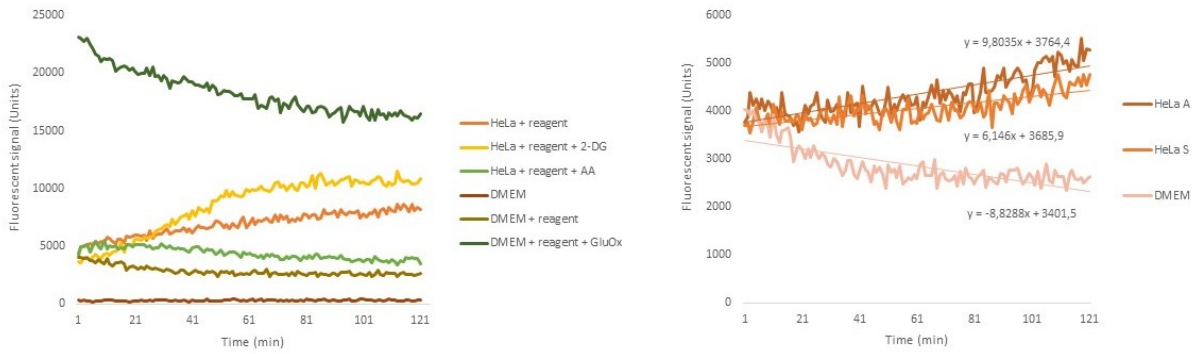
Following the manufacturer's instructions, a set of controls was used during the measurements: (1) blank control, medium or respiration buffer only; (2) cell-free negative control, medium or respiration buffer plus the corresponding reagent; and (3) cell-free positive control, medium or respiration buffer plus the corresponding reagent plus glucose oxidase. As a cell-based negative control (4), cells were treated with compounds that modulate lactate production (2-deoxy-d-glucose) or the electron transport chain (Antimycin A) (Figure 14: A and B, left).

Chemical compounds - final concentration per well:

2-deoxy-d-glucose (250 mM)	10 mM
Antimycin A (100 µM)	1 µM
Glucose oxidase (1 mg/ml)	0.1 mg/ml

SiRNA-mediated gene silencing, as a specific experimental pre-step, necessitated the use HeLa in a suspension mode (not attached to the plate surface) during measurement. The measurement with adherent HeLa cells was performed in parallel and served as a control. The change in signal was measured kinetically using a fluorescence plate reader. Although the fluorescent signal was lower in comparison to the control, it was considered a reliable indicator of appropriate metabolic activity (Figure 14: A and B, right).

**A**



**B**

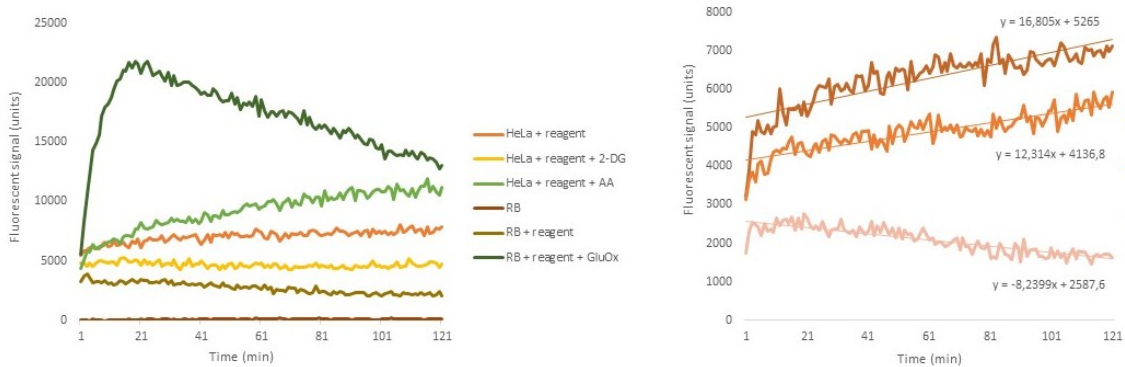


**Figure 14. The signal profile of MitoXpress Xtra and pH-Xtra.** HeLa cells were seeded in a 96-well plate (black well/clear bottom). The cell-free wells were served as negative control (A and B: left, brown and olive green; right, light orange) or positive control (A and B: left, dark green). For both assays, the fluorescent signal (units) was measured for 120 min. **(A: left)** The evaluation of oxidative phosphorylation. As cells respire, the concentration of dissolved oxygen decreases, causing an increase in fluorescent signal (orange). The addition of Antimycin A caused a signal drop (light green), while the addition of 2-DG (glycolysis inhibitor) resulted with an elevated signal (yellow). **(B: left)** The assessment of glycolytic activity. The conversion of pyruvate to lactate causes extracellular acidification, resulting with the pH-reduction in assay buffer that is detected as an increase in fluorescent signal (orange). The addition of 2-DG caused a signal drop (yellow). The Inhibition of oxidative phosphorylation by Antimycin A resulted with an elevated signal (light green). **(A, B: right)** For HeLa adherent cells (dark orange), measurement was performed after cells were seeded in a plate and incubated for 2.5 h at 37°C and 5% CO<sub>2</sub>. For HeLa suspension cells (orange), the measurement was performed right after cell seeding. The rate of change in fluorescent signal was calculated by a linear regression (slope calculation) and was the indicator of rate of measured metabolic activity. HeLa A, adherent HeLa cells; HeLa B, suspension HeLa cells; DMEM, cell medium, blank control; RB, respiration buffer (pH 7.4), blank control; DMEM or RB plus corresponding reagent, cell-free negative control; reagent, Mito Xpress or pH-Xtra; 2-DG, 2-deoxy-d-glucose, modulate the lactate production; AmA, Antimycin A, modulate electron transport chain; GluOx, glucose oxidase.

#### II.4.4.1. Measuring mitochondrial respiration

Mitochondrial respiration was measured in HeLa cells using the MitoXpress Xtra assay kit (Agilent). After 72 h of AXER-gene silencing (II.2.2), cells were harvested, counted, and the cell number was adjusted to  $1.665 \times 10^6$  cells/ml. Cells were seeded in two 96-well plates (black wall/clear bottom) at a density of  $1.5 \times 10^5$  cells per well (90  $\mu$ l). Before measurement, one plate was placed in the incubator with 5% CO<sub>2</sub> at 37°C for 2.5 h to allow for cell adhesion. The other plate, with non-adherent cells, was used for the experiment immediately after seeding. The MitoXpress reagent (10  $\mu$ l) was added to the corresponding wells, and each well was sealed by adding one drop of pre-warmed mineral oil, avoiding air bubbles. The plate was transferred to the fluorescence plate reader (M200 Tecan Infinite; Table 11), and the measurement was started.

#### II.4.4.2. Measuring glycolytic activity

Glycolytic activity was measured in HeLa cells using the pH-Xtra assay kit (Agilent). After 72 h of AXER-gene silencing (II.2.2), cells were harvested, and counted, and the cell number was adjusted to  $1.665 \times 10^6$  cells/ml. The reaction tubes containing the cell suspension were placed in a CO<sub>2</sub>-free incubator with 95% humidity, at 37°C for 2 hours. The cell medium and microplate were also purged of CO<sub>2</sub> which may contribute to acidification. Cells were centrifuged for 2 min at 3000 rpm, and the pellet was resuspended in respiration buffer (RB; pH 7.4) that was previously prepared according to the manufacturer's instructions. Afterwards, cells were seeded in the 96-well plate (black wall/clear bottom) at a density of  $1.5 \times 10^5$  cells per well (90  $\mu$ l). The pH-Xtra reagent (10  $\mu$ l) was added to the corresponding wells, and the plate was transferred in the fluorescence plate reader (M200 Tecan Infinite; Table 11), and the measurement was started.

### II.5. Statistical analysis

Collection and conversion of the values were carried out in Microsoft Excel 2010. Statistical analysis and graph design were performed using Graph Pad Prism 10. One-way ANOVA was used for statistical comparison of multiple groups. Analysed values were from at least three independent experiments and are shown with the standard error of the mean (SEM). Significant changes are indicated by asterisks as follows:

$p \geq 0.05$	ns	(non-significant);
$p < 0.05$	*	(significant);
$p < 0.01$	**	(very significant);
$p < 0.001$	***	(highly significant).

## II.6. Additional experiments

### II.6.1. Spot peptide array analysis

For the detection of protein-protein interaction sites, the spot peptide array analysis was performed by Professor Dr. Martin Jung.

The preparation of dog pancreatic rough microsomes (RM; ER membrane fragments) was based on the method by Walter and Blobel (1983). The RM-extracts (Ribosome Associated Membrane Proteins, RAMP) and the purified protein complexes (Sec61- and TRAP-complex) were produced and purified according to Görlich and Rapoport (1993).

The fully automated peptide synthesizer (ResPep SL, Intavis) was used to synthesize the peptide spots on derivatized cellulose membrane (CEM, 32100), following the manufacturer's instructions. The membrane was activated in methanol for one minute with gentle rocking. The full-length sequence of AXER (SLC35B1) was covalently coupled to the membrane in overlapping peptide fragments (15 amino acid length, with a shift of 3 amino acids from one peptide to the next). To prevent non-specific binding, the membrane was blocked in 1% (w/v) BSA dissolved in 1x PBS for 60 min at RT, with gentle rocking. The extracts or the purified protein complexes were diluted in 1x PBS containing 1% digitonin (detergent; 1:3 ratio) and incubated with the membrane at 4°C overnight, with gentle rocking. Subsequently, the washing step was performed three times in 1x PBS with 0.05% Tween 20 and once with 1x PBS.

The incubation with primary antibody (Sec61 $\alpha$ , Sec61 $\beta$ , TRAP $\alpha$ , TRAP $\beta$  or AXER) was carried out at a 1:1000 ratio for 90 min at RT, with gentle rocking. As before, the washing step was performed three times in 1x PBS with 0.05% Tween 20 and once in 1x PBS. Afterwards, the membrane was incubated with the anti-rabbit POD-coupled secondary antibody (1:1000 dilution) for 120 min at RT. The washing step was repeated. After adding the chemiluminescence substrates (1:1 ratio; SuperSignal West Pico PLUS kit, Thermo Scientific), the membrane was placed between two transparent plastic sheets. The Fusion SL (PepLab) chemiluminescence imager was used for antibody detection, and analysis was performed by the Fusion software.

### III. RESULTS

The main goal of this work was to verify and extend the set of AXER interaction partners and understand the regulation and metabolic integration of this functionally unique ER protein. In parallel, a set of the ER translocon protein-protein interactions (PPI) were detected in living cells and followed by further research regarding the PPI dynamics under different cellular conditions. Various scientific techniques were performed using a HeLa cell line and the HeLa- $\mu$ s cell model (Bakunts et al., 2017).

#### III.1. Evaluation of optimal time interval for AXER siRNA-mediated silencing

Small interfering RNA (siRNA) represents a valuable research tool for the prompt characterization of the function of target gene. To suppress the expression of the SLC35B1 (AXER) gene at the post-transcriptional level, HeLa cells were transfected with two AXER siRNAs (SLC35B1-UTR (AXER #1) or SLC35B1 (AXER #4)), or control siRNA (Ctrl; with no sequence homology to any known gene). The experimental design for AXER siRNA-mediated silencing was described in section II.2.2. Previous research in our lab was mostly based on the 96 hours AXER silencing (Klein et al., 2018). In this work, the intention was to investigate molecular changes caused by AXER depletion with duration less than 96 hours in order to avoid excessive toxic or detrimental side-effects from an extended silencing time. To evaluate the optimal time interval for AXER silencing, 48 h or 72 h post transfection, the cell viability was determined by an automated cell counter. Change in total cell number suggested the silencing influence on cell proliferation over time.

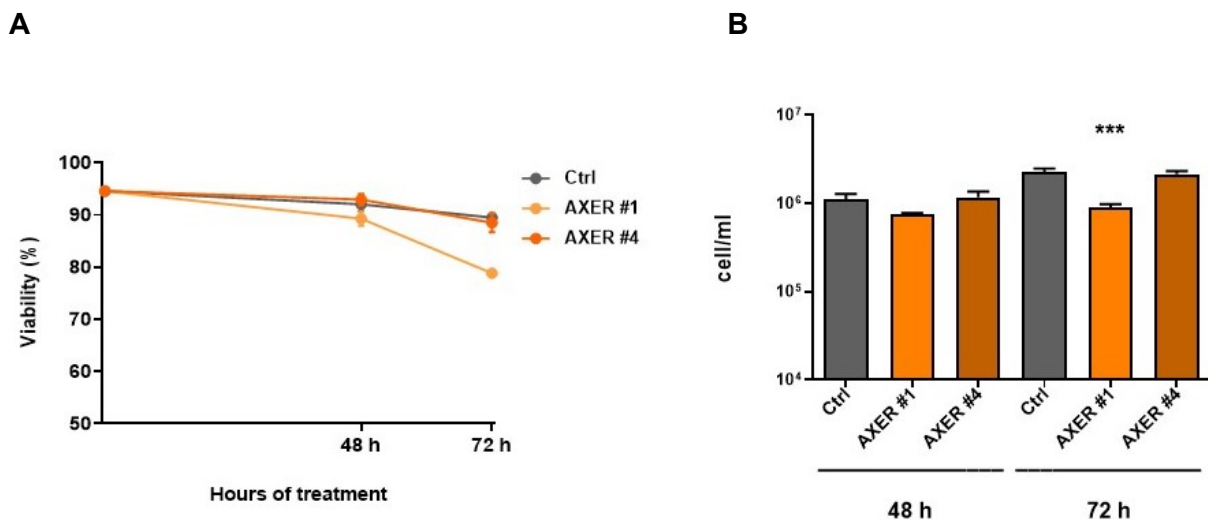


**Figure 15. AXER gene silencing affected cell viability and proliferation depending on different silencing duration and type of targeting siRNA.** HeLa cells were transfected with AXER (#1 or #4) targeting siRNA or with control siRNA (Ctrl). Cells were harvested after 48 and 72 hours, and (A) viability and (B) cell number (cell/ml) were determined by an automated cell counter using trypan blue staining. Reported data are from three independent experiments

and are shown with the standard error of the mean (SEM). Statistical significance between conditions was determined using one-way ANOVA. Significant changes are indicated by asterisks: \*\*\*  $p < 0.001$ . Statistical analyses were performed using GraphPad Prism version 10.

After 48 hours of AXER silencing, the cell viability was measured (Figure 15: A). AXER #4 showed a minor change, while the decline of cell viability for AXER #1 was slightly more pronounced. The cell viability dropped down further until 72 hours, showing the reduction for AXER #1 over 16%. The reduction for AXER #4 was approximately 7%. In line with this finding, the transfection with AXER #1 siRNA had a stronger effect on impeding cell proliferation, causing a significant change in the cell number after 72 hours, in comparison to control (Figure 15: B). The silencing efficiency was evaluated by real-time quantitative PCR (RT-qPCR; II.3.1.3). The analysis revealed that the knockdown of AXER-gene was effective: the 5' untranslated region (UTR)-targeting siRNA (AXER #1) depleted the mRNA level to ~5%, and the coding region-targeting siRNA (AXER #4) to ~10%. Similar depletion efficiency was observed for both 48 and 72 hours of AXER silencing (Figure 16).

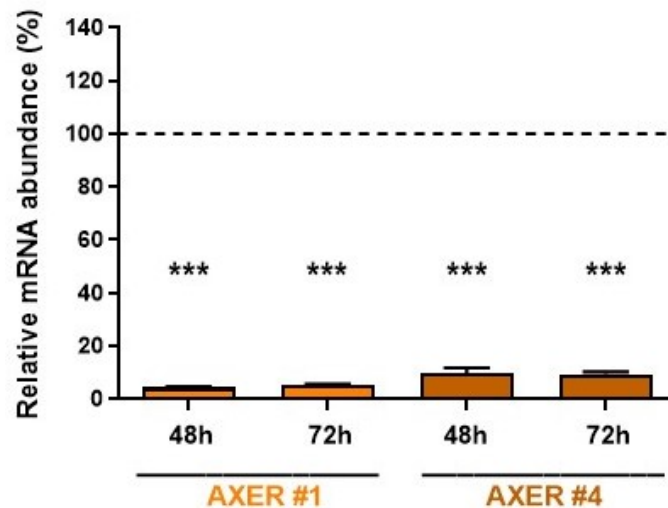


**Figure 16. AXER depletion efficiency validated by RT-qPCR.** The real-time quantitative PCR performed after HeLa cells were transfected with AXER (#1 or #4) targeting siRNA or with control siRNA for 48 and 72 h. The  $\Delta C_t$ -values were calculated using  $\beta$ -actin as a standard. Values were normalized based on the control siRNA-treated cells (Ctrl; dashed line). Reported data are from three independent experiments and shown with the standard error of the mean (SEM). Statistical significance between conditions was determined using one-way ANOVA. Significant changes are indicated by asterisks: \*\*\*  $p < 0.001$ . Statistical analyses were performed using Graph Pad Prism version 10.

Based on the cell viability, proliferation, and silencing efficiency for all downstream experiments in this work, 72 h silencing was considered as optimal duration for AXER silencing.

### III.2. RNA sequencing analysis after AXER depletion

The main purpose of the RNA sequencing (RNA-seq; transcriptomic) analysis was to characterize changes in the overall gene expression landscape of a cell after AXER silencing. The analysis was used to determine the genetic interaction partners of AXER, biological pathways it might be involved in, and what mechanisms cells use to compensate for its loss over time. After 72 h of AXER gene silencing (II.2.2), three independent batches of cells for each condition (Ctrl (1; 2; 3), AXER #1 (1; 2; 3) and AXER #4 (1; 2; 3)) were harvested, counted, and pelleted instantly. The total RNA isolation was performed using the RNeasy Mini Kit (Qiagen) (II.3.1). The quality control of RNA samples was performed by NanoDrop (II.3.1.1) and Bioanalyzer (II.3.1.2). Results are summarized in Table 12. The AXER silencing efficiency was confirmed by RT-qPCR (Figure 16) before sending the samples to NovoGene company for sequencing.

**Table 12. Quantity and quality of RNA samples prepared for RNA sequencing.** The results fulfilled the NovoGene company requirements. 260/280 ~ 2.0 for RNA; RIN = RNA integrity number (1-10; high quality > 8.0).

Sample	NanoDrop (ng/μl)	Bioanalyzer (ng/μl)	Average (ng/μl)	260/280	RIN
Ctrl-1	268.10	181	224.55	2.03	9.7
Ctrl-2	271.45	196	233.73	2.02	9.8
Ctrl-3	153.15	133	143.08	2.03	9.7
AXER #1-1	238.15	283	260.58	2.05	9.4
AXER #1-2	236.15	269	252.58	2.05	9.5
AXER #1-3	190.20	304	247.10	2.08	9.6
AXER #4-1	97.90	141	119.45	2.02	9.7
AXER #4-2	147.15	173	160.08	2.02	9.9
AXER #4-3	113.70	169	141.35	2.02	9.8

Transcriptomic (RNAseq) analysis revealed changes in gene expression caused by AXER depletion. In comparison to control (Ctrl), 8272 genes of AXER #1 and 6914 genes of AXER #4 were detected as significantly changed (differentially expressed genes, DEGs; Figure 17: B). The gene expression profiles of three conditions (Ctrl, AXER #1 and AXER #4) were compared, and the data was illustrated using heatmap, Venn diagram and volcano plot. The heatmap demonstrated that AXER (#1 and #4) siRNA-mediated silencing resulted in a different expression of various genes. The inter-sample correlations indicated more similarities between control and AXER #4, than between control and AXER #1 (Figure 17: A). The Venn diagram illustrated the DEGs-overlap, revealing that AXER #1 and AXER #4 were sharing 4481 differentially expressed genes, in comparison to control (Figure 17: C). Significantly

downregulated and upregulated genes upon AXER depletion were visualized by volcano plots (Figure 18).

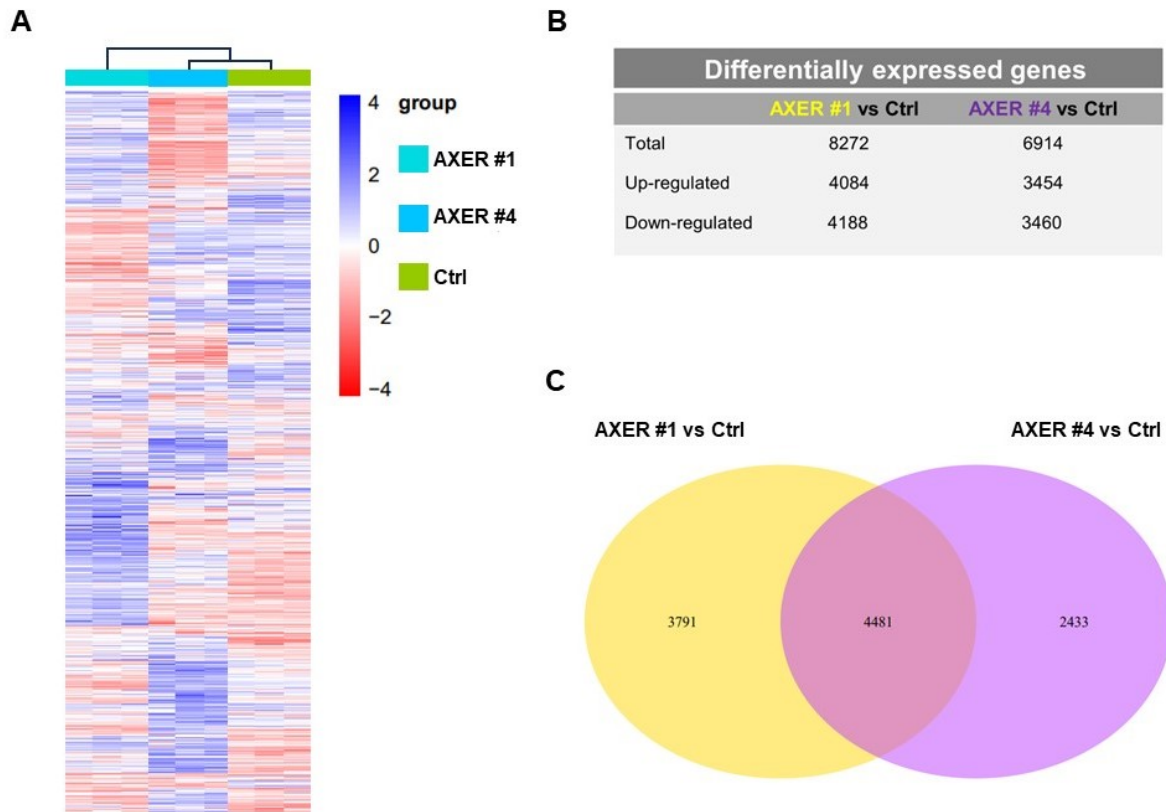


**Figure 17. Comparison of differentially expressed genes (DEGs) upon AXER depletion.** (A) Heatmap used for RNA-seq data visualization of differentially expressed genes for AXER depleted samples in comparison to control. Each column shows one of the conditions (AXER #1, light blue; AXER #4, blue; Ctrl, green), representing group of three independent samples. Intergroup correlations were presented at the top of the heatmap. Cool-to-warm schema shows gene expression: cooler colors (blue shades) show higher expression, while warmer colors (red shades) represent lower expression. The heatmap, created by NovoGene company, was slightly modified by removing additional columns of samples that were not part of this work. (B) The number of differentially expressed genes for AXER #1 and AXER #4 in comparison to control. (C) Venn diagram used for an illustration of the overlapping DEGs for AXER-depleted samples (#1 and #4) in comparison to control.

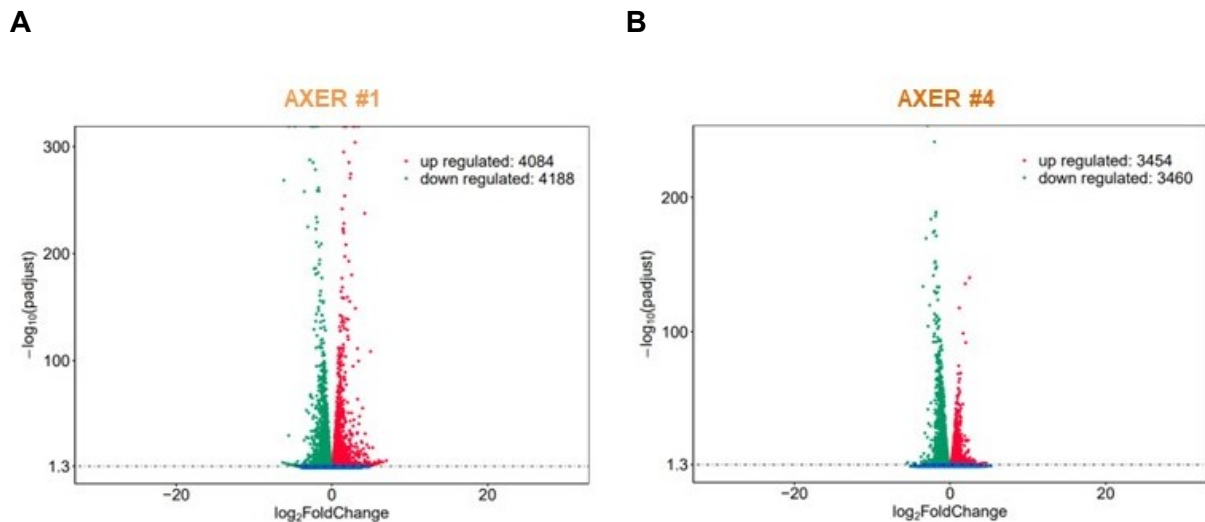


**Figure 18. Comparison of differentially expressed genes (DEGs) upon AXER depletion illustrated by volcano plots.** Volcano plots show log<sub>2</sub> fold change in gene expression in AXER depleted samples (#1 and #4), and statistical significance (padjust; calculated by NovoGene Company). Downregulated genes are shown in green and upregulated genes in red color. **(A)** DEGs for AXER #1, in comparison to control. **(B)** DEGs for AXER #4, in comparison to control.

Importantly, AXER was found as significantly downregulated gene for both AXER siRNA treated samples, in comparison to control. Among the DEGs were genes involved in the ER protein import, protein modification, ER calcium homeostasis, and cellular energy homeostasis. The genes are summarized in Table 14 (Appendix) and details are described below.

Protein-coding genes with specific role in the ER protein translocation were mainly downregulated upon AXER depletion, in comparison to control. The Sec61-complex-coding genes for subunits  $\alpha$  (SEC61A1) and  $\beta$  (SEC61B), showed a significantly decreased regulation, but only in the case of AXER #4. Contrary, the Sec61 $\gamma$ -coding gene (SEC61G) was upregulated (AXER #4). The HSPA5 gene, that encodes for the ER luminal chaperon BiP, was downregulated after the treatment with AXER siRNA #4. Moreover, the HYOU1 gene for the other ER chaperone, Grp170 was downregulated upon AXER depletion. Further, the TRAP-complex-coding genes for subunits  $\beta$  (SSR2) and  $\gamma$  (SSR3) were found to be significantly downregulated for both AXER-depleted samples (#1 and #4), while  $\alpha$  (SSR1) and  $\delta$  (SSR4) subunits -coding genes were significantly downregulated for AXER #1 only. Regarding the protein glycosylation, the genes for oligosaccharyl-transferase complex (OST) catalytic subunits, STT3A and STT3B, showed down-regulation, excluding STT3A for AXER #4. On the other hand, the gene that encodes for the signal recognition particle receptor subunit  $\alpha$  (SR $\alpha$ ; gene SRPRA), involved in the co-translational protein transport to the ER, showed a significant up-regulation for both AXER #1 and AXER #4. Furthermore, the translocating chain-

associating membrane protein1 (TRAM1) and protein 2 (TRAM2) -coding genes were significantly upregulated for AXER #1 and downregulated for AXER #4. The same dysregulation was detected regarding Sec62, involved in the post-translational protein transport to the ER.

The genes (and gene isoforms) that encode for proteins involved in the ER calcium homeostasis and cellular energy homeostasis show a different level of regulation after AXER silencing. A significant decreased regulation (AXER #4) was detected for the ATP2A2 gene that encodes for the ER membrane calcium pump SERCA2. The isoform of AMPK-coding gene for catalytic subunit- $\alpha$ 1, PRKAA1 was significantly upregulated for AXER #1 and downregulated for AXER #4, while the isoform PRKAA2 (subunit- $\alpha$ 2) showed a decreased regulation in the case of AXER #1. The isoform PRKAB2 (encodes for the regulatory subunit- $\beta$ 2) and isoform PRKAG2 (encodes for the regulatory subunit- $\gamma$ 2) were upregulated after AXER silencing. The gene that encodes the regulatory subunit- $\gamma$ 1 (isoform PRKAG1) was downregulated in the case of AXER #1. A decreased regulation was detected for the genes that encode for two AMPK-activators; the CAMKK2 gene (CaMKK2 or CaMKK $\beta$  activator) was downregulated for both AXER-depleted samples, while STK11 (LKB1 activator) was upregulated for AXER #1 only. Regarding the CALM1 gene, that encodes for Calmodulin1, AXER #1 showed reduced regulation, and AXER #4 showed elevated regulation. Further, the PFKFB gene, that codes for 6-phospho-2-fructo kinase (the regulator of glycolytic process, phosphorylated by an activated AMPK) was dysregulated by loss of AXER. Precisely, AXER #1 revealed an up-regulation, while AXER #4 revealed a down-regulation of PFKFB2.

The gene that was significantly upregulated for both AXER-depleted samples was SQSTM1. The multifunctional protein encoded by this gene, was found to take part in the AMPK-signaling pathway, and induces autophagy and apoptosis (Yu et al., 2021).

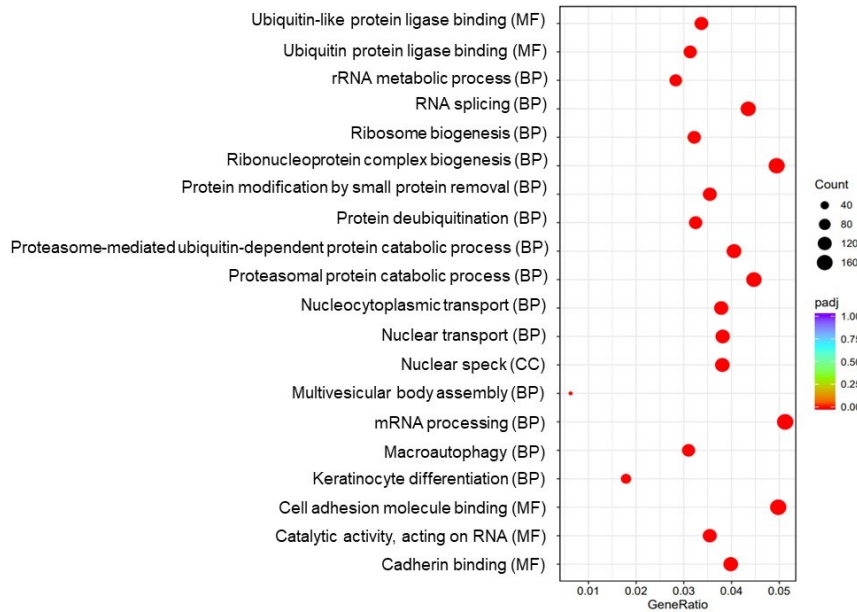
Regarding the ER stress and unfolded protein response (UPR), the three genes that code for IRE1 (ERN1), PERK (EIF2AK3) and ATF6 (ATF6) were downregulated after the treatment with AXER siRNA #4, while AXER #1 sample showed a decreased regulation of ATF6 only. On the other hand, the sample AXER #1 revealed an increased regulation of the CHOP-coding gene (DDIT3), that works as apoptosis inducer (Nishitoh, 2012).

### III.2.1. GO enrichment analysis

The Gene Ontology (GO) enrichment analysis was used to determine the biological significance of changes in the gene expression levels. The DEGs are categorized by GO annotations, and corresponding description is associated with one of the three GO terms: biological process (BP), cellular component (CC) and molecular function (MF).

Of note, some of the described GO terms (below) were not presented in Figure 19 (A and B) and Figure 20 (A and B), that include only the top 20 (n=20) GO terms of the DEGs from AXER #1 and AXER #4, respectively.

**A**



**B**

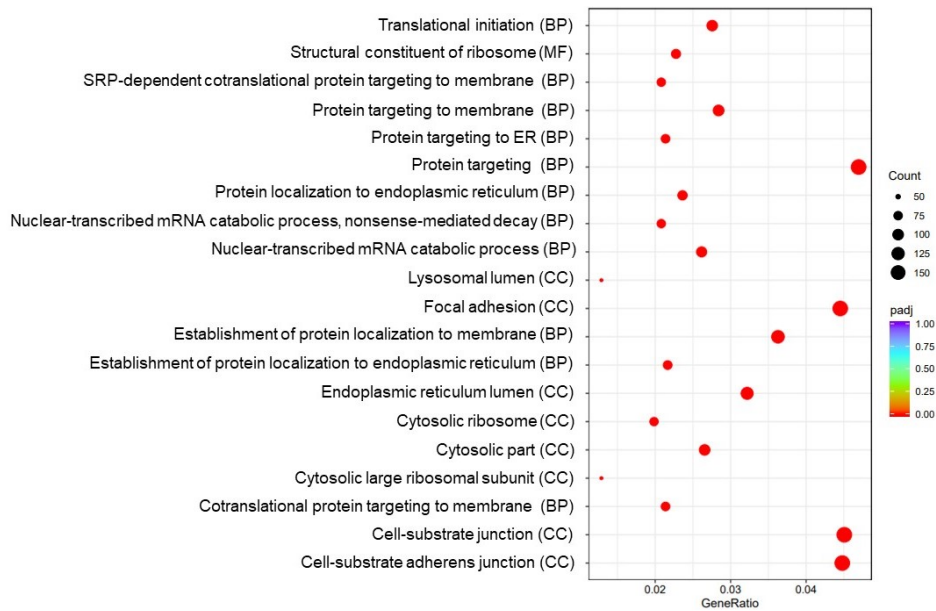
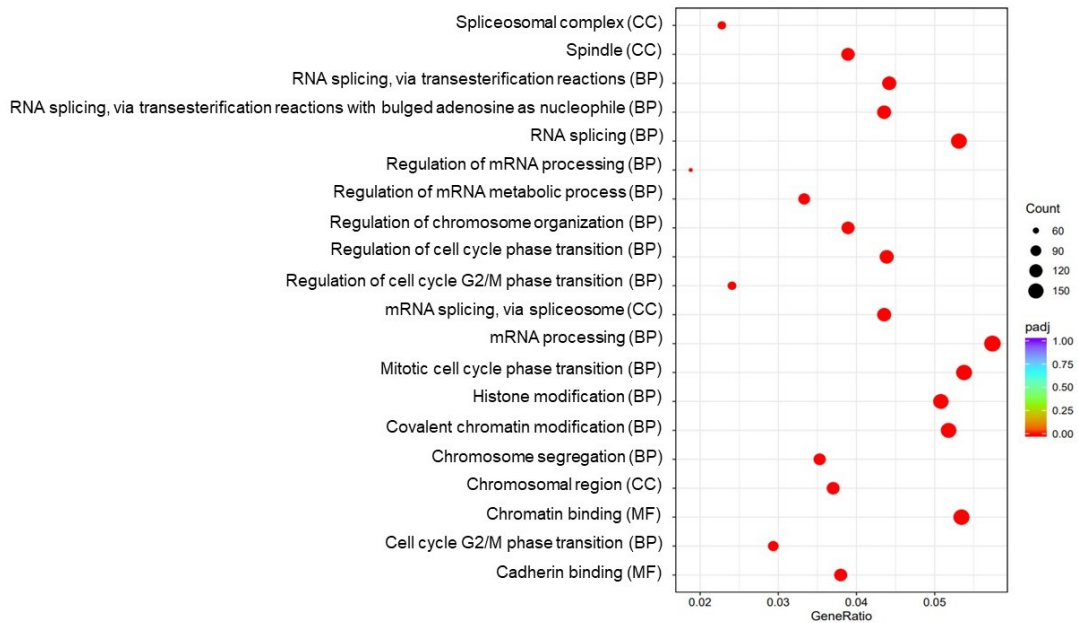


**Figure 19. Gene Ontology (GO) enrichment analysis of differentially expressed genes (DEGs) from the AXER siRNA #1 treatment.** The GO annotation (GO term) is on the y-axes; and the gene ratio on x-axis is the relative gene abundance in corresponding term. Rainbow schema shows adjusted p-value from statistical analysis. The bubble plots, created by NovoGene company, were slightly modified by adding the GO term (BP, biological process;

CC, cellular component; or MF, molecular function) next to the related GO annotation. **(A)** GO-terms (n=20) of upregulated genes. **(B)** GO-terms (n=20) of downregulated genes.

**A**



**B**

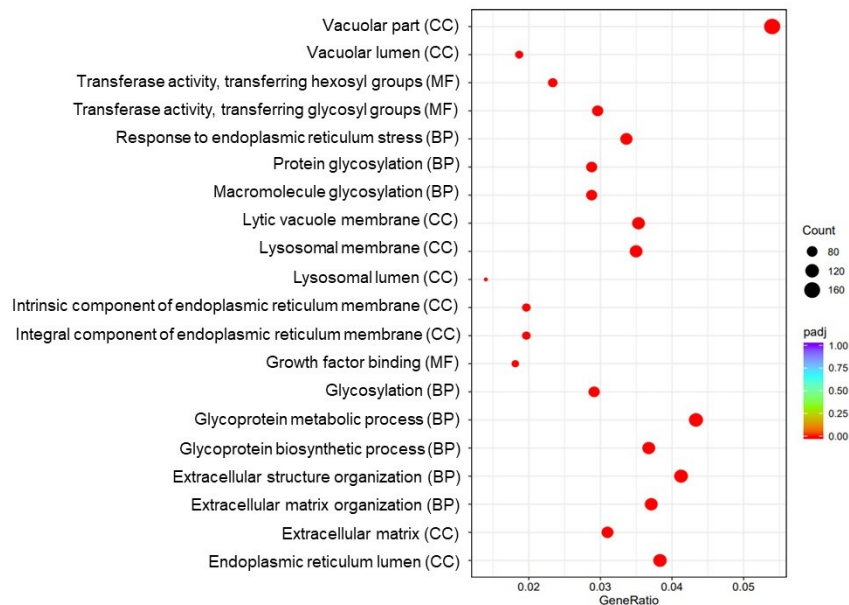


**Figure 20. Gene Ontology (GO) enrichment analysis of differentially expressed genes (DEGs) from the AXER siRNA #4 treatment.** The GO annotation (GO term) is on the y-axes; and the gene ratio on x-axis is the relative gene abundance in corresponding term. Rainbow schema shows adjusted p-value from statistical analysis. The bubble plots, created by NovoGene company, were slightly modified by adding the GO term (BP, biological process; CC, cellular component; or MF, molecular function) next to the related GO annotation. **(A)** GO-terms (n=20) of upregulated genes. **(B)** GO-terms (n=20) of downregulated genes.

In the case of AXER #1 it was found that some of the GO terms of significantly upregulated genes were “proteasome-mediated ubiquitin-dependent protein catabolic process”, “protein localization to mitochondrion”, “stress-activated protein kinase signaling cascade”, “protein serine-threonine kinase activity”, “modification-dependent protein binding”, “protein dephosphorylation” and “autophagy” (macroautophagy). Most of these terms included upregulated genes SQSTM1, STK11, and AMPK gene-isoforms (PRKAA1, PRKAB2 and PRKAG2). Among the GO terms of significantly downregulated genes were “SRP-dependent cotranslational protein targeting to membrane” and “protein localization to endoplasmic reticulum”. Both of these biological processes involved the SSR3 gene, RPL-genes that encode for the components of the large ribosomal subunit, and SRP-genes that encode for the components of the signal recognition particle (SRP) complex. Further, the GO terms that included downregulated genes were “response to endoplasmic reticulum stress”, “endoplasmic reticulum unfolded protein response”, “endoplasmic reticulum chaperone complex”, “protein N-linked glycosylation via asparagine”, “integral component of endoplasmic reticulum membrane”, and “intrinsic component of endoplasmic reticulum membrane” (with SLC35B1 (AXER) as one of the DEGs).

The GO terms of significantly upregulated genes for AXER #4 were mainly related to RNA splicing and regulation of cell cycle. Comparable to AXER #1, the GO term “protein serine/threonine kinase activity” that included genes SQSTM1, and AMPK gene-isoforms (PRKAB2 and PRKAG2), was upregulated as well as terms “modification-dependent protein binding” and “ubiquitin protein ligase binding” that included SQSTM1 gene. Moreover, the GO terms of significantly downregulated genes were “integral component of endoplasmic reticulum membrane” and “intrinsic component of endoplasmic reticulum membrane” with SLC35B1 (AXER) as one of the DEGs; then, “endoplasmic reticulum quality control compartment”, “endoplasmic reticulum lumen”, “response to endoplasmic reticulum stress”, “endoplasmic reticulum unfolded protein response”, “endoplasmic reticulum chaperone complex”, “protein glycosylation” and “protein exit from endoplasmic reticulum”.

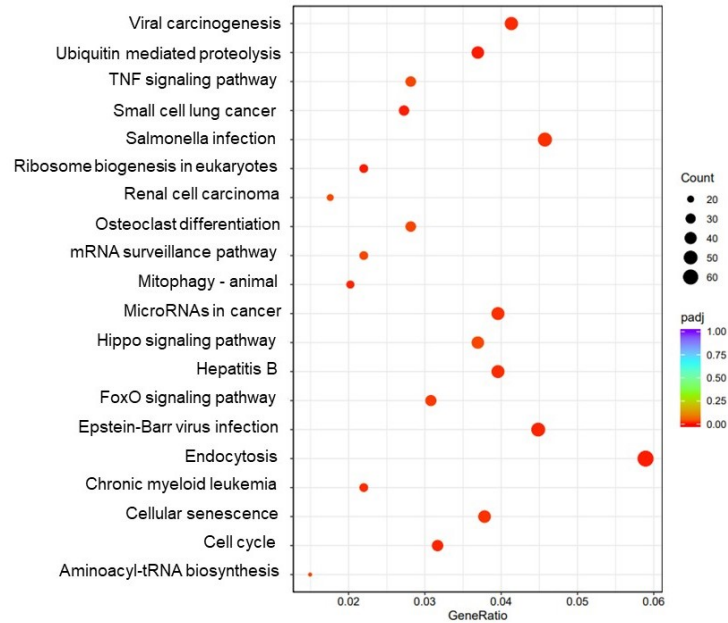
Taken together, AXER depleted samples (#1 and #4) revealed a significant gene dysregulation for various GO terms, including those related to the process of ubiquitination, protein serine/threonine kinase activity, ER membrane and ER lumen, ER stress, ER chaperones and protein glycosylation.

### **III.2.2. KEGG pathway analysis**

Further transcriptomic analysis was based on cellular pathways and their corresponding genes. The Kyoto Encyclopedia of Genes and Genome (KEGG) database was used to define

the gene-pathway relation. Significantly dysregulated pathways after AXER-gene silencing, in comparison to control are shown in Figure 21 (AXER #1) and Figure 22 (AXER #4).

**A**



**B**

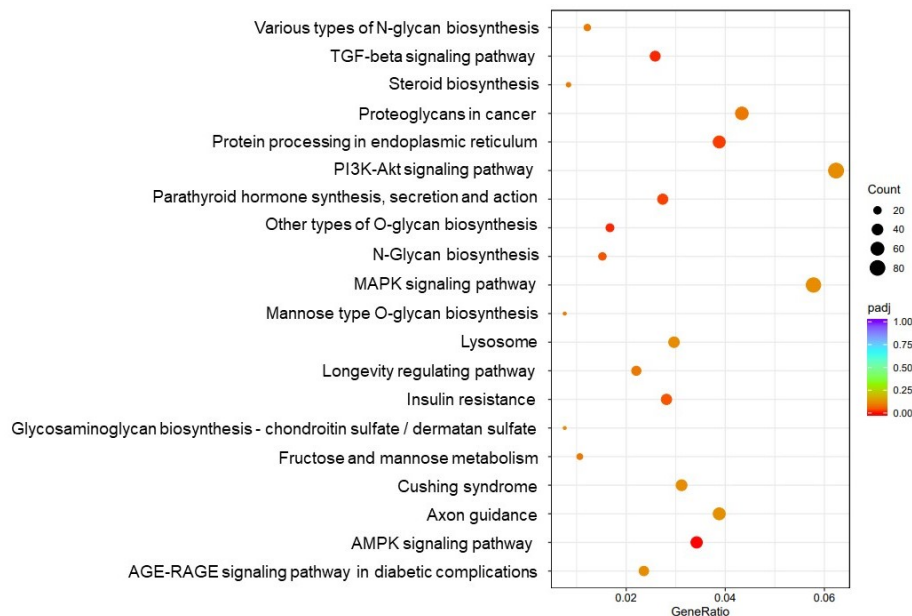
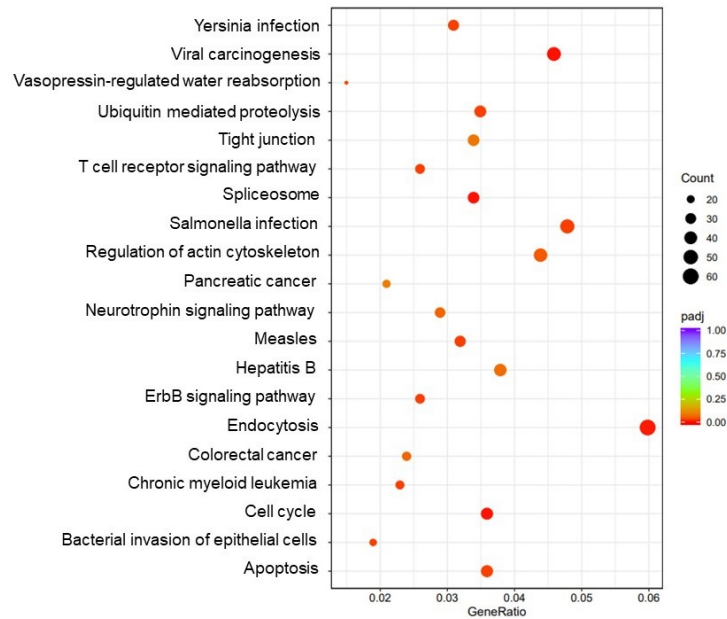


**Figure 21. KEGG enrichment analysis of differentially expressed genes from the AXER siRNA #1 treatment.** The KEGG term (pathway) is on the y-axes; and the gene ratio on x-axis is the relative gene abundance in corresponding term. Rainbow schema shows adjusted p-value from statistical analysis. The bubble plots were created by NovoGene company (to be readable, the pathway descriptions were re-written). **(A)** KEGG-terms (n=20) of upregulated genes. **(B)** KEGG-terms (n=20) of downregulated genes.

A



B

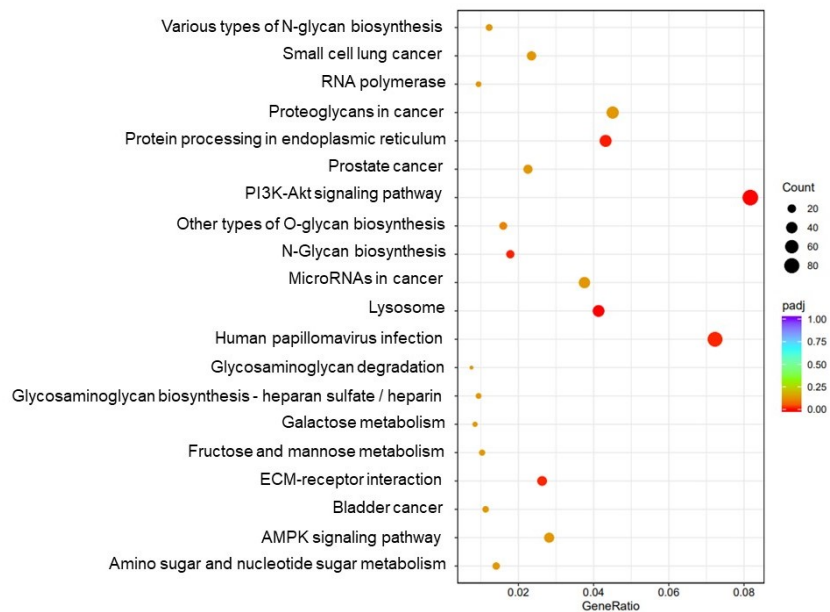


**Figure 22. KEGG enrichment analysis of differentially expressed genes from the AXER siRNA #4 treatment.** The KEGG term (pathway) is on the y-axes; and the gene ratio on x-axis is the relative gene abundance in corresponding term. Rainbow schema shows adjusted p-value from statistical analysis. The bubble plots were created by NovoGene company (to be readable, the pathway descriptions were re-written). **(A)** KEGG-terms (n=20) of upregulated genes. **(B)** KEGG-terms (n=20) of downregulated genes.

Both AXER-depleted samples showed up-regulation for various pathways, including those related to cell cycle and apoptosis. Considering that HeLa cells are cancer cells, most of the upregulated pathways were related to carcinogenesis. Significantly decreased gene regulation for pathway linked to the “protein processing in endoplasmic reticulum” was detected after AXER silencing. Also, the AMPK signaling pathway, that maintains the cellular energy homeostasis (I.1.3), was significantly downregulated but only for AXER #1. AXER #4 demonstrated a down-regulation regarding the AMPK signaling pathway, but this change was found as non-significant.

### III.3. Quantitative proteomic analysis after AXER silencing

A simplified view, “from DNA to RNA to protein” represents The Central Dogma of molecular biology (Crick, 1970). Although this concept suggests a direct connection between an RNA level and corresponding protein, there is a considerable doubt over the ideal mRNA-protein correlation (Gry et al., 2009; Vogel and Marcotte, 2012; Liu et al., 2016; Buccitelli and Selbach, 2020). All proteins that can be expressed by an organism are presented with the term “proteome”, coined by Marc Wilkins, in 1994 (Parker et al., 2010). One of the techniques for proteome analysis - mass spectrometry (MS), was used in this work with intention to identify the changes in the protein levels after AXER silencing, and subsequently verify the overlapping with the appropriate mRNA levels (from RNA-seq data, III.2).

After 72 h gene silencing, three independent cell samples for each condition (AXER #1, AXER #4, and Ctrl) were collected with a cell scraper and using PBS only (no trypsin; II.2.6). Cells were counted and pelleted instantly. Subsequent mass spectrometry was performed in collaboration with the working group of PD Dr. Andreas Roos (University of Duisburg-Essen). Statistical analysis of proteomic data revealed the differences in protein levels between AXER depleted samples (#1 and #4) and control. Intriguingly, AXER was not found on the list of differently expressed proteins. The reason might be the low level of native AXER in HeLa cells (Hein et al., 2015) as well as the flaw of proteomic approaches that perform less efficiently when implemented for the analysis of membrane proteins (Helbig et al., 2010). Furthermore, the RNA-seq analysis revealed that AXER #1 and AXER #4 share 4481 differentially expressed genes in comparison to control (Figure 17: C), while the proteomic analysis observed a level-alteration of approximately two times less proteins (2166; and only 55 proteins showed significant changes for both AXER-depleted samples compared with control ((AXER #1+AXER #4)/Ctrl). This also correlates with the abovementioned disparity between protein level and its coding transcript.

The results were selected focusing on the proteins that were previously identified as possible components of the AXER interactome (RNA-seq data; III.2) and summarized in Table 13.

**Table 13. Changes in protein level after AXER depletion.** The table shows a subset of the proteomic data. Proteins of interest were selected based on their association with the ER and other results of this work. The row-color indicates a main role of the target protein; biological process and/or molecular function: brown - autophagy; light blue - targeting receptors; olive green - post-translational protein transport; petroleum – ER translocon subunits; light green – ER translocation of proteins and protein glycosylation; light purple – protein glycosylation; red – ER chaperone; light red – the ER calcium homeostasis. For better understanding the extent of change in protein abundance, the detected highest and lowest values (fold change) are given: AXER #1, 5.89 and 0.17; AXER #4, 2.55 and 0.01. p-values are indicated as: \*\*\*  $p < 0.001$ ; \*\*  $p < 0.01$ ; \*  $p < 0.05$ ; or as non-significant (ns) if  $p \geq 0.05$ .

Protein	AXER#1/Ctrl (Fold change; <i>p</i> -value)	AXER#4/Ctrl (Fold change; <i>p</i> -value)	AXER#1/AXER#4 (Fold change; <i>p</i> -value)	(AXER#1+AXER#4)/Ctrl (Fold change; <i>p</i> -value)
SQSTM1	4.97; ***	1.24; **	4.00; ***	3.11; *
SR $\alpha$	1.08; *	1.12; ns	0.97; ns	1.10; ns
SR $\beta$	1.25; **	0.67; ***	1.87; ***	0.96; ns
Sec62	1.30; ***	0.88; ns	1.49; ***	1.09; ns
Sec61 $\alpha$ 1	0.89; ns	0.79; *	1.13; *	0.84; **
Sec61 $\beta$	0.81; **	0.68; ***	1.19; *	0.75; ***
Sec61 $\gamma$	0.77; **	0.59; ***	1.31; **	0.68; ***
TRAP $\alpha$	0.84; *	0.92; ns	0.91; ns	0.88; *
TRAP $\gamma$	0.81; **	0.84; **	0.97; ns	0.82; ***
TRAP $\delta$	0.81; **	0.93; ns	0.86; *	0.87; *
STT3A	0.85; *	1.06; ns	0.80; ***	0.96; ns
STT3B	0.59; ***	0.56; ***	1.04; ns	0.57; ***
BiP (Grp78)	0.91; ns	0.79; ***	1.16; *	0.85; **
SERCA2	0.87; *	0.65; ***	1.35; ***	0.76; **
Calmodulin1	0.35; ***	0.32; ***	1.08; ns	0.34; ***

Proteomic analysis showed that AXER depletion caused the changes in abundance of proteins that are involved in protein import to the ER (SR $\alpha$  and SR $\beta$ ; subunits of Sec61 and TRAP complex; BiP) and the ER calcium homeostasis (SERCA2; Calmodulin1; BiP). Overlapping with the RNA-seq results, the abundance of SQSTM1 was increased after AXER silencing. The change in protein expression was detected in samples treated with AXER siRNAs (#1 or #4) in comparison to control as well as compared to each other.

The Sec61-complex subunits ( $\alpha$ ,  $\beta$  and  $\gamma$ ) showed the reduced protein abundance, except in the case of AXER #1 regarding Sec61 $\alpha$ . A difference in the levels of all three Sec61-complex subunits was detected between AXER #1 and AXER #4. The subunit  $\gamma$  of TRAP-complex showed reduced abundance for AXER-depleted samples, while levels of subunits  $\alpha$  and  $\delta$  were lower for AXER #1 only. Compared to each other, conditions #1 and #4 showed the difference in TRAP $\delta$  levels. The subunit  $\beta$  of TRAP-complex was not found in the proteomic data. The abundance of the ER luminal chaperon BiP was reduced only for AXER #4, showing a difference between AXER-depleted samples. The ER membrane calcium pump SERCA2 and

Calmodulin1 showed a reduction after AXER depletion. While SERCA2 showed a difference between conditions #1 and #4, the significantly low levels of Calmodulin1 were almost identical for AXER #1 and AXER #4. Regarding OST-complex, only the catalytic subunits STT3B was reduced for both AXER-depleted samples. The SR subunits,  $\alpha$  and  $\beta$ , showed an elevation for AXER #1. Contrary, condition #4 revealed a reduction regarding SR $\beta$ . Increased abundance of Sec62 was detected for AXER #1 only.

Together, AXER #1 plus AXER #4, showed a difference in protein levels when compared to control. That applies for most selected proteins, excluding SR $\alpha$ , SR $\beta$ , Sec62 and STT3A.

#### **III.4. RT-qPCR and Western blot analysis used to verify the “-omic” results**

Both “-omic” data (transcriptomic, RNA-seq, III.2; and proteomic, III.3) revealed that potential interaction partners of AXER, at the genetic or protein level, are components of the ER. Many of those identified candidates are involved in the ER protein import and calcium homeostasis. Also, an extreme gene up-regulation and elevated protein abundance was detected for the cytosolically located protein SQSTM1. Genes/proteins with similar trend of regulation/ expression after AXER depletion are shown in Table 15 (Appendix).

To validate the differentially expressed genes (DEGs) identified by RNA-seq, the RT-qPCR was performed after 72 hours AXER siRNA-mediated silencing. Results showed differences in the mRNA expression levels between samples treated with AXER siRNA (#1 and #4), in comparison to control. Nine genes were selected to be verified: two subunits of the Sec61-complex,  $\alpha$  and  $\beta$ ; the translocon-associated protein (TRAP) complex subunits,  $\alpha$  and  $\beta$ ; signal recognition particle receptor (SR)  $\alpha$  and  $\beta$ ; the ER luminal chaperon BiP; sarco/endoplasmic reticulum calcium ATPase (SERCA); and sequestosome 1 (SQSTM1) (Figure 23).

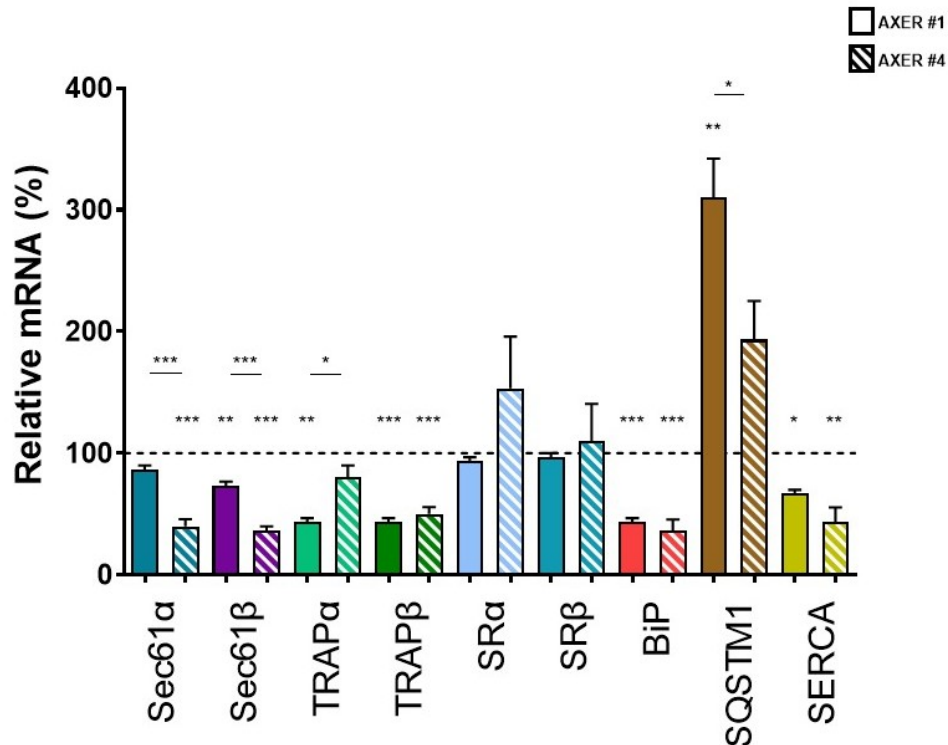


**Figure 23. mRNA expression levels after AXER silencing validated by RT-qPCR.** HeLa cells were transfected with AXER (#1 or #4) targeting siRNA or with control siRNA. After 72 hours cells were harvested, and the total RNA was isolated and transcribed into complementary DNA (cDNA). Equal amounts of cDNA for each condition were subjected to qRT-PCR, using gene-specific Taqman probes. The  $\Delta$ Ct-values were calculated using  $\beta$ -actin as a standard. Values were normalized based on control siRNA-treated cells (Ctrl; dashed line). AXER #1 – non-pattern bars; AXER #4 – bars with pattern. Reported data are from three independent experiments and shown with the standard error of the mean (SEM). Statistical significance between conditions was determined using one-way ANOVA. Significant changes are indicated by asterisks: \*\*\*  $p < 0.001$ ; \*\*  $p < 0.01$ ; \*  $p < 0.05$ ; or as non-significant (ns) if  $p \geq 0.05$ . Statistical analyses were performed using GraphPad Prism version 10.

The Sec61 $\alpha$  mRNA expression level was significantly decreased for AXER #4, while both AXER samples (#1 or #4) showed the significantly reduced Sec61 $\beta$  mRNA. Also, the significant reduction for TRAP $\beta$  mRNA was observed upon AXER depletion. Regarding TRAP $\alpha$ , significant reduction was detected for AXER #1 only. Interestingly, the BiP mRNA and SERCA2 mRNA levels were significantly decreased by AXER silencing, suggesting a mechanistic reduction in the ER calcium concentration as will be discussed later (IV.1). The levels of mRNA encoding for SR $\alpha$  and SR $\beta$  were elevated for AXER #4, but this change was found as non-significant. On the other hand, a strong increase of the SQSTM1 mRNA was observed after AXER knockdown, that was significant for AXER #1. Discrete differences were noticed between RT-qPCR results and RNA-seq data, most likely due to distinct sensitivity of these methods. In general, the expression pattern of the target DEGs was verified by RT-qPCR.

Next, Western blot (WB) analysis was performed to verify the changes in protein abundance after AXER depletion. Majority of the WB-target proteins were identified by mass spectrometry (selected in Table 13), including the ER translocon and its accessory proteins, receptors, and chaperone. As the RNA-seq analysis revealed that some of the differentially expressed genes are involved in the cellular energy homeostasis (e.g., AMPK and CaMKK2; l.1.3), Western blot analysis was also used to determine the abundance of their corresponding proteins. Considering that phosphorylation is a key-step of the AMPK activation, the abundance of the phosphorylated AMPK (pAMPK) was evaluated. As earlier, two different siRNAs were used for 72 h of AXER silencing (#1 and #4) and compared against the control siRNA treatment (Ctrl).

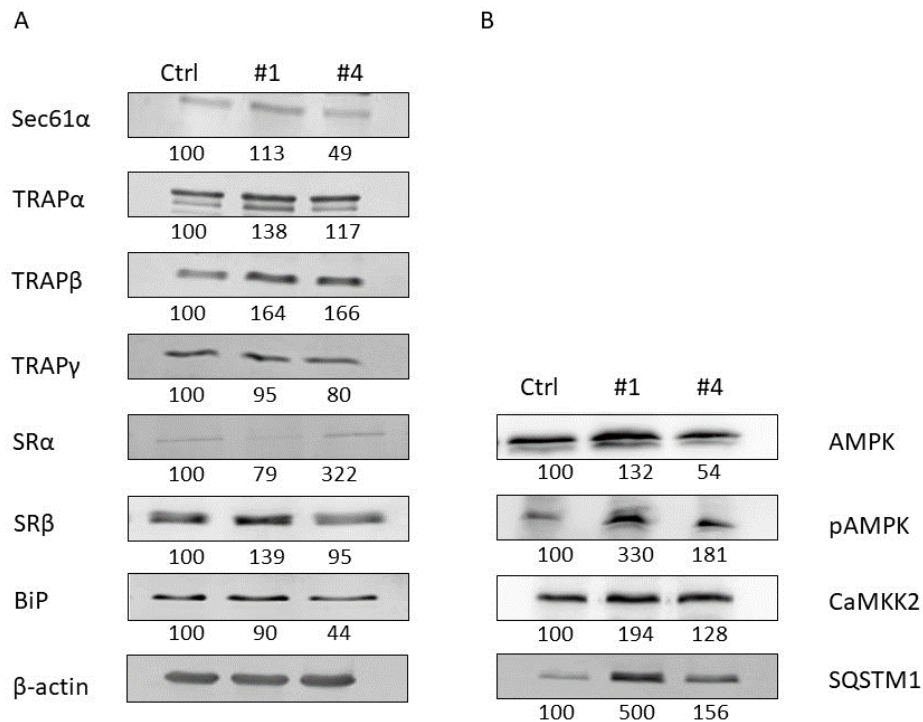


**Figure 24. Different protein abundance in response to AXER silencing, determined by Western blot analysis.** HeLa cells were transfected with AXER (#1 or #4) targeting siRNA or with control siRNA (Ctrl). After 72 hours cells were harvested, processed into lysate, and, following the SDS-PAGE (II.4.1), Western Blot (II.4.2) and immunological detection, a respective protein abundance was detected. Beta-actin served as a protein loading control. Evaluation was performed with the Fusion SL and ImageQuant software. The relative protein abundance for each condition was compared to control. Numbers show the average abundance of a specific protein for each condition. One representative blot is from three independent repeats. **(A)** Proteins involved in targeting the nascent polypeptide to the ER; polypeptide ER import, folding and modification; and ER calcium homeostasis **(B)** proteins involved in the AMPK-signaling pathway. Ctrl, control; #1, AXER #1; #4, AXER #4.

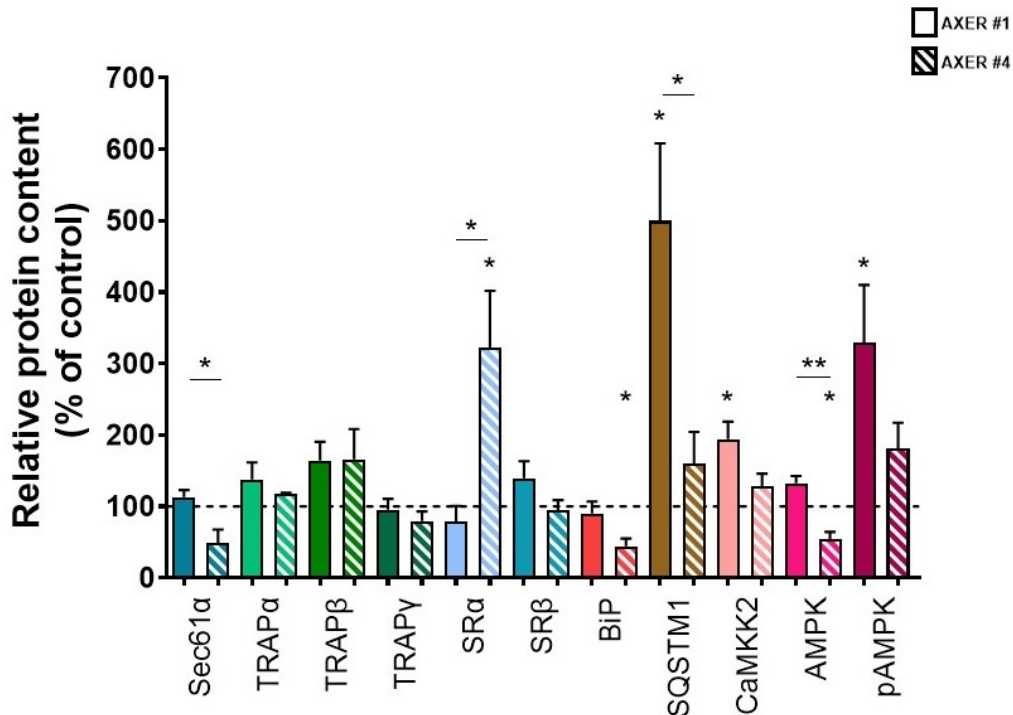


**Figure 25. Statistical analysis of Western blot results upon AXER depletion.** Protein levels are shown for AXER #1 (non-pattern bars) and AXER #4 (bars with pattern). Values were normalized based on the control (Ctrl; dashed line). Reported data are from three independent experiments and shown with the standard error of the mean (SEM). Statistical significance between conditions was determined using one-way ANOVA. Significant changes are indicated by asterisks: \*\*  $p < 0.01$ ; \*  $p < 0.05$ . Statistical analyses were performed using GraphPad Prism version 10.

Quantitative WB analysis revealed a different abundance of the target proteins between AXER conditions (#1 and #4) and control as well as in comparison to each other (Figure 24). However, the statistical analysis demonstrated a non-significant change in protein abundance for most of the target proteins; or significant change for only one of the AXER conditions (#1 or #4; Figure 25); most likely due to a result-fluctuation of the experimental repeats.

Sec61-complex subunit  $\alpha$ , was slightly elevated (AXER #1) or decreased (AXER #4), upon AXER depletion. TRAP-complex subunits,  $\alpha$  and  $\beta$  showed enhanced abundance, while  $\gamma$  subunit was reduced. SR $\beta$  displayed increased abundance by AXER #1 siRNA treatment, and slightly reduced level after the AXER #4 siRNA treatment. Yet, none of these changes was found as significant. On the other hand, SR $\alpha$  was slightly decreased for AXER #1, but significantly more abundant for AXER #4. The ER chaperone BiP showed reduced abundance after AXER silencing, and the change was significant in the case of AXER #4. Very similar to what was observed earlier by RNA-seq analysis (III.2), proteomic analysis (III.3) and RT-qPCR approach (above), the expression of SQSTM1 was increased (AXER #4) or significantly elevated (AXER #1). The results indicate that the AXER depletion triggers an autophagy event (Yu et al., 2021). Furthermore, the master regulator of cellular energy metabolism, AMPK

displayed an increased abundance, and the significantly increased level of phosphorylated AMPK (pAMPK) after the AXER #1 siRNA treatment. The AMPK:pAMPK ratio was 1:2.5. In the case of AXER #4, AMPK was significantly reduced, and the pAMPK abundance was increased, showing the AMPK:pAMPK ratio of 1:3.4. Therefore, both conditions (#1 and #4) revealed a pronounced phosphorylation of the available AMPK, indicating activation of this energy sensor. Moreover, CaMKK2 (CaMKK $\beta$ ), involved in the activation of AMPK, was significantly elevated for AXER #1, or increased in the case of AXER #4. In sum, abundance of the target proteins upon AXER depletion, probed by Western blot, showed only a slight overlap with the proteomic results (III.3). This could be due to the different sensitivity and specificity of the experimental techniques.

### III.5. Changes in cell metabolism due to AXER depletion

To comprehend involvement of AXER in the metabolic processes and possibly define its role in the ER energy homeostasis, two live-cell metabolic assays were established: a) the pH-Xtra assay to estimate glycolytic activity, and b) the MitoXpress Xtra oxygen consumption assay to evaluate mitochondrial respiration. For both assays a soluble metabolic sensor changes fluorescent signal intensity due to changes in extracellular acidification (indicator of glycolytic activity; Figure 13, and Figure 14: B) or oxygen level (indicator of mitochondrial respiration; Figure 13, and Figure 14: A). As described in II.4.4.1 and II.4.4.2, the AXER-depleted HeLa cells were used in suspension mode (Figure 26, and Figure 27: A), while adherent HeLa cells served as control (Figure 27: B).

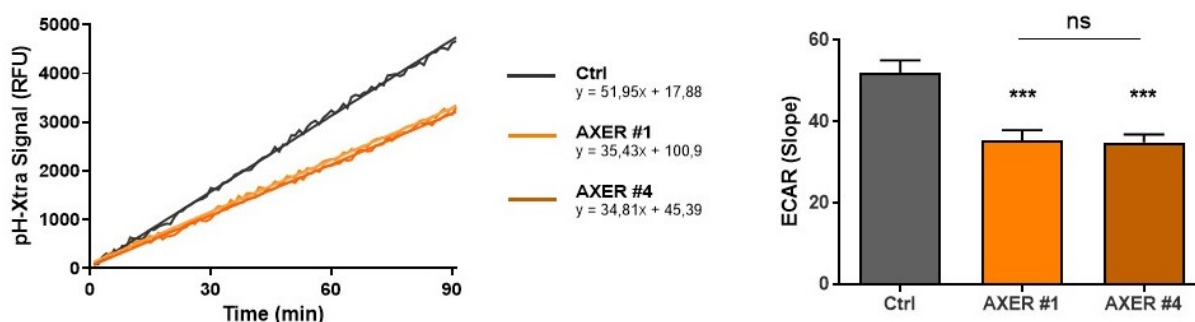
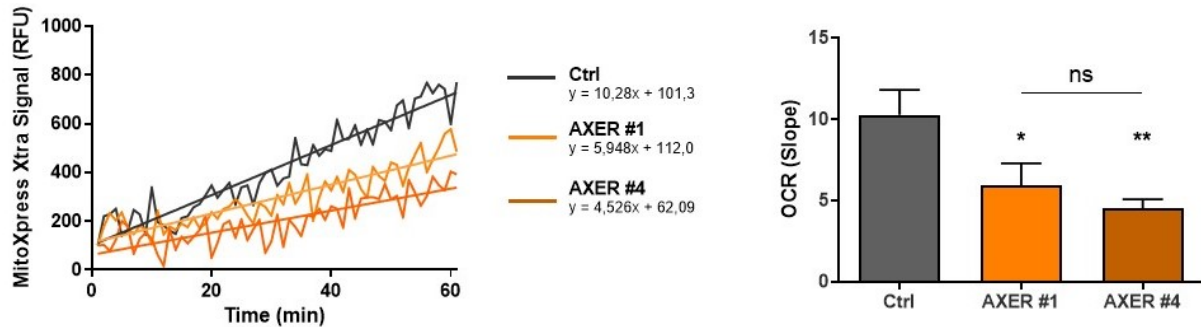


**Figure 26. Extracellular acidification upon AXER depletion.** As a pre-step, HeLa cells were transfected with two AXER siRNAs (#1 and #4) or control siRNA (Ctrl). After 72 hours cells were harvested, counted, and cell number was adjusted to  $1.5 \times 10^5$  cells per well (90  $\mu$ l) for each condition. To remove CO<sub>2</sub>, cells were placed in the CO<sub>2</sub>-free incubator for 2 hours. Afterwards, cells were seeded in a 96-well plate (black well/clear bottom), corresponding reagent was added to the wells, and measurement was started. Cells were considered as suspension cells (not attached to the plate surface). The fluorescent signal for each condition was evaluated for 90 min. The rate of change in fluorescent signal (pH-Xtra signal; relative fluorescence units, RFU) was calculated by linear regression (slope calculation; left graph) and

indicates the rate of measured metabolic activity; plotted as extracellular acidification rate (ECAR; right graph). The lower rates serve as indicator for reduced metabolic activity. Reported data are from at least three independent experiments and shown with the standard error of the mean (SEM). Statistical significance between groups was determined using one-way ANOVA. Significant changes are indicated by asterisks: \*\*\*  $p < 0.001$ ; or as non-significant (ns) if  $p \geq 0.05$ . Statistical analyses were performed using GraphPad Prism version 10.

A



B

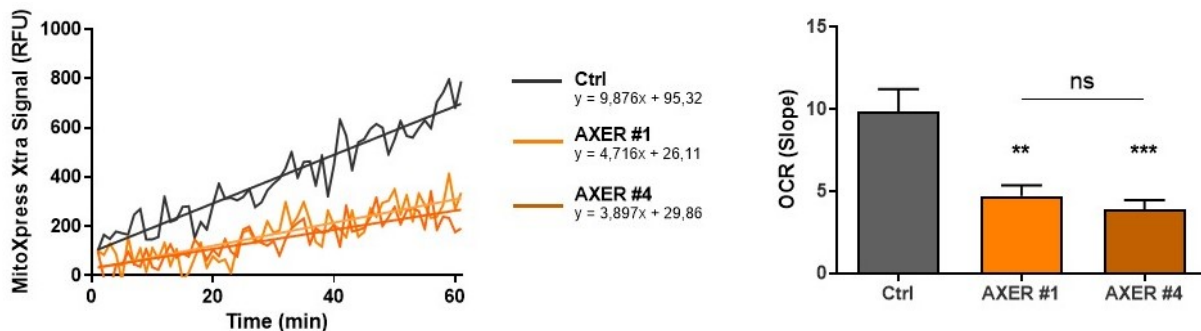


**Figure 27. Mitochondrial respiration upon AXER depletion.** As a pre-step, HeLa cells were transfected with two AXER siRNAs (#1 and #4) or control siRNA (Ctrl). After 72 hours cells were harvested, counted, and cell number was adjusted to  $1.5 \times 10^5$  cells per well (90  $\mu$ l) for each condition. Afterwards cells were seeded in a 96-well plate (black well/clear bottom), corresponding reagent was added to the wells, and measurement was started. The cells were in suspension mode (**A**). For cell adhesion, the plate (adherent cells; **B**) was placed in the incubator for 2.5 hours, before the measurement. The fluorescent signal for each condition was evaluated for 60 min. (**A**, **B**) The rate of change in fluorescent signal (MitoXpress Xtra signal; relative fluorescence units, RFU) was calculated by linear regression (slope calculation; A and B, left) and indicates the rate of measured metabolic activity; plotted as oxygen consumption rate (OCR; A and B, right). The lower rates serve as indicator for reduced metabolic activity. Reported data are from at least three independent experiments and shown with the standard error of the mean (SEM). Statistical significance between groups was determined using one-way ANOVA. Significant changes are indicated by asterisks: \*\*\*  $p < 0.001$ ; \*\*  $p < 0.01$ ; \*  $p < 0.05$ ; or as non-significant (ns) if  $p \geq 0.05$ . Statistical analyses were performed using GraphPad Prism version 10.

In comparison to control (Ctrl, dark grey), both samples transfected with AXER siRNAs (AXER #1, light orange; and AXER #4, dark orange) showed a reduction in fluorescent signal and a lower rate of the sensor signal change. This stays for both assays: pH-Xtra that measures extracellular acidification (Figure 26); and MitoXpress Xtra that measures mitochondrial respiration (Figure 27), suggesting the drop in total cell energy metabolism after AXER depletion. There was no significant difference between AXER #1 and AXER #4, for both measured metabolic activities (Figure 26, right; and Figure 27: A and B, right). Although the change in oxygen consumption rate (OCR; slope) between Ctrl and both AXER samples (#1 and #4) was a less pronounced in the case of suspension HeLa cells (Figure 27: A, right), in comparison with the adherent HeLa cells (Figure 27: B, right), this specific experimental condition did not affect the result reliability (statistical significance).

Biomolecular luminescence complementation (BiLC) approach was utilized to further investigate the AXER interactome as well as the ER translocon-BiP interaction in intact cells. The results are described in the subsequent sections.

### **III.6. Detection of dynamic protein-protein interactions in living cells using the NanoBiT system**

Transient, and thus labile protein-protein interactions (PPI) can be disrupted easily during the process of sample preparation. Consequently, the downstream protein analysis often provides limited and incomplete description of the “living” interactome. To avoid this, the interactions in living cells were measured using the NanoLuc Binary Technology (NanoBiT) system. As described earlier (II.4.3), the LgBiT and SmBiT subunits were fused to proteins of interest and the corresponding fusion constructs were expressed in cells for 24 hours. In case the fusion proteins interact, the luciferase subunits were brought into close contact and form a functional luciferase enzyme. After adding the substrate furimazine, the luciferase provided a bright, luminescent signal that was measured. The principle of NanoBiT system was presented in Figure 12. To confirm the sufficient expression of LgBiT-generated fusion constructs, two further measurements were performed after substrate (furimazine) addition. Cells were semi-permeabilized by adding digitonin, and eventually the expression of LgBiT-tagged construct was verified by complementation approach with the synthetic HaBiT peptide showing very high affinity for the LgBiT (Table 5; II.4.3; Sicking et al., 2021).

The live-cell assay was used to expand recent studies from our lab that demonstrate interactions of various ER membrane proteins that are part of the ER protein translocase. Of all described interactions (Sicking et al., 2021), the PPI between Sec61 $\beta$  and Sec63 was the only interaction with ER-luminally located subunits of the luciferase that was tested and

confirmed, demonstrating that the functional luciferase was efficiently reconstituted in the ER lumen. More available plasmids with lumenally located LgBiT and SmBiT tags (created by Dr. Sicking, Saarland University) enable further testing of PPI in the ER lumen. Also, new constructs were created in this work (Table 9) and AXER interactome was examined using a biomolecular luminescence complementation approach.

### III.6.1. The interactions of the Sec61-complex subunits $\beta$ and $\gamma$

Sec61 $\alpha$ , the channel-forming subunit of the Sec61-complex, is accompanied by the two tail-anchored proteins, Sec61 $\beta$  and Sec61 $\gamma$  (Pfeffer et al., 2015; 2016). In a 1:1:1 stoichiometry the three subunits form the functional Sec61-complex (Figure 28: A and B). The NanoBiT system was used to demonstrate the interaction of Sec61 $\beta$  and Sec61 $\gamma$  in living, intact cells (Figure 28: C-F). Next, the interaction was tested between proteins of different translocon subcomplexes, Sec61 $\gamma$  and Sec63, also with lumenally located LgBiT and SmBiT tags (Figure 28: E and F). As additional positive control, the previously measured Sec61 $\beta$  and Sec63 PPI (Sicking et al., 2021) was run in parallel and used for comparison (Figure 28: C and D).

Further, NanoBiT experiments were performed to demonstrate the interaction of Sec61-complex and the soluble Hsp70-type ER chaperon BiP. The luminal loop 7 of Sec61 $\alpha$  was determined as a BiP binding site (I.4.1; Figure 6; Schäuble et al., 2012). Since tags of the NanoBiT system must interact with each other for the proper determination of a PPI, it was crucial for both tags of fusion proteins to be located on the same side of the ER membrane. The topological structure of Sec61 $\alpha$  shows that it has both N- and C- terminus located in the cytosol (Figure 28: B), making it impractical to test the interactions with a lumenally located partner protein. To avoid possible disturbance of Sec61 $\alpha$  function by introducing the LgBiT- or SmBiT- tag in one of its luminal loops, the solution was to test the BiP interaction with Sec61 $\alpha$ 's "nearest neighbors", Sec61 $\beta$  and Sec61 $\gamma$ . As tail-anchored proteins, the C-terminus of Sec61 $\beta$  and Sec61 $\gamma$  is oriented on the luminal side of the ER (Figure 28: B). In case when luminal facing C-terminus of Sec61 $\beta$  subunit was tagged with LgBiT (Sec61 $\beta$  C LgBiT), the Sec61 $\gamma$  C-terminus was tagged with SmBiT (Sec61 $\gamma$  C SmBiT), and conversely. The SmBiT-tag of Sec63 was on the lumenally oriented N-terminus (Figure 28: B; Sec63 N SmBiT), while BiP SmBiT-tag was inserted upstream of the C-terminal KDEL-coding sequence (BiP SmBiT; Jin et al., 2017).

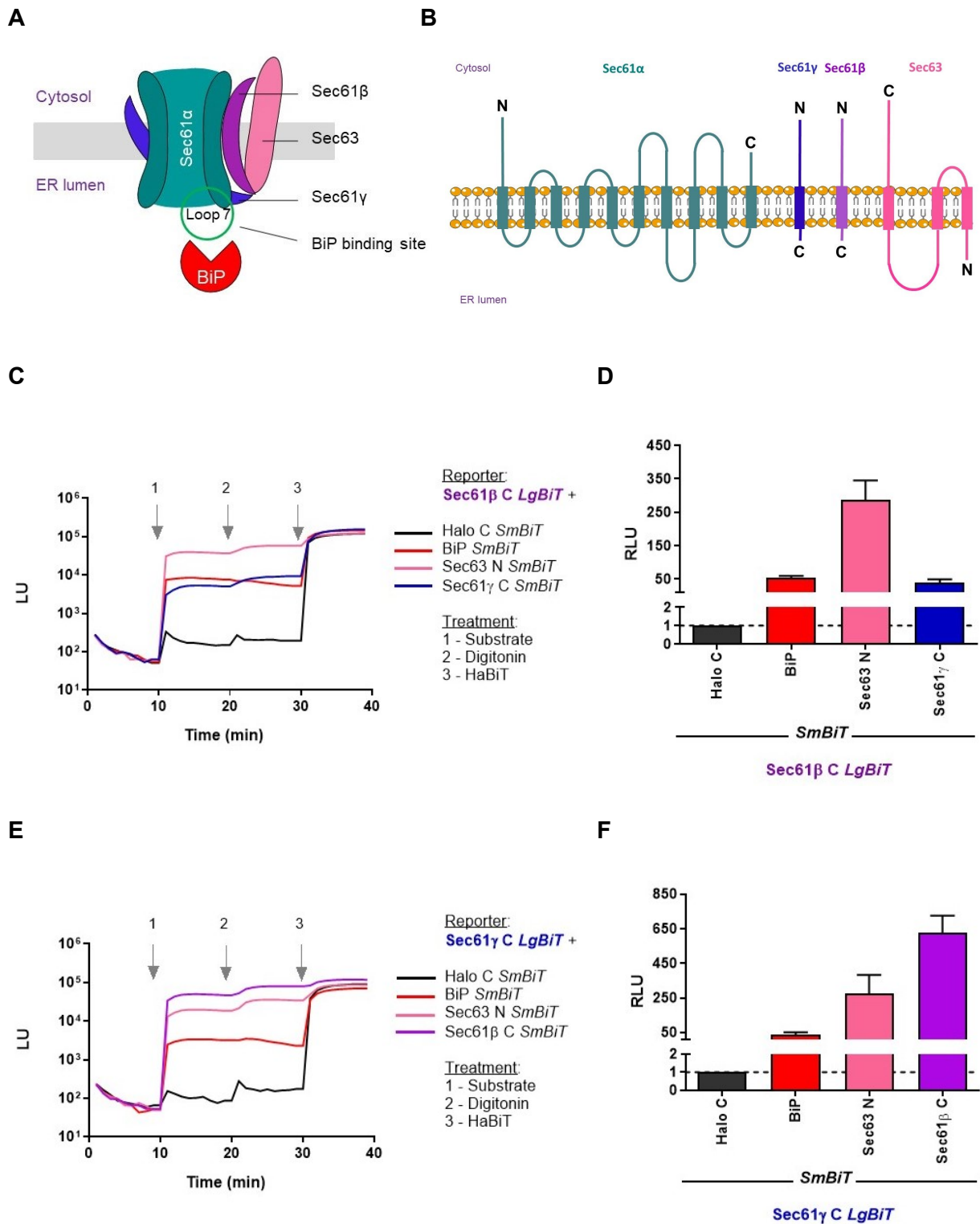


**Figure 28. ER-luminal protein-protein interactions of Sec61-complex.** (A) Structure of Sec61-complex, plus Sec63 and BiP; simplified, cartoon view. (B) Topology of the channel-forming Sec61 $\alpha$  (N- and C- termini are oriented in the cytosol) and associated tail-anchored subunits  $\beta$  and  $\gamma$ , both with N-terminus in cytosol and C-terminus in the ER lumen. Topology of Sec63 shows its cytosolic C-terminus and lumenally oriented N-terminus. (C, E) Total luminescent units (LU) were measured 24 hours after HeLa cells were transfected with the indicated constructs. Nine minutes after baseline read, the luciferase substrate, furimazine was

added to activate luminescence (marked as treatment 1). Digitonin (0.002%) was used for cell permeabilization (treatment 2, after 19 min) and followed by the addition of the synthetic HaBiT peptide (treatment 3, after 29 min). (**D**, **F**) The signal for each construct pair was evaluated 5 min after adding the furimazine and plotted as relative luminescent units (RLU). For normalization purposes the luminescence of the negative control pair (Sec61 $\beta$  C LgBiT plus Halo C SmBiT in **D**; and Sec61 $\gamma$  C LgBiT plus Halo C SmBiT in **F**) was used and set to 1. Reported data are from at least three independent experiments and shown with the standard error of the mean (SEM). Statistical analyses were performed using GraphPad Prism version 10. Letter N or C, coming after protein name, represents N or C terminally located LgBiT or SmBiT.

After confirmation of previously demonstrated interaction between Sec61 $\beta$  and Sec63 (Figure 28: C and D, pink; Sicking et al., 2021), the other PPIs were measured. In comparison to the non-interacting Sec61 $\beta$  C LgBiT plus Halo C SmBiT control pair (Figure 28: C and D, black), the other reporter pairs of Sec61 $\beta$  C LgBiT showed a higher luminescent signal. Also, contrary to the non-interacting Sec61 $\gamma$  C LgBiT plus Halo C SmBiT control pair (Figure 28: E and F, black), a stronger interaction was detected for the other reporter pairs of Sec61 $\gamma$  C LgBiT. Increased luminescent signal of Sec61 $\gamma$  C LgBiT plus Sec63 N SmBiT reporter pair (Figure 28: E and F, pink) indicated that the  $\gamma$  subunit of the Sec61-complex also interacts with Sec63. As it was expected, based on the Sec61-complex structure, interaction between Sec61 $\beta$  and Sec61 $\gamma$  was demonstrated using luminally located BiT-tags. Much stronger signal intensity was detected in the case of Sec61 $\gamma$  C LgBiT plus Sec61 $\beta$  C SmBiT reporter pair (Figure 28: E and F, purple) in comparison to Sec61 $\beta$  C LgBiT plus Sec61 $\gamma$  C SmBiT (Figure 28: C and D, blue). Both Sec61-complex subunits ( $\beta$  and  $\gamma$ ) showed interaction with luminal ER chaperone BiP (Figure 28; C-F, red). The synthetic complementation approach with HaBiT peptide revealed a sufficient expression of corresponding LgBiT-tagged fusion protein (Figure 28: C and E; treatment 3).

This unique and novel way to detect the BiP - Sec61-complex interaction in live cells, earlier referred to as “nearest neighbors” approach, deserved further consideration.

### III.6.2. How ER stress affects the Sec61-complex interaction with BiP

Disturbing the ER Ca<sup>2+</sup>-homeostasis or protein glycosylation causes the ER stress. This cellular condition leads to engagement of specific proteins in the ER lumen, at first place BiP, with the intention to restore the normal ER activity (Xu et al., 2005). Presuming that cellular adaptation during ER stress might have an impact on PPIs in the ER lumen, physiological and chemically caused ER stress were provoked and tested in HeLa and HeLa- $\mu_s$  cells (II.1.9.1.1).

### III.6.2.1. Effect of chemically caused ER stress

The beauty of the NanoBiT assay is its use in intact cells and in a 96-well format. This provides a unique opportunity to use diverse chemical stress inducers in a medium-throughput fashion, detecting the influence on the PPI landscape. To test the impact of ER stress on the luminal interaction between the Sec61-complex and BiP, two well-characterised chemical stressors were used, thapsigargin and tunicamycin. Thapsigargin (Tg) causes a decrease in the ER calcium concentration by specific inhibition of the ER calcium ATPase SERCA (Christensen et al., 2021). Tunicamycin (Tun) suppresses the ER lumenally catalyzed N-linked glycosylation and thereby prevents protein folding and protein passage through the ER (Wang et al., 2020). Thus, both chemicals trigger a rapid experimental ER stress. Their combined effect (indicated as Tg/Tun) on the PPI was tested in HeLa cells (Figure 29 and Figure 30).

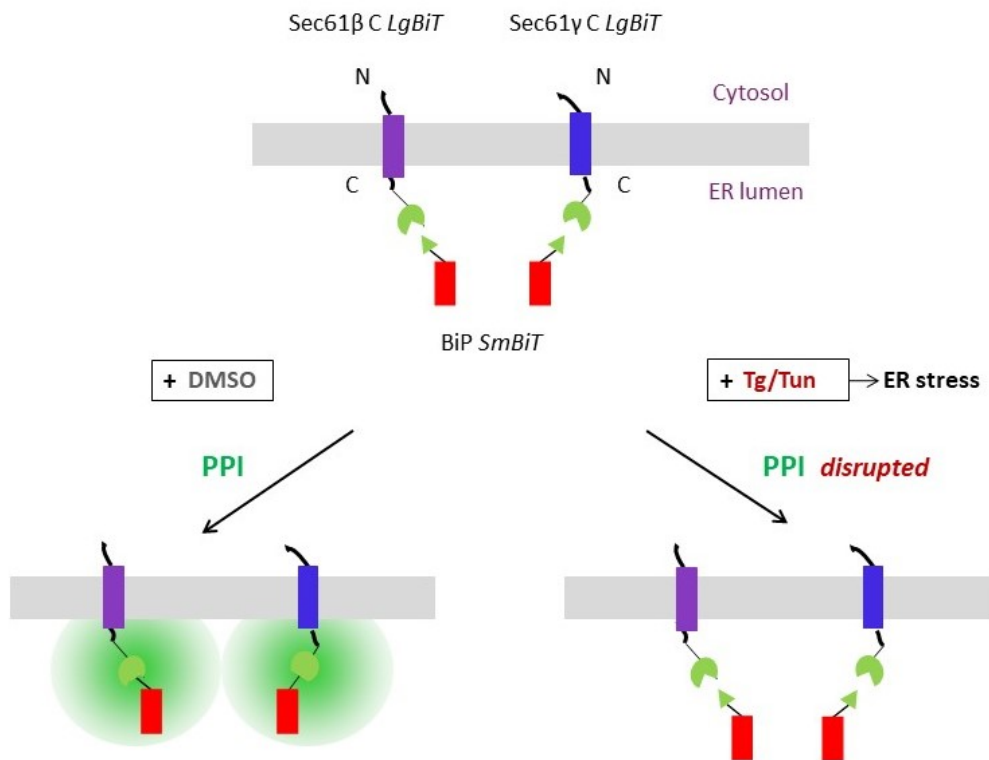


**Figure 29. Cartoon view of disrupted PPIs between Sec61 subunits ( $\beta$  and  $\gamma$ ) and BiP, caused by Tg/Tun treatment. (Upper panel)** The C-termini of Sec61 subunits ( $\beta$ , purple;  $\gamma$ , blue), on the luminal side of the ER were tagged with LgBiT (green orb with “missing triangle part”). The ER luminal chaperone BiP (red) was tagged with SmBiT (green triangle), inserted upstream of the C-terminal KDEL-coding sequence. **(Left lower panel)** Sec61 subunits ( $\beta$  and  $\gamma$ ) and BiP come in close proximity and their interactions (PPIs) result in re-assembly of the functional luciferase, providing a bright luminescent signal (green orb). The PPIs were not disrupted by DMSO addition (control). **(Right lower panel)** ER stress, caused by combined effect of two chemical stressors (thapsigargin, Tg; and tunicamycin, Tun) disrupted the interaction between Sec61 subunits ( $\beta$  and  $\gamma$ ) and BiP, that is verified by loss (significant reduction) of the luminescent signal.

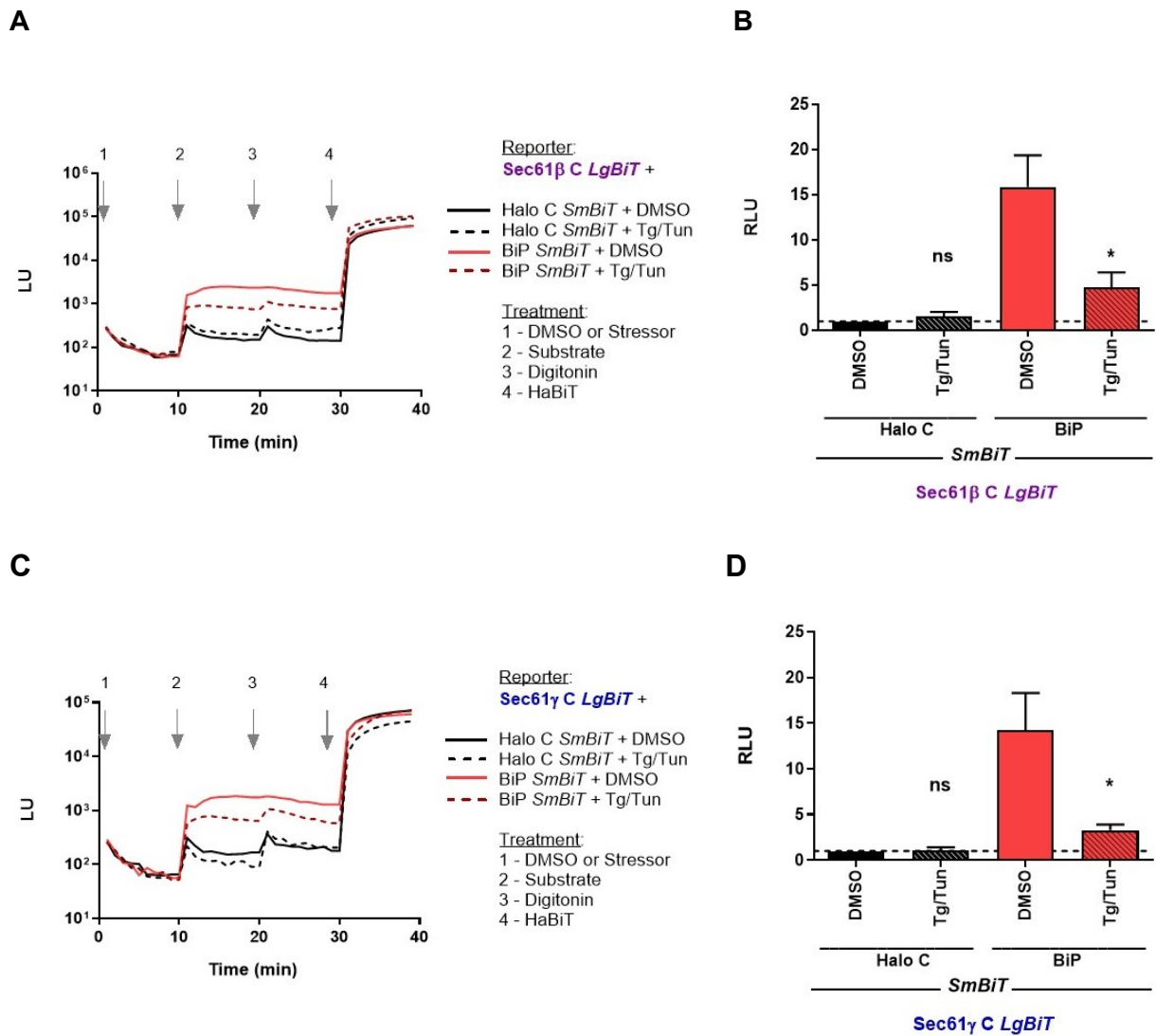


**Figure 30. Effect of chemically caused ER stress on Sec61-complex interaction with BiP in HeLa cells.** (A, C) Twenty-four hours post transfection, Tg/Tun mix (thapsigargin, Tg, f.c. 1  $\mu$ M; tunicamycin, Tun; f.c. 10  $\mu$ g/ml) was added in the wells with indicated constructs (treatment 1), and total luminescent units (LU) were measured. Wells containing DMSO served as control. Nine minutes after baseline read, furimazine was added to activate luminescence (treatment 2). Digitonin (0.002%) was used for cell permeabilization (treatment 3, after 19 min) and followed by the addition of the synthetic HaBiT peptide (treatment 4, after 29 min). (B, D) The signal for each construct pair was evaluated 5 min after adding the furimazine and plotted as relative luminescent units (RLU). For normalization purposes the luminescence of the negative control pair (Sec61β C LgBiT plus Halo C SmBiT in B; and Sec61γ C LgBiT plus Halo C SmBiT in D) with the addition of DMSO or stressors was used and set to 1. Reported data are from three independent experiments and shown with the standard error of the mean (SEM). Statistical significance between groups was determined using one-way ANOVA. Significant changes are indicated by asterisks: \*  $p < 0.05$ ; or as non-significant (ns) if  $p \geq 0.05$ . Statistical analyses were performed using GraphPad Prism version 10. Letter C, coming after protein name, represents C terminally located LgBiT or SmBiT.

Considering that DMSO was used to dilute the chemical stressors (Tg and Tun), it was added in the wells free of Tg/Tun and served as control. After the measurement, it was noticed that the DMSO treatment caused a certain decline of the luminescent signal of Sec61 $\beta$ -BiP and Sec61 $\gamma$ -BiP interaction (~15 RLU; Figure 30: B and D, red bars) in comparison to the earlier experiment without DMSO pre-treatment (~50 RLU; Figure 28: D and F, red bars). The study from Tjernberg et al. (2006) found that DMSO can affect PPIs by destabilizing proteins and changing their apparent binding properties. Yet, the detected signal decline caused by DMSO did not influence the main results nor their interpretation (i.e., the detected effect of ER stress). The wells with DMSO, containing Sec61 $\beta$  C LgBiT plus BiP SmBiT reporter pair (Figure 30: A, red line; B, red bar), and the Sec61 $\gamma$  C LgBiT plus BiP SmBiT reporter pair (Figure 30: C, red line; D, red bar) showed the higher luminescent signal in comparison to the appropriate non-interacting control pair with Halo C SmBiT (Figure 30: A and C, black line; B and D, black bar). In the wells with Tg/Tun, the Sec61 $\beta$ -BiP (Figure 30: A, red dashed line; B, red bar with pattern) and Sec61 $\gamma$ -BiP interactions (Figure 30: C, red dashed line; D, red bar with pattern) also showed the higher signal intensity, comparing to their corresponding non-interacting control pair (Figure 30: A and C, black dashed line; B and D, black bar with pattern). Compared to the DMSO treatment (Figure 30: B and D, red bar), statistical analysis revealed a significant reduction of luminescence when cells were treated with the ER stressors (Tg/Tun; Figure 30: B and D, red bar with pattern). On the other hand, the luminescent signal of the negative control (Figure 30: B and D, black bar) was not affected by stressors addition (Figure 30: B and D, black bar with pattern). The complementation approach with synthetic HaBiT peptide confirmed a sufficient expression of the LgBiT-tagged fusion protein in all tested conditions (Figure 30: A and C; treatment 4).

In sum, the treatment with ER stressors induced a reduction of the Sec61 $\beta$ -BiP and Sec61 $\gamma$ -BiP luminescent signal, indicating that the Sec61-complex interaction with BiP is susceptible to ER stress.

To further investigate the detected influence of ER stress on the Sec61-complex - BiP interaction, the experimental design with chemical stressors was repeated using the HeLa- $\mu_s$  cell model (II.1.9.1.1). In addition, the combined as well as individual effect of thapsigargin and tunicamycin was tested (Figure 31).

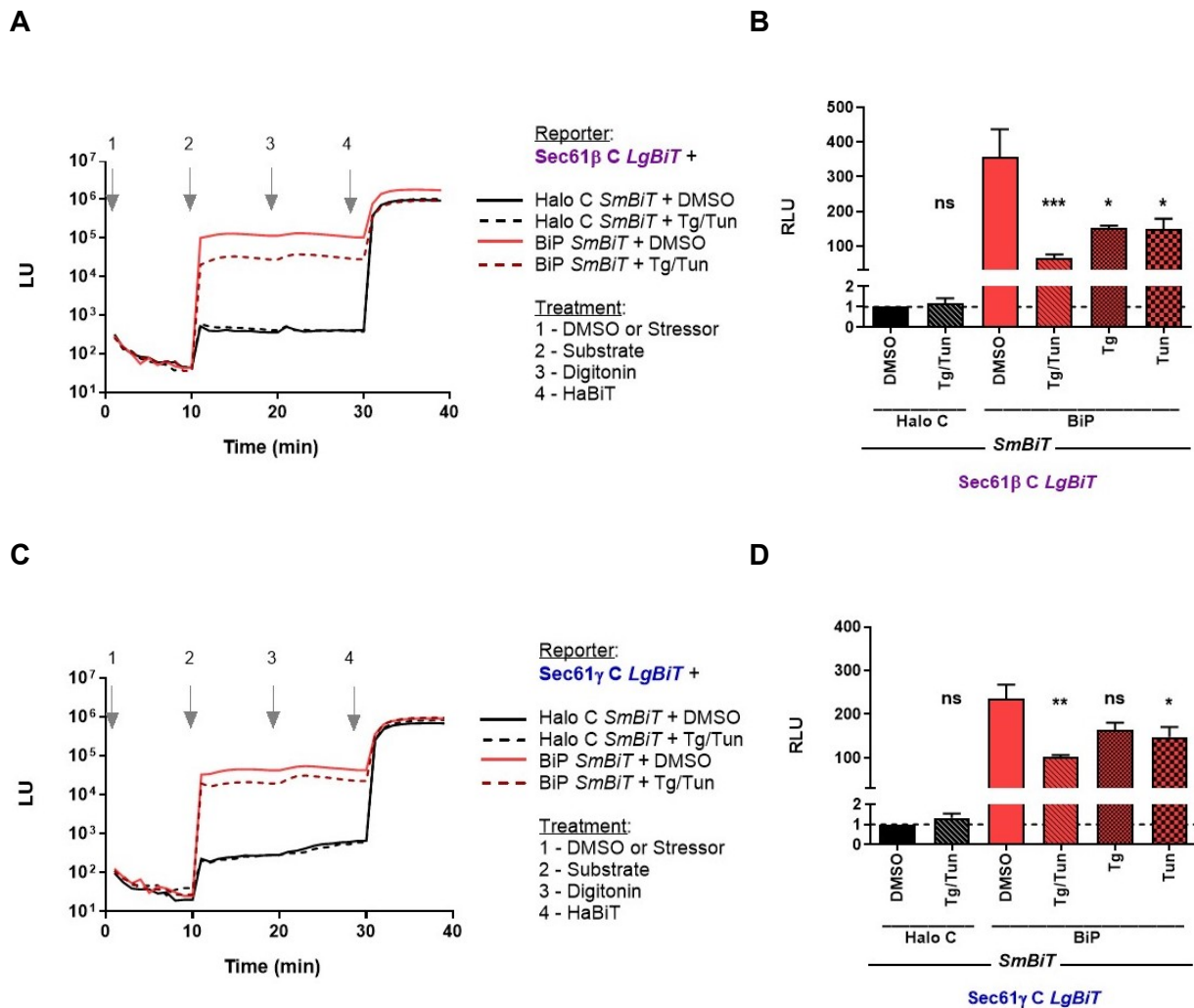


**Figure 31. Effect of chemically caused ER stress on Sec61-complex interaction with BiP in HeLa- $\mu_s$  cells.** (A, C) Twenty-four hours post transfection, thapsigargin (Tg; f.c. 1  $\mu$ M), tunicamycin (Tun; f.c. 10  $\mu$ g/ml) or Tg/Tun mix were added in the wells with indicated constructs (treatment 1), and total luminescent units (LU) were measured. Wells containing DMSO served as control. Nine minutes after baseline read, furimazine was added to activate luminescence (treatment 2). Digitonin (0.002%) was used for cell permeabilization (treatment 3, after 19 min) and followed by the addition of the synthetic HaBiT peptide (treatment 4, after 29 min). Only results for DMSO and combined Tg/Tn were shown. (B, D) The signal for each construct pair was evaluated 5 min after adding the furimazine and plotted as relative luminescent units (RLU). For normalization purposes the luminescence of the negative control pair (Sec61 $\beta$  C LgBiT plus Halo C SmBiT in B; and Sec61 $\gamma$  C LgBiT plus Halo C SmBiT in D) with the addition of DMSO or stressor(s) was used and set to 1. Reported data are from at least three independent experiments and shown with the standard error of the mean (SEM). Statistical significance between groups was determined using one-way ANOVA. Significant changes are indicated by asterisks: \*\*\*  $p < 0.001$ ; \*\*  $p < 0.01$ ; \*  $p < 0.05$ ; or as non-significant (ns) if  $p \geq 0.05$ . Statistical analyses were performed using GraphPad Prism version 10. Letter C, coming after protein name, represents C terminally located LgBiT or SmBiT.

In comparison to the appropriate non-interacting control pair with Halo C SmBiT (Figure 31: A and C, black line; B and D, black bar), the Sec61 $\beta$  C LgBiT plus BiP SmBiT reporter pair (Figure 31: A, red line; B, red bar), and the Sec61 $\gamma$  C LgBiT plus BiP SmBiT reporter pair (Figure 31: C, red line; D, red bar), treated with DMSO, showed a significantly higher luminescent signal. When cells were treated with ER stressors (individual or combined), a significant difference in signal intensity was noticed between reporter pair (Figure 31: A and C, red dashed line; B and D, red bar with pattern) and corresponding negative control (Figure 31: A and C, black dashed line; B and D, black bars with pattern). As in the experiment before, the statistical analysis revealed a significant reduction of luminescent signal in the wells treated with the ER stressors, individual or combined (Figure 31: B and D, red bars with pattern), in comparison to DMSO treatment (Figure 31: B and D, red bar). The signal was more reduced when the combined treatment was used (Tg/Tun; Figure 31: B and D, red bar with line pattern) in comparison to the individual stressor impact (Tg or Tun; Figure 31: B and D, red bars with dots pattern). The change of Sec61 $\gamma$ -BiP interaction under the Tg treatment was determined as statistically non-significant (Figure 31: D, red bar with dots pattern), most likely due to fluctuation in the measurements (from three independent experiments). Luminescent signal of negative control (Figure 31: B and D, black bar) was not affected by stressors addition (Tg/Tun mix; Figure 31: B and D, black bar with pattern). The complementation approach with synthetic HaBiT peptide confirmed a sufficient expression of the LgBiT-tagged fusion protein (Figure 31: A and C; treatment 4).

Overall, the experiment confirmed previous results, indicating that the PPI between Sec61-complex and BiP is changing during ER stress.

However, a significantly higher luminescent signal was detected during the measurements when the HeLa- $\mu_s$  cell model was used. Therefore, all following NanoBiT experiments were performed with the HeLa- $\mu_s$  cell model.

#### III.6.2.1.1. Is NanoBiT luciferase Ca<sup>2+</sup>-dependent?

Luciferases are enzymes commonly used to detect the expression level of proteins or protein-protein interactions. To emit light, these enzymes oxidize their substrate. However, there are additional requirements for luciferase reaction, like in case of the firefly luciferase which uses its substrate, but also depends on Mg<sup>2+</sup> (Oba et al., 2020).

Since thapsigargin and tunicamycin cause ER stress and Ca<sup>2+</sup> leakage from the ER lumen to the cytosol, one issue had to be clarified: was luminescence reduction, detected after stressor addition, caused by calcium dependency of the NanoBiT luciferase? To address this question, cells were transfected with construct pair of cAMP-dependent protein kinase A (PKA); rPKA C LgBiT plus cPKA C SmBiT (Sicking et al., 2021). Due to high signal intensity, this reporter pair

was used as positive control and treated with DMSO or the Tg/Tun mix. The non-interacting rPKA C LgBiT plus Halo C SmBiT served as negative control pair (Figure 32).

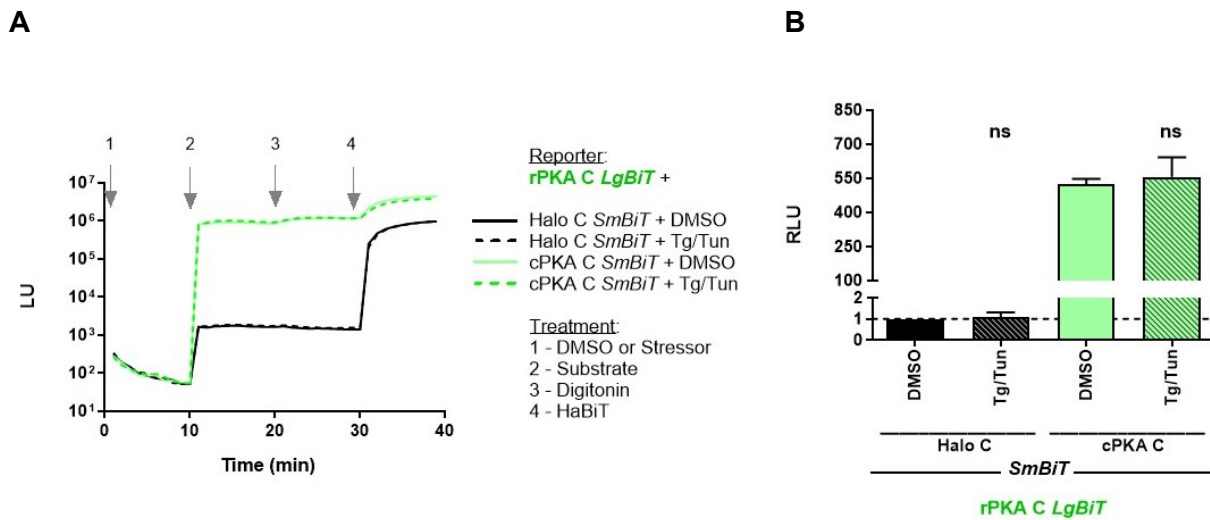


**Figure 32. cAMP-dependent protein kinase A (PKA) construct pair served as control for luciferase calcium dependency.** (A) Twenty-four hours post transfection, Tg/Tun mix (thapsigargin, Tg, f.c. 1  $\mu$ M; tunicamycin, Tun; f.c. 10  $\mu$ g/ml) was added in the wells with indicated constructs (treatment 1), and total luminescent units (LU) were measured. Wells containing DMSO served as control. Nine minutes after baseline read, furimazine was added to activate luminescence (treatment 2). Digitonin (0.002%) was used for cell permeabilization (treatment 3, after 19 min) and followed by the addition of the synthetic HaBiT peptide (treatment 4, after 29 min). (B) The signal for each construct pair was evaluated 5 min after adding the furimazine and plotted as relative luminescent units (RLU). For normalization purposes the luminescence of the negative control pair (rPKA C LgBiT plus Halo C SmBiT) with the addition of DMSO or stressors was used and set to 1. Reported data are from three independent experiments and shown with the standard error of the mean (SEM). Statistical significance between groups was determined using one-way ANOVA. p-values are indicated as non-significant (ns) if  $p \geq 0.05$ . Statistical analyses were performed using GraphPad Prism version 10. Letter C, coming after protein name, represents C terminally located LgBiT or SmBiT.

Considering that PKA is a cytosol-resident protein, in case that the NanoBiT luciferase is  $Ca^{2+}$ -dependent, a change of luminescent signal would be detected after Tg/Tun addition (i.e., a luminescent signal would increase due to a higher  $Ca^{2+}$  concentration in the cytosol induced by ER stress). However, the rPKA C LgBiT plus cPKA C SmBiT positive control pair showed non-significant difference between DMSO and stressors treatment (Figure 32: B, green bar, and green bar with pattern) as well as the negative control pair rPKA C LgBiT plus Halo C SmBiT (Figure 32: B, black bar, and black bar with pattern). This indicates that a) luciferase is  $Ca^{2+}$ -independent, and b) the PPI between BiP and the Sec61-complex is changing during ER stress.

Irrespective of treatment (DMSO or Tg/Tun), the complementation approach with synthetic HaBiT peptide (Figure 32: A; treatment 4) revealed that rPKA C LgBiT construct of the positive control pair was more sufficiently expressed in the presence of its fusion partner cPKA C SmBiT (Figure 32: A, green line, green dashed line) in comparison to the non-interacting Halo C SmBiT (Figure 32: A, black line and black dashed line). That is expected considering that rPKA C LgBiT represents the actual regulatory and cPKA C SmBiT the catalytic subunit of protein kinase A (Sicking et al., 2021).

### II.6.2.1.2. ER stress affects the additional luminal protein-protein interaction

A newly generated BiP plasmid enabled an extra NanoBiT experiments to be performed and an additional interaction was detected. The construct pair was BiP plus Sec63, where BiP was tagged with the LgBiT (inserted upstream of the C-terminal KDEL-coding sequence; BiP LgBiT), and SmBiT was fused on the N-terminus of Sec63 (Sec63 N SmBiT). As earlier, interaction was exposed to the ER stress triggered by the chemical mix of thapsigargin and tunicamycin (Tg/Tun; Figure 33).

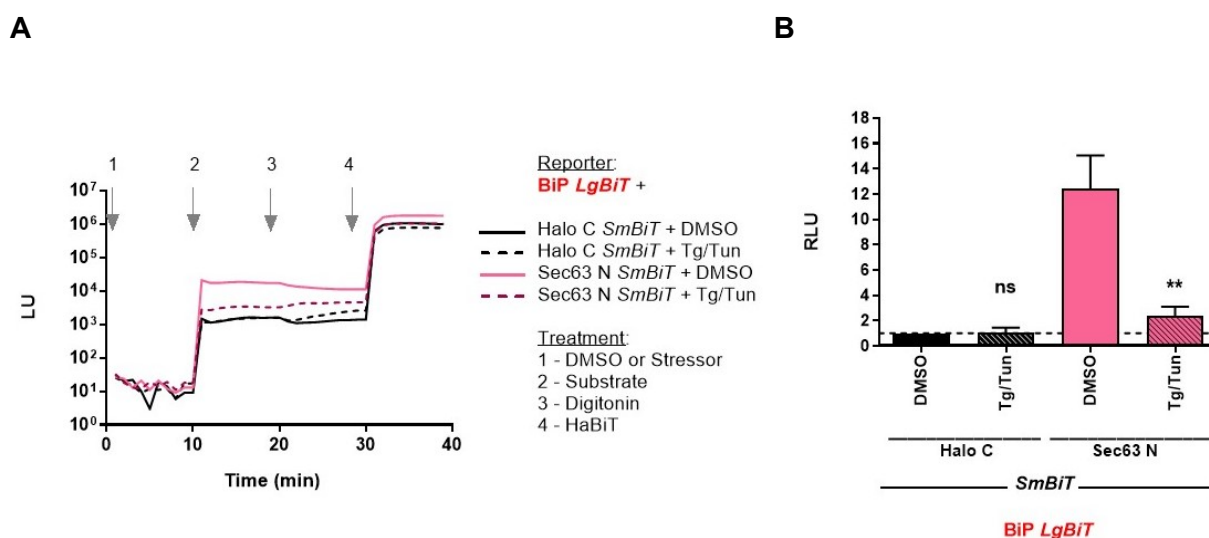


**Figure 33. Effect of chemically caused ER stress on BiP interaction with Sec63.** (A) Twenty-four hours post transfection, Tg/Tun mix (thapsigargin, Tg, f.c. 1  $\mu$ M; tunicamycin, Tun; f.c. 10  $\mu$ g/ml) was added in the wells with indicated constructs (treatment 1), and total luminescent units (LU) were measured. Wells containing DMSO served as control. Nine minutes after baseline read, furimazine was added to activate luminescence (treatment 2). Digitonin (0.002%) was used for cell permeabilization (treatment 3, after 19 min) and followed by the addition of the synthetic HaBiT peptide (treatment 4, after 29 min). (B) The signal for each construct pair was evaluated 5 min after adding the furimazine and plotted as relative luminescent units (RLU). For normalization purposes the luminescence of the negative control pair (BiP LgBiT plus Halo C SmBiT) with the addition of DMSO or stressors was used and set to 1. Reported data are from three independent experiments and shown with the standard error of the mean (SEM). Statistical significance between groups was determined using one-way

ANOVA. Significant changes are indicated by asterisks: \*\*  $p < 0.01$ ; or as non-significant (ns) if  $p \geq 0.05$ . Statistical analyses were performed using GraphPad Prism version 10. Letter N or C, coming after protein name, represents N or C terminally located LgBiT or SmBiT.

During the measurement, surprisingly high luminescent signal (approximately 10-fold higher than average) was detected for the negative control pair BiP LgBiT plus Halo C SmBiT (during all repeats of the experiment; Figure 33: A, black line, treatment 2). Still, statistical analysis showed that the relative luminescence units (RLU) representing the BiP-Sec63 interaction were over ten ( $RLU > 10$ ; Figure 33: B, pink bar), that is suggested as specific protein-protein interaction (Sicking et al., 2021). Moreover, Tg/Tun treatment induced a significant luminescent signal reduction for the BiP LgBiT plus Sec63 N SmBiT construct pair (Figure 33: B, pink bar with pattern) in comparison to the DMSO treatment (Figure 33: B, pink bar), indicating that ER stress disturbs the BiP-Sec63 interaction. A non-significant difference between DMSO and stressors treatment was detected for the negative control pair BiP LgBiT plus Halo C SmBiT (Figure 33: B, black bar, and black bar with pattern). A sufficient expression of the LgBiT-tagged protein was verified by the synthetic complementation approach with HaBiT peptide (Figure 33: A; treatment 4).

### III.6.2.2. Effect of physiological ER stress

Considering that the accumulation of unfolded proteins induces the ER stress, the overexpression of an ER-client protein was a useful strategy for inducing an overload of the ER folding capacity and thus testing the impact of “natural” ER stress on PPIs. In that case, the treatment with stress-eliciting drugs was avoided, and the provoked protein-driven ER stress could be defined as (patho-)physiological.

The stress was triggered using the mifepristone (Mif) responsive HeLa- $\mu_s$  cell model that persistently overexpressed the orphan secretory heavy chain ( $\mu_s$ ) of immunoglobulin M (IgM) (Bakunts et al., 2017). Identified as Ig heavy-chain binding protein (Haas and Wabl, 1983), BiP inhibits immunoglobulins secretion if they are not completely assembled. Overall, the bulk IgM- $\mu_s$  expression was an ideal tool to observe the BiP interaction with Sec61-complex upon the ER stress. Different lengths of treatment with the synthetic steroid were compared, and, in parallel, cells were treated with ethanol (EtOH) as control (Figure 34). Possible direct mifepristone influence on luciferase was tested using the PKA positive control pair (Figure 35).

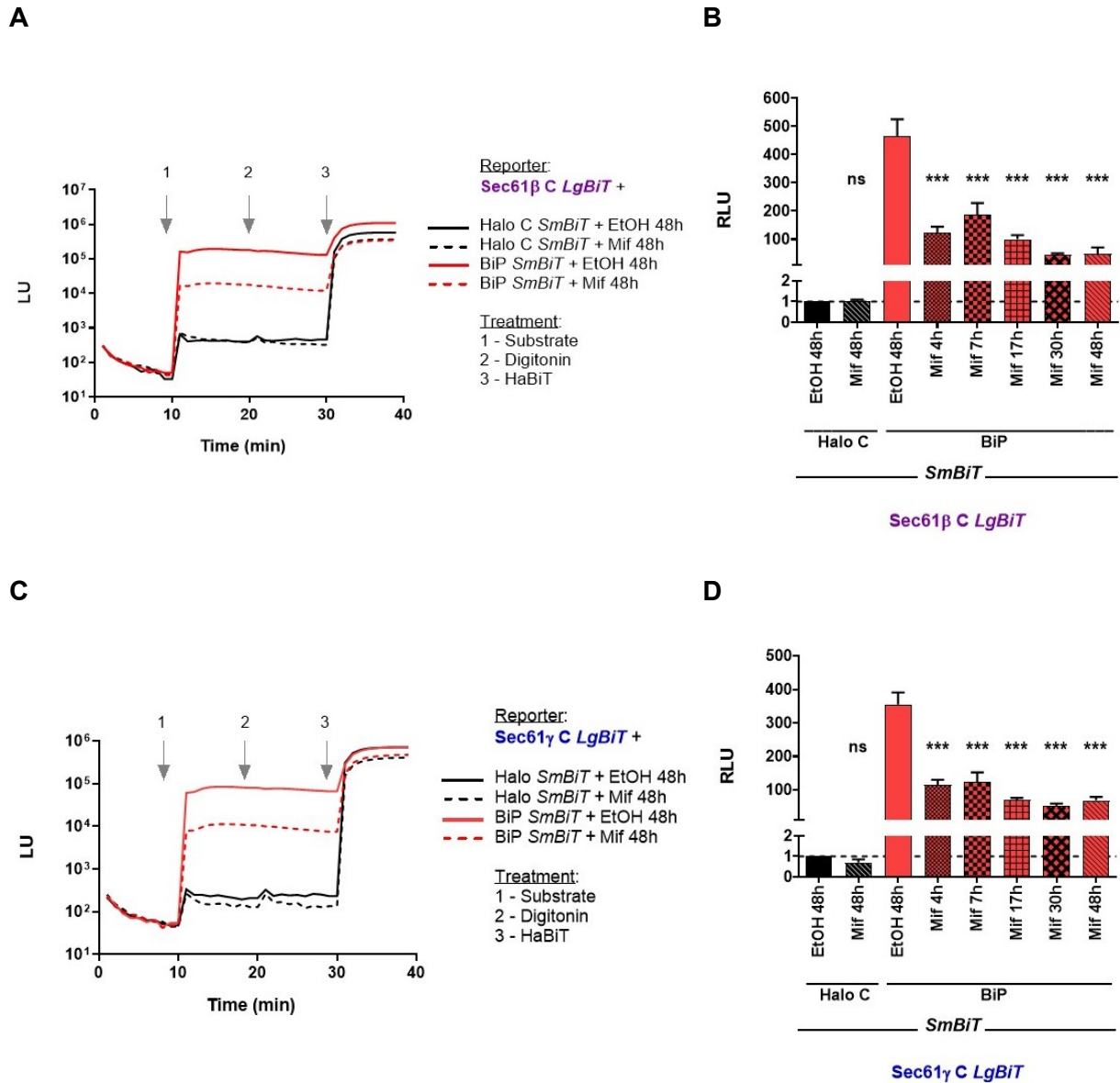


**Figure 34. Effect of physiological ER stress on Sec61-complex interaction with BiP.** (A, C) Cells were seeded in 96-well plate and treated with mifepristone (Mif; f.c. 0.5 nM) at different time points (48h, 30h, 17h, 7h and 4 h before measurement). Twenty-four hours after cell-seeding, transfection with indicated constructs was performed. Total luminescent units (LU) were measured after the next twenty-four hours. Wells containing ethanol (EtOH) served as control. Nine minutes after baseline read, furimazine was added to activate luminescence (treatment 1). Digitonin (0.002%) was used for cell permeabilization (treatment 2, after 19 min) and followed by the addition of the synthetic HaBIT peptide (treatment 3, after 29 min). Only results for 48h EtOH and Mif treatment were shown. (B, D) The signal for each construct pair was evaluated 5 min after adding the furimazine and plotted as relative luminescent units (RLU). For normalization purposes the luminescence of the negative control pair (Sec61 $\beta$  C LgBiT plus Halo C SmBiT in B; Sec61 $\gamma$  C LgBiT plus Halo C SmBiT in D) with the addition of EtOH or Mif was used and set to 1. Reported data are from at least three independent experiments and shown with the standard error of the mean (SEM). Statistical significance between groups was determined using one-way ANOVA. Significant changes are indicated by asterisks: \*\*\*  $p < 0.001$ ; or as non-significant (ns) if  $p \geq 0.05$ . Statistical analyses were

performed using GraphPad Prism version 10. Letter C, coming after protein name, represents C terminally located LgBiT or SmBiT.

In comparison to appropriate non-interacting control pair with Halo C SmBiT (Figure 34: A and C, black line; B and D, black bar), the Sec61 $\beta$  C LgBiT plus BiP SmBiT reporter pair (Figure 34: A, red line; B, red bar), and the Sec61 $\gamma$  C LgBiT plus BiP SmBiT reporter pair (Figure 34: C, red line; D, red bar), treated with EtOH, showed the significantly higher luminescent signal. Also, treated with mifepristone (Mif), the Sec61 $\beta$  C LgBiT plus BiP SmBiT pair (Figure 34: A, red dashed line; B, red bars with pattern), and the Sec61 $\gamma$  C LgBiT plus BiP SmBiT pair (Figure 34: C, red dashed line; D, red bars with pattern) showed the higher signal intensity, comparing to their corresponding non-interacting control pair (Figure 34: A and C, black dashed line; B and D, black bar with pattern). Compared to the EtOH treatment (Figure 34: B and D, red bar), the statistical analysis revealed a significant decline of the luminescent signal after treatment with Mif (Figure 34: B and D, red bars with pattern). On the other hand, the luminescent signal of negative control (Figure 34: B and D, black bar) was not affected by Mif addition (Mif 48h; Figure 34: B and D, black bar with pattern). The complementation approach with synthetic HaBiT peptide revealed the expression of LgBiT-tagged proteins upon Mif treatment (Sec61 $\beta$  and Sec61 $\gamma$ ; Figure 34: A and C; treatment 3).

The Mif-induction of ER luminal accumulation of immunoglobulin M heavy-chain caused ER stress. Next, the UPR was triggered by prolonged stress, and limited protein translation was started (1.4.2). Irrespective of Mif treatment duration, the decline of luminescent signal was statistically significant (Figure 34: B and D, red bars with pattern). Still, the drop of signal intensity was changing over time (RLU of Mif 4h-Mif 48h; Figure 34: B and D, red bars with pattern) indicating the change in BiP abundance regulated by the UPR (Bakunts et al., 2017). Shortly, the luminal accumulation of immunoglobulin M heavy-chain resulted with a significant reduction in the luminescent signal, indicating that ER stress has direct influence on the interaction between Sec61-complex and BiP.

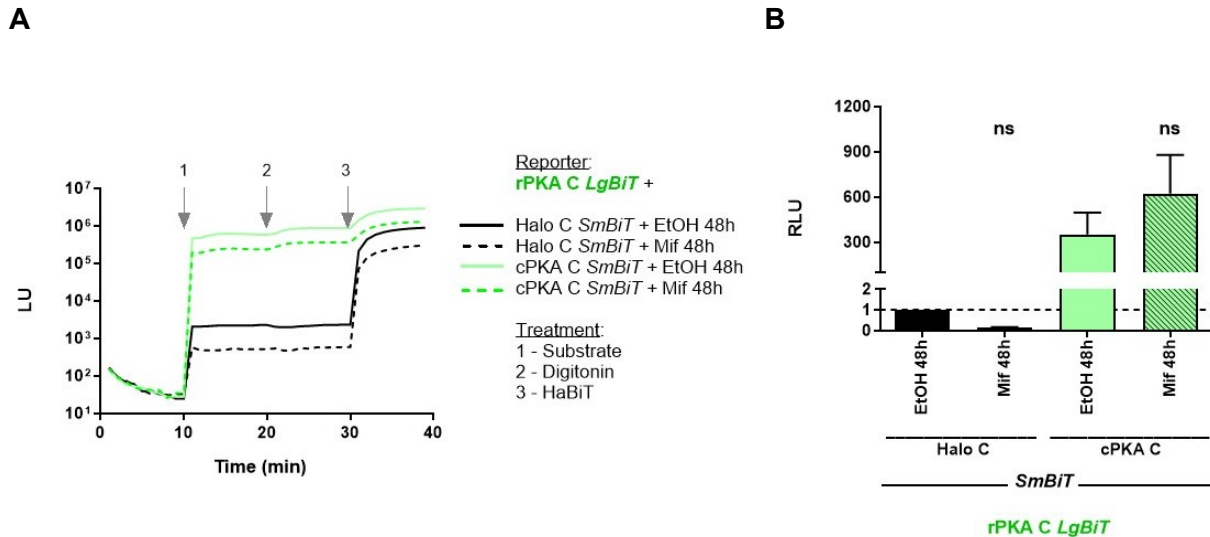


**Figure 35. Effect of physiological ER stress on PKA positive control pair.** (A) Cells were seeded in 96-well plate and treated with mifepristone (Mif; f.c. 0.5 nM) at different time points (48h, 30h, 17h, 7h and 4 h before measurement). Twenty-four hours after cell-seeding, transfection with indicated constructs was performed. Total luminescent units (LU) were measured after the next twenty-four hours. Wells containing ethanol (EtOH) served as control. Nine minutes after baseline read, furimazine was added to activate luminescence (treatment 1). Digitonin (0.002%) was used for cell permeabilization (treatment 2, after 19 min) and followed by the addition of the synthetic HaBiT peptide (treatment 3, after 29 min). (B) The signal for each construct pair was evaluated 5 min after adding the furimazine and plotted as relative luminescent units (RLU). For normalization purposes the luminescence of the negative control pair (rPKA C LgBiT plus Halo C SmBiT) with the addition of EtOH or Mif was used and set to 1. Reported data are from three independent experiments and shown with the standard error of the mean (SEM). Statistical significance between groups was determined using one-way ANOVA. p-values are indicated as non-significant (ns) if  $p \geq 0.05$ . Statistical analyses were performed using Graph PadPrism version 10. Letter C, coming after protein name, represents C terminally located LgBiT or SmBiT.

The rPKA C LgBiT plus cPKA C SmBiT positive control pair showed a non-significant difference between 48h EtOH and Mif treatment (Figure 35: B, green bar, and green bar with pattern) as well as the negative control pair rPKA C LgBiT plus Halo C SmBiT (Figure 35: B, black bar, and black bar with pattern (imperceptible)). This indicates that the mifepristone treatment has no influence on the luciferase. Yet, as expected, ER stress and consequently activated the unfolded protein response (UPR) decreased the expression of rPKA C LgBiT, revealed by complementation approach with synthetic HaBiT peptide (Figure 35: A; treatment 3).

### III.6.3. Identification of AXER playmates in intact cells

The AXER interactome was probed in living cells using a biomolecular luminescence complementation approach. With the unknown *in situ* structure of AXER, the experimental design was based on the hypothetical model of AXER (Figure 3) with both termini (N and C) on the cytosolic side of the ER membrane. Accordingly, four possible fusion constructs of AXER were generated (II.3.2; Table 9). The AXER constructs were paired with all available and functional constructs of the Sec61- and TRAP-complex subunits, which contain cytosolically oriented BiT-tags (Table 9). Luminescence data are summarized in Figure 43 (Appendix). The PPIs of AXER (N or C) LgBiT plus Sec61- and TRAP-complex are presented in Figure 36 and Figure 37, respectively.

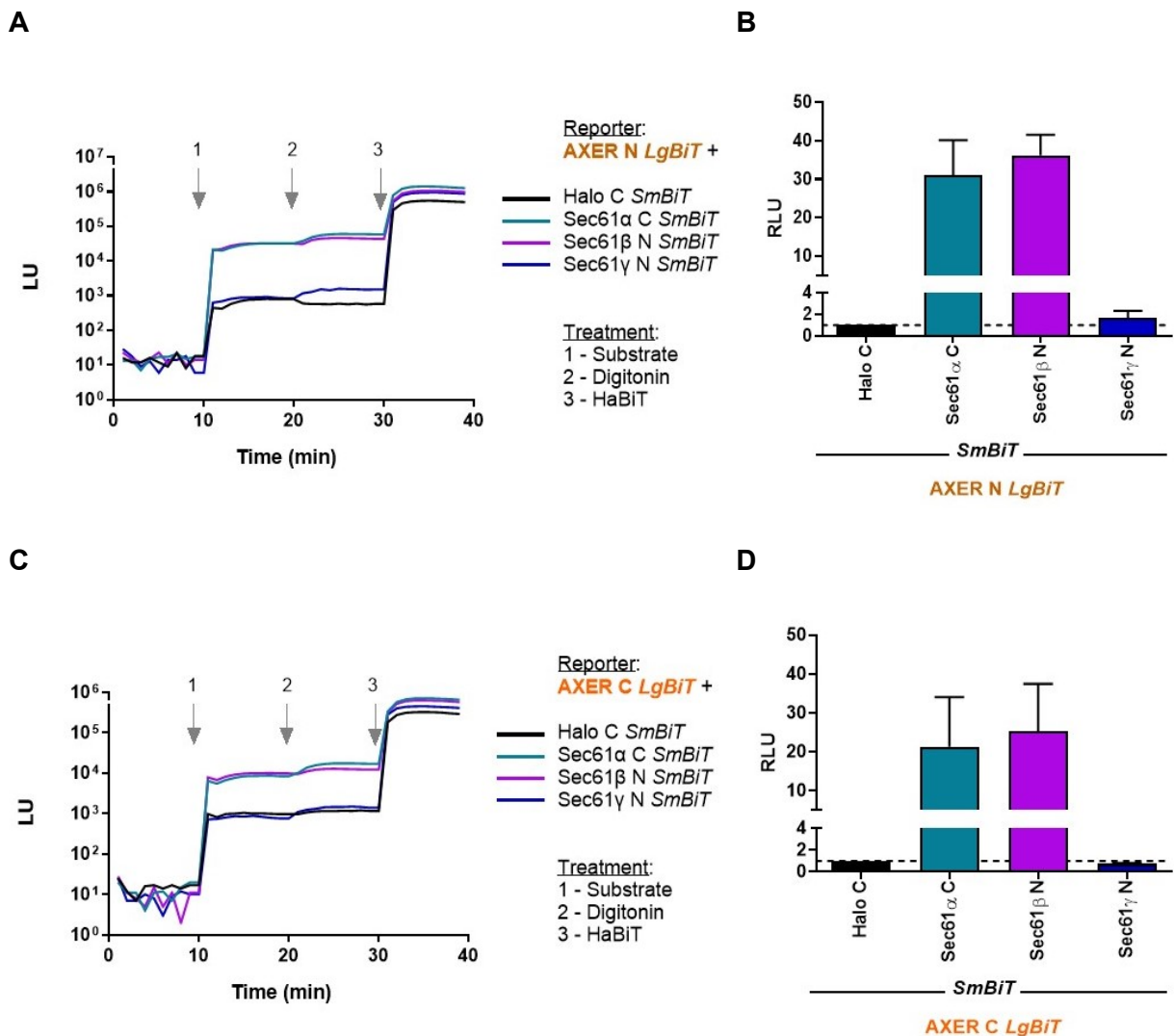


**Figure 36. AXER interaction with Sec61-complex.** (A, C) Total luminescent units (LU) were measured 24 hours after HeLa- $\mu$ s cells were transfected with the indicated constructs. Nine minutes after baseline read, the luciferase substrate, furimazine was added to activate luminescence (treatment 1). Digitonin (0.002%) was used for cell permeabilization (treatment 2, after 19 min) and followed by the addition of the synthetic HaBiT peptide (treatment 3, after

29 min). (**B**, **D**) The signal for each construct pair was evaluated 5 min after adding the furimazine and plotted as relative luminescent units (RLU). For normalization purposes the luminescence of the negative control pair (AXER N LgBiT plus Halo C SmBiT in **B**; and AXER C LgBiT plus Halo C SmBiT in **D**) and set to 1. Reported data are from at least three independent experiments and shown with the standard error of the mean (SEM). Statistical analyses were performed using GraphPad Prism version 10. Letter N or C, coming after protein name, represents N or C terminally located LgBiT or SmBiT.

In comparison to the corresponding non-interacting control pair with Halo C SmBiT (Figure 36: A, black line; B, black bar), the AXER N LgBiT plus Sec61 $\alpha$  C SmBiT reporter pair (Figure 36: A, petroleum line; B, petroleum bar) and the AXER N LgBiT plus Sec61 $\beta$  N SmBiT reporter pair (Figure 36: A, purple line; B, purple bar) showed the significantly higher luminescent signal. Also, contrary to appropriate negative control pair (Figure 36: C, black line; D, black bar), a stronger interaction was detected for the AXER C LgBiT plus Sec61 $\alpha$  C SmBiT reporter pair (Figure 36: C, petroleum line; D, petroleum bar) and the AXER C LgBiT plus Sec61 $\beta$  N SmBiT reporter pair (Figure 36: C, purple line; D, purple bar). The signal intensity suggested that AXER interacts with Sec61 $\alpha$  and Sec61 $\beta$ . Even though Sec61 $\alpha$  has both termini oriented on the cytosolic side of the ER membrane, only Sec61 $\alpha$  C SmBiT construct was functional and used as fusion partner of AXER N LgBiT or AXER C LgBiT. Yet, the reporter pair Sec61 $\alpha$  N LgBiT plus AXER (N or C) SmBiT provided luminescent signal that indicates a specific PPI (Figure 43, Appendix). Further, the signal intensity showed that AXER N- terminus interacts stronger with the Sec61  $\alpha$  and  $\beta$  subunits (Figure 36: B), in comparison to AXER C- terminus (Figure 36: D). In the case of AXER (N or C) LgBiT plus Sec61 $\gamma$  N SmBiT reporter pair (Figure 36: B and D, blue bar), the relative luminescence units (RLU) were almost equal to the RLU of negative control pair (Figure 36: B and D, black bar), indicating a non-specific interaction. Expression of the LgBiT-tagged protein was verified by the complementation approach with synthetic HaBiT peptide. For unexplained reason, it was observed that AXER (N or C) LgBiT construct was more sufficiently expressed in the presence of the Sec61 subunits  $\alpha$  or  $\beta$  in comparison to the subunit  $\gamma$  or non-interacting Halo (Figure 36: A and C; treatment 3).

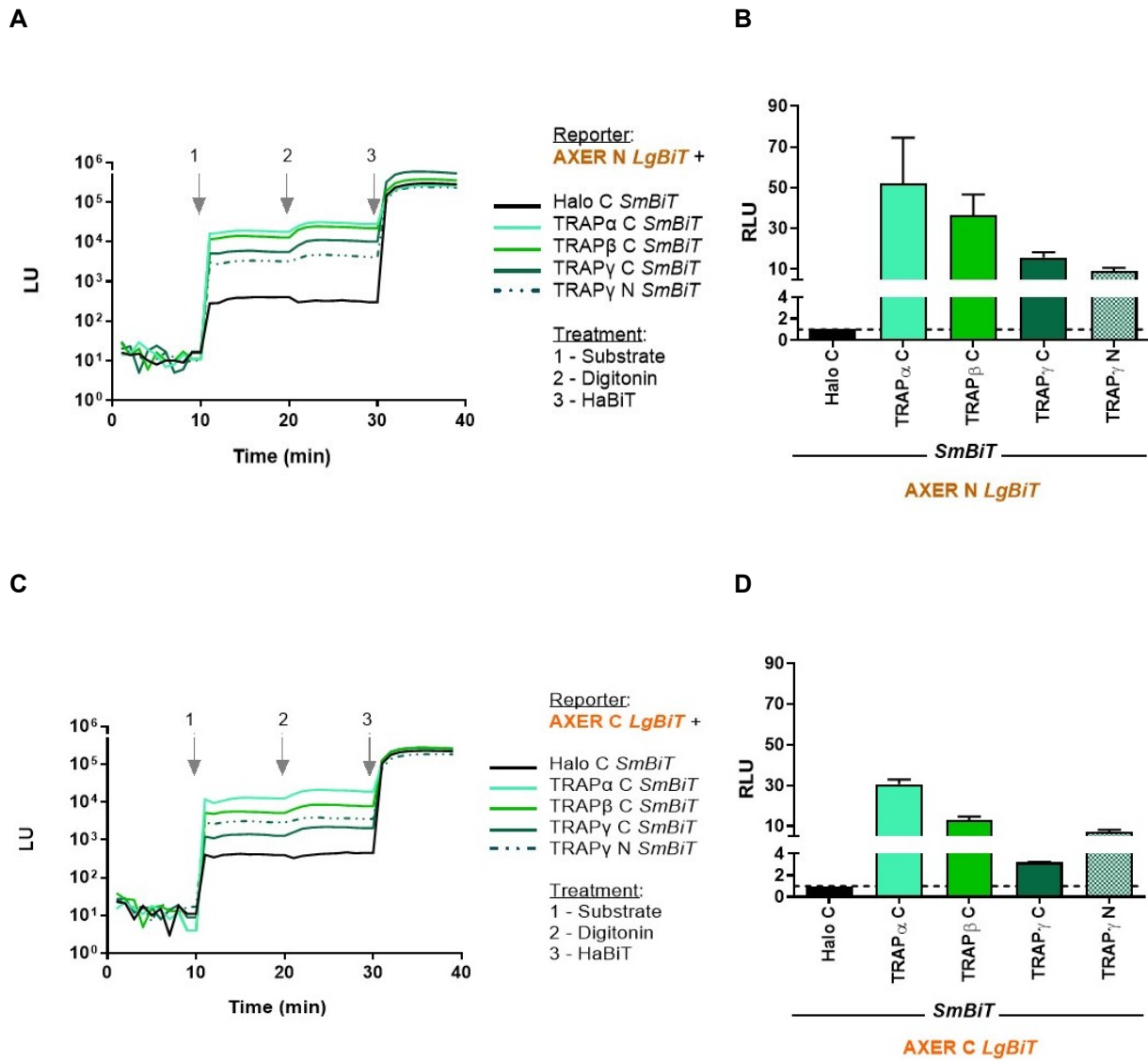


**Figure 37. AXER interaction with TRAP-complex.** (A, C) Total luminescent units (LU) were measured 24 hours after HeLa- $\mu$ s cells were transfected with the indicated constructs. Nine minutes after baseline read, the luciferase substrate, furimazine was added to activate luminescence (treatment 1). Digitonin (0.002%) was used for cell permeabilization (treatment 2, after 19 min) and followed by the addition of the synthetic HaBiT peptide (treatment 3, after 29 min). (B, D) The signal for each construct pair was evaluated 5 min after adding the furimazine and plotted as relative luminescent units (RLU). For normalization purposes the luminescence of the negative control pair (AXER N LgBiT plus Halo C SmBiT in B; and AXER C LgBiT plus Halo C SmBiT in D) was used and set to 1. Reported data are from at least three independent experiments and shown with the standard error of the mean (SEM). Statistical analyses were performed using GraphPad Prism version 10. Letter N or C, coming after protein name, represents N or C terminally located LgBiT or SmBiT.

The AXER N LgBiT plus TRAP $\alpha$  C SmBiT reporter pair (Figure 37: A, light green line; B, light green bar) and the AXER N LgBiT plus TRAP $\beta$  C SmBiT reporter pair (Figure 37: A, grass green line; B, grass green bar) showed the significantly higher luminescent signal, in comparison to appropriate negative control pair with Halo C SmBiT (Figure 37: A, black line;

B, black bar). Also, the AXER C LgBiT plus TRAP $\alpha$  C SmBiT reporter pair (Figure 37: C, light green line; D, light green bar) and the AXER C LgBiT plus TRAP $\beta$  C SmBiT reporter pair (Figure 37: C, grass green line; D, grass green bar) showed stronger interaction in comparison to corresponding non-interacting Halo C SmBiT (Figure 37: C, black line; D, black bar). The intensity of luminescent signal suggested that AXER interacts with TRAP $\alpha$  and TRAP $\beta$ . Further, it was detected that N-terminus of AXER interacts stronger with the TRAP subunits, including the TRAP $\gamma$  C (Figure 37: B, dark green bar). The relative luminescence units provided by reporter pairs AXER N LgBiT plus TRAP $\gamma$  N SmBiT (Figure 37: B, dark green bar with pattern) and AXER C LgBiT plus TRAP $\gamma$  (N or C) SmBiT (Figure 37: D, dark green bar, and dark green bar with pattern) were under ten (RLU<10), indicating a non-specific interaction. The synthetic complementation approach with HaBiT peptide revealed a sufficient expression of the AXER LgBiT fusion protein (Figure 37: A and C; treatment 3).

### III.6.3.1. Is AXER capable of homo-oligomerization?

Tending to self-associate, many soluble and membrane-bound proteins form a complex of two or more identical subunits. The phenomenon is known as homo-oligomerization and, among other benefits, it contributes to protein stability and biological function (Koch, 2020; Gaber and Pavšič, 2021). It was found that 20% of eukaryotic proteomes form homo-oligomers (Schweke et al., 2024). Thus, among the other PPIs inspected in this work (described before), the NanoBiT assay was used to investigate the AXER homo-oligomerisation (i.e., AXER-AXER interaction; Figure 38).

Contrary to non-interacting pairs, AXER N LgBiT plus Halo C SmBiT (Figure 38: A, black line; B, black bar) and AXER C LgBiT plus Halo C SmBiT (Figure 38: C, black line; D, black bar), other reporter pairs provided a higher luminescence. In comparison to the LgBiT-tagged C-terminus of AXER (Figure 38: D, orange bars), the LgBiT-tagged N-terminus showed a higher affinity to interact with another AXER (N or C) SmBiT (Figure 38: B, orange bars). In the case of AXER C LgBiT plus AXER N SmBiT construct pair, relative luminescence units were below ten (RLU<10; Figure 38: D, orange bar (right)), suggesting a non-specific interaction (Sicking et al., 2021). A sufficient expression of the AXER LgBiT fusion was verified by the complementation approach with synthetic HaBiT peptide (Figure 38: A and C; treatment 3). Results indicated that AXER is capable to form homo-oligomers.

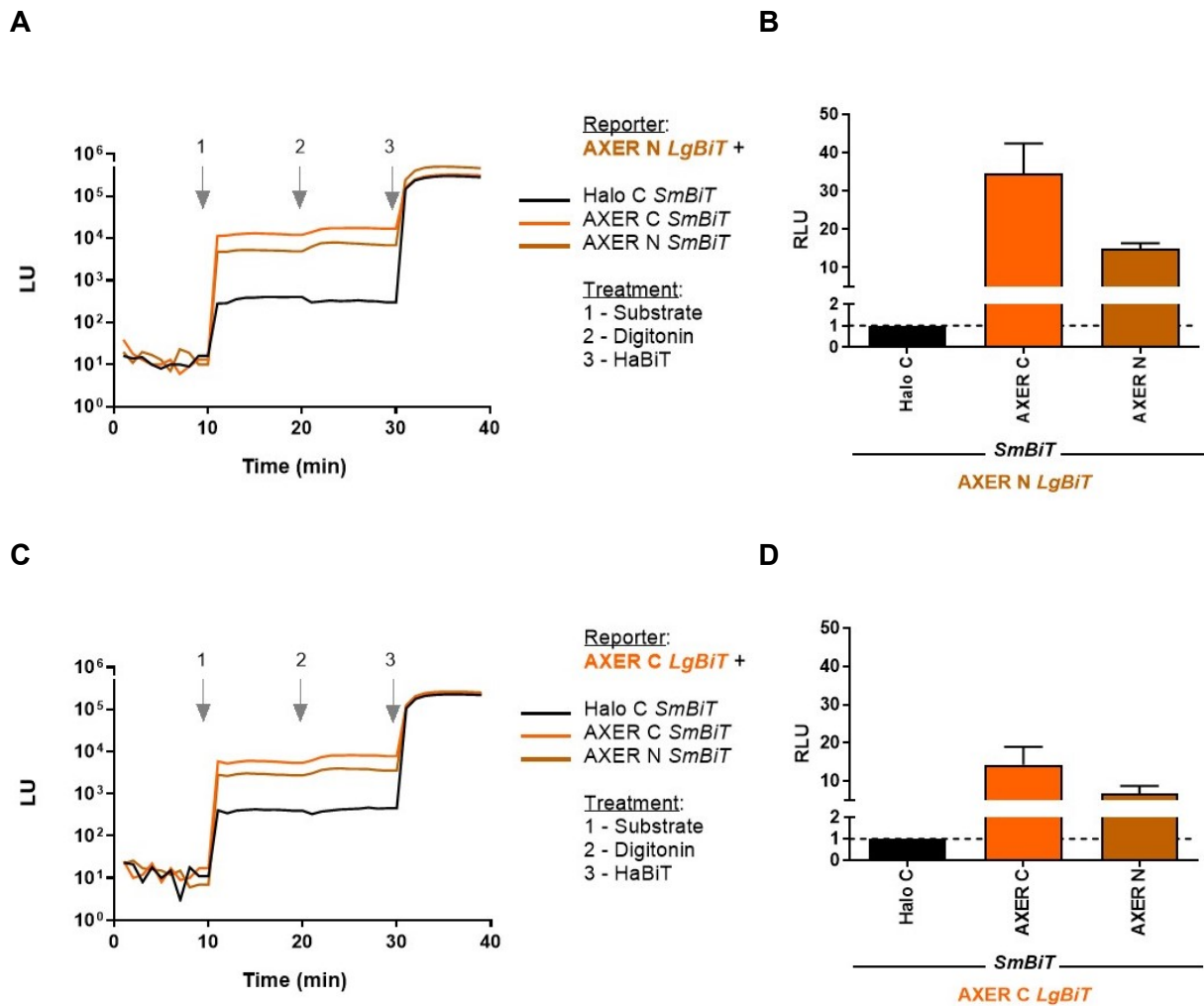


**Figure 38. AXER putative homo-oligomerization.** (A, C) Total luminescent units (LU) were measured 24 hours after HeLa cells were transfected with the indicated constructs. Nine minutes after baseline read, the luciferase substrate, furimazine was added to activate luminescence (marked as treatment 1). Digitonin (0.002%) was used for cell permeabilization (treatment 2, after 19 min) and followed by the addition of the synthetic HaBiT peptide (treatment 3, after 29 min). (B, D) The signal for each construct pair was evaluated 5 min after adding the furimazine and plotted as relative luminescent units (RLU). For normalization purposes the luminescence of the negative control pair (AXER N LgBiT plus Halo C SmBiT in B; and AXER C LgBiT plus Halo C SmBiT in D) was used and set to 1. Reported data are from three independent experiments and shown with the standard error of the mean (SEM). Statistical analyses were performed using GraphPad Prism version 10. Letter N or C, coming after protein name, represents N or C terminally located LgBiT or SmBiT.

### III.7. Additional results

#### III.7.1. Spot peptide array data

With the intention to verify the NanoBiT results which indicate the AXER interaction with subunits of Sec61- and TRAP-complex (III.6.3), the spot peptide array analysis was performed by Professor Dr. Martin Jung. As described earlier (II.6.1), the full-length sequence of AXER was covalently coupled to membranes in short, overlapping peptide fragments (15 amino acid length, shift of 3 amino acids from one peptide to the next). The membranes were incubated with ER membrane protein extracts, containing a high proportion of the Sec61- and TRAP-complex. Afterwards, protein detection was performed using the antibodies against the certain complex subunits.

The AXER-membranes, with the extract of ribosome-associated membrane protein (RAMP) fraction, showed a pronounced spot-pattern after incubation with the anti-Sec61 or anti-TRAP antibodies. With an extended exposure time, the small epitopes were detected; one corresponds to the cytosolic sequence of AXER, possibly interacting with TRAP $\alpha$  (Figure 39: A), and the other corresponds to the ER-luminally oriented AXER sequence that might interact with TRAP $\beta$  (Figure 39: B). Regarding the Sec61-complex, the detected small epitope (weak signal; Figure 39: C) corresponds to the membrane domain of AXER, indicating that the possible contact with Sec61 $\beta$  takes place in the ER membrane. With intention to achieve a better signal-to-noise ratio, the purified ER membrane protein complexes were used. However, the membranes incubated with the purified TRAP-complex showed a non-specific signal against the background level. On the other hand, the membranes incubated with the purified Sec61-complex revealed a difference in the spot-pattern signal. Yet, the signals were detected for the  $\alpha$  subunit only, while  $\beta$  subunit detection was at the background level. The detected signals of  $\alpha$  subunit (Figure 39: D) indicated the connection with sequence that is upstream of the AXER IQ motif (Figure 3). A repeat of the assay with the purified Sec61-complex confirmed this result.

To verify the putative AXER homo-oligomerization (III.6.3.1), the AXER-membrane was incubated with the RAMP fraction containing AXER. Subsequently, the AXER antibody were used for protein detection. Besides the antibody-specific epitope against which the antibody was directed (Figure 40, II 9-14), three possible contacts sites were determined (Figure 40), including the C-terminus (Figure 40, IV 9-14). The data indicated that AXER may form dimers or oligomers.

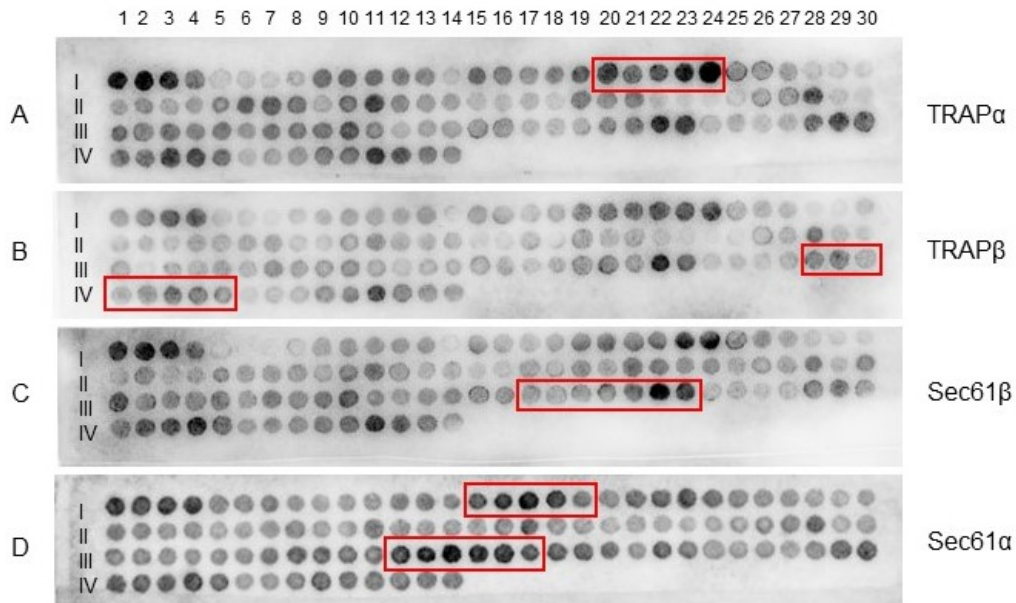


**Figure 39. Possible interaction sites of AXER-Sec61 and AXER-TRAP.** AXER peptide spots (15 amino acid length, shift of 3) incubation with RAMP or purified protein complex extract, and Sec61 or TRAP subunits antibodies. The highlighted area indicates the possible AXER interacting amino acid sequence; **(A)** I 20-24, IQC-VIN-AVF-AKI-LIQ-FFD-TAR-VDR-TRS (TRAP $\alpha$ ); **(B)** III 28-30, IV 1-5, VYF-GPL-TCS-IIT-TTR-KFF-TIL-ASV-ILF-ANP-ISP-MQW (TRAP $\beta$ ); **(C)** III 12-17, FAE-RYP-AII-YNI-LLF-GLT-SAL-GQS-FIF-MTV-VYF (Sec61 $\beta$ ); **(D)** I 15-19, GAK-QET-FTF-ALT-LVF-IQC-VIN-AVF-AKI and III 12-17, LLL-GMG-ILF-TGE-LWE-FLS-FAE-RYP-AII-YNI (Sec61 $\alpha$ ).

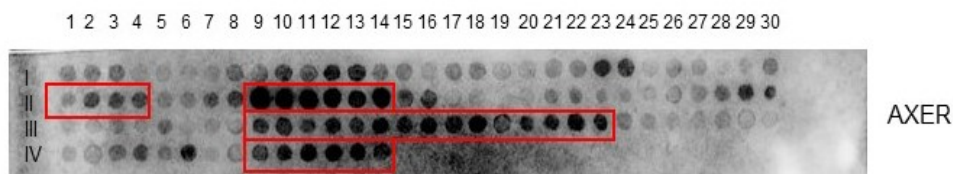


**Figure 40. Possible interaction sites of AXER-AXER.** AXER peptide spots (15 amino acid length, shift of 3) incubation with RAMP, and AXER antibody. The highlighted area indicates the possible interacting amino acid sequence; **II 1-4**, SIS-YLG-AMV-SSN-SAL-QFV-NYP-TQV; **II 9-14**, LGK-SCK-PIP-VML-LGV-TLL-KKK-YPL-AKY-LCV (AXER antibody-specific epitope); **III 9-23**, MLN-INL-WST-LLL-GMG-ILF-TGE-LWE-FLS-FAE-RYP-AII-YNI-LLF-GLT-SAL-GQS-FIF-MTV; and **IV 9-14**, MQW-VGT-VLV-FLG-LGL-DAK-FGK-GAK-KTSH.

## IV. DISCUSSION

Recently, Klein et al. (2018), the team from our lab, identified SLC35B1 (AXER) as the ATP/ADP exchanger in the mammalian ER membrane. Still, AXER's interactome remained insufficiently defined, becoming the main driving force of this work. The intention was to complement the current characterization of AXER by validating and broadening the scope of its interaction partners, that could provide valuable insights into its regulatory network. Considering AXER as the energy transporter in the ER, it was attractive to clarify its participation in the total cellular energy metabolism. In parallel, the aim was to continue the line of research regarding protein-protein interactions in living cells, focusing on the ER protein translocase and the Hsp70-family chaperone BiP.

### IV.1. “-Omic” analysis revealed the molecular changes occurring after AXER knockdown

The “-omic” technologies remarkably contributed to biological research, and the growing number of generated interaction maps significantly boosted the human knowledge about interdependency of genes and proteins, respectively (Hein et al., 2015; Uhlén et al., 2015; Horlbeck et al., 2018; Müller et al., 2020).

A powerful tool for studying transcriptome is RNA sequencing (RNA-seq) that allows quantification of expression of all genes at once (Geraci et al., 2020). In this work, the RNA-seq analysis allowed the comprehensive insights into the genomic landscape of AXER-depleted HeLa cells. The analysis revealed the changes in gene regulation, suggesting some of AXER's interaction partners as well as biological pathways it might be involved in. AXER was depleted in HeLa cells using two AXER siRNAs (#1 and #4), while the control (Ctrl) was treated with a scrambled siRNA (II.2.2). The interpretation of the RNA-seq data revealed the clear differences between these three conditions (AXER #1, AXER #4 and Ctrl), evident in the heatmap (Figure 17: A). This visualization also showed greater similarities between AXER #4 and control, compared to those observed between AXER #1 and control. The distinctions between AXER #1 and AXER #4 could arise from variations in the biological impact of the siRNAs used for AXER gene silencing, possibly due to unforeseen off-target effects (Birmingham et al., 2006; Ui-Tei et al., 2008). Yet, AXER #1 and AXER #4 showed high similarities in the gene regulation due to AXER knockdown (Figure 17: C). Importantly, the AXER gene was identified as downregulated (Table 14, Appendix), confirming successful gene silencing. The gene was detected among the DEGs annotated to the “integral component of endoplasmic reticulum membrane” (the GO term – cellular compartment), agreeing with the localization of human AXER (Klein et al., 2018). Furthermore, the RNA-seq data (Table 14, Appendix) revealed a downregulation of the Sec61  $\alpha$  and  $\beta$  subunits as well as subunits of the TRAP- and OST -complex. That fits well with the observed down-regulation of the GO terms

related to protein localization to ER, and protein glycosylation. Interestingly, the heatmap from the other, independent study (representing genes from UPR Perturb-seq experiment, Adamson et al., 2016) showed AXER in a position close to the Sec61 $\beta$  and STT3A indicating their similar expression pattern, that aligns with the findings in this work. In addition, the RNA-seq analysis after TRAP $\beta$  gene silencing revealed down-regulation of AXER (unpublished data from our lab), supporting the detected relation between these two ER membrane proteins. On the other hand, depletion of the gene encoding for Sec61 $\alpha$  did not significantly affect the regulation of AXER gene (unpublished RNA-seq data from our lab). These two proteins could interact as elements of the ER protein import; as a direct player (Sec61 $\alpha$ ; the key component of the ER translocon), and as an indirect participant (AXER; enables the ER ATP-supply, at first place for the ER luminal chaperone BiP). Moreover, the role of Sec61 $\alpha$  in facilitating the passive Ca<sup>2+</sup>-leakage from the ER lumen to the cytosol may have an impact on the AXER regulatory mechanism (I.3.1.1; Klein et al., 2018). However, the abundance of these two proteins might not be strictly influenced by each other. The SRP-dependent pathway serves as an example, where an up-regulation of the SR $\alpha$  gene was noted after Sec61 $\alpha$  knockdown (Lang et al., 2012), while silencing of SR $\alpha$  marginally reduced the abundance of Sec61 $\alpha$  (O'Keefe et al., 2021).

Interestingly, the gene encoding SR $\alpha$  exhibited up-regulation after AXER depletion as well. Conversely, the GO term associated with SRP-dependent protein targeting to the ER was downregulated (Figure 19: B), as majority of genes implicated in the ER protein processing, including the luminal chaperone BiP (Table 14, Appendix). BiP is ATP-dependent (I.4) and limited source of ATP<sub>ER</sub>, caused by loss of AXER, resulted with its dissociation from Sec61 $\alpha$  and consequent Ca<sup>2+</sup>-leakage into the cytosol (Schäuble et al., 2012; Klein et al., 2018). The detected BiP dysregulation and its low protein abundance (Figure 25) align with the downregulated GO term related to the ER chaperones. Depletion of Ca<sup>2+</sup> in the ER poses a risk of exacerbating the disruption of the ER energy homeostasis, leading to the excessive accumulation of misfolded proteins. In such cases, the activation of PERK and the subsequent reduction in energetically costly protein synthesis help mitigate the effect on overall energetics (Figure 7). However, the genes encoding for PERK and two other UPR proteins, IRE1 and ATF6, were identified as downregulated after AXER depletion (Table 14, Appendix). That is in agreement with the observed down-regulation of the GO term related to ER stress, and additionally supports the detected low BiP. Furthermore, a down-regulation was observed for the gene encoding for the sarcoplasmic/endoplasmic reticulum ATPase (SERCA; Table 14, Appendix), which maintains the Ca<sup>2+</sup> gradient between the ER lumen and cytosol (Wuytack et al., 2002). Inadequate SERCA abundance hindered the ER Ca<sup>2+</sup> recovery. SERCA is ATP-dependent and uses ATP from the cytosolic side of the ER membrane (Aguayo-Ortiz and

Espinoza-Fonseca, 2020). So, the identified drop of total cellular ATP-production after AXER knockdown (discussed in IV.2) could affect its gene regulation and protein level.

Even if cells attempt to replenish the ATP<sub>ER</sub> (by suggested regulatory mechanism(s); Figure 4; Klein et al., 2018; Yong et al., 2019; Zimmermann and Lang, 2020) as well as the BiP and SERCA levels, the ER energy homeostasis would still be compromised due to initial loss of AXER. This indicates a prolonged disruption of both the ER energy homeostasis and ER Ca<sup>2+</sup> homeostasis. Consequently, the constant Ca<sup>2+</sup>-leakage from the ER lumen to the cytosol might cause the Ca<sup>2+</sup> overload in mitochondria leading to autophagy, and apoptosis (Rimessi et al., 2008; A. Li et al., 2022; Matuz-Mares et al., 2022). This scenario is supported by the upregulated GO term related to mitophagy as well as the upregulated apoptotic pathway. Moreover, this might explain the observed low ATP-generation through both glycolytic activity and OXPHOS (IV.2). Namely, proposed by Yong et al. (2019), the “ATP usage in the ER may increase mitochondrial OXPHOS while decreasing glycolysis”; but the mitochondrial autophagy (mitophagy) decreased the ATP production by OXPHOS and subsequently caused a drop in total cellular ATP.

The autophagy and mitophagy could be regulated by the AMPK complex (Herzig and Shaw, 2018), a central player of signaling pathway which maintains the cellular energy balance. The ratio between protein abundance of AMPK and its phosphorylated form pAMPK was significantly elevated (Figure 25), indicating the AMPK complex activation. The increased level of pAMPK after AXER knockdown was also detected earlier by Klein et al. (2018). The authors suggested the kinase CaMKK2 (CaMKK $\beta$ ) as AMPK activator and PFK2 as its target-component for downstream glycolysis (Figure 4: A). However, the RNA-seq data (Table 14, Appendix) showed that AMPK subunit isoforms were differently regulated upon AXER siRNA treatment. Furthermore, the LKB1 (STK11) kinase was upregulated, while CaMKK2 was downregulated (with an elevated protein level; Figure 25). A different gene regulation was detected for PFK2 as well as Calmodulin1, which participates in the activation of CaMKK2 (Figure 4: A). These findings do not offer a clear backing for the regulatory mechanism suggested by Klein et al. (2018).

Previously, Vishnu et al. (2014) suggested that the Ca<sup>2+</sup>-regulated increase of ATP<sub>ER</sub> requires the AMPK activity. Intriguingly, one of the pathways observed as downregulated after AXER depletion was the AMPK-signaling pathway (Figure 21: B; Figure 22: B). Considering that some of the AMPK subunit isoforms were downregulated (Table 14, Appendix) it is possible that the downstream pathways regulated by the AMPK-complex(es) composed of these subunits (for better understanding, see I.1.3) were limited. Notably, antibodies used for the AMPK and pAMPK identification (Table 3) targeted the catalytic subunit isoforms,  $\alpha$ 1 and  $\alpha$ 2; so, the exact AMPK complex that was phosphorylated (activated) could not be determined. Based on the genes that were upregulated (Table 14, Appendix) it could be the AMPK complex

$\alpha 1\beta 2\gamma 2$ . However, none of AMPK substrates was identified as strictly or primarily phosphorylated by a specific AMPK complex, so far (Herzig and Shaw, 2018).

On the other hand, the detected up-regulation of autophagy and apoptosis could be governed by SQSTM1 (Sánchez-Martín and Komatsu, 2018), which was significantly upregulated upon AXER silencing (Table 14, Appendix). The accumulation of SQSTM1 was detected in multiple forms of cancer, including cervical cancer (Sánchez-Martín et al., 2019; [Expression of SQSTM1 in cancer - Summary - The Human Protein Atlas](#), last checked at 14/06/24). Furthermore, findings from Ha et al. (2017) indicate that SQSTM1, phosphorylated by AMPK, drives mitophagy (autophagy), serving as a mechanism for cell death in rat hippocampal neural (HCN) stem cells. The other findings, from Yu et al. (2021), suggest that SQSTM1 could promote autophagy and apoptosis by regulating the AMPK/AKT/mTOR signaling pathway in papillary thyroid cancer (PTC). Considering these findings, it is possible that a certain AMPK-SQSTM1 (inter)regulation was triggered by AXER knockdown, inducing autophagic and apoptotic events. However, SQSTM1 was also upregulated after SEC61A1 gene silencing in HeLa cells as well as after hSND2 and TMEM109 silencing, respectively (unpublished RNA-seq data from our lab). This indicates that an increased expression of SQSTM1 is not exclusively triggered by loss of AXER. Instead, it might be a stress-responsive reaction of cancer cells.

Collectively, the observed results indicate a complex interplay of processes that mutually influenced each other due to AXER depletion. It is unclear whether the identified molecular changes are linked to a certain adaptability of cancer cells or if they are the result of cell's efforts to restore the ER energy homeostasis, or both. Further investigation is needed to unravel the complexities of this question.

As earlier, the sample preparation for mass-spectrometry (proteomic approach) included siRNA-mediated gene silencing. The expression of the AXER gene was suppressed aiming to significantly deplete the level of corresponding protein. However, the mass-spectrometry-based protein abundance data did not show AXER as one of the differently expressed proteins. The low level of native AXER in HeLa cells (Hein et al., 2015) could elucidate the absence of AXER in the proteomic results. Proteomic approaches are primarily designed for investigating soluble proteins and often face limitations in identifying and characterizing proteins within biological membranes. The hydrophobic nature of membrane proteins and their low abundance frequently interfere with their analysis (Helbig et al., 2010). Despite of displaying different fold of changes, the expressions of target proteins for both AXER-depleted samples (#1 and #4) share similar trends of either reduction or elevation (Table 13). Furthermore, the data comparison revealed the fairly similar changes of the regulation of target genes (transcriptomic analysis) and the expression of corresponding proteins (proteomic analysis) after AXER knockdown. The certain disparity observed between protein levels and their coding

transcripts may be attributed to the spatiotemporal fluctuations of mRNAs, coupled with the abundance of resources for protein synthesis (Liu et al., 2016).

In sum, the “-omic” results collectively highlighted the key players in the ER protein import (i.g., Sec61-complex; TRAP-complex; BiP; Oligosaccharyltransferase) and/or the ER  $\text{Ca}^{2+}$ -homeostasis (i.g., SERCA) as AXER’s interaction partners. These findings are in accordance with the previous co-immunoprecipitation analysis conducted by Klein et al. (2018). Thus, the “-omic” analysis enabled an ex-post (“after the fact”) selection of proteins, which were prime candidates for further investigation of the AXER interactome in intact cells (IV.3.2).

#### **IV.2. Cellular energy-producing activities affected by loss of AXER**

One of the objectives of this work was to detect possible changes in cellular energy metabolism upon AXER depletion. To achieve that, the live-cell metabolic analysis was performed. It included two fluorescence-based assays: pH-Xtra assay, that monitors extracellular acidification rate (ECAR; glycolytic activity; II.4.4.2); and MitoXpress Xtra, that monitors oxygen consumption rate (OCR; mitochondrial respiration; II.4.4.1). The change in fluorescent signal was measured kinetically on a plate reader, and it was indicator of the rate of corresponding metabolic activity in real time. As a pre-step, HeLa cells were transfected with two AXER siRNAs (#1 and #4) or control siRNA (Ctrl). After 72 hours, cells were subjected to the live-cell metabolic analysis.

Due to the specific experimental conditions, HeLa cells were used as suspension cells in both assays (Figure 26; Figure 27: A). In addition, adherent HeLa cells were used (Figure 27: B) and served as control. The results demonstrated (i) that HeLa cells act in a more excellent manner when they are attached to a surface (in adherent mode) as well as (ii) that, if experimental approach requires, HeLa cells can be used as free-floating cells (in suspension mode), not affecting a result significantly (Figure 27: A and B, right).

Samples treated with the AXER siRNAs (#1 and #4) showed a non-significant difference in comparison to each other, for both measured activities (Figure 26, right; and Figure 27: A and B, right). On the other hand, the fluorescent signal was significantly reduced upon AXER depletion, in comparison to control. Data demonstrated that both metabolic pathways, glycolysis (Figure 26) and mitochondrial respiration (Figure 27), are perturbed, leading to conclusion that the loss of AXER causes a decline in total cellular ATP-production. However, Klein et al. (2018) detected a non-significant difference in the cytosolic ATP level between AXER-depleted samples and control, while the level of  $\text{ATP}_{\text{ER}}$  was significantly lower upon AXER depletion in HeLa cells. Still, considerable differences existed between experimental approaches, such as the duration of AXER siRNA-mediated silencing, the length of live-cell measurement/recording, and the number of examined cells.

Apparently, more studies are needed to investigate the role of AXER in energy metabolism. One experimental method that might be employed is the simultaneous live-cell measurement of glycolytic activity and mitochondrial respiration by the Seahorse assay (Caines et al., 2022). Furthermore, AXER's involvement in energy metabolism could be examined under different cellular conditions and perturbations. This could be achieved through pharmacological manipulations targeting various components of the AMPK pathway (e.g., CaM inhibitors, trifluoperazine, and ophiobolin A; CaMKK2 inhibitor, STO-609; AMPK inhibitor, dorsomorphin). Considering that cancer cells display markedly modified energy metabolism and adaptive abilities (Moreno-Sánchez et al., 2007), there is a possibility that they respond in a very specific way upon AXER depletion (i.e., energetic stress). Hence, it would be beneficial to conduct parallel experiments using non-cancer cells.

### **IV.3. Valuable insights into protein-protein interactions of the ER residents**

The identification of meaningful protein-protein interactions (PPIs) is performed best in intact cells. Recently, the NanoBiT assay was established in our lab and used to demonstrate the PPIs of several ER membrane proteins in living cells (Sicking et al., 2021). The applied luciferase (Nanoluciferase, NanoLuc) is composed of two complementary subunits, Large BiT (LgBiT) and Small BiT (SmBiT) that are fused to proteins of interest. If proteins come in close proximity, their interaction results in re-assembly of the functional luciferase, enabling catalysis of the luminescent reaction (Hall et al., 2012; Dixon et al., 2016). Importantly, luminescence of the properly reconstituted luciferase was emitted in the ER lumen and could efficiently be detected (Sicking et al., 2021). It was demonstrated by the interaction between Sec61 $\beta$  and Sec63 that were lumenally tagged with LgBiT and SmBiT, respectively.

#### **IV.3.1. Interactions of the ER protein translocase demonstrated in living cells**

One of the goals of this work was to extend the study from our lab and quantitatively analyse more PPIs of the ER protein translocase. Focus was on the reporter pairs with topological layout that allows ER-lumenally located BiT-tags (Figure 28: A and B). The set of construct pairs included Sec61 $\beta$  C LgBiT plus Sec63 N SmBiT pair that served as control (~290 RLU; Figure 28: D).

Considering that Sec61 $\beta$  and Sec61 $\gamma$  are subunits of the same protein-complex, their connection was expected. Yet, using NanoBiT approach, the Sec61 $\beta$ -Sec61 $\gamma$  interaction was verified in living mammalian cells. Even more, the reporter pair of Sec61 $\gamma$  C LgBiT and Sec61 $\beta$  C SmBiT provided luminescence of ~630 relative luminescent units (RLU; Figure 28: F). The RLUs indicate the strength and constancy of that PPI (Sicking et al., 2021). Thus, detected

high luminescent signal demonstrated that luminal C-termini of Sec61 $\beta$  and Sec61 $\gamma$  are closely located, and that subunits interact strongly. That agrees well with the structure of Sec61-complex (Lang et al., 2017). Interestingly, the Sec61 $\alpha$ -Sec61 $\beta$  construct pair provided a signal (141 RLU; Sicking et al., 2021) that is approximately 4.5-fold weaker than the signal detected for Sec61 $\beta$ -Sec61 $\gamma$ . Though, the construct pairs were tagged with a differently located subunits of the luciferase. While the Sec61 $\alpha$ -Sec61 $\beta$  interaction was measured using cytosolically BiT-tagged protein constructs, the Sec61 $\beta$  and Sec61 $\gamma$  were lumenally tagged.

Further, the Sec61 $\gamma$ -Sec63 interaction was demonstrated, providing the high luminescence of ~280 RLU that is similar as signal intensity of the Sec61 $\beta$ -Sec63 interaction (Figure 28: D and F). It was proposed earlier that Sec61 $\beta$  subunit keeps Sec63 near the Sec61-complex, to be available when protein transport requires its rapid inclusion (Sicking et al., 2021). The Sec61 $\beta$ -Sec63 and Sec61 $\gamma$ -Sec63 interactions, demonstrated in this work, support this idea, indicating that both  $\beta$  and  $\gamma$  subunits, act as mediators that keep Sec63 close to the Sec61-complex.

Moreover, interaction between the ER membrane translocase and ER luminal chaperone BiP was demonstrated in living cells. This was the first detection of PPI in the ER lumen that include a soluble protein. As the “nearest neighbors” of Sec61 $\alpha$ , it was presumed that subunits  $\beta$  and  $\gamma$  also associate with BiP, and luminescent signal of construct pairs Sec61 $\beta$  C LgBiT plus BiP SmBiT, and Sec61 $\gamma$  C LgBiT plus BiP SmBiT was measured in HeLa cells (Figure 28: D and F). The signal intensity for both detected interactions (Sec61 $\beta$ -BiP and Sec61 $\gamma$ -BiP) reached ~50 RLU, indicating a mid-strong or less-constant interaction that aligns well with the BiP’s lively role in the ER lumen (I.4). Also, the detected interactions indirectly verify the luminal BiP-binding site of the Sec61 $\alpha$ , determined by Schäuble et al. (2012) (Figure 6). This can be additionally tested in future using SEC61A1 Y344H mutant cells incapable to bind BiP. Furthermore, all detected PPIs can be supported by two methods: 1) Western blot analysis employing the in-house generated anti-SmBiT antibody which demonstrates the expression of SmBiT fusion protein (Sicking et al., 2021); and 2) overexpression of the native, untagged protein(s) as a competitive strategy (Sicking et al., 2021).

Altogether, the detected luminescent signal of PPIs with ER-lumenally located BiT-tags confirmed the efficient luminal reconstitution of the luciferase.

#### **IV.3.1.1. BiP-Sec61 interaction disrupted by ER stress**

Intending to examine the dynamics of detected interaction between BiP and Sec61-complex, the ER stress was provoked in HeLa (Figure 30) and HeLa- $\mu_s$  cells (Figure 31; Figure 34). Previously, it was demonstrated that BiP dissociates from the Sec61 $\alpha$  to deal with the excess number of misfolded proteins in the ER (Schäuble et al., 2012). Also, BiP acts as a chaperon dependent on Ca<sup>2+</sup>, and its functionality may be disrupted by an imbalanced ER calcium homeostasis (Preissler et al., 2020). Therefore, ER stress was induced by a) a short-term

treatment with thapsigargin (Tg) and/or tunicamycin (Tun) (i.e., chemical ER stress; Figure 30; Figure 31); and b) a different length of treatment with the synthetic steroid mifepristone (Mif) that triggers the ER luminal accumulation of immunoglobulin M heavy-chain in mutant HeLa- $\mu_s$  cells (here referred to as physiological ER stress; Figure 34). Under these specific conditions, the BiP-Sec61-complex interaction was challenged, and the changes in luminescence were monitored in living cells.

Indeed, the luminescent signal of corresponding interaction (Sec61 $\beta$ -BiP and Sec61 $\gamma$ -BiP) was significantly decreased (Figure 30; Figure 31), suggesting that BiP's connection with Sec61-complex is disrupted due to perturbation of the ER homeostasis. Also, the signal was significantly more reduced when the Tg/Tun mix was used in comparison to the individual stressor (Figure 31: B and D). This is in correlation with the abovementioned BiP Ca<sup>2+</sup>-dependency as well as with BiP engagement by misfolded proteins and subsequent dissociation from Sec61 $\alpha$ .

In addition, the stress-inducing drug treatment was found to significantly reduce the luminescent signal of the BiP-Sec63 interaction (Figure 33). The analysis revealed the BiP-Sec63 as a weak interacting pair (~13 RLU; Figure 33: B) under non-stress conditions. Yet, an unusually high luminescent signal of the negative control pair BiP LgBiT plus Halo C SmBiT (Figure 33: A) was the reason for such a low RLU-calculation. Although speculative, the LgBiT and SmBiT subunits might spontaneously associate (re-assembly) providing a luminescent signal, without interaction between BiP and Halo. This phenomenon could occur due to a millimolar concentration of BiP in the ER lumen (Lang et al., 2017) and its ability to form oligomers (Preissler et al., 2015), coupled with the successful expression of Halo throughout the cell ([NanoBiT® Protein:Protein Interaction System Technical Manual TM461 \(promega.de\)](https://www.promega.de), last checked at 14/06/24). Alternatively, a close association between BiP LgBiT and Halo C SmBiT could be based on BiP functioning as a chaperone supporting the folding of the Halo protein. Yet, both these scenarios of spontaneously re-assembly as well as chaperoning are unlikely considering the supposed localisation of BiP in the ER lumen and of Halo in the cytosol. Both proteins should not interact as they are physically separated by the intact ER membrane. Although not further investigated, maybe a significant portion of the synthesized BiP LgBiT remains in the cytosol instead of being imported into the ER. As a better suited negative control, it should be considered to construct a Halo C SmBiT targeted to the ER lumen by adding an efficient ER signal peptide at the N-terminus. Such an "ER-Halo C SmBiT" version would eventually serve as better negative control. Of note, the experiments with a luminal LgBiT and a cytosolic Halo C SmBiT did not show an extensively reduced total background luminescence compared to experiments where LgBiT and Halo C SmBiT were present in the cytosol. Hence, it is unlikely that the strength of interaction signals detected using ER-luminally located NanoBiT sensors are overestimated. The dynamic response to the

chemical stressors strongly supports the bona fide interaction partners detected in this work. This leads to conclusion that the BiP-Sec63 interaction is stronger than initially calculated, as expected considering their chaperone – co-chaperone relationship (Lang et al., 2012; Linxweiler et al., 2017).

The physiological ER stress (i.e., protein-driven ER stress), induced by long-term overload of the ER folding capacity, confirmed the detected stress-impact on the BiP-Sec61-complex interaction. Although certain fluctuations were noticed, the drop in luminescent signal intensity was equally significant irrespective of Mif treatment duration (Figure 34: B and D). The signal fluctuations indicate the changes in BiP abundance (SmBiT-tag) regulated by the unfolded protein response (UPR) over time (Bakunts et al., 2017).

Furthermore, it was necessary to clarify that the detected luminescence reduction under stress conditions was not caused by  $Ca^{2+}$ -dependency of the NanoLuc luciferase. For that purpose, the measurement of luminescence units (LU) was performed using the cytosolically located cAMP-dependent protein kinase A (PKA) construct pair (positive control; Figure 32 and Figure 35).

Overall, the observed change in luminescent signal in living cells demonstrated that (i) the interactions of BiP-Sec61-complex and BiP-Sec63 are changing during ER stress; (ii) a prolonged protein misfolding in the ER lumen activates the UPR; and (iii) the Nanoluciferase is  $Ca^{2+}$ -independent. The live-cell assay enabled to capture the transient and dynamic nature of the interactions between BiP and the ER membrane residents, offering insights into the kinetics of the ER events under stress conditions.

### IV.3.2. AXER interaction partners identified in intact cells

Indicated as AXER's interaction partners ("playmates") through various experimental methods, in this work and earlier (Klein et al., 2018), the subunits of the Sec61- and TRAP-complex were selected for a PPI investigation using the NanoBiT live-cell assay. This approach enabled the examination of AXER interactions with rationally picked target proteins in their natural cellular environment.

The AXER construct with the LgBiT-tag on the N-terminus (AXER N LgBiT; Figure 36: A and B; Figure 37: A and B) showed a more robust response, indicated by a greater luminescence, when paired with constructs of the Sec61 and TRAP subunits than the AXER construct with LgBiT-tag on the C-terminus (AXER C LgBiT; Figure 36: C and D; Figure 37: C and D). Therefore, the interactions of the AXER N LgBiT are preferentially discussed.

AXER demonstrated the connections with Sec61 $\alpha$  (~30 RLU; Figure 36: B, petroleum bar) and Sec61 $\beta$  (~35 RLU; Figure 36: B, purple bar), suggestive of a low-to-mid-strong PPI. Similar results were observed in the case of AXER-TRAP $\beta$  interaction (~35 RLU; Figure 37: B, grass green bar), while AXER-TRAP $\gamma$  was identified as a weak interacting pair (~15 RLU; Figure 37:

B, dark green bar). On the other hand, AXER-TRAP $\alpha$  showed luminescence of ~50 RLU (Figure 37: B, light green bar), suggesting a slightly stronger interaction. Considering a coexistence of the endogenous proteins (AXER, Sec61, and TRAP) alongside BiT-tagged expressed proteins in transfected cells, a potential competitive interaction might occur and reduce the observed luminescent signal intensity. For additional examination of strength of the detected interactions, a depletion of the endogenous proteins can be performed by siRNA-mediated silencing as experimental pre-step. Furthermore, the AXER construct with SmBiT-tag incorporated in its ER-luminal-loop 3 was generated in this work (Table 9) and can be tested with the constructs of the Sec61- and TRAP- complex containing ER-luminally located LgBiT-tags. Moreover, all AXER constructs utilized for the NanoBiT experiments were generated from the AXER-isoform 1 plasmid (Table 9); yet it is still unresolved which AXER isoform/isoforms is/are present in HeLa cells (Klein et al., 2018). Therefore, it may be useful to generate AXER BiT-tag constructs based on the other two known isoforms of human AXER, and additionally examine the detected PPIs.

The AXER proximity to  $\alpha$  and  $\beta$  subunits of both the Sec61 and TRAP, aligns well with the latest Sec61-TRAP complex atomic model, observed from the cytosolic side of the ER membrane (Jaskolowski et al., 2023). Moreover, spot peptide array analysis revealed the possible contact sites of the detected interactions (Figure 39). Noteworthy, the results suggest that Sec61 $\alpha$  interacts with the sequence that is close to the AXER IQ motif. These findings (i.e., the detected interactions of AXER with Sec61 $\alpha$  and TRAP $\alpha$ ), along with the Sec61 $\alpha$  containing IQ motif (Figure 6) and the characterization of TRAP $\alpha$  as a Ca<sup>2+</sup>-binding protein (Wada et al., 1991), strengthen the indications that AXER is part of an extensive signaling cascade where calcium (Ca<sup>2+</sup>) could serve as a potent regulator (Klein et al, 2018; Yong et al., 2019). However, additional studies are required to elucidate the mechanism of this regulation. Inducing ER stress (as discussed in IV.3.1.1) and evaluating the impact of Ca<sup>2+</sup>-leakage from the ER lumen to the cytosol on the detected interactions between AXER and the Sec61- or TRAP- complex could offer useful information. It might be interesting to investigate AXER's interactions with some other ER membrane proteins suggested to bind calcium, such as Sec62 (I.4.1; Linxweiler et al., 2013) and/or Calnexin, which also requires ATP for its interaction with substrate (Wada et al., 1991; Ou et al., 1995; Paskevicius et al., 2023). Moreover, exploring AXER's interactions with proteins at the mitochondrial–ER contact sites (MERCs; Klein et al., 2018) might generate valuable perspectives.

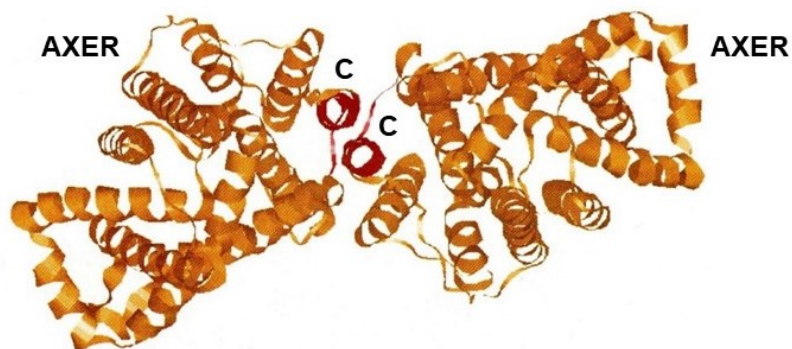
In sum, the identified interactions in living cells added a layer of authenticity to previous findings. Together with spot array analysis, they provided a more precise representation of how AXER interacts with Sec61- and TRAP-complex within the ER membrane. Future investigations employing cryo-electron microscopy (cryo-EM) and X-ray crystallography can verify and further explore the AXER interactome.

### IV.3.3. Putative AXER homo-oligomer

Aside from the AXER interactions with the Sec61 and TRAP subunits discussed before, the NanoBiT approach identified an AXER-AXER interaction indicative of homo-oligomerization (Figure 38). Spot peptide array analysis was performed to further support this finding. Indeed, the analysis revealed the potential contact sites of the AXER dimer or oligomer (Figure 40). In addition, the visualization of dimer molecular structure suggested that two AXER molecules could be oriented front-to-front (Figure 41: A) or front-to-back (Figure 41: B). Considering the detected possible interaction sites (III.7.1; Figure 40), the front-to-front model might be more authentic.

In the field of proteins, dimer formation is a common occurrence. Yet, defining the physiologically relevant structure of certain proteins can be challenging. An ongoing debate serves as a prime example, questioning whether the ATP/ADP carrier in the inner membrane of mitochondria, also known as the adenine nucleotide translocator (ANT), operates in form of a monomer or a dimer (Klingenberg, 2008; Liu and Chen, 2013; Kunji et al., 2016; Bernardi et al., 2023). It is interesting to speculate that, in a putative dimeric model, two AXER entities could operate synchronously, importing ATP into the ER and exporting ADP into the cytosol, jointly contributing to the regulation of energy balance within the organelle. Furthermore, the ER AXER dimer could interact with the mitochondrial ANT dimer at the mitochondrial-ER contact sites, where these two organelles might directly exchange nucleotides (i.e., ER  $\text{ATP}_{\text{in}}/\text{ADP}_{\text{out}}$  and mitochondria  $\text{ATP}_{\text{out}}/\text{ADP}_{\text{in}}$ ). Intriguing asymmetrical affinities of AXER for ATP transport across the ER membrane (I.3.1; Schwarzbaum et al., 2022) might be related to dimer formation as well; that remains to investigate. It would be interesting to check if the AXER dimer could integrate into the Sec61-TRAP complex proposed by Jaskolowski et al., (2023). Generating the BiT-tag constructs of other two human AXER isoforms may be useful for further exploration of dimer/oligomer formation. There is a possibility that multiple AXER molecules surround the Sec61-TRAP complex and act depending on the cellular conditions and ER energy requirements. Hence, investigating whether the oligomeric state of AXER is affected by ER stress could supply valuable information. Besides its preferential ATP/ADP exchange, AXER has been identified as contributor to the uptake of UDP-glucuronic acid (UDPGA; Ondo et al., 2020). Moreover, it is suggested to function as a broad-range antiporter for nucleotides (Schwarzbaum et al., 2022). For comparison, the mitochondrial ANT is also described as a multifunctional protein, involved in the energy homeostasis and cell death (Hoshino et al., 2019; Brourd et al., 2020). However, the precise nature of AXER-AXER interaction remains unclear and subsequent investigations are imperative to elucidate and validate these so-far-theoretical constructs of AXER dimerization or oligomerization (Figure 41).

A



B

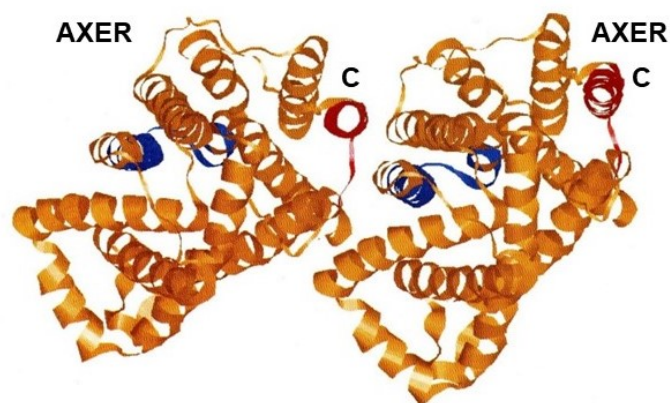


**Figure 41. Putative AXER dimer.** View from the cytosolic side of the ER membrane. Contact sites determined by the spot peptide array analysis (III.7.1). **(A)** Front-to-front orientation. The interaction between C-termini (red; for amino acid sequence, see Figure 40: IV 9-14) of two AXER molecules. **(B)** Front-to-back orientation. Interaction between the C-terminus (red) of one AXER molecule and the other detected possible contact site (blue; for amino acid sequence, see Figure 40: II 1-4) of the second AXER molecule. Visualization of the molecular structure by molecular graphic program RASWin (version 2.6). C, carboxy terminus.

#### IV.4 Conclusion and further directions

Nearly all cellular functions depend on the presence of adenosine triphosphate (ATP), used as primary energy source as well as a signaling molecule. Any disruption of energy-producing and/or energy-supplying activities potentially leads to cell collapse and subsequent apoptotic event. Therefore, the identified decline in total cellular ATP-production after the loss of AXER may not be so surprising. Although such an effect on the global cellular energetics after AXER depletion was not detected before, the differences in experimental approaches between this and the previous research should be considered. However, AXER's involvement in the complex signaling cascade and the role of  $\text{Ca}^{2+}$  as its regulator remain an active area of investigation. Since AXER knockdown indicates a “domino effect” and wide-ranging consequences on cell survival, one of the possibilities to continue this line of research is to generate mutation in the AXER IQ motif, making it unable to bind calmodulin, and subsequently measure the changes in  $\text{Ca}^{2+}$  and ATP/ADP levels in the ER and cytoplasm. On the other hand, some companies already offer the SLC35B1 (AXER) knockout kit (CRISPR), suggesting that the total loss of AXER on the transcriptional level might be compatible with life. It is possible that some adaptive cellular mechanism compensates for total AXER loss and/or another ER membrane protein with a similar function maintains sufficient ATP supply for the ER. To what extent the loss of AXER reshapes the energy metabolism in the cell is an important question that demands attention in forthcoming studies.

Using a variety of experimental methodologies in this work, preferentially relying on the bimolecular luminescence complementation (BiLC) approach in intact cells, the components of AXER interactome were successfully identified. Accumulating data suggest AXER's interaction with the ER proteins crucial for protein import and/or ER  $\text{Ca}^{2+}$  homeostasis, strongly supporting previous findings. The putative AXER form of a dimer/oligomer may serve as a foundation for subsequent studies, including both structural and biochemical analysis, with the aim of yielding a comprehensive mechanistic understanding of AXER activity. The BiLC approach was also instrumental in demonstrating the impact of ER stress on the interactions between the ER protein translocase and the luminal chaperone BiP. This work highlights the significance of exploring protein interactions in living cells, offering valuable insights into how protein interactions occur within the complex biological milieu.

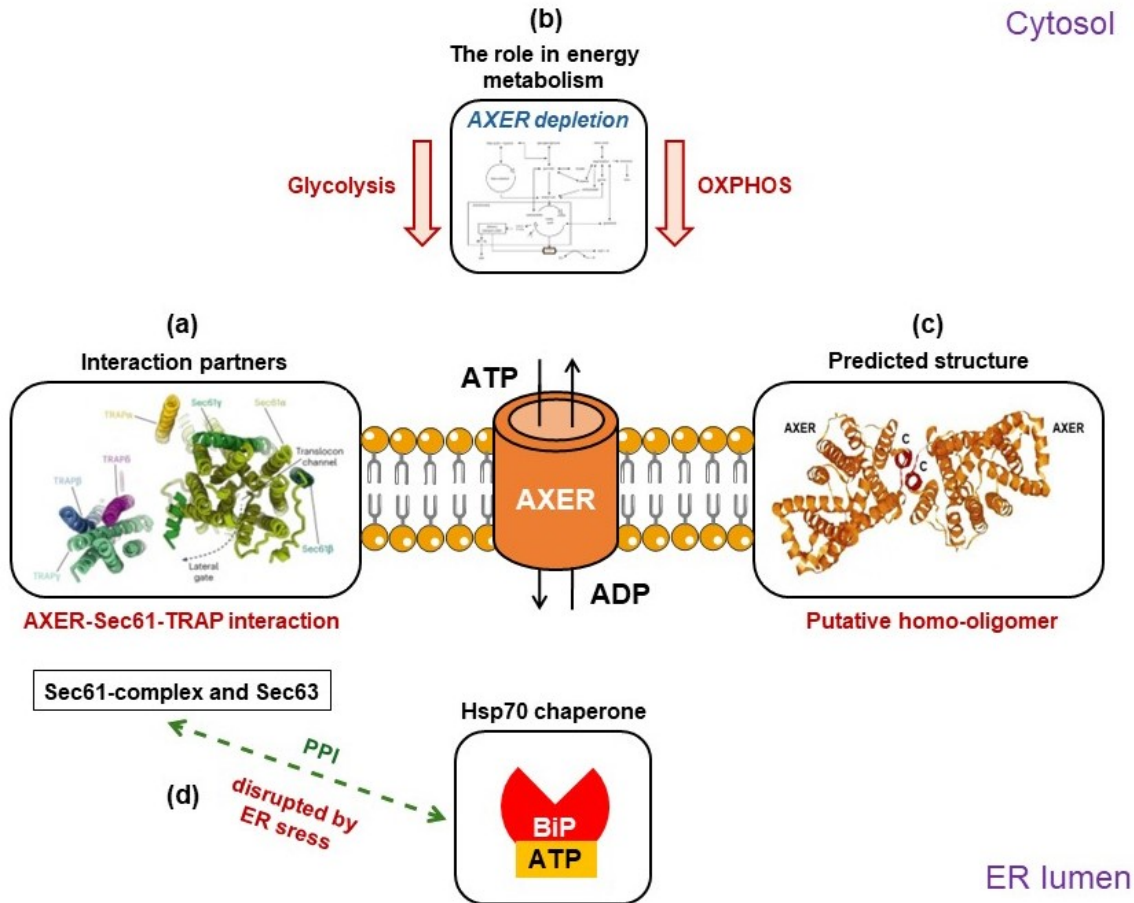


**Figure 42. Graphical summary of the main findings of the study.** The study centered around AXER, the ER ATP/ADP exchanger. (a) The Sec61-TRAP-complex subunits are components of AXER's interactome; (b) The loss of AXER causes a decline in total cellular ATP-production (glycolysis and OXPHOS); (c) AXER potentially operates in form of a dimer/oligomer; (d) The interactions of BiP-Sec61-complex and BiP-Sec63 are changing during ER stress. PPIs, protein-protein interactions.

[(a) Model of Sec61-TRAP-complex, Jaskolowski et al., 2023]

## Appendix

**Table 14. Differently expressed genes (DEGs) upon AXER depletion.** Down-regulation (blue) or up-regulation (red) of specific genes after 72 hours AXER silencing (AXER siRNA #1 and #4) in comparison to control siRNA treatment. The table contains genes involved in the ER protein import, protein modification, the unfolded protein response (UPR), ER calcium homeostasis, cellular energy homeostasis and autophagy.

Gene	siRNA	Gene regulation	
		AXER #1	AXER #4
SLC35B1 (AXER)		down	down
SEC61A1 (Sec61 $\alpha$ )		/	down
SEC61B (Sec61 $\beta$ )		/	down
SEC61G (Sec61 $\gamma$ )		/	up
HSPA5 (BiP)		/	down
HYOU1 (Grp170)		down	down
SSR1 (TRAP $\alpha$ )		down	/
SSR2 (TRAP $\beta$ )		down	down
SSR3 (TRAP $\gamma$ )		down	down
SSR4 (TRAP $\delta$ )		down	/
STT3A		down	/
STT3B		down	down
SRPRA (SR $\alpha$ )		up	up
TRAM1		up	down
TRAM2		up	down
SEC62		up	down
ATP2A2 (SERCA2)		/	down
PRKAA1 (AMPK $\alpha$ 1)		up	down
PRKAA2 (AMPK $\alpha$ 2)		down	/
PRKAB2 (AMPK $\beta$ 2)		up	up
PRKAG1 (AMPK $\gamma$ 1)		down	/
PRKAG2 (AMPK $\gamma$ 2)		up	up
CAMKK2 (CAMKK $\beta$ )		down	down
STK11 (LKB1)		up	/
CALM1 (Calmodulin1)		down	up
PFKFB2 (PFK2)		up	down
SQSTM1		up	up
ERN1 (IRE1)		/	down
EIF2AK3 (PERK)		/	down
ATF6		down	down
DDIT3 (CHOP)		up	/

**Table 15. Genes/proteins with similar trends of regulation/expression upon AXER depletion.** The “-omic” (transcriptomic and proteomic) data analysis revealed the changes in gene regulation/protein expression after 72 hours AXER silencing (AXER siRNA #1 and #4) in comparison to control siRNA treatment. The table contains genes/proteins involved in the ER protein import, protein modification, ER calcium homeostasis and autophagy, displaying different fold of changes, yet sharing similar trend of regulation/expression (down or up).

Gene / Protein	AXER #1		AXER #4	
	Transcriptomic	Proteomic	Transcriptomic	Proteomic
SEC61A1 / Sec61 $\alpha$	down	down	down	down
SEC61B / Sec61 $\beta$	down	down	down	down
HSPA5 / BiP	down	down	down	down
SSR3 / TRAP $\gamma$	down	down	down	down
SSR4 / TRAP $\delta$	down	down	down	down
STT3B	down	down	down	down
ATP2A2 / SERCA2	down	down	down	down
SRPRA / SR $\alpha$	up	up	up	up
SQSTM1	up	up	up	up

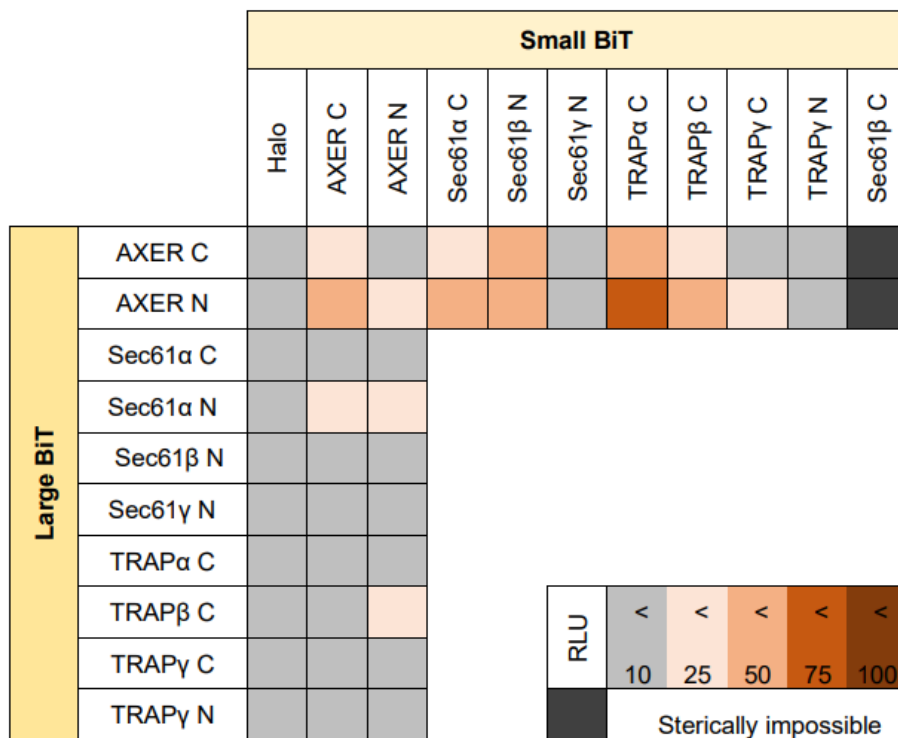


**Figure 43. Heatmap summarizing the tested PPIs of AXER.** AXER interactions with Sec61 and TRAP subunits, identified using construct pairs with cytosolically oriented BiT-tags. Detected AXER-AXER interaction indicates homo-oligomerization. RLU, relative luminescence units; RLU <10 suggests non-specific interaction (Sicking et al., 2021).

**References**

- Adams CJ, Kopp MC, Larburu N, Nowak PR, Ali MMU (2019) Structure and Molecular Mechanism of ER Stress Signaling by the Unfolded Protein Response Signal Activator IRE1. *Frontiers in Molecular Biosciences* 6 (11)
- Adams BM, Canniff NP, Guay KP, Hebert DN (2021) The role of ER chaperones in protein folding and quality control. *Progress in Molecular and Subcellular Biology* 59: 27-50
- Adamson B, Norman TM, Jost M, Cho MY, Nuñez JK, Chen Y, Villalta JE, Gilbert LA, Horlbeck MA, Hein MY, Pak RA, Gray AN, Gross CA, Dixit A, Parnas O, Regev A, Weissman JS (2016) A multiplexed single-cell CRISPR screening platform enables systematic dissection of the unfolded protein response. *Cell* 167(7): 1867-1882.e21
- Aguayo-Ortiz R, Espinoza-Fonseca LM (2020) Linking Biochemical and Structural States of SERCA: Achievements, Challenges, and New Opportunities. *International Journal of Molecular Sciences* 21(11): 4146
- Alder NN, Shen Y, Brodsky JL, Hendershot LM, Johnson AE (2005) The molecular mechanisms underlying BiP-mediated gating of the Sec61 translocon of the endoplasmic reticulum. *Journal of Cell Biology* 168(3): 389-399
- Ali R, Ramadurai S, Barry F, Nasheuer HP (2018) Optimizing fluorescent protein expression for quantitative fluorescence microscopy and spectroscopy using herpes simplex thymidine kinase promoter sequences. *FEBS Open Bio* 8(6): 1043-1060
- Almanza A, Carlesso A, Chinthra C, Creedican S, Doultinos D, Leuzzi B, Luís A, McCarthy N, Montibeller L, More S, Papaioannou A, Püschel F, Sassano ML, Skoko J, Agostinis P, de Belleruche J, Eriksson LA, Fulda S, Gorman AM, Healy S, Kozlov A, Muñoz-Pinedo C, Rehm M, Chevet E, Samali A (2019) Endoplasmic reticulum stress signalling – from basic mechanisms to clinical applications. *FEBS Journal* 286(2): 241-278
- Amador FJ, Stathopoulos PB, Enomoto M, Ikura M (2013) Ryanodine receptor calcium release channels: lessons from structure–function studies. *FEBS Journal* 280(21): 5456-5470
- Andhavarapu S, Mubariz F, Arvas M, Bever Jr C, Makar TK (2019) Interplay between ER stress and autophagy: A possible mechanism in multiple sclerosis pathology. *Experimental and Molecular Pathology* 108: 183-190
- Bakunts A, Orsi A, Vitale M, Cattaneo A, Lari F, Tadè L, Sitia R, Raimondi A, Bachi A, van Anken E (2017) Ratiometric sensing of BiP-client versus BiP levels by the unfolded protein response determines its signaling amplitude. *Elife* 6: e27518
- Balchin D, Hayer-Hartl M, Hartl FU (2020) Recent advances in understanding catalysis of protein folding by molecular chaperones. *FEBS Letters* 594(17): 2770-2781
- Behnke J, Feige MJ, Hendershot LM (2015) BiP and its nucleotide exchange factors Grp170 and Sil1: mechanisms of action and biological functions. *Journal of Molecular Biology* 427(7): 1589-1608
- Bernardi P, Gerle C, Halestrap AP, Jonas EA, Karch J, Mnatsakanyan N, Pavlov E, Sheu S-S, Soukas AA (2023) Identity, structure, and function of the mitochondrial permeability

transition pore: controversies, consensus, recent advances, and future directions. *Cell Death and Differentiation* 30: 1869-1885

Birmingham A, Anderson EM, Reynolds A, Ilsley-Tyree D, Leake D, Fedorov Y, Baskerville S, Maksimova E, Robinson K, Karpilow J, Marshall WS, Khvorova A (2006) 3' UTR seed matches, but not overall identity, are associated with RNAi off-targets. *Nature Methods* 3(3): 199-204

Bonora M, Patergnani S, Rimessi A, De Marchi E, Suski JM, Bononi A, Giorgi C, Marchi S, Missiroli S, Poletti F, Wieckowski MR, Pinton P (2012) ATP synthesis and storage. *Purinergic Signal* 8(3): 343-357

Braunger K, Pfeffer S, Shrimal S, Gilmore R, Berninghausen O, Mandon EC, Becker T, Förster F, Beckmann R (2018) Structural basis for coupling of protein transport and N-glycosylation at the mammalian endoplasmic reticulum. *Science* 360(6385): 215-219

Bround MJ, Bers DM, Molckentin JD (2020) A 20/20 view of ANT function in mitochondrial biology and necrotic cell death. *Journal of Molecular and Cellular Cardiology* 144: A3-A13

Buccitelli C, Selbach M (2020) mRNAs, proteins and the emerging principles of gene expression control. *Nature Review Genetics* 21: 630-644

Caines JK, Barnes DA, Berry MD (2022) The use of Seahorse XF assays to interrogate real-time energy metabolism in cancer cell lines. *Methods in Molecular Biology* 2508: 225-234

Chandel NS (2021) Glycolysis. *Cold Spring Harbor Perspectives in Biology* 13(5): a040535

Cherepanova N, Shrimal S, Gilmore R (2016) N-linked glycosylation and homeostasis of the endoplasmic reticulum. *Current Opinion in Cell Biology* 41: 57-65

Chipurupalli S, Samavedam U, Robinson N (2021) Crosstalk between ER stress, autophagy and inflammation. *Frontiers in Medicine (Lausanne)* 8: 758311

Christensen SB, Simonsen HT, Engedal N, Nissen P, Møller JV, Denmeade SR, Isaacs JT (2021) From Plant to Patient: Thapsigargin, a Tool for Understanding Natural Product Chemistry, Total Syntheses, Biosynthesis, Taxonomy, ATPases, Cell Death, and Drug Development. *Progress in the Chemistry of Organic Natural Products* 115: 59-114

Christianson JC, Carvalho P (2022) Order through destruction: how ER-associated protein degradation contributes to organelle homeostasis. *EMBO Journal* 41(6): e109845

Chu L, Gruber A, Ast M, Schmitz-Esser S, Altensell J, Neuhaus HE, Kroth PG, Haferkamp I (2017) Shuttling of (deoxy-) purine nucleotides between compartments of the diatom *Phaeodactylum tricornutum*. *New Phytologist* 213(1): 193-205

Clairmont CA, De Maio A, Hirschberg CB (1992) Translocation of ATP into the lumen of rough endoplasmic reticulum-derived vesicles and its binding to luminal proteins including BiP (GRP 78) and GRP 94. *Journal of Biological Chemistry* 267(6): 3983-3990

Clapham DE (2007) Calcium signaling. *Cell* 131(6): 1047-1058

Corchete LA, Rojas EA, Alonso-López D, De Las Rivas J, Gutiérrez NC, Burguillo FJ (2020) Systematic comparison and assessment of RNA-seq procedures for gene expression quantitative analysis. *Scientific Reports* 10(1): 19737

- Crick F (1970) Central dogma of molecular biology. *Nature* 227(5258): 561-563
- Csala M, Marcolongo P, Lizák B, Senesi S, Margittai É, Fulceri R, Magyar JÉ, Benedetti A, Bánhegyi G (2007) Transport and transporters in the endoplasmic reticulum. *Biochimica et Biophysica Acta* 1768(6): 1325-1341
- Cui W, Li J, Ron D, Sha B (2011) The structure of the PERK kinase domain suggests the mechanism for its activation. *Acta Crystallographica Section D Biological Crystallography* 67(5): 423-428
- Danilczyk UG, Cohen-Doyle MF, Williams DB (2000) Functional relationship between calreticulin, calnexin, and the endoplasmic reticulum luminal domain of calnexin. *Journal of Biological Chemistry* 275(17): 13089-13097
- Davies SP, Helps NR, Cohen PT, Hardie DG (1995) 5'-AMP inhibits dephosphorylation, as well as promoting phosphorylation, of the AMP-activated protein kinase. Studies using bacterially expressed human protein phosphatase-2C alpha and native bovine protein phosphatase-2AC. *FEBS Letters* 377(3): 421-425
- Dejima K, Murata D, Mizuguchi S, Nomura KH, Gengyo-Ando K, Mitani S, Kamiyama S, Nishihara S, Nomura K (2009) The ortholog of human solute carrier family 35 member B1 (UDP-galactose transporter-related protein 1) is involved in maintenance of ER homeostasis and essential for larval development in *Caenorhabditis elegans*. *FASEB Journal* 23(7): 2215-2225
- Depaoli MR, Hay JC, Graier WF, Malli R (2019) The enigmatic ATP supply of the endoplasmic reticulum. *Biological Reviews of the Cambridge Philosophical Society* 94(2): 610-628
- Dixon AS, Schwinn MK, Hall MP, Zimmerman K, Otto P, Lubben TH, Butler BL, Binkowski BF, Machleidt T, Kirkland TA, Wood MG, Eggers CT, Encell LP, Wood KV (2016) NanoLuc Complementation Reporter Optimized for Accurate Measurement of Protein Interactions in Cells. *ACS Chemical Biology* 11(2): 400-408
- Dudek J, Benedix J, Cappel S, Greiner M, Jalal C, Müller L, Zimmermann R (2009) Functions and pathologies of BiP and its interaction partners. *Cellular and Molecular Life Science* 66(9): 1556-1569
- Dudek J, Pfeffer S, Lee P, Jung M, Cavalié A, Helms V, Förster F, Zimmermann R (2015) Protein transport into the human endoplasmic reticulum. *Journal of Molecular Biology* 427(6): 1159-1175
- Ellgaard L, Helenius A (2003) Quality control in the endoplasmic reticulum. *Nature Reviews Molecular Cell Biology* 4(3): 181-191
- England CG, Ehlerding EB, Cai W (2016) NanoLuc: A Small Luciferase Is Brightening Up the Field of Bioluminescence. *Bioconjugate Chemistry* 27(5): 1175-1187
- Erdmann F, Schäuble N, Lang S, Jung M, Honigmann A, Ahmad M, Dudek J, Benedix J, Harsman A, Kopp A, Helms V, Cavalié A, Wagner R, Zimmermann R (2011) Interaction of calmodulin with Sec61 $\alpha$  limits Ca<sup>2+</sup> leakage from the endoplasmic reticulum. *EMBO Journal* 30(1): 17-31

- Fan HY, Heerklotz H (2017) Digitonin does not flip across cholesterol-poor membranes. *Journal of Colloid and Interface Science* 504: 283-293
- Ferri E, Thomas AL, Wallweber HA, Day ES, Walters BT, Kaufman SE, Braun M-G, Clark KR, Beresini MH, Mortara K, Chen Y-CA, Canter B, Phung W, Liu PS, Lammens A, Ashkenazi A, Rudolph J, Wang W (2020) Activation of the IRE1 RNase through remodeling of the kinase front pocket by ATP-competitive ligands. *Nature Communications* 11: 6387
- Fire A, Xu S, Montgomery MK, Kostas SA, Driver SE, Mello CC (1998) Potent and specific genetic interference by double-stranded RNA in *Caenorhabditis elegans*. *Nature* 391: 806-811
- Frenkel N, Makky A, Sudji IR, Wink M, Tanaka M (2014) Mechanistic investigation of interactions between steroidal saponin digitonin and cell membrane models. *Journal of Physical Chemistry B* 118(50): 14632-14639
- Gaber A, Pavšič M (2021) Modeling and Structure Determination of Homo-Oligomeric Proteins: An Overview of Challenges and Current Approaches. *International Journal of Molecular Sciences* 22(16): 9081
- Ganapathy-Kanniappan S, Geschwind J-FH (2013) Tumor glycolysis as a target for cancer therapy: progress and prospects. *Molecular Cancer* 12: 152
- Genest O, Wickner S, Doyle SM (2019) Hsp90 and Hsp70 chaperones: Collaborators in protein remodeling. *Journal of Biological Chemistry* 294(6): 2109-2120
- Geraci F, Saha I, Bianchini M (2020) Editorial: RNA-Seq Analysis: Methods, Applications and Challenges. *Frontiers in Genetics* 11: 220
- Giacomello M, Pellegrini L (2016) The coming of age of the mitochondria-ER contact: a matter of thickness. *Cell Death Differ* 23(9): 1417-1427
- Gladden LB (2004) Lactate metabolism: a new paradigm for the third millennium. *Journal of Physiology* 558(1) 5-30
- Gomez-Suaga P, Paillusson S, Stoica R, Noble W, Hanger DP, Miller CCJ (2017) The ER-Mitochondria Tethering Complex VAPB-PTPIP51 Regulates Autophagy. *Current Biology* 27(3): 371-385
- Görlich D, Rapoport TA (1993) Protein translocation into proteoliposomes reconstituted from purified components of the endoplasmic reticulum membrane. *Cell* 75(4): 615-630
- Gry M, Rimini R, Strömberg S, Asplund A, Pontén F, Uhlén M, Nilsson P (2009) Correlations between RNA and protein expression profiles in 23 human cell lines. *BMC Genomics* 10: 365
- Guillén E, Hirschberg CB (1995) Transport of adenosine triphosphate into endoplasmic reticulum proteoliposomes. *Biochemistry* 34(16): 5472-5476
- Gülow K, Bienert D, Haas IG (2002) BiP is feed-back regulated by control of protein translation efficiency. *Journal of Cell Science* 115(11): 2443-2452
- Gültekin H, Heermann KH (1988) The use of polyvinylidenedifluoride membranes as a general blotting matrix. *Analytical Biochemistry* 172(2): 320-329

- Ha S, Jeong S-H, Yi K, Chung KM, Hong CJ, Kim SW, Kim E-K, Yu S-W (2017) Phosphorylation of p62 by AMP-activated protein kinase mediates autophagic cell death in adult hippocampal neural stem cells. *Journal of Biological Chemistry* 292(33): 13795-13808
- Haas IG, Wabl M (1983) Immunoglobulin heavy chain binding protein. *Nature* 306(5941): 387-389
- Hadley B, Litfin T, Day CJ, Haselhorst T, Zhou Y, Tiralongo J (2019) Nucleotide Sugar Transporter SLC35 Family Structure and Function. *Computational and Structural Biotechnology Journal* 17: 1123-1134
- Hall MP, Unch J, Binkowski BF, Valley MP, Butler BL, Wood MG, Otto P, Zimmerman K, Vidugiris G, Machleidt T, Roberts MB, Benink HA, Eggers CT, Slater MR, Meisenheimer PL, Klaubert DH, Fan F, Encell LP, Wood KV (2012) Engineered Luciferase Reporter from a Deep Sea Shrimp Utilizing a Novel Imidazopyrazinone Substrate. *ACS Chemical Biology* 7(11): 1848-1857
- Hamman BD, Chen JC, Johnson EE, Johnson AE (1997) The aqueous pore through the translocon has a diameter of 40–60 Å during cotranslational protein translocation at the ER membrane. *Cell* 89(4): 535-544
- Harding HP, Novoa I, Zhang Y, Zeng H, Wek R, Schapira M, Ron D (2000) Regulated translation initiation controls stress-induced gene expression in mammalian cells. *Molecular Cell* 6(5): 1099-1108
- Hebert DN, Molinari M (2007) In and out of the ER: protein folding, quality control, degradation, and related human diseases. *Physiological Reviews* 87(4): 1377-1408
- Hediger MA, Clémenton B, Burrier RE, Bruford EA (2013) The ABCs of membrane transporters in health and disease (SLC series): Introduction. *Molecular Aspects of Medicine* 34(2-3): 95-107
- Hein MY, Hubner NC, Poser I, Cox J, Nagaraj N, Toyoda Y, Gak IA, Weisswange I, Mansfeld J, Buchholz F, Hyman AA, Mann M (2015) A human interactome in three quantitative dimensions organized by stoichiometries and abundances. *Cell* 163(3): 712-723
- Helbig AO, Heck AJR, Slijper M (2010) Exploring the membrane proteome—challenges and analytical strategies. *Journal of Proteomics* 73(5): 868-878
- Hendershot LM, Ting J, Lee AS (1988) Identity of the immunoglobulin heavy-chain-binding protein with the 78,000-dalton glucose-regulated protein and the role of posttranslational modifications in its binding function. *Molecular and Cellular Biology* 8(10): 4250-4256
- Herzig S, Shaw RJ (2018) AMPK: guardian of metabolism and mitochondrial homeostasis. *Nature Reviews Molecular Cell Biology* 19(2) 121-135
- Hillary RF, FitzGerald U (2018) A lifetime of stress: ATF6 in development and homeostasis. *Journal of Biomedical Science* 25(1): 48
- Hirschberg CB, Robbins PW, Abeijon C (1998) Transporters of nucleotide sugars, ATP, and nucleotide sulfate in the endoplasmic reticulum and Golgi apparatus. *Annual Review of Biochemistry* 67: 49-69

- Hoffmann C, Plochanski B, Haferkamp I, Leroch M, Ewald R, Bauwe H, Riemer J, Herrmann JM, Neuhaus HE (2013) From endoplasmic reticulum to mitochondria: absence of the Arabidopsis ATP antiporter endoplasmic Reticulum Adenylate Transporter1 perturbs photorespiration. *Plant Cell* 25(7): 2647-2660
- Horlbeck MA, Xu A, Wang M, Bennett NK, Park CY, Bogdanoff D, Adamson B, Chow ED, Kampmann M, Peterson TR, Nakamura K, Fischbach MA, Weissman JS, Gilbert L (2018) Mapping the Genetic Landscape of Human Cells. *Cell* 174(4): 953-967.e22
- Hoshino A, Wang W-J, Wada S, McDermott-Roe C, Evans CS, Gosis B, Morley MP, Rathi KS, Li J, Li K, Yang S, McManus MJ, Bowman C, Potluri P, Levin M, Damrauer S, Wallace DC, Holzbaur ELF, Arany Z (2019) The ADP/ATP translocase drives mitophagy independent of nucleotide exchange. *Nature* 575(7782): 375-379
- Jaskolowski M, Jomaa A, Gamerdinger M, Shrestha S, Leibundgut M, Deuerling E, Ban N (2023) Molecular basis of the TRAP complex function in ER protein biogenesis. *Nature Structural & Molecular Biology* 30(6): 770-777
- Jin H, Komita M, Aoe T (2017) The Role of BiP Retrieval by the KDEL Receptor in the Early Secretory Pathway and its Effect on Protein Quality Control and Neurodegeneration. *Frontiers in Molecular Neuroscience* 10: 222
- Jung S-J, Kim H (2021) Emerging View on the Molecular Functions of Sec62 and Sec63 in Protein Translocation. *International Journal of Molecular Sciences* 22(23): 12757
- Kamerlin SCL, Sharma PK, Prasad RB, Warshel A (2013) Why nature really chose phosphate. *Quarterly Reviews of Biophysics* 46(1): 1-132
- Kennedy EP, Lehninger AL (1949) Oxidation of fatty acids and tricarboxylic acid cycle intermediates by isolated rat liver mitochondria. *Journal of Biological Chemistry* 179(2): 957-972
- Kim J, Yang G, Kim Y, Kim J, Ha J (2016) AMPK activators: mechanisms of action and physiological activities. *Experimental & Molecular Medicine* 48(4): e224
- Kim SH, Shin SJ, Park JS (1996) Identification of the ATP transporter of rat liver rough endoplasmic reticulum via photoaffinity labeling and partial purification. *Biochemistry* 35(17): 5418-5425
- Kiviluoto S, Vervliet T, Ivanova H, Decuypere J-P, De Smedt H, Missiaen L, Bultynck G, Parys JB (2013) Regulation of inositol 1,4,5-trisphosphate receptors during endoplasmic reticulum stress. *Biochimica et Biophysica Acta* 1833(7): 1612-1624
- Klein M-C, Lerner M, Nguyen D, Pfeffer S, Dudek J, Förster F, Helms V, Lang S, Zimmermann R (2020) TRAM1 protein may support ER protein import by modulating the phospholipid bilayer near the lateral gate of the Sec61-channel. *Channels (Austin)* 14(1): 28-44
- Klein M-C, Zimmermann K, Schorr S, Landini M, Klemens PAW, Altensell J, Jung M, Krause E, Nguyen D, Helms V, Rettig J, Fecher-Trost C, Cavalié A, Hoth M, Bogeski I, Neuhaus HE, Zimmermann R, Lang S, Haferkamp I (2018) AXER is an ATP/ADP exchanger in the membrane of the endoplasmic reticulum. *Nature Communications* 9: 3489

- Klingenberg M (2008) The ADP and ATP transport in mitochondria and its carrier. *Biochimica et Biophysica Acta* 1778(10): 1978-2021
- Koch D (2020) Homo-Oligomerisation in Signal Transduction: Dynamics, Homeostasis, Ultrasensitivity, Bistability. *Journal of Theoretical Biology* 499: 110305
- Koch CM, Chiu SF, Akbarpour M, Bharat A, Ridge KM, Bartom ET, Winter DR (2018) A Beginner's Guide to Analysis of RNA Sequencing Data. *American Journal of Respiratory Cell and Molecular Biology* 59(2): 145-157
- Kochendörfer KU, Then AR, Kearns BG, Bankaitis VA, Mayinger P (1999) Sac1p plays a crucial role in microsomal ATP transport, which is distinct from its function in Golgi phospholipid metabolism. *EMBO Journal* 18(6): 1506-1515
- Kukurba KR, Montgomery SB (2015) RNA Sequencing and Analysis. *Cold Spring Harbor Protocols* 2015(11): 951-969
- Kumar DP, Vorvis C, Sarbeng EB, Ledesma VCC, Willis JE, Liu Q (2011) The Four Hydrophobic Residues on the Hsp70 Inter-Domain Linker Have Two Distinct Roles. *Journal of Molecular Biology* 411(5): 1099-1113
- Kunji ERS, Aleksandrova A, King MS, Majd H, Ashton VL, Cerson E, Springett R, Kibalchenko M, Tavoulari S, Crichton PG, Ruprecht JJ (2016) The transport mechanism of the mitochondrial ADP/ATP carrier. *Biochimica et Biophysica Acta* 1863(10): 2379-2393
- Kutay U, Ahnert-Hilger G, Hartmann E, Wiedenmann B, Rapoport TA (1995) Transport route for synaptobrevin via a novel pathway of insertion into the endoplasmic reticulum membrane. *EMBO Journal* 14(2): 217-223
- Laemmli UK (1970) Cleavage of structural proteins during the assembly of the head of bacteriophage T4. *Nature* 227(5259): 680-685
- Lakkaraju AKK, Thankappan R, Mary C, Garrison JL, Taunton J, Strub K (2012) Efficient secretion of small proteins in mammalian cells relies on Sec62-dependent posttranslational translocation. *Molecular Biology of the Cell* 23(14): 2712-2722
- Lam JKW, Chow MYT, Zhang Y, Leung SWS (2015) siRNA Versus miRNA as Therapeutics for Gene Silencing. *Molecular Therapy – Nucleic Acids* 4(9): e252
- Landry JJM, Pyl PT, Rausch T, Zichner T, Tekkedil MM, Stütz AM, Jauch A, Aiyar RS, Pau G, Delhomme N, Gagneur J, Korbel JO, Huber W, Steinmetz LM (2013) The genomic and transcriptomic landscape of a HeLa cell line. *G3 (Bethesda)* 3(8): 1213-1224
- Lang S, Benedix J, Fedeles SV, Schorr S, Schirra C, Schäuble N, Jalal C, Greiner M, Haßdenteufel S, Tatzelt J, Kreutzer B, Edelmann L, Krause E, Rettig J, Somlo S, Zimmermann R, Dudek J (2012) Different effects of Sec61 $\alpha$ , Sec62 and Sec63 depletion on transport of polypeptides into the endoplasmic reticulum of mammalian cells. *Journal of Cell Science* 125(8): 1958-1969
- Lang S, Erdmann F, Jung M, Wagner R, Cavalié A, Zimmermann R (2011) Sec61 complexes form ubiquitous ER Ca<sup>2+</sup> leak channels. *Channels (Austin)* 5(3): 228-235

- Lang S, Pfeffer S, Lee P-H, Cavalié A, Helms V, Förster F, Zimmermann R (2017) An Update on Sec61 Channel Functions, Mechanisms, and Related Diseases. *Frontiers in Physiology* 8: 887
- Lee K, Tirasophon W, Shen X, Michalak M, Prywes R, Okada T, Yoshida H, Mori K, Kaufman RJ (2002) IRE1-mediated unconventional mRNA splicing and S2P-mediated ATF6 cleavage merge to regulate XBP1 in signaling the unfolded protein response. *Genes & Development* 16(4): 452-466
- Lee T-Y (2021) Lactate: a multifunctional signaling molecule. *Yeungnam University Journal of Medicine* 38(3): 183-193
- Lee PY, Costumbrado J, Hsu C-Y, Kim YH (2012) Agarose gel electrophoresis for the separation of DNA fragments. *Journal of Visualized Experiments* (62): 3923
- Lemmer IL, Willemsen N, Hilal N, Bartelt A (2021) A guide to understanding endoplasmic reticulum stress in metabolic disorders. *Molecular Metabolism* 47: 101169
- Leroch M, Neuhaus HE, Kirchberger S, Zimmermann S, Melzer M, Gerhold J, Tjaden J (2008) Identification of a novel adenine nucleotide transporter in the endoplasmic reticulum of *Arabidopsis*. *Plant Cell* 20(2): 438-451
- Li A, Gao M, Liu B, Qin Y, Chen L, Liu H, Wu H, Gong G (2022) Mitochondrial autophagy: molecular mechanisms and implications for cardiovascular disease. *Cell Death & Disease* 13(5): 444
- Li X, Yang Y, Zhang B, Lin X, Fu X, An Y, Zou Y, Wang J-X, Wang Z, Yu T (2022) Lactate metabolism in human health and disease. *Signal Transduction and Targeted Therapy* 7: 305
- Liberti MV, Locasale JW (2016) The Warburg Effect: How Does it Benefit Cancer Cells?. *Trends in Biochemical Sciences* 41(3): 211-218
- Lièvre J-P, Rizzuto R, Hendershot L, Meldolesi J (1997) BiP, a major chaperone protein of the endoplasmic reticulum lumen, plays a direct and important role in the storage of the rapidly exchanging pool of Ca<sup>2+</sup>. *Journal of Biological Chemistry* 272(49): 30873-30879
- Lin J, Chen L, Jiang W, Zhang H, Shi Y, Cai W (2019) Rapid detection of low-level HeLa cell contamination in cell culture using nested PCR. *Journal of Cellular and Molecular Medicine* 23(1): 227-236
- Linxweiler M, Schick B, Zimmermann R (2017) Let's talk about secs: Sec61, sec62 and sec63 in signal transduction, oncology and personalized medicine. *Signal Transduction and Targeted Therapy* 2:17002
- Linxweiler M, Schorr S, Schäuble N, Jung M, Linxweiler J, Langer F, Schäfers H-J, Cavalié A, Zimmermann R, Greiner M (2013) Targeting cell migration and the endoplasmic reticulum stress response with calmodulin antagonists: a clinically tested small molecule phenocopy of SEC62 gene silencing in human tumor cells. *BMC Cancer* 13: 574
- Liu Y, Chen XJ (2013) Adenine Nucleotide Translocase, Mitochondrial Stress, and Degenerative Cell Death. *Oxidative Medicine and Cellular Longevity* 2013: 146860

Liu Y, Beyer A, Aebersold R (2016) On the Dependency of Cellular Protein Levels on mRNA Abundance. *Cell* 165(3): 535-550

Lodish H, Berk A, Kaiser CA, Krieger M, Bretscher A, Ploegh H, Amon A, Martin K (eds) (2016) *Molecular Cell Biology*. 8th ed. Macmillan Learning

Losfeld ME, Ng BG, Kircher M, Buckingham KJ, Turner EH, Eroshkin A, Smith JD, Shendure J, Nickerson DA, Bamshad MJ; University of Washington Center for Mendelian Genomics; Freeze HH (2014) A new congenital disorder of glycosylation caused by a mutation in SSR4, the signal sequence receptor 4 protein of the TRAP complex. *Human Molecular Genetics* 23(6): 1602-1605

Lucey BP, Nelson-Rees WA, Hutchins GM (2009) Henrietta Lacks, HeLa cells, and cell culture contamination. *Archives of Pathology and Laboratory Medicine* 133(9): 1463-1467

Lyman SK, Schekman R (1995) Interaction between BiP and Sec63p is required for the completion of protein translocation into the ER of *Saccharomyces cerevisiae*. *Journal of Cell Biology* 131(5) 1163-1171

Malmersjö S, Meyer T (2013) Inside-Out Connections: The ER Meets the Plasma Membrane. *Cell* 153(7): 1423-1424

Marcelo KL, Means AR, York B (2016) The Ca<sup>2+</sup>/Calmodulin/CaMKK2 Axis: Nature's Metabolic CaMshaft. *Trends in Endocrinology & Metabolism* 27(10) 706-718

Marchi S, Patergnani S, Pinton P (2013) The endoplasmic reticulum–mitochondria connection: One touch, multiple functions. *Biochimica et Biophysica Acta* 1837(4): 461-469

Matlack KE, Mothes W, Rapoport TA (1998) Protein translocation: tunnel vision. *Cell* 92(3): 381-390

Matuz-Mares D, González-Andrade M, Araiza-Villanueva MG, Vilchis-Landeros MM, Vázquez-Meza H (2022) Mitochondrial Calcium: Effects of Its Imbalance in Disease. *Antioxidants (Basel)* 11(5): 801

Mayinger P, Meyer DI (1993) An ATP transporter is required for protein translocation into the yeast endoplasmic reticulum. *EMBO Journal* 12(2): 659-666

Melnyk A, Lang S, Sicking M, Zimmermann R, Jung M (2022) Co-chaperones of the Human Endoplasmic Reticulum: An Update. In Edkins AL, Blatch GL (eds) *The Networking of Chaperones by Co-chaperones*. 3rd ed: 247-291. Springer

Mohorko E, Glockshuber R, Aebi M (2011) Oligosaccharyltransferase: the central enzyme of N-linked protein glycosylation. *Journal of Inherited Metabolic Disease* 34(4): 869-878

Moreno-Sánchez R, Rodríguez-Enríquez S, Marín-Hernández A, Saavedra E (2007) Energy metabolism in tumor cells. *FEBS Journal* 274(6): 1393-1418

Müller JB, Geyer PE, Colaço AR, Treit PV, Strauss MT, Oroshi M, Doll S, Winter SV, Bader JM, Köhler N, Theis F, Santos A, Mann M (2020) The proteome landscape of the kingdoms of life. *Nature* 582(7813): 592-596

- Nakanishi H, Nakayama K, Yokota A, Tachikawa H, Takahashi N, Jigami Y (2001) Hsc70 proteins identified in *Saccharomyces cerevisiae* and *Schizosaccharomyces pombe* are functional homologues involved in the protein-folding process at the endoplasmic reticulum. *Yeast* (Chichester, England) 18(6): 543-554
- Nguyen D, Stutz R, Schorr S, Lang S, Pfeffer S, Freeze HH, Förster F, Helms V, Dudek J, Zimmermann R (2018) Proteomics reveals signal peptide features determining the client specificity in human TRAP-dependent ER protein import. *Nature Communications* 9(1): 3765
- Nguyen TH, Law DT, Williams DB (1991) Binding protein BiP is required for translocation of secretory proteins into the endoplasmic reticulum in *Saccharomyces cerevisiae*. *Proceedings of the National Academy of Sciences USA* 88(4): 1565-1569
- Nicchitta CV, Blobel G (1993) Luminal proteins of the mammalian endoplasmic reticulum are required to complete protein translocation. *Cell* 73(5): 989-998
- Nishitoh H (2012) CHOP is a multifunctional transcription factor in the ER stress response. *Journal of Biochemistry* 151(3): 217-219
- Nolfi-Donagan D, Braganza A, Shiva S (2020) Mitochondrial electron transport chain: Oxidative phosphorylation, oxidant production, and methods of measurement. *Redox Biology* 37: 101674
- Oba Y, Konishi K, Yano D, Shibata H, Kato D, Shirai T (2020) Resurrecting the ancient glow of the fireflies. *Science Advances* 6(49): eabc5705
- Oh-Hashi K, Hirata Y, Kiuchi K (2016) SOD1 dimerization monitoring using a novel split NanoLuc, NanoBit. *Cell Biochemistry and Function* 34(7): 497-504
- Ondo K, Arakawa H, Nakano M, Fukami T, Nakajima M (2020) SLC35B1 significantly contributes to the uptake of UDPGA into the endoplasmic reticulum for glucuronidation catalyzed by UDP-glucuronosyltransferases. *Biochemical Pharmacology* 175: 113916
- O'Keefe S, Zong G, Duah KB, Andrews LE, Shi WQ, High S (2021) An alternative pathway for membrane protein biogenesis at the endoplasmic reticulum. *Communications Biology* 4(1): 828
- Otero JH, Lizák B, Hendershot LM (2010) Life and death of a BiP substrate. *Seminars in Cell & Developmental Biology* 21(5): 472-478
- Ou WJ, Bergeron JJ, Li Y, Kang CY, Thomas DY (1995) Conformational changes induced in the endoplasmic reticulum luminal domain of calnexin by Mg-ATP and Ca<sup>2+</sup>. *Journal of Biological Chemistry* 270(30): 18051-18059
- Palade GE, Porter KR (1954) Studies on the endoplasmic reticulum. I. Its identification in cells in situ. *Journal of Experimental Medicine* 100(6): 641-656
- Panda S, Behera S, Alam MF, Syed GH (2021) Endoplasmic reticulum & mitochondrial calcium homeostasis: The interplay with viruses. *Mitochondrion* 58: 227-242
- Park S-M, Kang T-I, So J-S (2021) Roles of XBP1s in Transcriptional Regulation of Target Genes. *Biomedicines* 9(7): 791

- Parker CE, Warren MR, Mocanu V (2010) Mass Spectrometry for Proteomics. In Alzate O (eds) Neuroproteomics. CRC Press/Taylor and Francis
- Parys JB, Van Coppenolle F (2022) Sec61 complex/translocon: The role of an atypical ER Ca<sup>2+</sup>-leak channel in health and disease. *Frontiers in Physiology* 13: 991149
- Pascale RM, Calvisi DF, Simile MM, Feo CF, Feo F (2020) The Warburg Effect 97 Years after Its Discovery. *Cancers (Basel)* 12(10): 2819
- Paskevicius T, Farraj RA, Michalak M, Agellon LB (2023) Calnexin, More Than Just a Molecular Chaperone. *Cells* 12(3): 403
- Paton AW, Beddoe T, Thorpe CM, Whisstock JC, Wilche MC, Rossjohn J, Talbot UM, Paton JC (2006) AB5 subtilase cytotoxin inactivates the endoplasmic reticulum chaperone BiP. *Nature* 443(7111): 548-552
- Pavlova NN, Thompson CB (2016) The Emerging Hallmarks of Cancer Metabolism. *Cell Metabolism* 23(1): 27-47
- Pavlova NN, Zhu J, Thompson CB (2022) The Hallmarks of Cancer Metabolism: Still Emerging. *Cell Metabolism* 34(3): 355-377
- Pfeffer S, Burbaum L, Unverdorben P, Pech M, Chen Y, Zimmermann R, Beckmann R, Förster F (2015) Structure of the native Sec61 protein-conducting channel. *Nature Communications* 6: 8403
- Pfeffer S, Dudek J, Gogala M, Schorr S, Linxweiler J, Lang S, Becker T, Beckmann R, Zimmermann R, Förster F (2014) Structure of the mammalian oligosaccharyl-transferase complex in the native ER protein translocon. *Nature Communications* 5: 3072
- Pfeffer S, Dudek J, Schaffer M, Ng BG, Albert S, Plietzko JM, Baumeister W, Zimmermann R, Freeze HH, Engel BD, Förster F (2017) Dissecting the molecular organization of the translocon-associated protein complex. *Nature Communications* 8: 14516
- Pfeffer S, Dudek J, Zimmermann R, Förster F (2016) Organization of the native ribosome-translocon complex at the mammalian endoplasmic reticulum membrane. *Biochimica et Biophysica Acta* 1860(10): 2122-2129
- Phillips MJ, Voeltz GK (2016) Structure and function of ER membrane contact sites with other organelles. *Nature Reviews Molecular Cell Biology* 17(2): 69-82
- Pobre KFR, Poet GJ, Hendershot LM (2019) The endoplasmic reticulum (ER) chaperone BiP is a master regulator of ER functions: Getting by with a little help from ERdj friends. *Journal of Biological Chemistry* 294(6) 2098-2108
- Porter KR, Palade GE (1957) Studies on the endoplasmic reticulum: III. Its form and distribution in striated muscle cells. *Journal of Biophysical and Biochemical Cytology* 3(2): 269-300
- Porter KR, Claude A, Fullam EF (1945) A study of tissue culture cells by electron microscopy: methods and preliminary observations. *Journal of Experimental Medicine* 81(3): 233-246
- Preissler S, Rato C, Yan Y, Perera LA, Czako A, Ron D (2020) Calcium depletion challenges endoplasmic reticulum proteostasis by destabilising BiP-substrate complexes. *Elife* 9: e62601

- Preissler S, Chambers JE, Crespillo-Casado A, Avezov E, Miranda E, Perez J, Hendershot LM, Harding HP, Ron D (2015) Physiological modulation of BiP activity by trans-protomer engagement of the interdomain linker. *Elife* 4: e08961
- Puhka M, Vihinen H, Joensuu M, Jokitalo E (2007) Endoplasmic reticulum remains continuous and undergoes sheet-to-tubule transformation during cell division in mammalian cells. *Journal of Cell Biology* 179(5): 895-909
- Rajendran M, Dane E, Conley J, Tantama M (2016) Imaging Adenosine Triphosphate (ATP). *Biological Bulletin* 231(1): 73-84
- Rapoport TA, Rolls MM, Jungnickel B (1996) Approaching the mechanism of protein transport across the ER membrane. *Current Opinion in Cell Biology* 8(4): 499-504
- Read A, Schröder M (2021) The Unfolded Protein Response: An Overview. *Biology (Basel)* 10(5): 384
- Rimessi A, Giorgi C, Pinton P, Rizzuto R (2008) The versatility of mitochondrial calcium signals: from stimulation of cell metabolism to induction of cell death. *Biochimica et Biophysica Acta* 1777(7-8): 808-816
- Ross FA, MacKintosh C, Hardie DG (2016) AMP-activated protein kinase: a cellular energy sensor that comes in 12 flavours. *FEBS Journal* 283(16): 2987-3001
- Sánchez-Martín P, Komatsu M (2018) p62/SQSTM1 – steering the cell through health and disease. *Journal of Cell Science* 131(21): jcs222836
- Sánchez-Martín P, Saito T, Komatsu M (2019) p62/SQSTM1: ‘Jack of all trades’ in health and cancer. *FEBS Journal* 286(1): 8-23
- Sano R, Reed JC (2013) ER stress-induced cell death mechanisms. *Biochimica et Biophysica Acta* 1833(12): 3460-3470
- Schäuble N, Lang S, Jung M, Cappel S, Schorr S, Ulucan Ö, Linxweiler J, Dudek J, Blum R, Helms V, Paton AW, Paton JC, Cavalié A, Zimmermann R (2012) BiP-mediated closing of the Sec61 channel limits Ca<sup>2+</sup> leakage from the ER. *EMBO Journal* 31(15): 3282-3296
- Schlenstedt G, Zimmermann R (1987) Import of frog prepropeptide GLa into microsomes requires ATP but does not involve docking protein or ribosomes. *EMBO Journal* 6(3): 699-703
- Schlessinger A, Yee SW, Sali A, Giacomini KM (2013) SLC classification: An update. *Clinical Pharmacology & Therapeutics* 94(1): 19-23
- Schönbrunner ER, Schmid FX (1992) Peptidyl-prolyl cis-trans isomerase improves the efficiency of protein disulfide isomerase as a catalyst of protein folding. *Proceedings of the National Academy of Sciences USA* 89(10): 4510-4513
- Schorr S, Klein M-C, Gamayun I, Melnyk A, Jung M, Schäuble N, Wang Q, Hemmis B, Bochen F, Greiner M, Lampel P, Urban SK, Hassdenteufel S, Dudek J, Chen X-Z, Wagner R, Cavalié A, Zimmermann R (2015) Co-chaperone Specificity in Gating of the Polypeptide Conducting Channel in the Membrane of the Human Endoplasmic Reticulum. *Journal of Biological Chemistry* 290(30): 18621-18635

Schwarz DS, Blower MD (2016) The endoplasmic reticulum: structure, function and response to cellular signaling. *Cellular and Molecular Life Sciences* 73(1): 79-94

Schwarzbaum PJ, Schachter J, Bredeston LM (2022) The broad range di- and tri-nucleotide exchanger SLC35B1 displays asymmetrical affinities for ATP transport across the ER membrane. *Journal of Biological Chemistry* 298(4): 101537

Schweke H, Pacesa M, Levin T, Goverde CA, Kumar P, Duhoo Y, Dornfeld LJ, Dubreuil B, Georgeon S, Ovchinnikov S, Woolfson DN, Correia BE, Dey S, Levy ED (2024) An atlas of protein homo-oligomerization across domains of life. *Cell* 187(4): 999-1010.e15

Seo M-D, Enomoto M, Ishiyama N, Stathopoulos PB, Ikura M (2015) Structural insights into endoplasmic reticulum stored calcium regulation by inositol 1,4,5-trisphosphate and ryanodine receptors. *Biochimica et Biophysica Acta* 1853(9): 1980-1991

Shackelford DB, Shaw RJ (2009) The LKB1-AMPK pathway: metabolism and growth control in tumor suppression. *Nature Reviews Cancer* 9(8): 563-575

Shen J, Chen X, Hendershot L, Prywes R (2002) ER stress regulation of ATF6 localization by dissociation of BiP/GRP78 binding and unmasking of Golgi localization signals. *Developmental Cell* 3(1): 99-111

Shibata Y, Shemesh T, Prinz WA, Palazzo AF, Kozlov MM, Rapoport TA (2010) Mechanisms determining the morphology of the peripheral ER. *Cell* 143(5): 774-788

Shibata Y, Voeltz GK, Rapoport TA (2006) Rough sheets and smooth tubules. *Cell* 126(3): 435-439

Shin SJ, Lee WK, Lim HW, Park J (2000) Characterization of the ATP transporter in the reconstituted rough endoplasmic reticulum proteoliposomes. *Biochimica et Biophysica Acta* 1468(1-2): 55-62

Shukla GC, Singh J, Barik S (2011) MicroRNAs: Processing, Maturation, Target Recognition and Regulatory Functions. *Molecular and Cellular Pharmacology* 3(3): 83-92

Sicking M, Jung M, Lang S (2021) Lights, Camera, Interaction: Studying Protein–Protein Interactions of the ER Protein Translocase in Living Cells. *International Journal of Molecular Sciences* 22(19): 10358

Simmen T, Herrera-Cruz MS (2018) Plastic mitochondria-endoplasmic reticulum (ER) contacts use chaperones and tethers to mould their structure and signaling. *Current Opinion in Cell Biology* 53: 61-69

Smith M, Wilkinson S (2017) ER homeostasis and autophagy. *Essays in Biochemistry* 61(6): 625-635

Smith BJ (1984) SDS polyacrylamide gel electrophoresis of proteins. *Methods in Molecular Biology* 1: 41-55

Smock RG, Rivoire O, Russ WP, Swain JF, Leibler S, Ranganathan R, Gierasch LM (2010) An interdomain sector mediating allostery in Hsp70 molecular chaperones. *Molecular Systems Biology* 6: 414

- Sommer N, Junne T, Kalies K-U, Spiess M, Hartmann E (2013) TRAP assists membrane protein topogenesis at the mammalian ER membrane. *Biochimica et Biophysica Acta* 1833(12): 3104-3111
- Sriram M, Osipiuk J, Freeman B, Morimoto R, Joachimiak A (1997) Human Hsp70 molecular chaperone binds two calcium ions within the ATPase domain. *Structure* 5(3): 403-414
- Stein SC, Woods A, Jones NA, Davison MD, Carling D (2000) The regulation of AMP-activated protein kinase by phosphorylation. *Biochemical Journal* 345(3): 437-443
- Stryer L (1995) *Biochemistry*. 4th ed. Freeman & Company, WH
- Tjernberg A, Markova N, Griffiths WJ, Hallén D (2006) DMSO-related effects in protein characterization. *Journal of Biomolecular Screening* 11(2): 131-137
- Towbin H, Staehelin T, Gordon J (1979) Electrophoretic transfer of proteins from polyacrylamide gels to nitrocellulose sheets: procedure and some applications. *Proceedings of the National Academy of Sciences USA* 76(9): 4350-4354
- Trefts E, Shaw RJ (2021) AMPK: restoring metabolic homeostasis over space and time. *Molecular Cell* 81(18): 3677-3690
- Tyedmers J, Lerner M, Wiedmann M, Volkmer J, Zimmermann R (2003) Polypeptide-binding proteins mediate completion of co-translational protein translocation into the mammalian endoplasmic reticulum. *EMBO Reports* 4(5): 505-510
- Uhlén M, Fagerberg L, Hallström BM, Lindskog C, Oksvold P, Mardinoglu A, Sivertsson Å, Kampf C, Sjöstedt E, Asplund A, Olsson I, Edlund K, Lundberg E, Navani S, Szigartyo CA-K, Odeberg J, Djureinovic D, Takanen JO, Hober S, Alm T, et al. (2015) Proteomics. Tissue-based map of the human proteome. *Science* 347(6220):1260419
- Ui-Tei K, Naito Y, Nishi K, Juni A, Saigo K (2008) Thermodynamic stability and Watson–Crick base pairing in the seed duplex are major determinants of the efficiency of the siRNA-based off-target effect. *Nucleic Acids Research* 36(22): 7100-7109
- Valm AM, Cohen S, Legant WR, Melunis J, Hershberg U, Wait E, Cohen AR, Davidson MW, Betzig E, Lippincott-Schwartz J (2017) Applying systems-level spectral imaging and analysis to reveal the organelle interactome. *Nature* 546(7656): 162-167
- Van Coppenolle F, Abeele FV, Slomianny C, Flourakis M, Hesketh J, Dewailly E, Prevarskaya N (2004) Ribosome-translocon complex mediates calcium leakage from endoplasmic reticulum stores. *Journal of Cell Science* 117(18): 4135-4142
- Van Wijk R, Van Solinge WW (2005) The energy-less red blood cell is lost: erythrocyte enzyme abnormalities of glycolysis. *Blood* 106(13): 4034-4042
- Vander Heiden MG, Cantley LC, Thompson CB (2009) Understanding the Warburg Effect: the metabolic requirements of cell proliferation. *Science* 324(5930): 1029-1033
- Vattem KM, Wek RC (2004) Reinitiation involving upstream ORFs regulates ATF4 mRNA translation in mammalian cells. *Proceedings of the National Academy of Sciences USA* 101(31): 11269-11274

- Vaupel P, Multhoff G (2021) Revisiting the Warburg effect: historical dogma versus current understanding. *Journal of Physiology* 599(6): 1745-1757
- Vishnu N, Khan MJ, Karsten F, Groschner LN, Waldeck-Weiermair M, Rost R, Hallström S, Imamura H, Graier WF, Malli R (2014) ATP increases within the lumen of the endoplasmic reticulum upon intracellular Ca<sup>2+</sup> release. *Molecular Biology of the Cell* 25(3): 368-379
- Voeltz GK, Rolls MM, Rapoport TA (2002) Structural organization of the endoplasmic reticulum. *EMBO Reports* 3(10): 944-950
- Vogel C, Marcotte EM (2012) Insights into the regulation of protein abundance from proteomic and transcriptomic analyses. *Nature Reviews Genetics* 13(4): 227-232
- Wada I, Rindress D, Cameron PH, Ou WJ, Doherty 2nd JJ, Louvard D, Bell AW, Dignard D, Thomas DY, Bergeron JJ (1991) SSR alpha and associated calnexin are major calcium binding proteins of the endoplasmic reticulum. *Journal of Biological Chemistry* 266(29): 19599-19610
- Walter P, Ibrahimi I, Blobel G (1981) Translocation of proteins across the endoplasmic reticulum. I. Signal recognition protein (SRP) binds to in-vitro-assembled polysomes synthesizing secretory protein. *Journal of Cell Biology* 91(2): 545-550
- Walter P, Ron D (2011) The unfolded protein response: from stress pathway to homeostatic regulation. *Science* 334(6059): 1081-1086
- Walter P, Blobel G (1983) Preparation of microsomal membranes for cotranslational protein translocation. *Methods in Enzymology* 96: 84-93
- Wang J, Lee J, Liem D, Ping P (2017) HSPA5 Gene Encoding Hsp70 Chaperone BiP in the Endoplasmic Reticulum. *Gene* 618: 14-23
- Wang Y, Zhang L, He Z, Deng J, Zhang Z, Liu L, Ye W, Liu S (2020) Tunicamycin induces ER stress and inhibits tumorigenesis of head and neck cancer cells by inhibiting N-glycosylation. *American Journal of Translational Research* 12(2): 541-550
- Warburg O (1956a) On the origin of cancer cells. *Science* 123(3191): 309-314
- Warburg O (1956b) On the respiratory impairment in cancer cells. *Science* 124(3215): 269-270
- Warburg O, Wind F, Negelein E (1927) The Metabolism of Tumors in the Body. *Journal of General Physiology* 8(6): 519-530
- Weber K, Osborn M (1969) The reliability of molecular weight determinations by dodecyl sulfate-polyacrylamide gel electrophoresis. *Journal of Biological Chemistry* 244(16): 4406-4412
- Wirth A, Jung M, Bies C, Friebe M, Tyedmers J, Zimmermann R, Wagner R (2003) The Sec61p complex is a dynamic precursor activated channel. *Molecular Cell* 12(1): 261-268
- Woods A, Dickerson K, Heath R, Hong S-P, Momcilovic M, Johnstone SR, Carlson M, Carling D (2005) Ca<sup>2+</sup>/calmodulin-dependent protein kinase kinase-β acts upstream of AMP-activated protein kinase in mammalian cells. *Cell Metabolism* 2(1): 21-33

- Wuytack F, Raeymaekers L, Missiaen L (2002) Molecular physiology of the SERCA and SPCA pumps. *Cell Calcium* 32(5-6): 279-305
- Xu C, Bailly-Maitre B, Reed JC (2005) Endoplasmic reticulum stress: cell life and death decisions. *Journal of Clinical Investigation* 115(10): 2656-2664
- Yan Y, Zhou XE, Xu HE, Melcher K (2018) Structure and Physiological Regulation of AMPK. *International Journal of Molecular Sciences* 19(11): 3534
- Yong J, Bischof H, Burgstaller S, Siirin M, Murphy A, Malli R, Kaufman RJ (2019) Mitochondria supply ATP to the ER through a mechanism antagonized by cytosolic Ca<sup>2+</sup>. *Elife* 8: e49682
- Yoshida H, Matsui T, Yamamoto A, Okada T, Mori K (2001) XBP1 mRNA is induced by ATF6 and spliced by IRE1 in response to ER stress to produce a highly active transcription factor. *Cell* 107(7): 881-891
- Yu F, Ma R, Liu C, Zhang L, Feng K, Wang M, Yin D (2021) SQSTM1/p62 Promotes Cell Growth and Triggers Autophagy in Papillary Thyroid Cancer by Regulating the AKT/AMPK/mTOR Signaling Pathway. *Frontiers in Oncology* 11: 638701
- Zimmerman JJ, von Saint André-von Arnim A, McLaughlin J (2011) Cellular Respiration. In Fuhrman BP, Zimmerman JJ (eds) *Pediatric Critical Care*. 4th ed:1058-1072. Mosby.
- Zimmermann R (2016) Components and Mechanisms of Import, Modification, Folding, and Assembly of Immunoglobulins in the Endoplasmic Reticulum. *Journal of Clinical Immunology* 36(1): 5-11
- Zimmermann R, Lang S (2020) A Little AXER ABC: ATP, BiP, and Calcium Form a Triumvirate Orchestrating Energy Homeostasis of the Endoplasmic Reticulum. *SAGE Journals* 3: 1-12
- Zimmermann R, Eyrisch S, Ahmad M, Helms V (2011) Protein translocation across the ER membrane. *Biochimica et Biophysica Acta* 1808(3): 912-924

## Publications

Andrea Tirincsi, Sarah O'Keefe, Duy Nguyen, Mark Sicking, Johanna Dudek, Friedrich Förster, Martin Jung, **Drazena Hadzibeganovic**, Volkhard Helms, Stephen High, Richard Zimmermann, Sven Lang (2022) Proteomics identifies substrates and a novel component in hSnd2-dependent ER protein targeting. *Cells* 11(18): 2925

Mark Sicking, Martina Živná, Pratiti Bhadra, Veronika Barešová, Andrea Tirincsi, **Drazena Hadzibeganovic**, Kateřina Hodaňová, Petr Vyleťal, Jana Sovová, Ivana Jedličková, Martin Jung, Thomas Bell, Volkhard Helms, Anthony Bleyer, Stanislav Kmoch, Adolfo Cavalié, Sven Lang (2022) Phenylbutyrate rescues the transport defect of the Sec61 $\alpha$  mutations V67G and T185A for renin. *Life Science Alliance* 5(4): e202101150

Andrea Tirincsi, Mark Sicking, **Drazena Hadzibeganovic**, Sarah Haßdenteufel, Sven Lang (2021) The Molecular Biodiversity of Protein Targeting and Protein Transport Related to the Endoplasmic Reticulum. *International Journal of Molecular Sciences* 23(1): 143

**Dražena Hadžibeganović**, Rifet Terzić, Amela Jusić, Aldijana Avdić (2017) Association between insertion/deletion polymorphism of the angiotensin-converting enzyme gene and coronary artery disease in Bosnian population. *Genetics & Applications* 1(2): 44-49

Aldijana Avdić, Rifet Terzić, Amela Karić, Amela Hercegovac, Samra Međedović, Lejla Riđanović, Mustafa Bačinović, Selma Bačinović, **Dražena Hadžibeganović** (2016) Populaciono-genetička analiza hromozomopatija u uzorku novorođenčadi Tuzlanskog kantona (Bosna i Hercegovina) [Population-genetical analysis of chromosomal anomalies in a sample of newborns of Tuzla Canton (Bosnia and Herzegovina)]. *Educa* 9:18-27

## **Acknowledgements**

First and foremost, I express my deepest appreciation to my supervisor, Dr. Sven Lang, who believed in my abilities and gave me the opportunity to complete my Ph.D. studies. Your expertise, wisdom, and encouragement have been a guiding light, shaping my understanding and fueling my enthusiasm for learning. Your generosity, kindness, and leadership made this journey both rewarding and memorable. Thank you for being an exceptional mentor.

I am sincerely grateful to Professor Dr. Martin Jung. Your proficiency and great support have enriched my experience throughout the entire research process.

To my dedicated teammates, Dr. Mark Sicking, Dr. Andrea Tirinci, and Gamar Musayeva, thank you for the hard work and commitment to our collective success that have transformed challenges into triumphs. I am fortunate to have worked alongside such a talented and supportive team. Together, we have forged a bond that goes beyond the professional realm.

A special acknowledgment goes to Monika Lerner whose "behind-the-scenes" effort ensured the smooth functioning of my lab work. Your technical expertise is truly commendable, and I am thankful for the seamless support you provided, especially during the last year of my research.

Many thanks to Sabine Pelvay, Petra Endlein, Iris Dlugosch, Holger Unruh, Lisa Ludes, Oliver Rößler, and Ina Maria Hierlmeier. I am truly grateful for the privilege of working with such an exceptional group of individuals.

Gratitude is also extended to the CRC/SFB 894 research foundation for the financial support. I am grateful for your belief in the significance of this work and your commitment to advancing knowledge in this field of study.

Last but not least, I want to express my heartfelt gratitude to my family members. Thank you for your love, encouragement, and patience throughout this academic endeavor. Your boundless support and understanding empowered me to pursue my dreams and overcome obstacles along the way.

THANK YOU ALL!

## **Curriculum Vitae**

The curriculum vitae was removed from the electronic version of the doctoral thesis for reasons of data protection.

